Durham E-Theses

Growth of CdTe bulk crystals by the multi tube physical vapour transport process

Cantwell, Benjamin John

How to cite:

Growth of CdTe Bulk Crystals by the Multi Tube Physical Vapour Transport Process

by

Benjamin John Cantwell
MSci (Hons)

A thesis presented in candidature for the degree of

Doctor of Philosophy in the University of Durham

Department of Physics

September 2004

ABSTRACT

This thesis is primarily concerned with the growth of bulk cadmium telluride (CdTe) crystals. The work relates to a modified physical vapour transport system which also enables the growth of ternary II-VI compounds, in particular cadmium zinc telluride (CdZnTe). A computer simulation to model the CdTe growth process is developed, along with a system to measure the partial pressures *in situ* during growth.

The modified Multi Tube Physical Vapour Transport (MTPVT) system, which is essentially a combination of the Markov annulus and Rosenberger flow restrictor designs, consists of two source tubes and a growth tube connected by a crossmember. This crossmember, which is optically heated, contains two capillaries which act as flow restrictors, and allows physical displacement, and therefore better thermal decoupling, of the source and growth areas.

The growth of CdTe in the MTPVT system is investigated, in particular, factors affecting the optimal design for the growth tube. The design of the pedestal, on which the seed crystal is located, is of prime importance in preventing polycrystalline growth, and the size and shape of the seed crystal is also critical. Increasing the inner diameter of the growth tube from 32 mm to 52 mm reduces the effect of the annulus gap around the seed, and increases the controllability of the growth process.

A computer simulation is used to model the vapour flow from the subliming source, through the capillary, and to the growing crystal and down the annulus. The trends predicted closely match those obtained experimentally, and imply, as expected, the growth process is controlled by the mass transport rate through the capillary. Further comparison with experiment gives an upper limit of 0.45 eV for the activation energy of the incorporation of atoms into the CdTe seed, although no lower limit can be set.

The partial pressure – optical density relationships are derived for $Cd_{(g)}$, $Zn_{(g)}$ and $Te_{2(g)}$, with the 214 nm absorption line of $Zn_{(g)}$ observed to deviate significantly from Beer's Law. Optical monitoring during CdTe growth by a computer controlled optical absorption measurement system allows *in situ* monitoring of the partial pressures. The measurements of the source side partial pressures match those predicted by the computer simulation, with the partial pressure ratio of around 1.7 also consistent with the model.

DECLARATION

I declare that all of the work in this thesis was carried out by the candidate unless stated otherwise. I also declare that none of this work has previously been submitted for any degree and that it is not being submitted for any other degree.

Dr A W Brinkman

Supervisor

Benjamin John Cantwell

Candidate

ACKNOWLEDGEMENTS

Dedicated to my Mam and Dad

CONTENTS

Chapter 1 Introduction

Chapter 2 Properties and Vapour Growth of II–VI Compounds

Chapter 3 MTPVT System

Chapter 5 Modelling the Growth of CdTe in the MTPVT System

Chapter 8 Conclusions and Scope for Future Work

Appendices

Chapter 1

Introduction

1.1 INTRODUCTION

Cadmium telluride and cadmium zinc telluride are semiconductor compounds with an increasingly wide range of applications [1]. The high average atomic number of the compounds, along with their high quantum efficiency, good mobility-lifetime product and energy resolution, make CdTe and CdZnTe excellent materials for use in room temperature X-ray and γ-ray detector systems [2-8]. In the past the main application of bulk CdTe crystals has been as a substrate for the epitaxial growth of mercury cadmium telluride (MCT), a material of tuneable bandgap for infrared detection applications, although CdZnTe is now the substrate of choice due to its better lattice match to MCT. [9-11]

The current market size for CdTe and CdZnTe is estimated at between $10 and $15 million per annum [10], and is approximately split into the sectors as shown in Figure 1.1
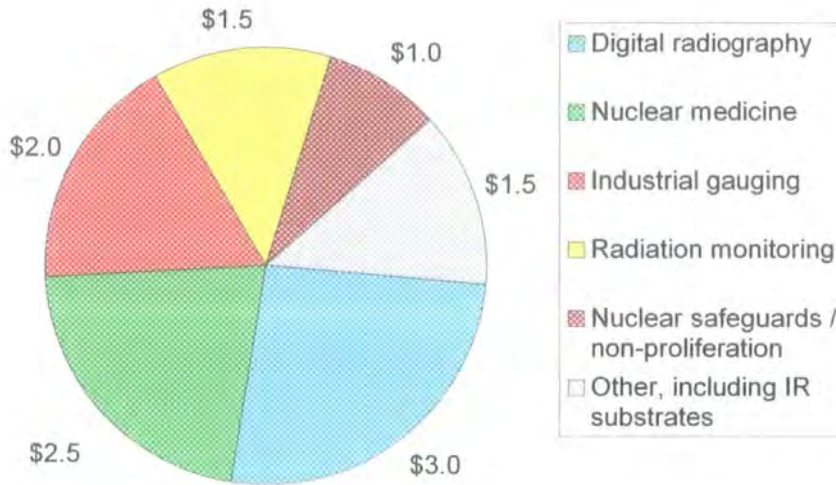
Figure 1.1: World market for 2003 for CdTe and CdZnTe split into market sectors (figures in $million) (from [10])

In the medical sector CdTe and CdZnTe based detectors are used for dental imaging, bone densitometry and digital mammography [12-19], while industrial uses include gauging and non-destructive testing. The importance of security in the current political climate has increased the demand for the use of these cadmium compounds in baggage and human scanners at airports [20], while personal radiation monitors are also increasing in importance. Hand-held detectors have also been produced to combat nuclear proliferation and as safeguards when using nuclear technology [13, 21-24]. The European Space Agency has, for many years, been developing a range of compound semiconductors for potential applications in planetary and astrophysics missions [25]. It currently has plans for a detector array using sixty-four 1cm^3 CdZnTe crystals which is to be placed on a satellite due to be launched in 2015 for the detection of γ rays.

Other applications of bulk crystals include their use as infra-red windows and as targets in sputtering systems.

This thesis outlines the further development of a vapour growth system designed to grow the binary CdTe from a CdTe source, and also grow the ternary compound CdZnTe from the binary sources CdTe and ZnTe. The growth of CdTe was studied in detail, while several preliminary experiments to grow CdZnTe are included. A computer simulation of the CdTe growth process was produced, with the results compared to the real data, and allowed the effect of changes in certain growth parameters to be modelled. A system to measure the partial vapour pressures *in situ* by optical absorption during growth has also been developed.

1.2 MOTIVATION OF THE PRESENT WORK

Direct conversion solid state radiation detectors based upon compound semiconductors allow much greater energy resolution than conventional silicon-based scintillator detectors [12], but the standard germanium-based solid state detectors which are available require cryogenic cooling. CdTe and CdZnTe based detectors, however, can operate at room temperatures [26-28] and have a number of advantages over the scintillator systems, with the high atomic number (~50) [29] and high density (~6 g cm^{-3} [30]) giving high quantum efficiency with high stopping power. The CdTe and CdZnTe detectors have a far superior energy resolution [23, 31], with the ability to detect much lower radiation levels [16, 32], and the good spatial resolution [33] allows much sharper imaging. These factors, along with the ability of the

detectors to work at room temperatures, permit hand-held detectors made of CdTe and CdZnTe to be produced.

The requirements of the crystal depend greatly upon their final use. High resistivity crystals are important for some detector applications [34], although low resistivity can be dealt with by the use of non-ohmic contacts [10, 16, 35, 36]. Large-area applications, such as medicine, require large crystals, while spectroscopic detectors require only small crystals [10]. Detectors require low densities of inclusions [22], while the absence of twin boundaries is one of the main requirements for IR substrates [37]. Sputtering targets may use polycrystalline CdTe providing it is robust and very pure.

One of the main reasons II-VI detectors have yet to be fully developed is the difficulty in obtaining the crystals reliably and at a reasonable price [10, 17]. Currently all commercially available CdTe is produced through melt techniques [38], which contain some intrinsic problems which are explained further in Chapter 2. This provided the motivation to develop a system to reliably grow high-quality CdTe and CdZnTe crystals from the vapour phase.

1.3 SCOPE OF THE PRESENT WORK

As mentioned in the previous section, this thesis is devoted to the development of a vapour growth system capable of reliably producing bulk crystals of CdTe and CdZnTe. This chapter has provided a brief background of the compounds and their applications.

The first part of Chapter 2 reviews the properties of CdTe and CdZnTe which are relevant to the vapour growth, including information about their

mechanical and thermal properties. The chapter also includes a brief review of other vapour growth techniques, particularly those relevant to CdTe and CdZnTe. The intention of the chapter was not to provide a comprehensive review of all of the techniques and results, but to outline the main developments and highlight the advantages and disadvantages of each method.

Chapter 3 outlines the redeveloped Multi-Tube Physical Vapour Transport (MTPVT) system. The system, which is based on modified Markov [39, 40] and Rosenberger [41] designs, was originally designed solely for the growth of CdTe by Dr J. T. Mullins [42]. The main elements of the system are presented in this chapter, along with the redesign of the system to enable the growth of CdZnTe from the binary sources CdTe and ZnTe.

Chapter 4 focuses on the development of the growth of CdTe crystals in the MTPVT system. Special reference is made to the development of the design of the pedestal on which the seed crystal resides. The chapter also details the changes in the tube diameter, growth profiles and temperatures designed to improve the quality of the crystals. Various types of seed crystal were used, with crystals of different size, shape and material, and the results of growth on each type are presented and discussed. A series of photographs taken during the growth on a multigrain seed crystal are included to show the development of different grains. The preliminary experiments for the growth of CdZnTe in the MTPVT system are introduced, and the results of some basic characterisation data are given.

Chapter 5 introduces a simulation for the growth of CdTe in the MTPVT system. The system is analysed in terms of a series of flows from the source to the growing crystal and beyond, and the theoretical basis for each flow is presented. Equations of flow are derived, and the computer algorithm for the simulation is presented. The results of a simulation of a growth run are shown graphically, with the changes in flows, pressures and partial pressure ratios during the growth displayed.

An optical absorption system designed to allow *in situ* measurement of the partial vapour pressures during growth is presented in Chapter 6. The physical basis for the relationship between the optical density and the pressure is outlined, and benchtop measurements used to calibrate the system are shown. Partial pressures derived from the measurements during the growth of CdTe are given, and their validity discussed.

Chapter 7 draws together the results of the growth, the simulations and the partial pressure measurements and attempts to deduce some of the growth parameters. Trends observed during the growth, via both the *in situ* measurements and measurements of weight loss and gain, are compared to simulations of growth under different conditions.

The concluding chapter provides a summary of all of the results presented and discussed in the previous chapters, and presents some ideas to extend the work in the future.

1.4 REFERENCES FOR CHAPTER 1

[1]   T. E. Schlesinger and R. B. James. *"Introduction and Overview"*. in *"Semiconductors for Room Temperature Nuclear Detectors"*. Edited by T. E. Schlesinger and R. B. James 43 Academic Press San Diego. (1995).

[2]   M. Funaki, T. Ozaki, K. Satoh and R. Ohno. *"Growth and Characterization of CdTe Single Crystals for Radiation Detectors"*. Nuclear Instruments and Methods in Physics Research Section A: Accelerators, Spectrometers, Detectors and Associated Equipment **436** (1999) 120.

[3]   J. E. Toney, R. B. James, J. Butler, P. Doty, T. E. Schlesinger, B. A. Brunett, H. Yoon, J. M. Van Scyoc, J. Lund, A. Antolak, R. W. Olsen, H. Hermon, D. H. Morse, M. Scheiber and R. H. Stulen *"Cadmium Zinc Telluride Charged Particle Nuclear Detectors"* Sandia National Laboratories (1997).

[4]   P. Fougeres, P. Siffert, M. Hageali, J. M. Koebel and R. Regal. *"CdTe and Cd$_{1-x}$Zn$_x$Te for Nuclear Detectors: Facts and Fictions"*. Nuclear Instruments and Methods in Physics Research Section A: Accelerators, Spectrometers, Detectors and Associated Equipment **428** (1999) 45.

[5]   J. Franc, P. Höschl, E. Belas, R. Grill, P. Hlídek, P. Moravec and J. Bok. *"CdTe and CdZnTe Crystals for Room Temperature Gamma-Ray Detectors"*. Nuclear Instruments and Methods in Physics Research Section A: Accelerators, Spectrometers, Detectors and Associated Equipment **434** (1999) 146.

[6]   F. Glasser, V. Gerbe, P. Ouvrier-Buffet, M. Accensi, J. L. Girard, M. Renaud and J. L. Gersten-mayer. *"CdZnTe High-Energy Radiography Detector"*. Nuclear Instruments and Methods In Physics Research A **458** (2001) 544.

[7]   B. Ramsey, D. P. Sharma, R. Austin, V. Gostilo, V. Ivanov, A. Loupilov, A. Sokolov and H. Sipila. *"Preliminary Performance of CdZnTe Imaging Detector Prototypes"*. Nuclear Instruments and Methods in Physics Research A **458** (2001) 55.

[8]   L. Verger, M. Boitel, M. C. Gentet, R. Hamelin, C. Mestais, F. Mongellaz, J. Rustique and G. Sanchez. *"Characterization of CdTe and CdZnTe Detectors for Gamma-Ray Imaging Applications"*. Nuclear Instruments and Methods In Physics Research A **458** (2001) 297.

[9]   M. G. Astles. *"Growth of Hgcdte by Liquid Phase Epitaxy"*. in *"Properties of Narrow Gap Cadmium-Based Compounds"*. Edited by P. Capper 10 Institute of Electrical Engineers London. (1993).

[10]   Research-Associates *"Market Study for Durham Scientific Crystals"* (2003).

[11]   M. Fiederle, T. Feltgen, J. Meinhardt, M. Rogalla and K. W. Benz. *"State of the Art of (Cd,Zn)Te as a Gamma Detector"*. Journal of Crystal Growth **197** (1999) 635.

[12]   D. G. Darambara and A. Todd-Pokropek. *"Solid State Detectors in Nuclear Medicine"*. The Quarterly Journal of Nuclear Medicine **46** (2002) 3.

[13]   N. Gross. *"A Revolution in Medical Imaging"* BusinessWeek (July 7, 1997) 134.

[14]   F. Glasser, P. Villard, J. P. Rostaing, M. Accensi, N. Baffert and J. L. Girard. *"Large Dynamic Range 64-Channel Asic for CZT or CdTe Detectors".* Nuclear Instruments and Methods In Physics Research A **509** (2003) 183.

[15]   V. Gostilo, V. Ivanov, S. Kostenko, I. Lisjutin, A. Loupilov, S. Nenonen, H. Sipila and K. Valpas. *"Technological Aspects of Development of Pixel and Strip Detectors Based on CdTe and CdZnTe".* Nuclear Instruments and Methods In Physics Research A **460** (2001) 27.

[16]   C. Scheiber and G. C. Giakos. *"Medical Applications of CdTe and CdZnTe Detectors".* Nuclear Instruments and Methods In Physics Research A **458** (2001) 12.

[17]   C. Scheiber. *"CdTe and CdZnTe Detectors in Nuclear Medicine".* Nuclear Instruments and Methods In Physics Research A **448** (2000) 513.

[18]   M. Schieber, H. Hermon, A. Zuck, A. Vilensky, L. Melekhov, R. Shatunovsky, E. Meerson and H. Saaso. *"Theoretical and Experimental Sensitivity to X-Rays of Single and Polycrystalline HgI_2 Compared with Different Single-Crystal Detectors".* Nuclear Instruments and Methods In Physics Research A **458** (2001) 41.

[19]   S. Yin, T. O. Tumer, D. Maeding, J. Mainprize, G. Mawdsley, M. J. Yaffe, E. E. Gordon and W. J. Hamilton. *"Direct Conversion Si and CdZnTe Detectors for Digital Mammography".* Nuclear Instruments and Metohds in Physics Research **448** (2000) 591.

[20]   C. H. Malden and R. D. Speller. *"A CdZnTe Array for the Detection of Explosives in Baggage by Energy-Dispersive X-Ray Diffraction Signatures at Multiple Scatter Angles".* Nuclear Instruments and Methods In Physics Research A **449** (2000) 408.

[21]   R. B. James.*"Revealed Weapons"* Discover Magazine (July 1997)88.

[22]   P. N. Luke, M. Amman, J. S. Lee, B. A. Ludewigt and H. Yaver. *"A CdZnTe Coplanar-Grid Detector Array for Environmental Remadiation".* Nuclear Instruments and Methods In Physics Research A **458** (2001) 319.

[23]   P. Mortreau and R. Berndt. *"Characterisation of Cadmium Zinc Telluride Detector Spectra- Application to the Analysis of Spent Fuel Spectra".* Nuclear Instruments and Methods In Physics Research A **458** (2001) 183.

[24]   K. Parnham, C. Szeles, T. H. Prettyman, M. Smith, C. Stahle, B. H. Parker and L. L. Wang. *"Further Studies on the Modified Two-Terminal Geometry for CdZnTe Detectors".* Nuclear Instruments and Methods In Physics Research A **458** (2001) 334.

[25]   M. Bavdaz, A. Peacock and A. Owens. *"Future Space Applications of Compound Semiconductor X-Ray Detectors".* Nuclear Instruments and Methods In Physics Research A **458** (2001) 123.

[26]   I. Kuvvetli, C. Butz-Jorgensen, L. Gerward and C. M. Stahle. *"Response of CZT Drift-Strip Detector to X- and Gamma Rays".* Radiation Physics and Chemistry **61** (2001) 457.

[27]   A. Owens, M. Bavdaz, H. Andersson, T. Gagliardi, M. Krumrey, S. Nenonen, A. Peacock, I. Taylor and L. Troger. *"The X-Ray Response of CdZnTe".* Nuclear Instruments and Methods In Physics Research A **484** (2002) 242.

[28]   S. M. Vincent, P. H. Regan, K. E. Owen, C. J. Pearson and A. S. Clough. *"In-Beam Performance of CdZnTe Detectors for Proton and*

Alpha-Particle Measurement". Nuclear Instruments and Methods In Physics Research A **483** (2002) 758.

[29] C. J. Pearson, P. H. Regan and A. Divoli. *"The Application of CdZnTe Detectors for Coincident a-G Spectroscopy".* Nuclear Instruments and Methods In Physics Research A **462** (2001) 393.

[30] D. J. Williams. *"Densities and Lattice Parameters of CdTe, CdZnTe and CdTeSe".* in *"Properties of Narrow Gap Cadmium-Based Compounds".* Edited by P. Capper 1 INSPEC London. (1994).

[31] O. Limousin. *"New Trends in CdTe and CdZnTe Detectors for X- and Gamma-Ray Applications".* Nuclear Instruments and Methods in Physics Research Section A: Accelerators, Spectrometers, Detectors and Associated Equipment **504** (2003) 24.

[32] C. E. Moss, K. D. Ianakiev, T. H. Prettyman, M. K. Smith and M. R. Sweet. *"Multi-Element Large-Volume CdZnTe Detectors".* Nuclear Instruments and Methods In Physics Research A **458** (2001) 455.

[33] C. Mestais, N. Baffert, J. P. Bonnefoy, A. Chapuis, A. Koenig, O. Monnet, P. O. Buffet, J. O. Rostaing, F. Sauvage and L. Verger. *"A New Design for a High Resolution, High Efficiency CZT Gamma Camera Detector".* Nuclear Instruments and Methods In Physics Research A **458** (2001) 62.

[34] U. Lachish. *"Semiconductor Crystal Optimization of Gamma Detection".* Journal of Crystal Growth **225** (2001) 114.

[35] A. V. Rybka, S. A. Leonov, I. M. Prokhoretz, A. S. Abyzov, L. N. Davydov, V. E. Kutny, M. S. Rowland and C. F. Smith. *"Influence of Detector Surface Processing on Detector Performance".* Nuclear Instruments and Methods In Physics Research A **458** (2001) 248.

[36] M. Hage-Ali and P. Siffert. *"Growth Methods of CdTe Nuclear Detector Materials".* in *"Semiconductors for Room Temperature Nuclear Detectors".* Edited by T. E. Schlesinger and R. B. James 43 Academic Press San Diego. (1995).

[37] J. Zeigler, M. Bruder, M. Fink, R. Kruger, P. Menger, T. Simon and R. Wollrab. *"Advanced Sensor Technologies for High Perforemance Infrared Detectors".* Infrared Physics & Technology **43** (2002) 239.

[38] A. W. Brinkman and P. Capper. *"Growth of CdTe, CdZnTe and CdTese by Bulk Methods".* in *"Properties of Narrow Gap Cadmium-Based Compounds".* Edited by P. Capper 10 Institute of Electrical Engineers London. (1994).

[39] E. V. Markov and A. A. Davydov. *"Sublimation of CdS Crystals".* Inorg. Mater. **7** (1971) 503.

[40] E. V. Markov and A. A. Davydov. *"Growing Oriented Single Crystals of Cadmium Sulphide from the Vapour Phase".* Inorg. Mater. **11** (1975) 104.

[41] F. Rosenberger, M. Banish and M. B. Duval *"Vapour Crystal Growth Technology Development - Application to Cadmium Telluride"* (1991).

[42] J. T. Mullins, J. Carles, N. M. Aitken and A. W. Brinkman. *"A Novel "Multi-Tube" Vapour Growth System and Its Application to the Growth of Bulk Crystals of Cadmium Telluride".* (1999).

Chapter **2**

Properties and Vapour Growth of II-VI Compounds

2.1 INTRODUCTION

The growth of II-VI compounds from the vapour phase is possible due to their relatively high vapour partial pressures over the solid. This thesis is concerned with the vapour growth of CdTe and CdZnTe, through the use of binary sources CdTe and ZnTe. This chapter will detail the properties of CdTe and ZnTe relevant to their use as sources, and the properties of CdTe and CdZnTe in respect of the growing crystal. A short description of the historical methods of vapour growth is presented, along with a short critique of the associated problems.

2.2 THERMODYNAMIC PROPERTIES

The pressure-temperature (P-T) phase relationships of binary compounds are dependent upon the composition (x) of the compound. Phase diagrams displaying the relationships at set values of one of the parameters allow the

variations of the other two to be represented graphically. This section will describe the thermodynamic properties of CdTe through the use of phase diagrams, and subsequently the phase relationships relevant to the growth of CdZnTe will follow.

2.2.1 P-T-X Phase Relations of CdTe

Early studies on the sublimation of CdTe found the solid dissociated upon heating into a vapour containing only Cd and Te_2 [1-5]

$$CdTe_{(s)} \Leftrightarrow Cd_{(g)} + \frac{1}{2}Te_{2(g)} \qquad (2.1)$$

If the source is truly stoichiometric with no inclusions or precipitates then the ratio of the partial pressures would be

$$p_{Cd} = 2p_{Te_2} \qquad (2.2)$$

Greenberg [6-8], however, through mass spectra studies found tellurium formed seven gaseous polymers Te_k where k=1 to 7, giving

$$p_{Cd} = \sum_{k=1}^{7} kp_{Te_k} \qquad (2.3)$$

although Te_2 was by far the majority species. Given the latter, and since there have been no other corroborating reports of equation (2.3), in this thesis it will be assumed the tellurium dimer is the only species present.

The temperature-dependent equilibrium constant $(K_{CdTe}(T))$ for the CdTe dissociation in equation (2.1) is given by [3]

$$K_{CdTe}(T) = p_{Cd}(p_{Te_2})^{\frac{1}{2}} = \exp\left(\frac{\Delta G}{RT}\right) \qquad (2.4)$$

where ΔG is the Gibbs Free Energy of Formation and R is the ideal gas constant.

Brebrick and Strauss [4, 9] used optical absorption studies to determine the partial pressures in mbar of p_{Cd} and p_{Te2} over subliming CdTe, and obtained the following relationships

$$\log(p_{Cd}[mbar]) = 10.039 - \frac{1.00 \cdot 10^4}{T} \qquad (2.5)$$

and

$$\log(p_{Te_2}[mbar]) = 9.346 - \frac{1.00 \cdot 10^4}{T} \qquad (2.6)$$

and were able to obtain an equation for the Gibbs Free Energy of Formation

$$\Delta G\left[\frac{kcal}{mol}\right] = 68.64 - 0.04494T \qquad (2.7)$$

De Largy *et al* [1] used a modified entrainment method to determine the equilibrium constant

$$\ln K_{CdTe} = \frac{45.842T - 69446}{1.9872T} \qquad (2.8)$$

For a vapour with partial pressure ratio α_{CdTe}, i.e.

$$p_{Cd} = \alpha_{CdTe} p_{Te_2} \qquad (2.9)$$

then from (2.4), (2.8) and (2.9)

$$p_{Cd}[Pa] = \alpha_{CdTe}^{1/3}\left(K_{CdTe}\right)^{2/3} = \alpha_{CdTe}^{1/3} \cdot 4.839 \times 10^{11} \cdot \exp\left(-\frac{23297}{T}\right) \qquad (2.10)$$

This is an oversimplification, however, as non-stoichiometries in the source need to be accounted for [10, 11]. The partial pressures are also determined by the history and pre-treatment of the source, as found by Su *et al* [12] and also by Palosz *et al* [13].

Greenberg [14] published a P-T phase diagram obtained by stoichiometry scanning which accounted for a range of tellurium compositions and is displayed in Figure 2.1. The vapour pressures for Cd-saturated CdTe and in

equilibrium with the liquid and Cd-rich vapour (VLS) were about an order of magnitude higher than those of Te-saturated CdTe in equilibrium with the liquid and Te-rich vapour (SLV) at the same temperature.
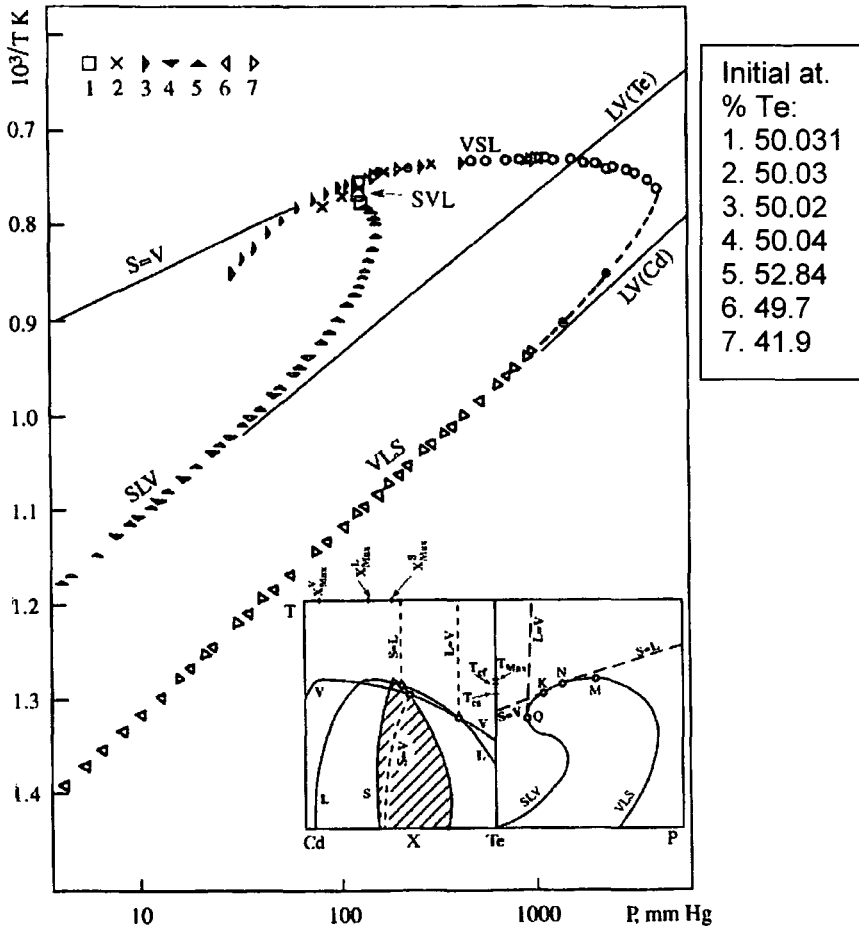
Figure 2.1: Greenberg's P-T projection of the Cd-Te phase diagram (from [14])

The temperature-composition (T-x) projection of the CdTe phase diagram [15] is presented in Figure 2.2, and its shape is characteristic of binary II-VI compounds. It implies that a source providing a stoichiometric vapour is the only requirement to obtain a stoichiometric crystal, and in terms of phase stability at the growth temperature, any temperature can in principle be

13

selected for growth. The melting point of stoichiometric CdTe is 1092°C, while

Cd and Te have eutectic melting points of 321 and 450°C respectively.
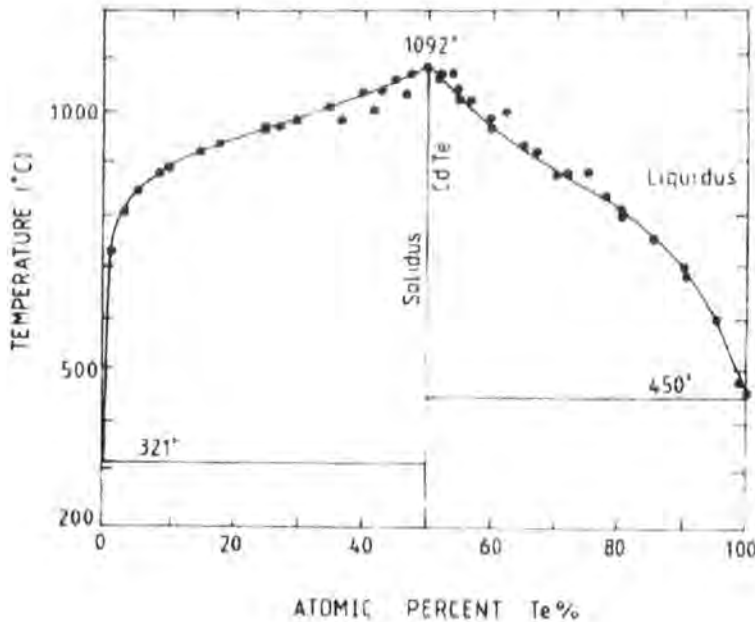
Figure 2.2: T-x projection of the CdTe phase diagram

The vertical solidus line which indicates the formation of CdTe is an

oversimplification, however. Greenberg [16] scanned the range of

homogeneity of CdTe with a stoichiometry sensitivity down to 10^{-4} at. %, and

found a range of stability on either side of the 50% composition line, as given

in Figure 2.3. The solidus is shown to be strongly asymmetrical; the

maximum Cd nonstoichiometry is almost an order of magnitude less than that

of Te and the asymmetry increases with temperature.

The retrograde solubility signified by the sharp kink in the Te-solidus in Figure

2.3, and the trend of the congruent sublimation line (S=V) towards the Te-rich

region have severe implications to the growth of CdTe from the melt [17].

During the cooling from the melt at high temperature Te precipitates will tend

to form in the crystal. This may be compensated through the use of a Cd

reservoir, although this is difficult to control accurately. These asymmetries in

14

the homogeneity favour the use of lower growth temperatures from the vapour to reduce the level of precipitates.
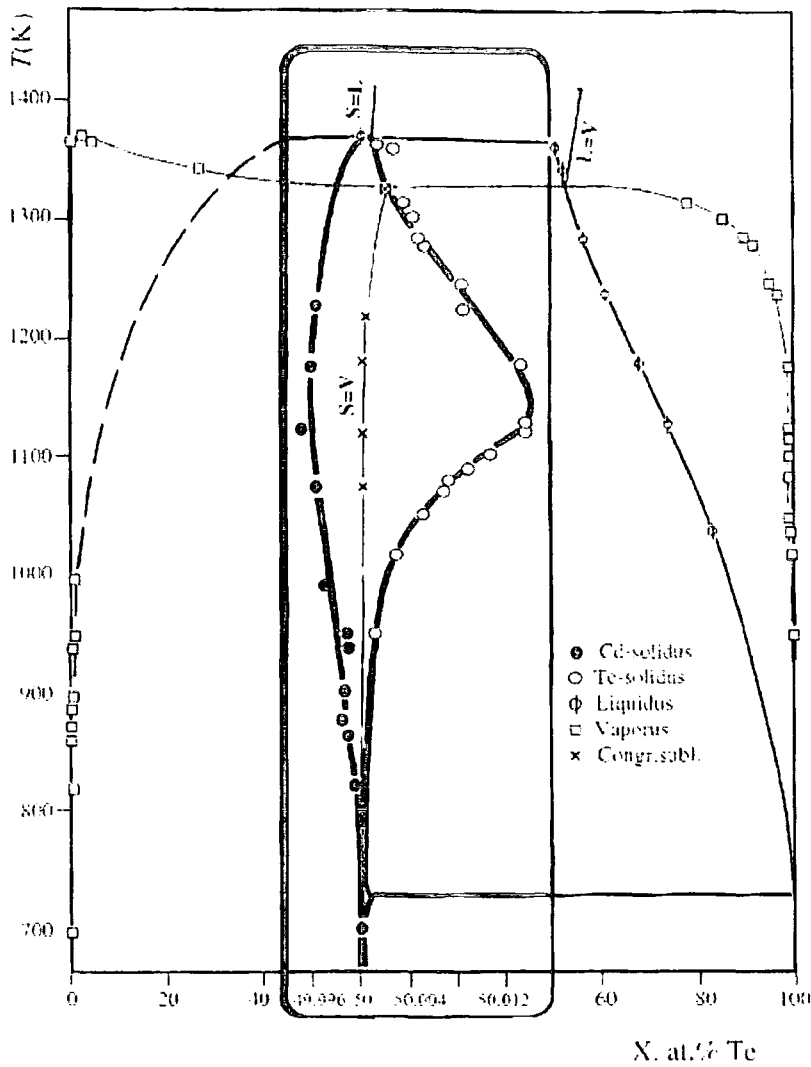
Figure 2.3: Range of homogeneity of CdTe as a function of temperature

2.2.2 Partial Pressures over ZnTe

ZnTe undergoes a similar dissociative reaction to that of CdTe (see equation 2.1) [2]

$$ZnTe_{(s)} \Leftrightarrow Zn_{(g)} + \frac{1}{2}Te_{2(g)} \qquad (2.11)$$

Brebrick [9, 18] again used optical absorption measurements to determine the equilibrium constant of the reaction

$$\ln\left(K_{ZnTe}\right) = 22.29 - \frac{37647}{T}$$ (2.12)

which translates to the partial pressure relationship

$$p_{Zn}[Pa] = \alpha^{\frac{1}{3}} \cdot 2.84 \times 10^{11} \cdot \exp\left(-\frac{25098}{T}\right)$$ (2.13)

A comparison with the equilibrium vapour pressure of Cd over CdTe in equation (2.10) is displayed graphically in Figure 2.4. It is apparent that at the same temperature the equilibrium partial pressure of Zn over ZnTe is about an order of magnitude lower than its Cd equivalent.
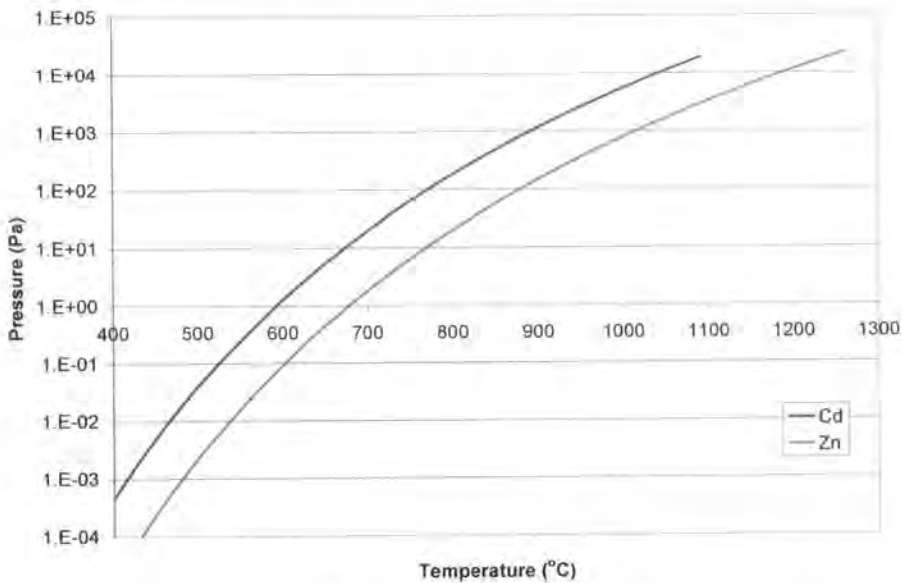
Figure 2.4: Comparison of equilibrium partial pressures of Cd and Zn over their binary telluride compounds.

The T-X diagram [17] of the ZnTe system (Figure 2.5) demonstrates a maximum stoichiometric melting temperature of 1300°C, with the Zn and Te eutectics melting at 419.5 and 449°C respectively. With the stoichiometric melting temperature over 200°C higher than that of CdTe, a higher source

temperature may be used to compensate for the lower Zn partial pressure, if equal partial pressures of Cd and Zn are required.
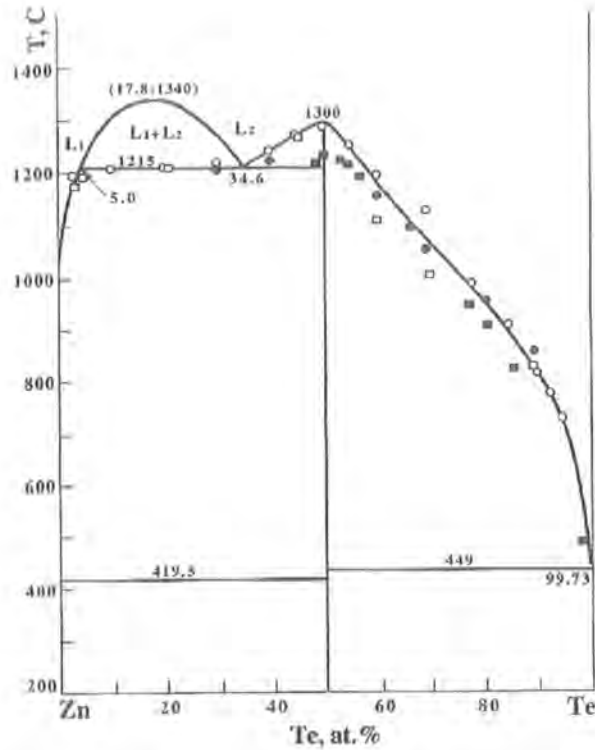
Figure 2.5: T-X projection of the ZnTe phase diagram

2.2.3 Cadmium Zinc Telluride Ternary Compound

The phase relationships of the CdZnTe depend upon the fraction of Zn in the compound, thus further complicating the phase diagrams, and only limited studies have been undertaken for fixed Zn fractions. Steininger *et al* [19] used differential thermal analysis (DTA) to study the solidus and liquidus points on a temperature – ZnTe content diagram (Figure 2.6). The liquidus is found to vary linearly with ZnTe content, but the solidus can not be extrapolated directly from the content [20]. The gap between the two is very small (about 60°C for 50% ZnTe) and no congruent composition was observed.
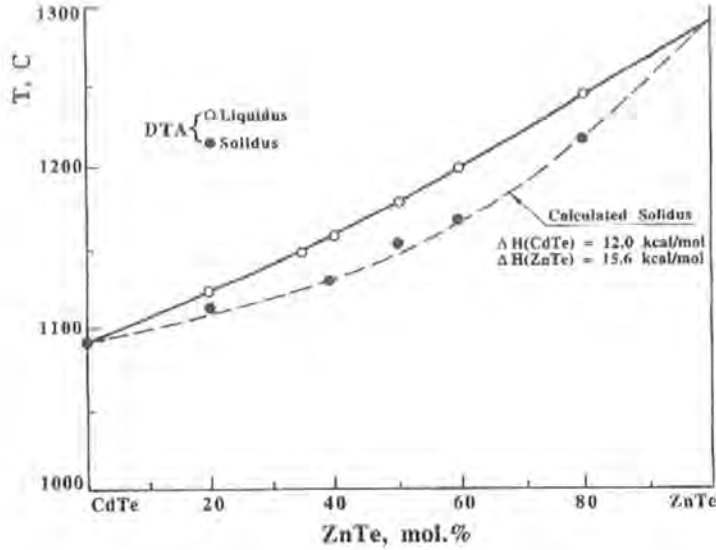
Figure 2.6: T-X projection of the CdTe-ZnTe system

Alikhanian *et al* [21] used thermodynamic calculations to determine the partial pressures in CdZnTe systems. They defined an activity a_{MeTe} of the species MeTe

$$a_{MeTe} = \frac{p_{MeTe}}{p^0_{MeTe}} \qquad\qquad Me = Cd, Zn \qquad (2.14)$$

where p_{MeTe} was the partial pressure of the MeTe species for the solid solution $Cd_{1-x}Zn_xTe$, and p^0_{MeTe} was the corresponding value for pure MeTe. Through the equilibrium constants

$$a_{MeTe} = \frac{p_{Me}\left(p_{Te_2}\right)^{\frac{1}{2}}}{p^0_{Me}\left(p^0_{Te_2}\right)^{\frac{1}{2}}} \qquad (2.15)$$

Assuming stoichiometry of the species, i.e.

$$p_{Zn} + p_{Cd} = 2p_{Te_2} \qquad (2.16)$$

the Te$_2$ partial pressures could be calculated via

$$a_{ZnTe}\, p^0_{Zn}\left(p^0_{Te_2}\right)^{\frac{1}{2}} + a_{CdTe}\, p^0_{Cd}\left(p^0_{Te_2}\right)^{\frac{1}{2}} = 2\left(p_{Te_2}\right)^{\frac{3}{2}} \qquad (2.17)$$

and subsequently, from equation (2.15), p_{Cd} and p_{Zn} could be derived. The author published a graph (Figure 2.7) of the activities of CdTe and ZnTe vs composition at 900 K.
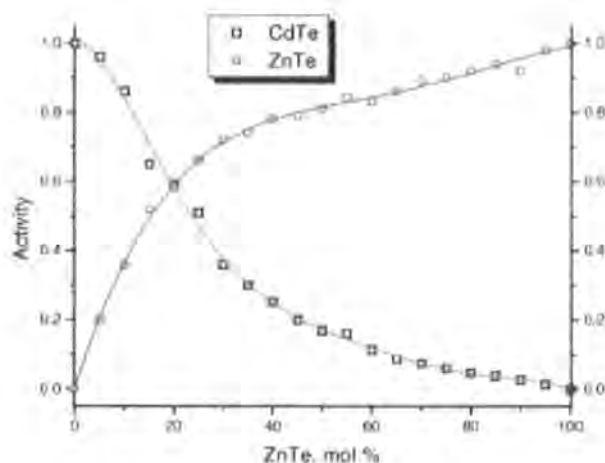
Figure 2.7: Activities of CdTe and ZnTe vs composition

Mass spectrometric studies by the authors also highlighted the problems of differential sublimation of the Cd and Zn species. For a $Cd_{0.9}Zn_{0.1}Te$ sample at 900 K the Cd was seen to sublime preferentially over Zn. The initial continuous decrease of the Cd^+ and Te_2^+ mass spectrometer ion currents (which were proportional to the partial pressures) and increase of the Zn^+ ion current corresponded to a progressive variation of the condensed phase composition towards ZnTe in Figure 2.8. The subsequent constant Zn^+ and Te_2^+ ion currents corresponded to the sublimation of pure ZnTe. These differential sublimation rates make it difficult to control the composition of the vapour during vapour growth from the ternary, leading to preference for the growth from the binaries CdTe and ZnTe.
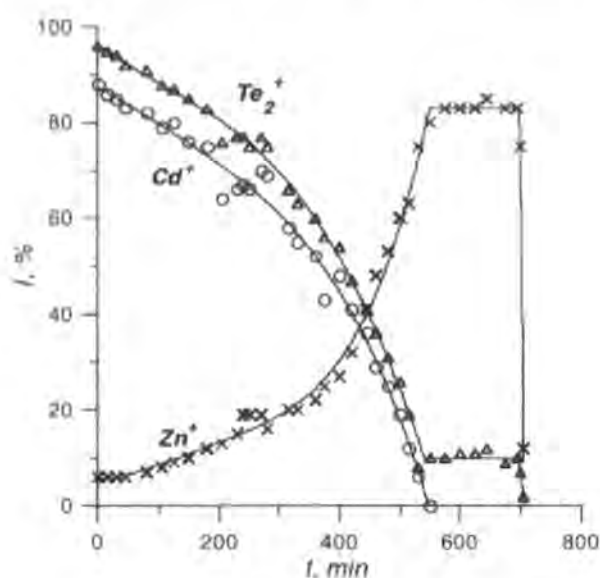
Figure 2.8: Isotherm of complete sublimation of the $Cd_{0.9}Zn_{0.1}Te$ ternary

2.3 MECHANICAL PROPERTIES

The low stacking fault energy and critical resolved sheer stress (CRSS) of the mechanically weak and brittle CdTe and CdZnTe require the minimisation of the stress and strain applied to the crystal during the growth process. Differences in the thermal expansion coefficient between crystal and quartz silica can lead to large thermal stresses applied to the crystal during the cooldown process after crystal growth, which in turn can lead to the propagation and multiplication of dislocations in the crystal.

The mechanical properties of CdTe and CdZnTe have been reviewed by Williams [22-25], while Schlesinger *et al* undertook a comprehensive review of CdZnTe [26]. The density of CdTe was reported as 5.854 ± 0.005 g cm^{-3}, with the density of ZnTe 5.636 g cm^{-3}, and the density of the ternary $Cd_{0.52}Zn_{0.48}Te$ between the densities of the two binaries at 5.811 g cm^{-3}. However, it was noted that non-stoichiometry in these types of material could lead to significant variations in the density.

The lattice parameter of CdTe was also noted to vary according to the stoichiometry, with Cd-rich melts providing material with a lattice parameter of 6.480 Å, compared to 6.488 Å for material from Te-rich melts [27], although other workers did not confirm these results [28]. With the lattice parameter of ZnTe of 6.1037 Å, that of the $Cd_{1-x}Zn_xTe$ system varied linearly with composition from CdTe to ZnTe, in accordance with Vegard's Law, and the measured lattice parameters of several zinc fractions are given in Figure 2.9:

Compound	Lattice Parameter (Å)
CdTe	*6.481*
$Cd_{0.95}Zn_{0.05}Te$	*6.465*
$Cd_{0.70}Zn_{0.30}Te$	*6.364*
$Cd_{0.50}Zn_{0.50}Te$	*6.287*
ZnTe	*6.104*

Figure 2.9: Room temperature lattice parameters of various $Cd_{1-x}Zn_xTe$ compounds

Williams also published an equation for the temperature dependence of the lattice parameter a_t of CdTe at $T\,°C$ between 20 and 420°C [29].

$$a_t = 6.4802 + (31.94 \times 10^{-6} T) + (7.55 \times 10^{-9} T^2) + (9.25 \times 10^{-12} T^3) \quad (2.18)$$

The linear expansion coefficient of CdTe, $\alpha_{CdTe}(T)$, is also given for the same range by Williams [29] as

$$\alpha_{CdTe}[°C^{-1}] = 4.932 \times 10^{-6} + (1.165 \times 10^{-9} T) + (1.1428 \times 10^{-12} T^2) \quad (2.19)$$

This agrees broadly with a constant value of 5.5×10^{-6} °C^{-1} between 25 and 800°C recommended by Hartmann *et al* [30], while Woods [31] gave an average value of 4.9×10^{-6} °C^{-1}. The average linear coefficient of expansion of silica over the similar range is 5.5×10^{-7} °C^{-1}, about one order of magnitude lower than CdTe [32]. Consequently, thermal stress can be induced in the crystal, as CdTe tends to adhere to the walls of the growth vessel due to the existence of oxides such as CdO and TeO$_2$, which are unavoidable due to outgassing from the silica [33]. A recent study [34] found sticking to the ampoule walls leads to higher dislocation densities ($\sim 10^5$ cm^{-2}) compared to growth free from the walls ($\sim 10^4$ cm^{-2}).

The CRSS of CdTe is about an order of magnitude lower than that of Si, Ge or III-V compounds at the melting point, leading to higher dislocation densities in CdTe than these other semiconductors [35]. A study by Balasubramanian and Wilcox [36] demonstrated the CRSS of CdTe ranges from 5 MPa at 300 K to about 0.2 MPa at 1353 K. The CRSS decreases sharply up to 400 K, and also above 800 K, with an almost constant region between 400 and 800 K. Williams [25], however, reports of work which translated microhardness data into CRSS values, which gave a substantially higher CRSS values for CdTe of 84MPa. The incorporation of Zn into the CdTe lattice is reported to substantially harden the material, with a calculated peak CRSS of Cd$_{0.96}$Zn$_{0.04}$Te at 159 MPa. The study predicts a strengthening effect of approximately 1.7 over most of the composition range, with the maximum at a Zn content around 75%. This study indicates the growth of CdZnTe under similar conditions should have a lower density of stress-related defects than CdTe. Kurilo *et al* [37] estimate an average value of Young's Modulus for CdTe of 4.52×10^{10} Pa.

2.4 THERMAL PROPERTIES

The thermal properties of Cd and Zn tellurides have been reviewed by Maleki and Holland [38]. The thermal conductivity of solid CdTe was observed to fall from 75 to 5.2 kW $m^{-1} K^{-1}$ between room temperature and 700 K. No data was given for high-temperature CdZnTe or ZnTe, although the room-temperature conductivity of ZnTe was calculated to be 116 kW $m^{-1} K^{-1}$. The thermal conductivity is important in vapour crystal growth since it governs the formation of temperature gradients within the growing crystal [39], and also the latent heat formed at the growth interface has to be removed to avoid superheating and the consequent morphological instabilities [40-42]. When the thermal conductivity of the crystal is lower than that of the ampoule the interface tends to be concave, and convex for the contrary. The convex condition is generally preferable because it reduces the risk of unwanted parasitic nucleation at the ampoule walls.

The emissivity of the growing crystal is another factor which affects the growth. The effect of the radiative heat exchange between the crystal and surrounding furnaces upon the mass transfer and surface kinetics has been extensively studied for the growth of mercury iodide crystals [43-46]. These studies illustrated that even in supersaturation conditions the growth process may be halted by the radiative heat transport. A study on the emissivity of CdTe crystals by Mullins *et al* [47] found the crystal behaved as a grey body not as a perfect black body. The emissivity of CdTe in the temperature range 827-1104 K, which is relevant to the MTPVT growth system, was obtained between 600 and 1800 nm. This study demonstrated the influence of surface

conditions on emissivity, and suggested its use as a measure of the surface quality and stoichiometry during growth.

2.5 VAPOUR GROWTH

Vapour growth techniques have been used to grow a range of materials, with many different techniques used to grow CdTe and CdZnTe. Several extensive reviews are available in the literature [26, 48-50], and this section will provide a short review of the development of the important techniques.

2.5.1 Advantages and Disadvantages of Vapour Growth

Modified Bridgman techniques and gradient freezing methods are used to produce all of the CdTe and CdZnTe currently commercially available, with possibly one exception [51]. In both methods large (up to 100 mm diameter) multi-grain boules are grown from the melt, and single crystals are cut out of the larger boules. The low thermal conductivity, stacking fault energy and critical resolved sheer stress of CdTe make it difficult to grow large-diameter single crystals with low dislocation density, according to Asahi *et al* [52, 53], while Rudolph *et al* [54] state that unless the pressures over the melt are controlled the melt is always Te-rich, since the nearly stoichiometric melt sublimes incongruently. Rudolph *et al* also indicate the further complication caused by the liquidus shape, and there is a high degree of association in the melt.

Considering these factors, vapour growth has a number of *a priori* advantages over melt growth.

      i.   The relatively high vapour pressure of II-VI compounds allow these crystals to be grown from the vapour at temperatures

below their congruent melting point (1092°C). This tends to reduced problems with precipitation and inclusions [49].

ii.   The lower growth temperature also reduces thermal stress applied to the crystal.

iii. Contamination from the crucible is also reduced by the lower growth temperature.

iv.   Non-volatile impurities present in the source are not transported to the growing crystal.

Despite these inherent advantages vapour growth has been held back by considerable technical difficulties. Vapour growth has suffered from the widely held perception that growth rates are necessarily low and reproducibility is poor [50], and has generally only been used for research and academic purposes. The main problems associated with vapour growth are the difficulties in controlling the seeding and stoichiometry of the source and vapour, which in turn result in low growth rates, complex transport mechanisms and irreproducibility of results. However, the traditional sublimation methods employed are cited by Rosenberger *et al* [32] as the main reason for the failure to consistently obtain high-quality single crystals.

Vapour growth methods may be divided into several categories, depending upon the nature of the source – whether the source is a solid which must be sublimed or a vapour itself – and the transport mechanism, which may be purely physical (physical vapour transport PVT) or carried by some chemical agent (chemical vapour transport CVT). This section will only deal with the PVT method of growth, which can itself be divided into closed-tube

techniques and semi-open methods, with seeded and unseeded versions of both.

2.5.2 Closed-Tube Physical Vapour Transport Techniques

Closed-tube PVT methods are all derivatives of the technique devised by Czyzak *et al* [55] for the unseeded growth of CdS, in which a source was sublimed at one end of a sealed ampoule and transported to a sink at a lower temperature at the other end of the tube. This process was simple to produce and operate, but was virtually impossible to control, with the process of sealing the ampoule itself introducing residual gases which altered the transport properties. The technique, which was improved by Greene *et al* [56] and established by Piper and Polich [57], enabled the growth of bulk crystals up to a few cm^3 to be grown in horizontal furnaces containing a parabolic temperature gradient. An inert carrier gas could be used to alter the transport process through the design of the source end of the growth tube, which was not tightly sealed in the initial state, but was gradually sealed by the condensing vapours during preheating.

Hoschl and Konák [58] modified the Piper-Polich technique through the use of molten cadmium to control the partial pressure and sublimation rate, growing crystals of 5 x 5 x 15 mm^3, while Itagi *et al* [59] demonstrated the dependence of the growth rate on the partial pressure of the controlling constituent element. Mochizuki [60, 61] studied the effects of supersaturation and deviation of source stoichiometry, and concluded that the history of the source determined the growth rate.
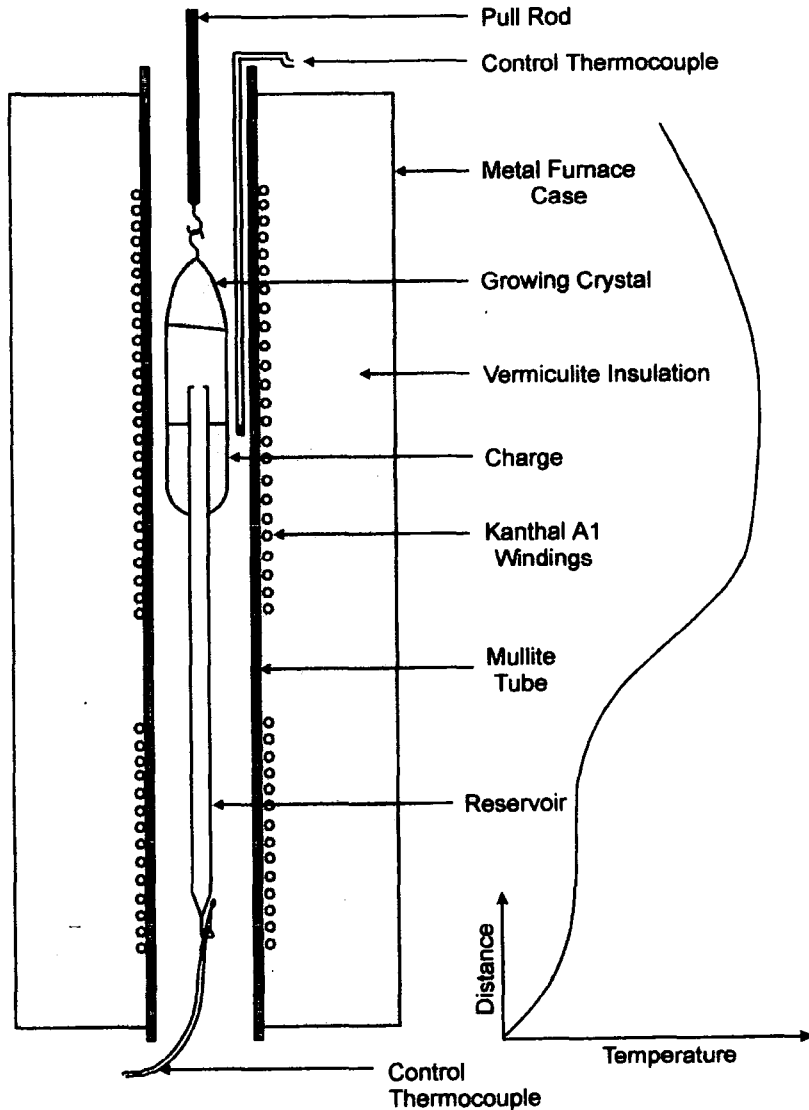
Figure 2.10: Durham Method of Closed Tube Growth

The Durham group, including Clark and Woods, adapted the technology to develop the "Durham method" (see Figure 2.10) which was used to grow a range of II-VI compounds, including CdTe and CdZnTe [62-66]. The technique was a vertical unseeded growth procedure, where material from the source (such as the CdTe binary or CdZnTe ternary) was transported from bottom to top in an evacuated source ampoule at growth temperatures between 950 and 1060°C. A separate reservoir containing one of the species,

heated to between 600 and 700°C, was connected to the main ampoule via a small orifice and allowed the independent control of the constituent partial pressures. The Durham method was used to routinely grow boules of up to 29 mm in diameter and ~ 70 mm in length and consisting of a small number of large grains [67, 68]. However, the boules were always twinned and always charcterised by high densities of dislocations and precipitates, which resulted from the long growth times allowing the defects to reach a state of equilibrium [69].

Faktor and Garret [3, 70-72] highlighted the difficulties of growth in closed ampoules by dissociative sublimation, through a theoretical description of the growth. Using the dissociation of CdTe as an example, a closed system can be modelled considering a simple setup (see Figure 2.11) with the growing crystal at position $x = 0$, at temperature $T(0)$, and the source of CdTe at position $x = l$ at temperature $T(l)$.
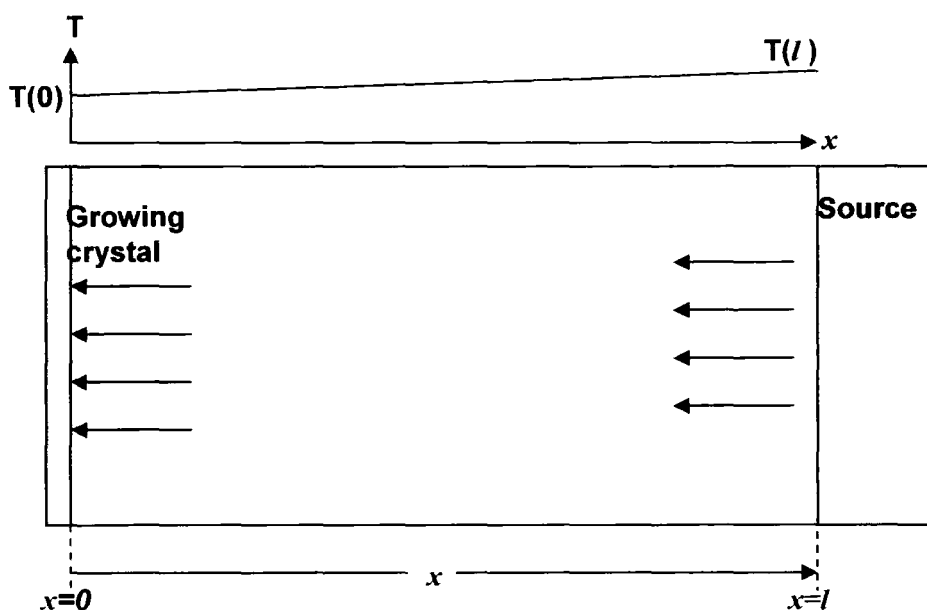
Figure 2.11: Closed Tube Transport Schematic

As a first approximation, the temperature difference along x is considered small compared to $T(l)$, and the temperature may be approximated to $T=T(l)$. The flux (J) of each component is the sum of the flow velocity U which acts on the gas as a whole, and a diffusion term (D) proportional to the concentration gradient of the particular component.

$$J_{Cd} = \frac{U}{RT} p_{Cd} - \frac{D}{RT} \frac{dp_{Cd}}{dx} \qquad (2.20)$$

$$J_{Te_2} = \frac{U}{RT} p_{Te_2} - \frac{D}{RT} \frac{dp_{Te_2}}{dx} \qquad (2.21)$$

Substituting for the diffusion terms

$$J_{Cd} + J_{Te_2} = \frac{UP}{RT} = \frac{3}{2} J \qquad (2.22)$$

Since the net flux of the component must be in the same ratio as to give equal fluxes of the Cd and Te atoms

$$J_{Cd} = 2J_{Te_2} \equiv J \qquad (2.23)$$

where J is the growth rate of CdTe, and P is the total pressure from

$$P = p_{Cd} + p_{Te_2} \qquad (2.24)$$

Equations (2.20) and (2.21) can be rewritten, eliminating U, as

$$J_{Cd} = \frac{\frac{3}{2} J}{P} p_{Cd} - \frac{D}{RT} \frac{dp_{Cd}}{dx} \qquad (2.25)$$

$$J_{Te_2} = \frac{\frac{3}{2} J}{P} p_{Te_2} - \frac{D}{RT} \frac{dp_{Te_2}}{dx} \qquad (2.26)$$

The flux equations can be integrated from $x = 0$ to $x = l$, and this is simplified if the variations of P are very small with respect to x.

$$p_{Cd}(x) - \frac{2}{3} P = \left[p_{Cd}(l) - \frac{2}{3} P \right] \exp\left\{ \frac{3JRT}{2DP}(x-l) \right\} \qquad (2.27)$$

$$p_{Te_2}(x) - \frac{1}{3}P = \left[p_{Te_2}(l) - \frac{1}{3}P \right] \exp\left\{ \frac{3JRT}{2DP}(x-l) \right\} \qquad (2.28)$$

The quantities (p_{Cd}- 2P/3) and (p_{Te2} – P/3) show simple exponential variations dependent upon the growth rate. If the vapour was stoichiometric over the CdTe solid, the ratio $\alpha = p_{Cd}/p_{Te2}$ would be 2, and there would be

$$p_{Cd} = \frac{2}{3}P \qquad \text{and} \qquad p_{Te_2} = \frac{1}{3}P \qquad (2.29)$$

Therefore the quantities which occur in Equations (2.27) and (2.28) are the departures from stoichiometry in the vapour. If the vapour over the source is not stoichiometric, then the non-stoichiometry will increase exponentially as the distance from the source increases. As described earlier, in general the vapour at the source will not be stoichiometric, causing higher non-stoichiometry at the seed. The seed will remove Cd atoms and Te_2 from the vapour in the stoichiometric ratio 2:1, but the vapour flow brings vapour from the source in the ratio α. If $\alpha \neq 2$, the vapour next to the seed becomes depleted in one component, while the excess of the other accumulates. For example, if the vapour is tellurium rich $\alpha < 2$, the tellurium accumulates and the vapour becomes depleted in cadmium.

The change in the vapour composition developing at the seed produces diffusion currents which carry the excess component away, and bring up more of the minority component. The flow of vapour and the diffusion currents of the component species combine to give net fluxes of Cd and Te_2 in the ratio 2 at steady state, in spite of the non-stoichiometry of the vapour.

The growth rate J of the solid can be expressed in terms of the vapour compositions over the source and seed by rearranging (2.27) and (2.28):

$$J = \frac{2DP}{3RTl}\ln\left(\frac{p_{Cd}(l) - \frac{2}{3}P}{p_{Cd}(0) - \frac{2}{3}P}\right) = \frac{2DP}{3RTl}\ln\left(\frac{p_{Te_2}(l) - \frac{1}{3}P}{p_{Te_2}(0) - \frac{1}{3}P}\right) \qquad (2.30)$$

Therefore the growth rate can be calculated, if the values of $p_{Cd}(l)$ and $p_{Cd}(0)$ are known. If it is assumed the vapour over the source and seed is in equilibrium with the solid, then the equilibrium condition at $x = 0$ and $x = l$ is

$$K_P(x) = p_{Cd}(x)\left[p_{Te_2}(x)\right]^{\frac{1}{2}} = \frac{(p_{Cd}(x))^{\frac{3}{2}}}{(\alpha(x))^{\frac{1}{2}}} \qquad (2.31)$$

where $K_p(x)$ is the value of the equilibrium constant at temperature $T(x)$.

Faktor and Garrett used these equations to calculate numerically the growth rate of the II-VI compound CdS, which dissociates in the same manner as CdTe, and demonstrated the dramatic effect of $\alpha(l)$ on the growth rate. Figures 2.12 and 2.13 display the variations in growth rate with the temperature difference between the source and seed for cadmium- and sulphur-rich vapours respectively.

A variation in the values of $\alpha(l)$ from 2.01 to 1000 leads to a decrease of three orders of magnitude for the growth rate, with a similar decrease seen in the S-rich variations from 1.99 to 0.001. From equation (2.31) a cadmium partial pressure of 0.0009 atm would be required to give a value of 1000 for $\alpha(l)$. Faktor and Garret convert this to a Cd excess of only 10 p.p.m. in 30 g of source material with a growth capsule volume of 30 cm^3, and claim alternatively 10 monolayers of oxide over 100 cm^2 of surface material would tie up enough sulphur in the vapour through the production of SO_2 to produce this excess of Cd.
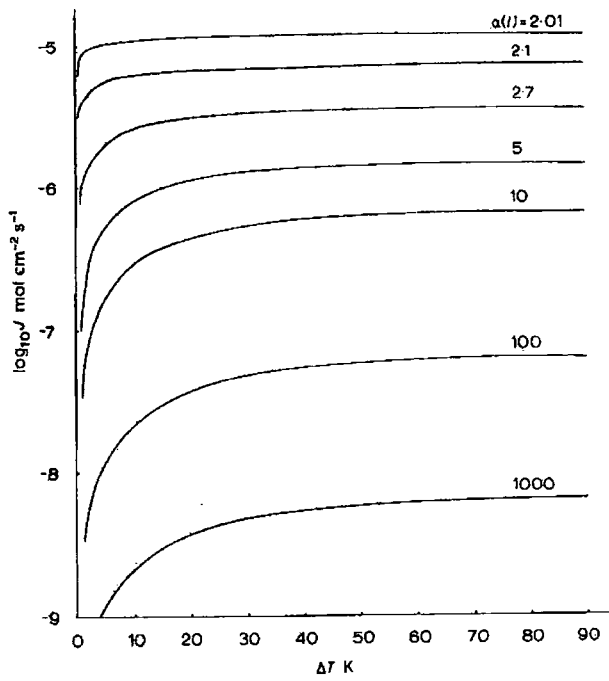
Figure 2.12: **Transport rate as a function of temperature difference between the source and seed of CdS with a Cd-rich vapour (from [3])**
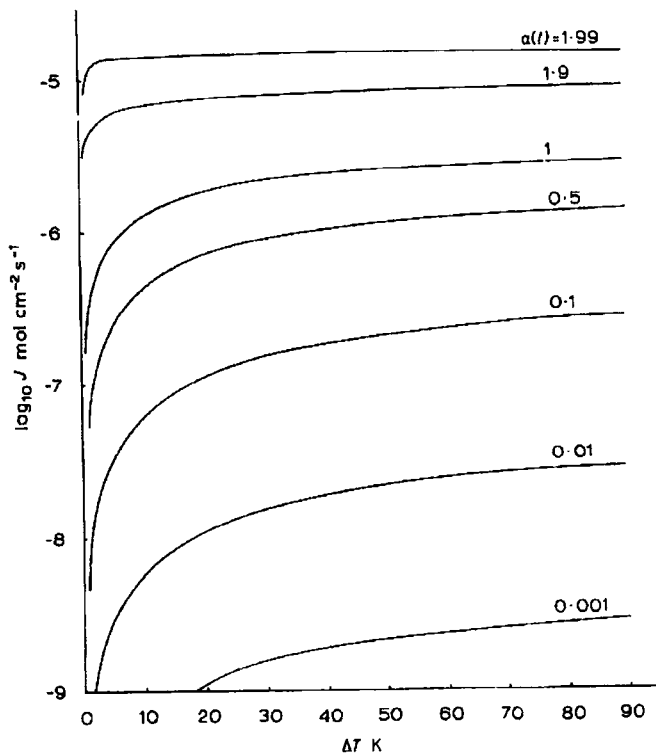
Figure 2.13: **Transport rate as a function of temperature difference between the source and seed of CdS with an S-rich vapour (from [3])**

32

Rosenberger *et al* [48, 73] also highlighted the limitations of closed-tube growth of dissociative compounds through the build up of diffusion barriers, but several workers have continued to use closed-tube methods. A vertical unseeded vapour growth (VUVG) method was used by Yellin *et al* [74-76] to study the effects of the source stoichiometry. They introduced a long quartz tube, which extended outside the furnace, attached to the top of the capsule to provide a heat pipe to create a cooler area for nucleation.

The Sublimation Travelling Heater Method (STHM) was developed from the melt-growth THM by Triboulet *et al* [77]. The Te-rich molten zone in the conventional THM was replaced by an empty space or vapour zone, with the stoichiometry controlled by the connection of a capillary to the sublimation chamber, one end of which was at room temperature. The large multigrained crystals obtained via STHM tended to have fewer Te precipitates than the THM material, but were found to be less pure. Undoped and halogen-doped crystals were grown from the STHM, but the crystal quality was not further improved.

2.5.3 Semi-Open Physical Vapour Transport

Piper and Polich [57] recognised the need to remove initial gaseous components from outgassing, surface contamination and source oxidation during their growth of CdS and ZnS. They used an ampoule which was partially open at the crystal end and allowed to self-seal during growth, and the system effectively became a closed tube. Faktor *et al* [3] understood that if a leak or effusion hole were maintained throughout growth it would continue to be effective in removing impurities and excess components with only a small loss of source material. They drilled 0.2 mm effusion holes though the

capsule wall near the source, allowing a link to a surrounding vacuum jacket or alternatively to a controlled pressure of an inert gas.

Rosenberger *et al* [78, 79] further developed the technology for the seeded growth of KCl and KBr, and obtained growth rates up to three orders of magnitude higher than in closed ampoules. The growth ampoule (see Figure 2.14) comprised of three separate components: a cooled tip, the main body with the seed receptacle and the source material chamber, which all fitted together with ground glass joints and were surrounded by a vacuum jacket. Two 0.3 mm effusion holes were drilled near the seed, and the cooled tip resulted in a radial temperature distribution to suppress the radial growth of the seed and ensure growth free of the container walls. The crystals grown were found to have dislocation densities three orders of magnitude lower than melt-growth equivalents.

Kuwamoto [80] added a heat pipe to cool the seed pedestal to grow quite large (~18 cm^3) crystals of CdTe, and found the existence of thin voids parallel to the growth direction, which he attributed to high growth rates. It was found an overpressure of ~100 torr of argon was required to prevent the sublimation and subsequent re-crystallisation of the seed during the heating process, and growth only started once the argon had been rapidly removed.
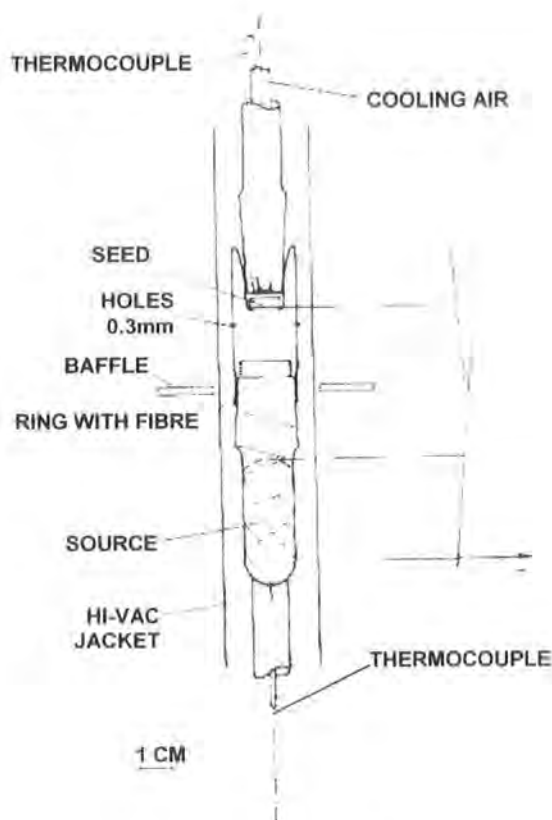
Figure 2.14: Ampoule arrangement used by Rosenberger [78]

Along with the development of effusion holes, these semi-open growth techniques highlighted the need to ensure the growth took place free from the crystal walls. Markov and Davydov [81, 82] (growing CdS) pioneered the use of an annulus around a seed-supporting sapphire rod which allowed both removal of excess components and growth free from the walls. A cold trap beneath the seed proved an effective sink for volatile impurities, and a relationship between the necessary length of rod and the vapour pressure at the source and seed was obtained. The length of rod appeared to be crucial to obtain wall-free growth. Golacki et al [83] used the Markov method to grow CdTe boules 8 mm in diameter and up to 15 mm in length. They also report

[84] the contactless growth of uniform $Cd_{0.8}Zn_{0.2}Te$ monocrystals of about 12 mm in size using a self-selecting vapour growth technique.

A horizontal semi-open growth technique was used by Lauk *et al* [85, 86], to produce twin-free seeded and unseeded CdTe crystals, and they compared the results with a model of the purification during the growth. They found impurities with a segregation coefficient less than unity were not transferred into the growing crystal, while those with a coefficient greater than 1 accumulated in the crystal and no purification took place.

The seeded growth of p-type CdTe crystals under an argon atmosphere in a horizontal arrangement were used by Boone *et al* [87]. The crystals, which were up to 100 cm^3 in volume with 5 cm diameter, contained etch pit densities in the range $3 - 7 \times 10^4$ cm^{-2}. No visual or X-ray detectable twins or grain boundaries were found, although the outer parts of the crystal were much poorer since they were in contact with the ampoule walls. It was found empirically that crystals of greater length than radius could not be grown due to parasitic nucleation at the walls, which was believed to be due to the difficulty in removing heat away from the centre of the growing crystal.

Grasza *et al* [88-91] exploited the behaviour of compacted source material in an axial temperature profile to nucleate seed crystals *in situ*. Increasing radial gradients and steeper isotherms were introduced to produce a single crystal, which stuck to the surface of a silica rod, but not the ampoule wall, as in Figure 2.15. Once the seed was formed, the temperature profile was manipulated to separate the seed and the source and initiated a conventional vapour growth. The growth directions of the single crystals were close to

<100>, and the crystals were twinned in 30-80% of the volume. The high-quality crystals had etch pit densities (EPDs) as low as 2×10^3 cm^{-2}, but successful seeding relied on the skill of the crystal grower, returning the growth to the status of a "black art".
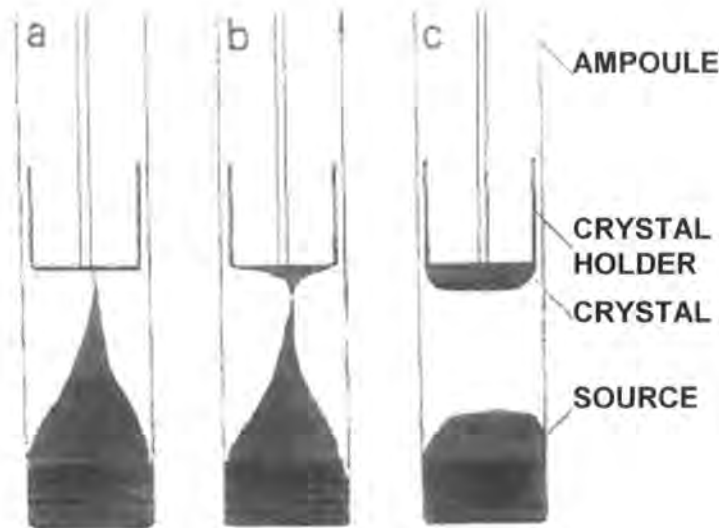
Figure 2.15: Three stages of *in situ* nucleation in the technique of Grasza *et al*

Modified Markov methods (also called free growth methods) appear to be the most promising route for CdTe and II-VI solid solutions bulk vapour growth. Large-diameter crystals, up to 100 mm^3 in volume, were regularly grown through one of these methods by the ELMA Research and Development Association of Moscow [92]. Their seed was mounted on an optically heated sapphire rod heat pipe in a continuously pumped chamber, which could be back-filled with He to control growth rates. One crystal was found to contain no large angle twin boundaries and only one small twin lamella. The crystals

however were always short, ~ 1 cm, and it appeared heat transfer prevented further growth.

The modified Markov method has been used by Laasch *et al* [93, 94] to produce twin-free seeded and unseeded single CdTe crystals. A comparison of the strain of crystals grown with and without wall contact showed no evidence of stress without wall contact. The authors demonstrated that the stoichiometry of the source did not influence the vapour composition at the growing surface if the sink remained at room temperature.

Trower [95] recognised the problems associated with the differences in vapour pressures over CdZnTe, with the consequent inhomogeneous growth. In a vapour phase growth ampoule Trower attempted to control the partial pressures by spatially separating the CdTe and ZnTe using calibrated channels and orifices. Polycrystals of up to 50 mm diameter and 25 mm height with Zn content from 4 to 40% were grown with encouraging preliminary results.

Rosenberger *et al* [32] conducted an extensive study on bulk vapour growth and drew on the conclusions to develop the effusive ampoule physical vapour transport (EAPVT) technique based on the Markov method. The system permitted either seeded or unseeded growth free from the walls with continuous removal of the excess component and impurities, along with a cadmium or tellurium reservoir. The innovative use of a capillary between the source and the seed allowed control of the mass transport rate, and, although unseeded growth was unsuccessful, the seeded growth of ~20 cm^3 crystals produced very low (~2x10^3 cm^{-2}) EPD.

2.6 CONCLUSIONS

A brief review of the relevant properties of CdTe, ZnTe and CdZnTe has been presented, along with the outline of several other vapour growth methods. Several important conclusions can be drawn from the review, which affect the choice of growth method and conditions. The review of the properties of the material suggests:

- Low temperatures are required to avoid, in particular, tellurium inclusions caused by the narrow range of homogeneity of CdTe.

- Temperature fluctuations across the crystal should also be minimised, as the low stacking fault energies of CdTe and CdZnTe encourage defects.

- The crystal should be grown free from the ampoule wall. The differential thermal expansion coefficients of the growing crystal and the silica ampoules promote dislocation formation in the crystal, due to the crystal's low critical resolved sheer stress.

- Radial temperature gradients should be minimised and radiative heat transfer encouraged since the low thermal conductivity of the compounds can influence the morphological stability.

The experience of other growth techniques provides other guidelines for growth:

- Closed-tube growth methods have intrinsic problems with the control of growth. Impurities introduced in the sealing of the ampoule, outgassing from the glassware and non-stoichiometries in the source make the sensitive partial pressure ratios, which control the growth rates, too variable and hence the growth uncontrollable.

- The use of reservoirs of one of the constituent elements allows a measure of control of the partial pressures, but without complete control of mass transport.

- Self-sealing ampoules allow the removal of some impurities from the sealing and outgassing of the glassware, but do not allow for non-stoichiometries in the vapour.

- Permanently semi-open ampoules allow the continuous removal of volatile impurities, outgassing products and excess components, preventing the build up of diffusion barriers and ensuring high growth rates.

- The Markov technique allows both removal of gaseous components and growth free of the ampoule walls.

- Self-seeding methods can produce the single-grain crystals required for good growth, but require considerable skill on behalf of the crystal grower.

- A capillary placed between the source and growing crystal can allow greater control of the mass transport rate.

2.7 REFERENCES FOR CHAPTER 2

[1]   B. De-Largy, A. Finch and P. J. Gardner. *"Thermodynamic Functions for the Congruent Sublimation of Cadmiun-Telluride"*. Journal of Crystal Growth **61** (1983) 194.

[2]   P. Goldfinger and M. Jeunehomme. *"Mass Spectroscopic and Knudsen-Cell Vaporization Studies of Group 2b-6b Compounds"*. Trans. Faraday Soc. **59** (1963) 2851.

[3]   M. M. Faktor and I. Garrett. *"Growth of Crystals from the Vapour"*. Chapman and Hall London (1974).

[4]   R. F. Brebrick and A. J. Strauss. *"Partial Pressures and Gibbs Free Energy of Formation for Congruently Subliming CdTe$_{(C)}$"*. J Phys Chem Solids **25** (1964) 1441.

[5]   D. De Nobel. *"Phase Equilibria and Semiconducting Properties of Cadmium Telluride"*. Philips Res. Repts **14** (1959) 361.

[6]   J. H. Greenberg, V. N. Guskov, V. B. Lazarev and O. V. Shebershneva. *"Vapor Pressure Scanning of Non-Stoichiometry in Cadmium Telluride"*. Materials Research Bulletin **27** (1992) 847.

[7]   J. H. Greenberg, V. N. Guskov, V. B. Lazarev and O. V. Shebershneva. *"Vapor Pressure Scanning of Nonstoichiometry in CdTe"*. Journal of Solid State Chemistry **102** (1993) 382.

[8]   J. H. Greenberg, V. N. Guskov and V. B. Lazarev. *"P-T-X Phase Diagram Cadmium-Telluride"*. Materials Research Bulletin **27** (1992) 997.

[9]   R. F. Brebrick. *"Partial Pressures in the Cd-Te and Zn-Te Systems"*. Journal of Electrochemical Society: Solid State Science **118** (1971) 2014.

[10]   J. Carles Alabert. *"Optical Vapour Pressure Monitoring and Mass Transport Control During Bulk CdTe Crystal Growth in a Novel Multi-Tube PVT System"*. PhD Thesis. University of Durham. (1998).

[11]   R. Fang and R. F. Brebrick. *"CdTe I: Solidus Curve and Composition-Temperature-Tellurium Partial Pressure Data for Te-Rich CdTe$_{(S)}$ from Optical Density Measurements"*. Journal of Physics and Chemistry of Solids **57** (1996) 443.

[12]   C.-H. Su, Y.-G. Sha, S. L. Lehoczky, H.-C. Lui, R. Fang and R. F. Brebrick. *"Vapor-Phase Stoichiometry and Heat Treatment of CdTe Starting Material for Physical Vapor Transport"*. Journal of Crystal Growth **183** (1998) 519.

[13]   W. Palosz and H. Weidemeier. *"Physical Vapour Transport of Cadmium Telluride in Closed Ampoules"*. Journal of Crystal Growth **129** (1993) 653.

[14]   J. H. Greenberg. *"Vapor Pressure Scanning Implications of CdTe Crystal Growth"*. Journal of Crystal Growth **197** (1999) 406.

[15]   M. Hage-Ali and P. Siffert. *"Growth Methods of CdTe Nuclear Detector Materials"*. in *"Semiconductors for Room Temperature Nuclear Detectors"*. Edited by T. E. Schlesinger and R. B. James 43 Academic Press San Diego. (1995).

[16]   J. H. Greenberg. *"P-T-X Phase Equilibrium and Vapor Pressure Scanning of Non-Stoichiometry in CdTe"*. Journal of Crystal Growth **161** (1996) 1.

[17]   J. H. Greenberg. *"Thermodynamic Basis of Crystal Growth"*. Springer Berlin (2002).

[18]   R. F. Brebrick. *"Partial Pressures of Zn and Te₂ over ZnTe up to 917°C".* J Electrochem. Soc. **116** (1969) 1274.

[19]   J. Steininger, A. J. Strauss and R. F. Brebrick. J. Electrochem. Soc. **117** (1970) 1305.

[20]   T. C. Yu and R. F. Brebrick. *"Phase Diagrams of Cd/Zn/Te/Se Compounds".* in *"Properties of Narrow Gap Cadmium-Based Compounds".* Edited by P. Capper 1 INSPEC London. (1994).

[21]   A. S. Alikhanian, V. N. Guskov, A. M. Natarovsky, J. H. Greenberg, M. Fiederle and K. W. Benz. *"Mass Spectrometric Study of the CdTe-ZnTe System".* Journal of Crystal Growth **240** (2002) 73.

[22]   D. J. Williams. *"Densities and Lattice Parameters of CdTe, CdZnTe and CdTeSe".* in *"Properties of Narrow Gap Cadmium-Based Compounds".* Edited by P. Capper 1 INSPEC London. (1994).

[23]   D. J. Williams. *"Thermal Expansion Coefficients of CdTe".* in *"Properties of Narrow Gap Cadmium-Based Compounds".* Edited by P. Capper 1 INSPEC London. (1994).

[24]   D. J. Williams. *"Mechanical Properties of CdTe and CdZnTe".* in *"Properties of Narrow Gap Cadmium-Based Compounds".* Edited by P. Capper 1 INSPEC London. (1994).

[25]   D. J. Williams. *"Yield Stress and Hardness of CdTe and CdZnTe".* in *"Properties of Narrow Gap Cadmium-Based Compounds".* Edited by P. Capper 1 INSPEC London. (1994).

[26]   T. E. Schlesinger, J. E. Toney, H. Yoon, E. Y. Lee, B. A. Brunett, L. Franks and R. B. James. *"Cadmium Zinc Telluride and Its Use as a Nuclear Radiation Detector Material".* Materials Science and Engineering **32** (2001) 103.

[27]   S. A. Medvedev, Y. V. Kluevkov, K. V. Kiseleva and N. N. Sentyurina. Inorg. Mater. **8** (1972) 1064.

[28]   A. Vaipolin and Y. V. Rud. Inorg. Mater. **10** (1974) 470.

[29]   M. G. Williams, R. D. Tomlinson and M. J. Hampshire. *"X-Ray Determication of the Lattice Parameters and Thermal Expansion of Cadmium Telluride in the Temperature Range 20-420°c".* Solid State Communications **7** (1969) 1831.

[30]   H. Hartmann, R. Mach and B. Selle. *"Wide Gap Ii-Vi Compounds as Electronic Materials".* in *"Current Topics in Materials Science".* Edited by E. Kaldis 9 North-Holland Amsterdam. (1982).

[31]   J. Woods. *"Group Ii-Vi Semiconductors".* in *"The Chemistry of the Semiconductor Industry".* Edited by S. J. Moss and A. Ledwith Blackie & Son Glasgow. (1987).

[32]   F. Rosenberger, M. Banish and M. B. Duval *"Vapour Crystal Growth Technology Development - Application to Cadmium Telluride"* (1991).

[33]   R. K. Bagai, R. D. S. Yadava, B. S. Sundersheshu, G. L. Seth, M. Anandan and W. N. Borle. *"A Study on Contaminations During Bulk Growth of CdTe Crystals".* Journal of Crystal Growth **139** (1994) 259.

[34]   W. Palosz, K. Grasza, K. Durose, D. P. Halliday, N. M. Boyall, M. Dudley, B. Raghothamachar and L. Cai. *"The Effects of the Wall Contact and Post-Growth Cool-Down on Defects in CdTe Crystals Grown by 'Contactless' Physical Vapour Transport".* Journal of Crystal Growth **254** (2003) 316.

[35]   R. N. Thomas, H. M. Hobgood, P. S. Ravishankar and T. T. Braggins. *"Meeting Device Needs through Melt Growth of Large-Diameter Elemental and Compound Semiconductors".* Journal of Crystal Growth **99** (1990) 643.

[36]   R. Balasubramanian and W. R. Wilcox. *"Mechanical Properties of CdTe"*. Mat. Sci. Eng. **B16** (1993) 1.

[37]   I. V. Kurilo, V. P. Alekhin, I. O. Rudyi, S. I. Bulychev and L. I. Osypyshin. *"Mechanical Properties of ZnTe, CdTe, CdHgTe and HgTe Crystals from Microchemical Investigation"*. Phys. Stat. Sol (a) **163** (1997) 47.

[38]   H. Maleki and L. R. Holland. *"Thermal Properties of Cd/Zn/Te/Se Compounds"*. in *"Properties of Narrow Gap Cadmium-Based Compounds"*. Edited by P. Capper 1 INSPEC London. (1994).

[39]   M. Isshiki. *"Bulk Growth of Widegap II-VI Single Crystals"*. in *"Compounds for Opto-Electronic Applications"*. Edited by H. E. Ruda 1 Chapman & Hall London. (1992).

[40]   J. Nelson. *"Heat Conduction Problems in Crystal Growth from the Vapour"*. Journal of Crystal Growth **132** (1993) 538.

[41]   F. Rosenberger. *"Fundamentals of Crystal Growth I: Macroscopic Equilibrium and Transport Concepts"*. Springer Berlin (1979).

[42]   A. A. Chernov. *"Notes on Interface Growth Kinetics 50 Years after Burton, Cabera and Frank"*. Journal of Crystal Growth **264** (2004) 499.

[43]   M. Piechotka. *"Mechanism of Vapour Growth and Defect Formation in Large Mercury Iodide Crystals"*. Journal of Crystal Growth **146** (1995) 1.

[44]   E. Kaldis and M. Piechotka. *"Bulk Crystal Growth by Physical Vapour Transport"*. in *"Handbook of Crystal Growth, Vol 2"*. Edited by D. T. J. Hurle 2 Elsevier Amsterdam. (1994).

[45]   A. A. Chernov, E. Kaldis, M. Piechotka and M. Zha. *"Conductive and Radiative Heat Transfer, Diffusion and Interface Kinetics in Spherically Symmetric Vapour Growth; Application to HgI_2"*. Journal of Crystal Growth **125** (1992) 627.

[46]   A. Roux, A. Fedoseyev and B. Roux. *"Thermal Radiation and Low Temperature Vapour Growth of HgI_2 Crystal in Production Furnace"*. Journal of Crystal Growth **130** (1993) 523.

[47]   J. T. Mullins, J. Carles and A. W. Brinkman. *"High Temperature Optical Properties of Cadmium Telluride"*. Journal of Applied Physics **81** (1997) 6374.

[48]   F. Rosenberger, J. Ouazzani, I. Viohl and N. Buchan. *"Physical Vapour Transport Revisited"*. Journal of Crystal Growth **171** (1997) 270.

[49]   A. W. Brinkman and P. Capper. *"Growth of CdTe, CdZnTe and CdTeSe by Bulk Methods"*. in *"Properties of Narrow Gap Cadmium-Based Compounds"*. Edited by P. Capper 10 Institute of Electrical Engineers London. (1994).

[50]   A. W. Brinkman and J. Carles. *"The Growth of Crystals from the Vapour"*. Progress in Crystal Growth and Characterization of Materials **37** (1998) 169.

[51]   Research-Associates *"Market Study for Durham Scientific Crystals"* (2003).

[52]   T. Asahi, O. Oda, Y. Taniguchi and A. Koyama. *"Characterization of 100mm Diameter CdZnTe Single Crystals Grown by the Vertical Gradient Freeezing Method"*. Journal of Crystal Growth **149** (1995) 23.

[53]   T. Asahi, O. Oda, Y. Taniguchi and A. Koyama. *"Growth and Characterization of 100 Mm Diameter CdZnTe Single Crystals by the*

Vertical Gradient Freezing Method". Journal of Crystal Growth **161** (1996) 20.

[54]   P. Rudolph and M. Muhlberg. *"Basic Problems of Vertical Bridgman Growth of CdTe"*. Mat. Sci. Eng. **B16** (1993) 8.

[55]   S. J. Czyzak, D. G. Craig, C. E. McCain and D. C. Reynolds. *"Single Synthetic Cadmium Sulphide Crystals"*. Journal of Applied Physics **23** (1952) 932.

[56]   L. C. Greene, D. C. Reynolds, S. J. Czyzak and W. M. Baker. *"Method for Growing Large CdS and ZnS Single Crystals"*. Journal of Applied Physics **29** (1958) 1357.

[57]   W. W. Piper and S. J. Polich. *"Vapour Phase Growth of Single Crystals of II-VI Compounds"*. Journal of Applied Physics **32** (1961) 1278.

[58]   P. Hoschl and C. Konak. *"Sublimation of Cadmium Telluride and Cadmium Selenide under a Vapour Pressure of One of Their Components and the Equilibrium Form of Crystal Growth"*. Phys. Stat. Sol **9** (1965) 167.

[59]   K. Itagi, N. Ohashi and K. Mochizuki. *"Vapour Phase of Cadmium Telluride under Controlled Partial Pressure of Constituent Element"*. Jap. J. Appl. Phys. **8** (1976) 1429.

[60]   K. Mochizuki. *"Effect of the Deviation from Stoichiometry of a Source Specimen on the Vapour Transport of CdTe"*. Journal of Crystal Growth **51** (1981) 453.

[61]   K. Mochizuki. *"Effect of Supersaturation on the Vapour Phase Transport of CdTe"*. Journal of Crystal Growth **53** (1981) 355.

[62]   L. Clark and J. Woods. *"Growth of Single Crystals of Cadmium Sulphide"*. Journal of Crystal Growth **3/4** (1968) 127.

[63]   K. E. Burr and J. Woods. *"Growth of ZnSe Single Crystals from the Vapour Phase"*. Journal of Crystal Growth **9** (1971) 183.

[64]   J. R. Cutter. *"The Crystal Growth and Properties of Some Chalcogenides of Zinc and Cadmium"*. PhD Thesis Thesis. University of Durham. (1977).

[65]   G. J. Russell and J. Woods. *"The Growth of CdS in Sealed Silica Capsules"*. Journal of Crystal Growth **46** (1979) 323.

[66]   I. E. Ture, F. Poulin, A. W. Brinkman and J. Woods. *"Electron Traps and Deep Levels in Cadmium Selenide"*. Phys. Stat. Sol **A 77** (1983) 535.

[67]   K. Durose, G. Russell and J. Woods. *"Structural Properties of Crystals of CdTe Grown from the Vapour Phase"*. Journal of Crystal Growth **72** (1985) 85.

[68]   K. Durose and G. J. Russell. *"Structural Defects in CdTe Crystals Grown by Two Different Vapour Phase Techniques"*. Journal of Crystal Growth **86** (1988) 471.

[69]   K. Durose and G. J. Russell. *"Twinning in CdTe"*. Journal of Crystal Growth **72** (1990) 85.

[70]   M. M. Faktor, R. Heckingbottom and I. Garrett. *"Growth of Crystals from the Gas Phase. Part I. Diffusional Limitations and Interfacial Stability in Crystal Growth by Dissociative Sublimation"*. J. Chem. Soc. A (1970) 2657.

[71]   M. M. Faktor, R. Heckingbottom and I. Garrett. *"Growth of Crystals from the Gas Phase. Part II. Diffusional Limitations and Interfacial Stability in Crystal Growth by Disscoiative Sublimation with an Inert Third Gas Present"*. J. Chem. Soc. A (1970) I.

[72]   M. M. Faktor, I. Garrett and R. Heckingbottom. *"Diffusional Limitations in the Gas Phase Growth of Crystals"*. Journal of Crystal Growth **9** (1971) 3.

[73]   D. W. Greenwell, B. L. Markham and F. Rosenberger. *"Numerical Modelling of Diffusive Physical Vapour Transport in Cylindrical Ampoules"*. Journal of Crystal Growth **51** (1981) 413.

[74]   N. Yellin, D. Eger and A. Shachna. *"Vertical Unseeded Vapour Growth of Large CdTe Crystals"*. Journal of Crystal Growth **60** (1982) 343.

[75]   N. Yellin and S. Szapiro. *"Vapour Transport of Nonstoichiometric CdTe in Closed Ampoules"*. Journal of Crystal Growth **69** (1984) 555.

[76]   N. Yellin and S. Szapiro. *"Calculation of the Partial Vapour Pressures of Tellurium and Cadmium over Non-Stoichiometric CdTe in the Temperature Range 750-1050°C"*. Journal of Crystal Growth **73** (1985) 77.

[77]   R. Triboulet and Y. Marfaing. *"CdTe Growth by Multipass THM and Sublimation THM"*. Journal of Crystal Growth **51** (1981) 89.

[78]   F. Rosenberger and G. H. Westphal. *"Low-Stress Physical Vapour Growth (PVT)"*. Journal of Crystal Growth **43** (1978) 148.

[79]   J. R. Abernathey, D. W. Greenwell and F. Rosenberger. *"Congruent (Diffusionless) Vapour Transport"*. Journal of Crystal Growth **47** (1978) 145.

[80]   H. Kuwamoto. *"Seeded Growth of Large Single-Grain CdTe from the Vapour Phase"*. Journal of Crystal Growth **69** (1984) 204.

[81]   E. V. Markov and A. A. Davydov. *"Sublimation of CdS Crystals"*. Inorg. Mater. **7** (1971) 503.

[82]   E. V. Markov and A. A. Davydov. *"Growing Oriented Single Crystals of Cadmium Sulphide from the Vapour Phase"*. Inorg. Mater. **11** (1975) 104.

[83]   Z. Golacki, M. Gorska, J. Makowski and A. Szcerbakow. *"Vapour Phase Growth of CdTe"*. Journal of Crystal Growth **56** (1982) 213.

[84]   Z. Golacki, J. Z. Domagala, K. Swiatek and A. Szxzerbakow. *"Contactless Growth of Uniform $Cd_{0.8}Zn_{0.2}Te$ Monocrystals from the Vapour"*. Materials Letters **In press** (2003).

[85]   R. Lauk and G. Muller-Vogt. *"Vapour Transport of Impurities in Semi-Closed Ampoules, I: Theory"*. Journal of Crystal Growth **74** (1986) 523.

[86]   R. Lauk, G. Muller-Vogt and W. Wendl. *"Vapour Transport of Impurities in Semi-Closed Ampoules. Ii. Doping Profiles, Refining and Stoichiometry in Crystal Growth of Ii-Vi Compounds"*. Journal of Crystal Growth **74** (1986) 520.

[87]   J. L. Boone, G. Cantwell, W. C. Harsch, J. E. Thomas and B. A. Foreman. *"Electrical and Crystallographic Characterization of CdTe Grown by the Transport Method"*. Journal of Crystal Growth **139** (1994) 27.

[88]   K. Grasza. *"Bulk Vapour Growth of CdTe"*. Journal of Crystal Growth **146** (1995) 65.

[89]   K. Grasza and M. Pawlowska. *"Morphological Instabilities in CdTe Crystal Growth from the Vapour Phase"*. Journal of Crystal Growth **203** (1999) 371.

[90]   K. Grasza. *"Computational Modeling of the Low Supersaturation Nucleation in Crystal Growth by "Contactless" Physical Vapor Transport"*. Journal of Crystal Growth **193** (1998) 426.

[91]   K. Grasza. *"Effect of Temperature Field on Growth Stability"*. Journal of Crystal Growth **146** (1995) 69.

[92]   Cited By [10]. .

[93]   M. Laasch, G. Kloess, T. Kunz, R. Schwarz, K. Grasza, C. Eiche and K. W. Benz. *"Stress Birefringence in Vapour-Grown CdTe and Its Correlation to Growth Techniques"*. Journal of Crystal Growth **161** (1996) 34.

[94]   M. Laasch, T. Kunz, C. Eiche, M. Fiederle, W. Joerger, G. Kloess and K. W. Benz. *"Growth of Twin-Free CdTe Single Crystals in a Semi-Closed Vapour Phase System"*. Journal of Crystal Growth **174** (1997) 696.

[95]   W. P. Trower. *"Modified Vapour Phase Growth of Cadmium Zinc Telluride: A Progress Report"*. in *"Semiconductors for Room-Temperature Radiation Detector Applications II"*. Edited by R. B. James, T. E. Schlesinger, P. Siffert, W. Dusi, M. R. Squillante, M. O'Connell and M. Cuzin 487 Materials Research Society Boston. (1997).

Chapter **3**

MTPVT System

3.1 INTRODUCTION

The original single-source Multi Tube Physical Vapour Transport (MTPVT) system was designed and developed by Dr John Mullins for the growth of CdTe [1]. The addition of a second source tube should allow the growth of ternary compounds such as cadmium zinc telluride from the binary sources CdTe and ZnTe, the growth of CdTe from the elements or the inclusion of a dopant such as chlorine.

To accommodate the addition of this extra source tube the system was comprehensively redesigned and rebuilt, and a new computer control program written. This chapter will introduce the principles of the MTPVT system, with specific reference to the changes to the glassware and furnaces, outline the new computer control system and detail the mechanics of a typical growth run.

3.2   PRINCIPLES OF THE MTPVT SYSTEM

3.2.1 Original Design

The MTPVT system is a seeded vapour phase growth system, in which the sources are sublimed and allowed to condense on a cooler seed crystal. It is based on the Markov [2] method of physical vapour transport, where the seed is separated from the container walls, ensuring wall-free growth. One of the main innovations of the MTPVT was the decoupling of the source and seed temperatures through its 'U' tube design.

The original MTPVT system was designed solely for the growth of cadmium telluride from its binary source. It comprised of one source and one growth tube, each heated by three zone PBN/PG furnaces, and connected by a capillary-containing quartz crossmember, which was heated by two quartz halogen lamps. (For further information consult [1, 3, 4]).

3.2.2 Development of Design

The MTPVT system has been comprehensively redesigned and rebuilt to allow the addition of the second source tube. These changes included the use of new source tube heaters, a significant redesign of the glassware, and the construction of new top and bottom plates of the vacuum chamber to accommodate the new setup.

The redeveloped MTPVT system, illustrated in Figure 3.1, contains two vertical source, and a single vertical growth, quartz silica glass tubes, connected by an optically heated crossmember. Polycrystalline source material, in an ampoule contained in a source tube, is heated for sublimation to occur, e.g.
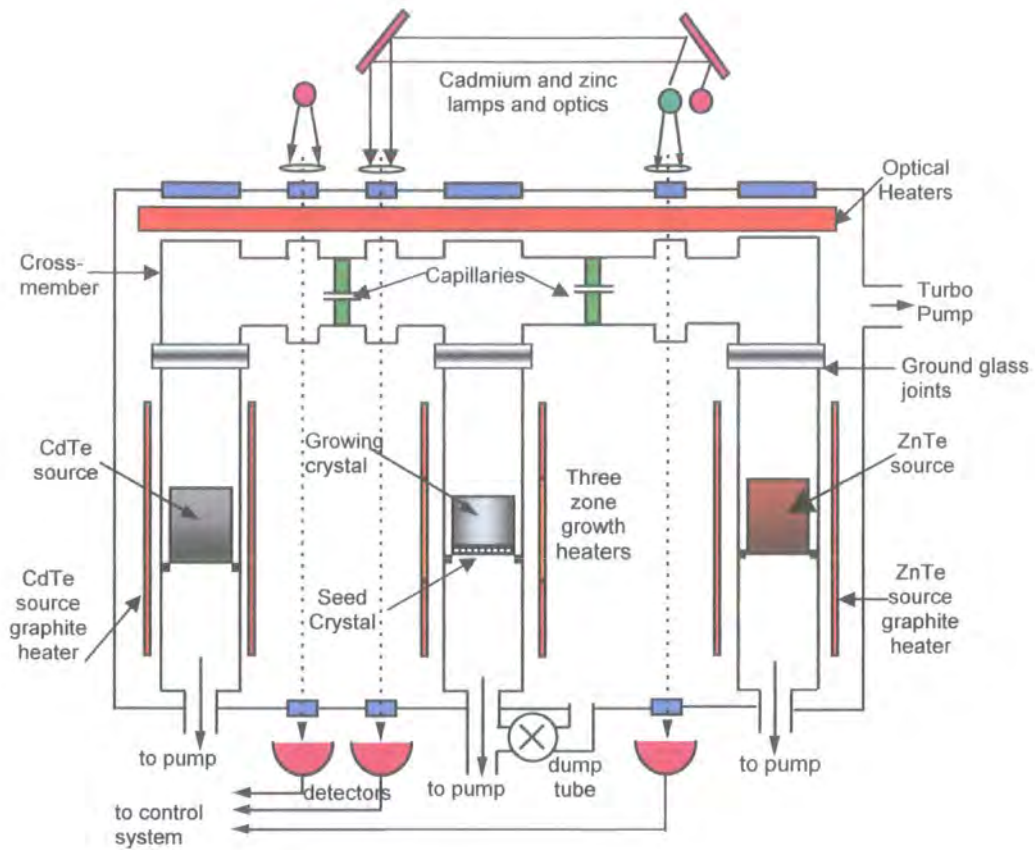
Figure 3.1: Three legged MTPVT system for growth of CdZnTe

$$MTe_{(s)} \Leftrightarrow M_{(g)} + \frac{1}{2}Te_{2(g)} \qquad\qquad M=Cd,Zn \qquad (3.1)$$

These vapours flow through the capillaries acting as flow restrictors in the crossmember, and nucleate on the cooler seed crystal in the growth tube. The flow restricting capillaries, along with the independent heating zone, allow the transport and growth rates to be well controlled.

The use of optical heating around the crossmember, together with optical windows on either side of the capillaries, enable the partial pressures in the source and growth tubes to be determined through optical absorption measurements.

A stainless steel drum encases the MTPVT system, and is pumped by a turbo-pump, allowing vacuum pressures below 10^{-6} mbar to be achieved. The vacuum reduces impurities incorporated into the crystals, improves thermal insulation between the system components, allows sublimation at lower temperatures and stops the oxidation of the furnaces and shields.

3.2.3 Glassware

The crossmember, source tubes and growth tubes are made of quartz silica glass to permit growth at temperatures in excess of 900°C. The crossmember is built to a T-shape to fit in the steel drum which encases the MTPVT system.
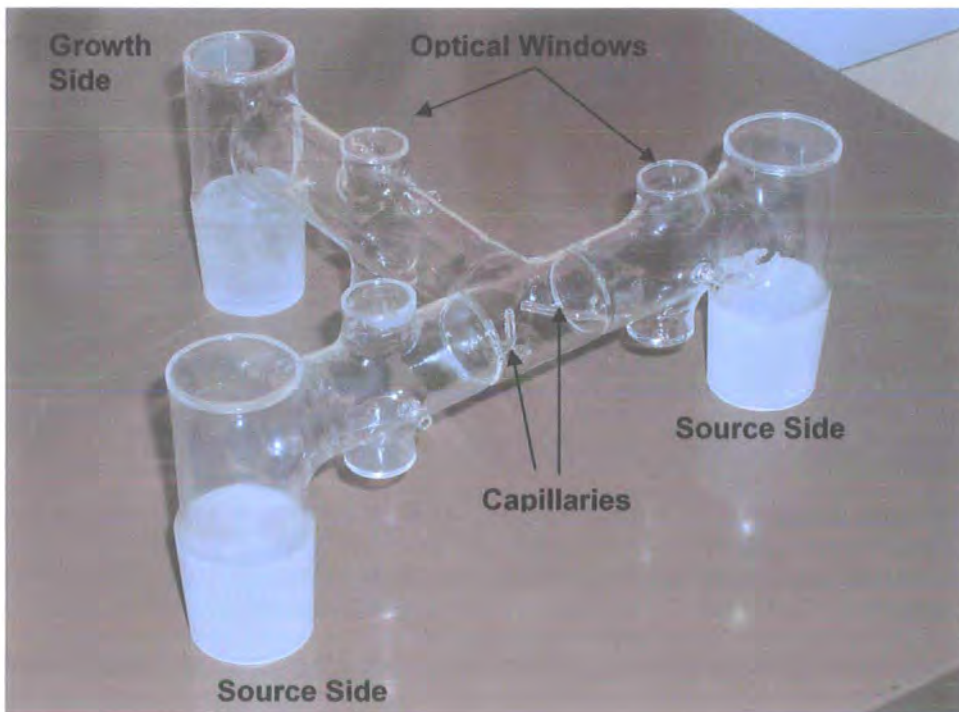
Figure 3.2: T-shaped quartz silica crossmember

Two capillaries in the crossmember restrict flow into the growth tube from each source tube. As can be seen in Figure 3.2, six optical windows exist to enable the partial pressures in each area to be determined *in situ* by optical absorption measurements. A large window above the growth tube allows the

growing crystal to be observed during growth, and the possibility of using an optical pyrometer to measure the crystal surface temperature.

The ground glass cones on the base of the crossmember are connected into ground glass sockets in the top of the vertical growth and source tubes, allowing the glassware to be dismountable, for loading of the seed and sources, and reusable. This also provides the opportunity to change the design of one of the tubes without the need to remanufacture the entire glassware.

Figure 3.3: Source Tube

The source materials are placed in the 455 mm long, 35 mm outer diameter (O.D.) quartz silica source tube with a B35 socket at the top to connect to the crossmember, as displayed in Figure 3.3. A B14 cone sits at the base of the growth tube to connect to a rotary pump during the initial roughing out. The capillary near the middle of the tube allows the volume around the source to be evacuated by the rotary pump, and also in principle permits the introduction of a carrier gas to alter the capillary flow. During the growth runs described in this thesis, however, no carrier gas was introduced, and the design of the capillary and heaters ensured the capillary was sealed off by the condensing source, allowing the source pressure to build up.

Several growth tube designs have been used in this MTPVT system. The initial design placed a sealed silica cone in a socket in the 35mm internal diameter (I.D.) silica tube on which the seed crystal sat, with wires placed between the cone and socket to accurately control the annulus gap. A second design replaced this cone and socket with a 10 mm thick 32 mm diameter quartz silica disc which rested on 3 indentations in the growth tube, with the annulus gap determined by the specifications of the internal bore of the growth tube and the diameter of the disc. The manufacturer's tolerance of the internal bore of the standard tube was ±0.5 mm, and this bore could vary to this degree along the length of the tube, consequently a matching disc needed to be produced individually to fit each growth tube. This led to large inaccuracies in the size of the annulus gap, with variations as great as 1 mm.

Figure 3.4: Growth Tube containing solid pedestal

The third major design of the growth tube (exhibited in Figure 3.4) increased the I.D. to 50 mm while maintaining the overall length, thus doubling the area of the growing crystal. Two quartz silica rods were attached to the internal wall of the growth tube to form a cross-hair table, on which a 25 mm spacer tube sat to hold a ~50 mm diameter, 10 mm long pedestal disc. This design allows the pedestal disc to sit more horizontally in the tube than the previous design, where the hand-made indentations could not be made level. Special "Precision Bore" quartz silica tube with a manufacture's tolerance of ±0.25 mm was used for the growth section of the tube, ensuring a greater control on the annulus gap.

3.2.4 Heaters

A three-zone heater is used to ensure the precise control of the vertical temperature profile, which determines the growth on the seed crystal. The 3 separate pyrolytic graphite (PG) / pyrolytic boron nitride (PBN) growth side furnaces, displayed in Figure 3.5, slot together to provide the three zone profile, with the larger central furnace enabling a large controllable area around the crystal, and smaller heaters above and below further defining the profile.

Figure 3.5: Three-zone PG/PBN growth tube heater (left) and graphite source tube heater (right)

The temperature profiles around the source tubes do not require the same precise control as the growth side. Graphite furnaces 250 mm long with a 52 mm I.D. provide sufficient heating on the source side to readily raise the source to 870°C. 3 mm thick graphite is required for the mechanical stability of the heater, therefore to provide a resistance of 1 Ω a picket-fence design is

required. At this low resistance, high currents of up to 60 A at a low voltage of 40 V are needed to give sufficient power output to achieve the desired temperatures.
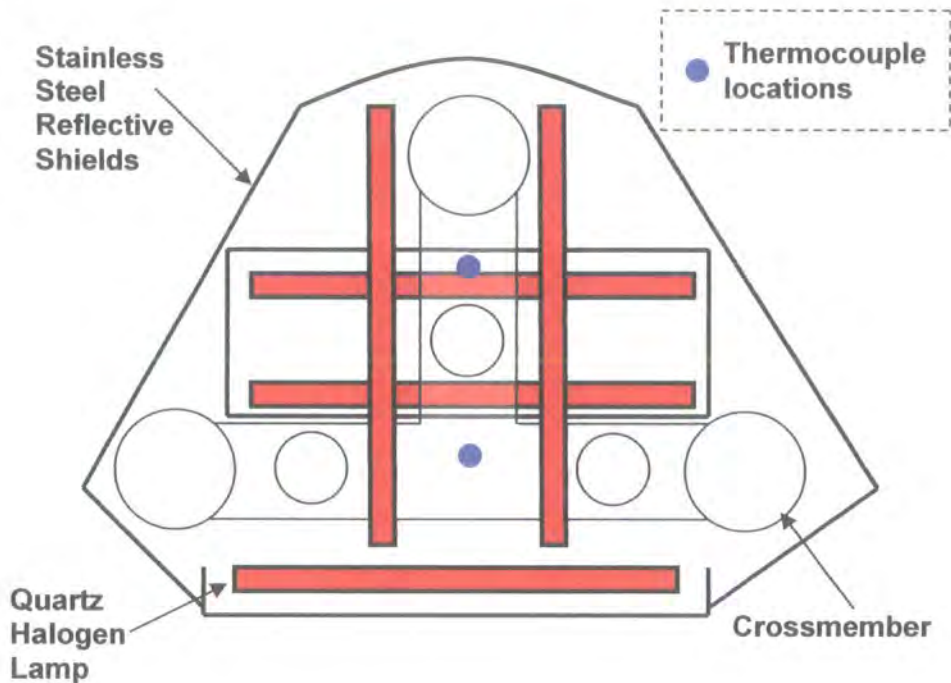
Figure 3.6: Five-lamp design of crossmember heating

It is important that no cold spots existed on the glassware as they acted as condensation points for the vapours, yet the T-design of the crossmember, together with the optical windows which protrude out of the tube, make it difficult to heat uniformly. Lines of sight have to be left clear above and below the windows to allow the passage of light for optical absorption partial pressure monitoring. Several designs of heaters and shielding have been tested to reach the required temperatures with minimal cold spots, including arranging three 1 kW, 254 mm long quartz halogen lamps in a triangle around the crossmember. The final design, presented in Figure 3.6, places five 1.5 kW lamps around the crossmember with considerable stainless steel shielding, and allows crossmember temperatures to reach up to 940°C without cold spots on the glassware. Source temperatures of 870°C can be

used without crossmember condensation, thus reasonable consistent flow rates can be accomplished.

3.2.5 Other Features of the MTPVT system

The heaters and quartz silica tubes are mounted on a 25 mm thick stainless steel base plate, which is fitted to a wheeled trolley frame, allowing the system to be easily assembled. Once wheeled into place, a motor enables the apparatus to be raised into the steel drum, with a VITON O-ring providing the vacuum seal between the drum and base plate. The drum exhibited in Figure 3.7 is clamped to a stainless steel top plate, on which an Edwards turbo-pump is connected to provide vacuums with pressures less than 10^{-6} mbar. Chilled water is piped around the drum to keep the O-rings cool, as the outer surface temperature of the drum exceeds $200°C$ during growth.

Figure 3.7: MTPVT system

3.3 ADVANTAGES OF THE MTPVT SYSTEM

The design specifications of the MTPVT system described earlier in this chapter gave the system considerable advantages over other growth techniques described in Chapter 2, overcoming some of the problems associated with these methods;

1) The annulus gap between the growing crystal and growth tube allows excess components and impurities to be removed from the growth region, and stops the build up of growth perturbing diffusion barriers around the crystal surface.

2) The annulus gap also minimises crystal contact with the silica growth tube, reducing the stress applied to the crystal.

3) The use of different temperature zones for the source tubes, growth tube and crossmember decouples the source and growth temperatures. Lower growth temperatures are required, further reducing the thermal stress applied to the crystal.

4) The crossmember capillary further decouples the source and growth zones, giving greater control of growth and transport rates.

5) The two source tubes allow flexibility in the methods of growth. For example, ternary compounds may in principle be grown from binary sources, or binary compounds grown from their elements.

6) The crossmember design permits *in situ* pressure monitoring of the constituent vapours through optical absorption measurements.

3.4 TEMPERATURE CONTROL

3.4.1 Thermocouples

During the growth of crystals accurate control of the temperatures is required, and has to be maintained at a constant level over a period of several days. R-

type Pt — 87%Pt 13%Rd thermocouples are used due to the high temperatures involved, the high level of vacuum and the requirement to minimise the amount of transition metals within the system. On the growth and source sides, thermocouples placed between the furnaces and the tubes measure the temperature of each zone. Two thermocouples fit into pockets on the crossmember, one to control the output from the bottom three lamps and the other for the top two lamps.

3.4.2 Computer Control of Temperatures

The temperatures of each zone are controlled via the use of a personal computer (PC) and thyristor packs, as indicated in Figure 3.8. A computer program was written in the Microsoft Visual C++ language to allow accurate automated control of the temperatures, with the thermocouples connected to an PCI PC card, which converts their voltages into corresponding temperatures. The computer program calculates the required power level for each furnace based on the measured and target temperatures, and supplies a control signal between 0 and 10 V, through a 14-bit Digital to Analogue (DA) converter, to the corresponding thyristor pack. For the mains voltage powered lamps, these currents are fed directly to the lamps, but for the growth and source furnaces, transformers are required to reduce these output voltages to increase the currents.
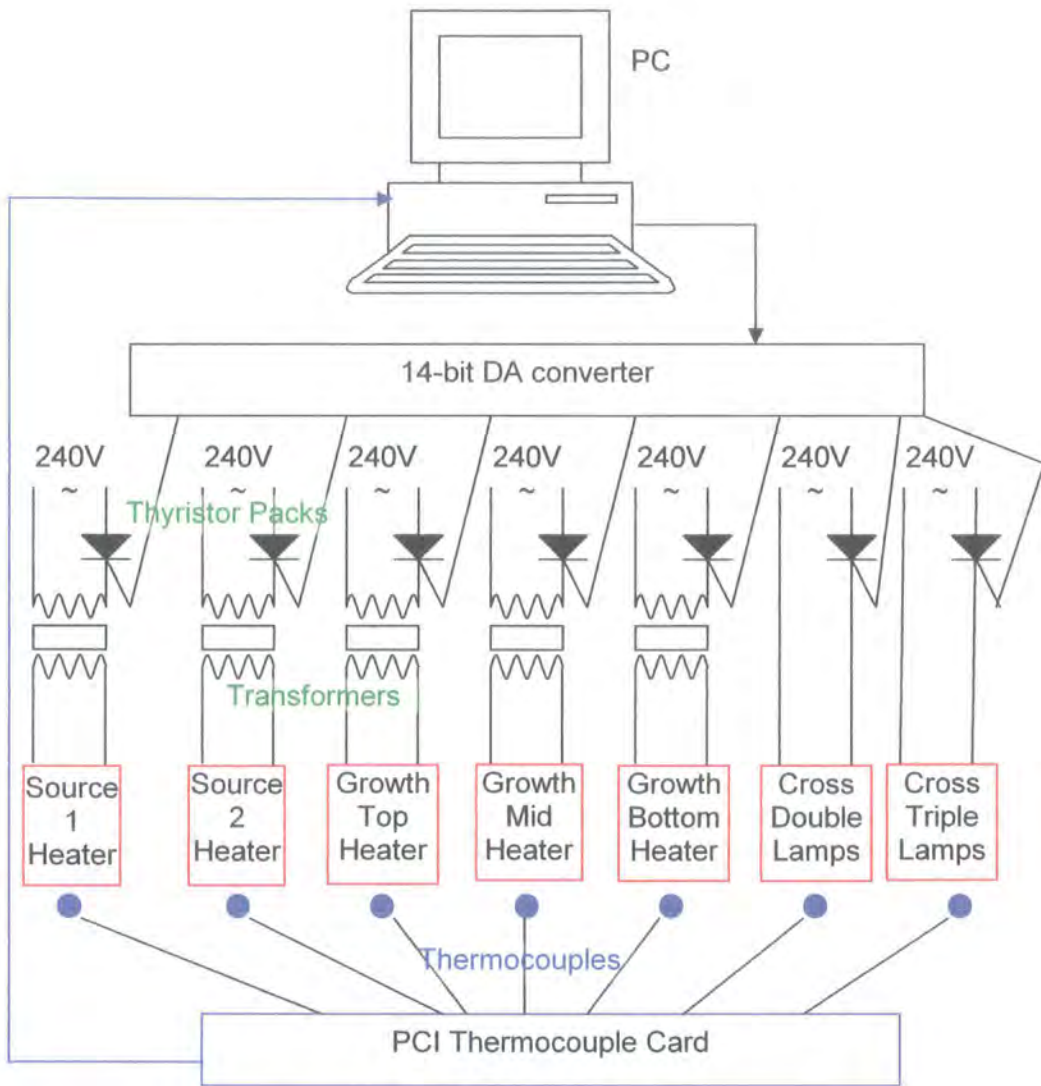
Figure 3.8: Computer control of heaters

3.4.3 Control Algorithm

The small magnitude of the voltages produced by the thermocouples mean any interference can cause small fluctuations in the temperature measurements of the Thermocouple Card. In the MPTVT control program a running average temperature reduces these fluctuations, increasing the stability of the control. After each temperature input T_i, the new running average temperature A_i is calculated from the previous running average A_{i-1} from [5]

$$A_i = \frac{(n-1)A_{i-1} + T_i}{n}$$
(3.2)

where *n* = *1.5* in the MTPVT controller. In the MTPVT system the temperature sample rate is limited to one second by the PCI Thermocouple Input card, which can read all 16 thermocouple voltages in one cycle, but can only sample these signals at 1 Hz.

The most commonly used control algorithm is the proportional-integral-derivative (PID) [6]. The PID acts to set the output *u* to decrease the difference between the target value and the measured value, the error *e*.

$$u(t) = K\left(e(t) + \frac{1}{T_I} \int_0^t e(\tau)d\tau + T_d \frac{de(t)}{dt} \right) + M_R$$
(3.3)

with the proportional gain *K*, T_I = integral action constant, T_d = derivative action constant and M_R is the output when the control action began.

The proportional control simply sets the output voltage proportional to the error.

$$u_p(t) = Ke(t)$$
(3.4)

With the 14-bit DA output card in the MTPVT computer, an output value of 0 gives 0% output, with full 100% output achieved by an output value of 16383. The gain could be set to give full output for a given error e_p

$$K = \frac{16383}{e_p}$$
(3.5)

For example, to achieve full power until the actual temperature was only 50°C less than the target *K*= 16383/50 $\approx$ 327. An offset always occurs with a proportional controller, since some error must persist for an output signal to be maintained. Figure 3.9 presents the temperature and power levels for a

proportional controller algorithm through the MTPVT controller computer on a benchtop furnace, with a target temperature of 550°C.
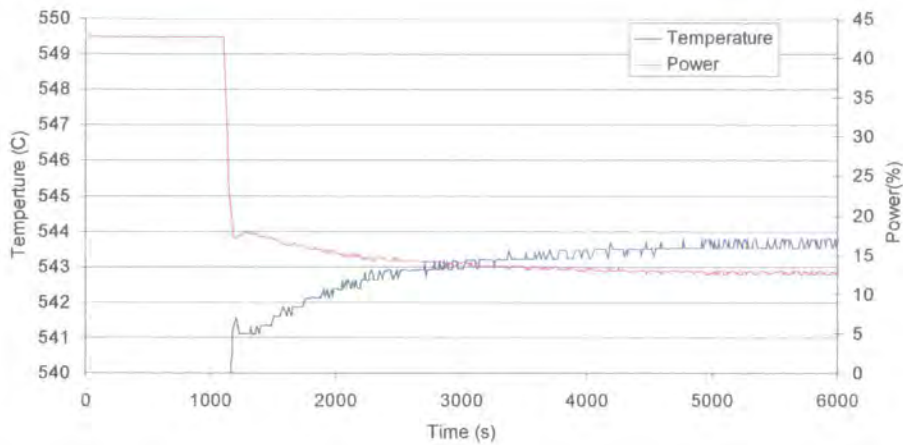
Figure 3.9: Temperature and power levels for proportional controller on benchtop furnace

The temperature settles to a level around 543°C, still 7°C below the target, and stable to within 0.5°C after 3000 s. Increasing the gain would reduce the error level but increase the instabilities.

Integral control produces an output which is a function of the time integral of the error, acting to reduce the error to zero.

$$u_I = \frac{K}{T_I} \int_0^t e(\tau)d\tau \tag{3.6}$$

The integral action acts as long as an error exists, but can take a period of time to build up as it is a time integral. Although integral controllers can be used alone, combining the proportional and integral controllers allows the system to react efficiently to changes. With a sudden change in the error, the proportional action produces a rapid response in output to counter the error, and the integral action follows to decrease the error. When the error falls to

zero, the proportional control stops, but the integral contribution remains as an output offset, maintaining the temperature.
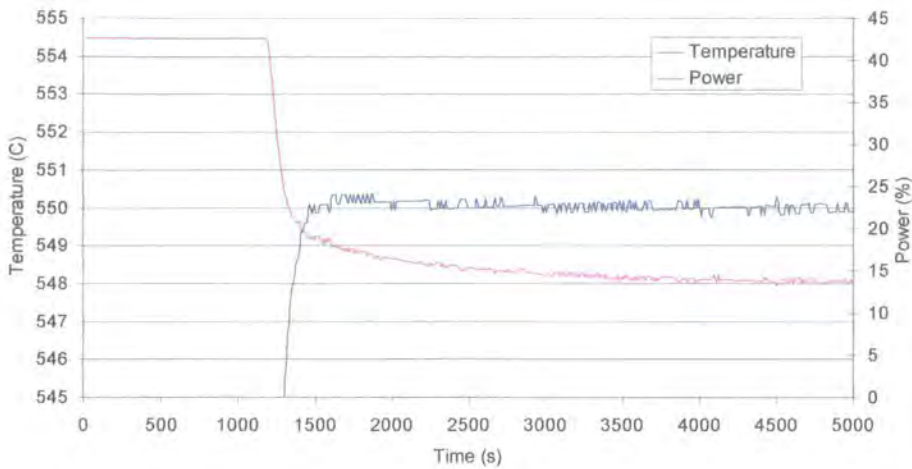
Figure 3.10: Proportional and Integral (PI) control combined

The effects of the combined PI controller in Figure 3.10 illustrate the temperature settling on the target 550°C after 1500 s with the instability reduced to 0.2°C. The step-like nature of these instabilities indicates the controller is acting at the limit of the PCI Thermocouple card.

If allowed to, the integral action can build up over a period of time. If a small error exists for a long period of time the sum will continue to rise, and the integral contribution to the control will become disproportionately large, known as integral wind-up. To prevent this, in the MTPVT algorithm the integration term by default only began when the actual temperature was within 50°C of the target. If the gain was set at 327 (from 16383 / 50), with the error greater than 50°C, the proportional term gave full power without the integration term.

The differential controller

$$u_d = KT_d \frac{de(t)}{dt} \tag{3.7}$$

produces an output proportional to the rate of change of the error. Whilst the proportional and integral controllers operate on past control errors, the derivative controller attempts to predict future errors, reducing overshoot when controlling about a set point. However, the derivative action can be very difficult to implement and over 75% of applications do not include this controller. As Figure 3.11 illustrates, the heater system is well controlled by the PI controller and therefore the MTPVT controller would not greatly benefit from the inclusion of the derivative.

The PI equation from (3.3) must be translated into a form suitable for inclusion in a digital computer control algorithm. The integral may be replaced by a summation for a small time interval Δt, giving an output for the *n*th sample

$$u_n = K\left(e_n + \frac{\Delta t}{T_I}\sum_{i=0}^{n}e_i\right) + M_R \tag{3.8}$$

This output needs to take account of its value when the output begins, M_R. If this is rewritten for the previous sampling time, M_{n-1}, and subtracted from the current sample then the change in output is

$$\Delta u = K\left((e_n - e_{n-1}) + \frac{T}{T_I}e_n\right) \tag{3.9}$$

This form does not require the value of the output when the control began, and can be easily implemented with only the previous power level, the current error and the previous error required. Therefore a version of this equation was included in the MTPVT control algorithm, extracts of which can be seen in Appendix I.

3.4.4 Ramp Speed Control

The control algorithm detailed above deals with achieving the target temperature in an optimum time period. In the MTPVT system, however, it is necessary to control the rate of temperature increase, or ramp speed, to maintain the vacuum, protect the furnaces and ensure controlled temperature profiles. To achieve this, without drastically altering the PI controller, the MTPVT algorithm increases the target temperature incrementally until the final target is reached. For the time period Δt, the target T_n at sample n increased at speed S

$$T_{n+1} = T_n + S\Delta t \qquad (3.10)$$

3.4.5 Control Program

The C++ program developed incorporates control algorithms for each furnace zone, and allows the user to build the temperature profiles by entering a series of target temperatures (T_i), ramp speeds (S_i) and plateaux lengths or delays (D_i), as displayed in Figure 3.11. Up to seven stages can be set for each zone.
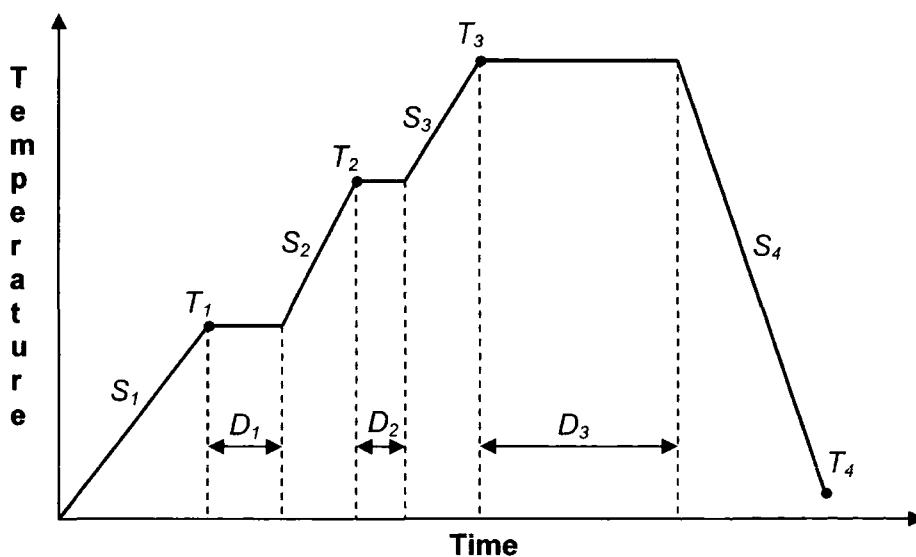
Figure 3.11: Temperature Profiles

The profile is constructed via a dialog window (Figure 3.12) which appears when the program starts. Up to seven target temperatures may be set for each of the seven temperature zones, together with the speed to reach the temperature and delay after the temperature is achieved.

Temperature Profile							
	Cadmium	Zinc	Growth Top	Growth Mid	Growth Bot	CrMem 2	CrMem 3
Temp 1 (C)	100	100	100	100	100	100	100
Speed 1 (C/min)	2	2	2	2	2	2	2
Delay 1 (min)	240	240	240			240	
Temp 2 (C)	200	200	200	200	200	250	250
Speed 2 (C/min)	2	2	2	2	2	2	2
Delay 2 (min)	240	240	240			240	
Temp 3 (C)	400	400	300	275	250	450	450
Speed 3 (C/min)	2	2	2	2	2	2	2
Delay 3 (min)	2880	1440	2880			2880	
Temp 4 (C)	400	400	300	275	250	550	550
Speed 4 (C/min)	2	2	2	2	2	2	2
Delay 4 (min)	5	5	5			5	
Temp 5 (C)	870	870	675	600	600	900	900
Speed 5 (C/min)	2	2	2	2	2	2	2
Delay 5 (min)	1	1	1			1	
Temp 6 (C)	870	870	775	700	700	900	900
Speed 6 (C/min)	2	2	2	2	2	2	2
Delay 6 (min)	2880	2880	2880			2880	
Temp 7 (C)	0	0	0	0	0	0	0
Speed 7 (C/min)	2	2	2	2	2	1.5	1.5

Set

Synchronisation

Figure 3.12: Temperature Profile input dialog box

A method of zone synchronisation enables the user to ensure the ramps for each zone start at the same time. A popup Synchronisation dialog box (Figure 3.13), accessible by clicking the Synchronisation button on the Profile dialog box, selects which zones are synchronised with each other.

Once the measured temperature reaches the zone target temperature, a flag is raised and the program waits for all of the flags of the synchronised zones to be raised before the delay plateau period begins.
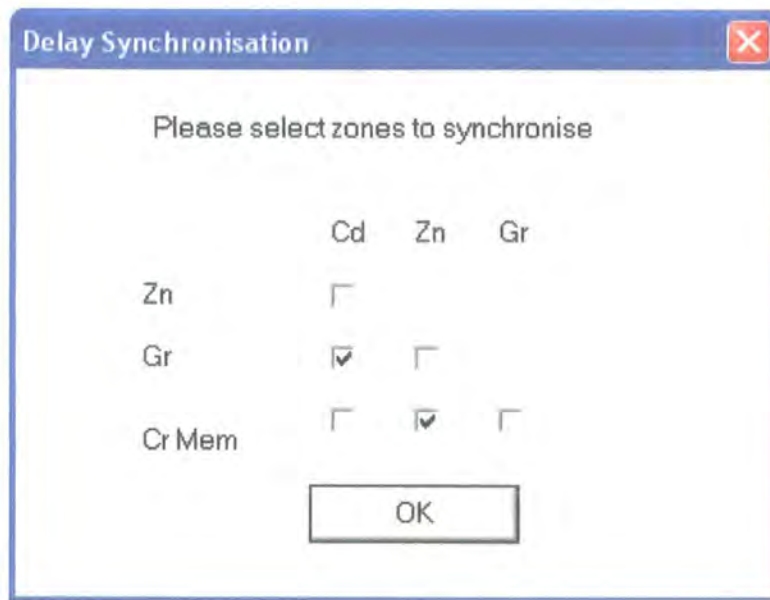
Figure 3.13: Delay Synchronisation dialog box

After the temperature profile has been entered and the synchronisation configuration set up, the main dialog window begins. This window, shown in Figure 3.14, displays the current growth information, including the current temperatures, the target temperatures, the power levels, the ramping state, the profile stage and the growth time, all updated every second. Access to the Profile input dialog box, to change the profile during the growth run, is possible from the main window by selecting the appropriate button, along with access to the Control Parameters dialog box. This Control Parameters dialog box, displayed in Figure 3.15, permits changes to the maximum powers, gain, integration time and integration set-in time for each heater zone.
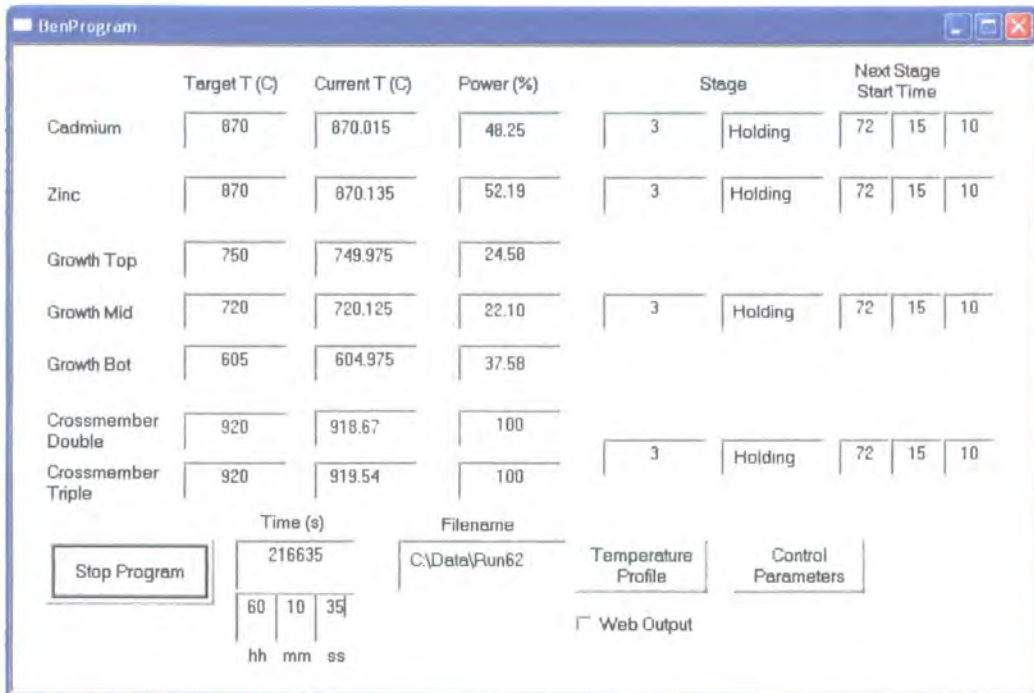
Figure 3.14: Main program dialog box
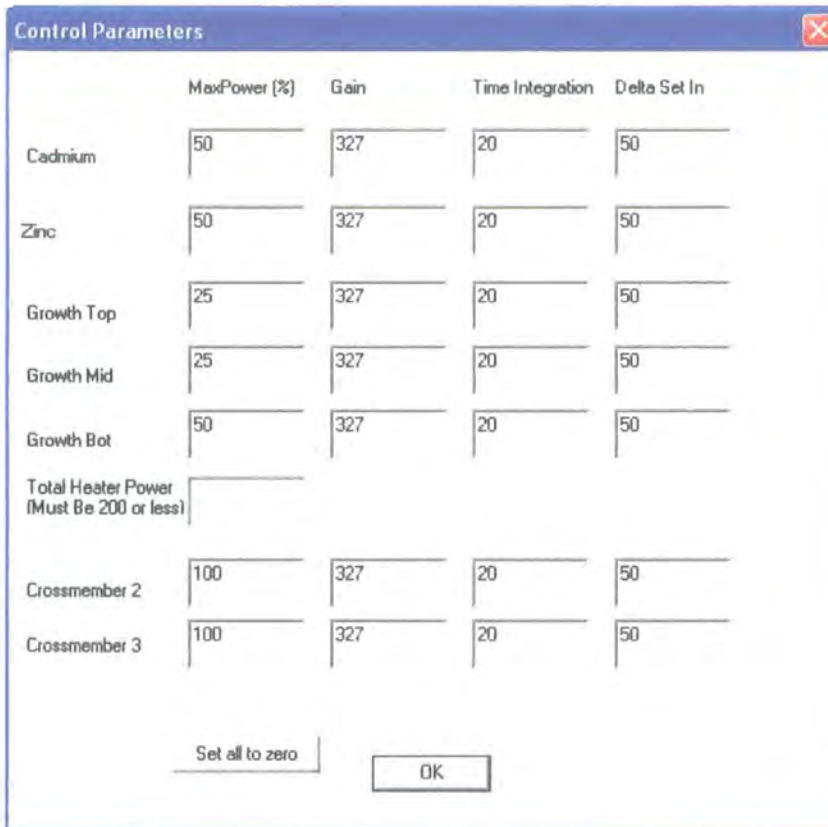
Figure 3.15: Control Parameters dialog box

Throughout the growth run temperature data and power levels are written to an output file every 100 seconds to give an electronic record of the growth. There is also an option to output the temperature and power data to a website during the run, which enables monitoring of the growth away from the laboratory.

3.5 STRUCTURE OF GROWTH RUNS

3.5.1 General Structure

The general structure of the growth run is displayed in the flow diagram in Figure 3.16.
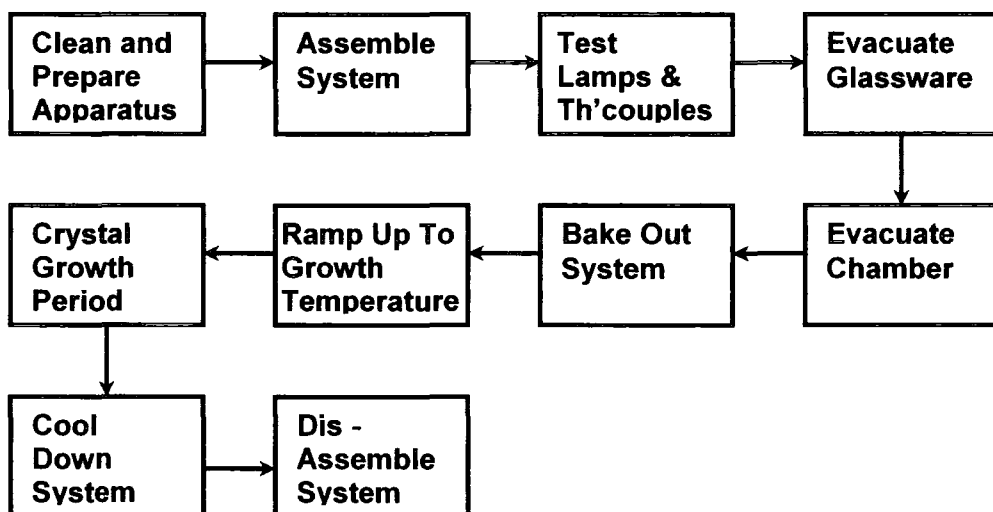
Figure 3.16: Flow diagram of structure of growth run

3.5.2 Preparation of Apparatus

Before the MTPVT system was assembled all of the stainless steel shields were cleaned with scouring pads to increase their reflectivity. Prior to insertion in the MTPVT system, the glassware was cleaned in aqua regia (3 $HCl_{(aq)}$: 1 $HNO_{3(aq)}$ by volume), rinsed with de-ionised water and dried in a drying oven overnight to ensure the glassware was clean and dry. The

source materials were poured directly from their supplier packaging into test-tube shaped quartz silica ampoules to minimise contamination, and all of the glassware was weighed before and after each run to allow determination of mass flows and losses.

The apparatus was assembled in a standard procedure to ensure all pieces were in place. Care was taken when assembling the glassware to reduce leaks, and it was found that twisting the tubes with respect to the crossmember helped lock together the cone and socket, giving a better seal.

Once the glassware, heaters and shields were assembled, but before they were raised onto the drum, the thermocouples were tested by directing hot air from a heat gun to ensure there was no open circuit or short circuit before the measuring point. The lamps were also tested by confirming their illumination when supplied with 15% of total power.

3.5.3 Vacuum and Bake Out

A specific sequence to pump out the glassware was established to prevent an imbalance in pressures which could cause the pedestal to accelerate up the growth tube and crash into the crossmember. Once the system was loaded, the source and growth tubes were connected to the rotary pump. The valve to the growth tube was opened and the growth tube roughed out for over an hour. The valves to the source tube were then slowly opened, allowing the evacuation of all of the glassware. It was necessary to rough out the glassware to a low pressure to prevent the joints being pushed apart when the whole chamber was evacuated using the turbo pump.

After allowing the whole glassware to pump for an hour the source tube valves were closed and the turbo pump started. As the turbo pump reached three quarters speed the pressure outside the glassware was close to the pressure inside, and the growth tube valve was closed and the dump tube opened to allow continuous pumping of the annulus by the turbo pump. The system was left pumping overnight, and by the morning the pressure had normally fallen below 10^{-5} mbar.

Providing the pressure was not too high, the growth program was started and the system baked out to dispel water vapour and other impurities. The bake out was a three-stage process, in which initially the temperatures of all zones were raised to 100°C at 2 °/min and held for over 4 hours. All temperatures were then raised at the same rate to 200°C, and again held for over 4 hours before being raised further. The crossmember was raised to 450°C and the source sides to 400°C, while the growth top, middle and bottom were only raised to 300, 275 and 250°C respectively, to avoid sublimation and thermal etching of the seed during the bake out period.

3.5.4   Ramp Up, Growth Period and Cooldown

Several methods of ramping the zones up to growth temperatures have been tested. In all cases the crossmember was raised up to 550°C, held for 5 minutes and then the final growth ramp commenced, giving the crossmember a 150°C lead on the source side, thus reducing the chances of condensation during the ramp. In the final growth ramp the crossmember was raised up to 920°C and the sources to 870°C at 2 °/min. During some growth runs the growth middle temperature was raised at the same time and rate to 600°C, held until the sources reached 870°C, and then raised up to growth

temperatures around 700°C. This allowed time for sufficient flow through the capillary to build up the growth-side pressure, reducing the possibility of seed-crystal sublimation. However, during this period material tended to condense around the cold annulus, often leading to a blocking of the annulus. To combat this, during other growth runs the growth ramp was started at the same time as the source ramp, and raised directly to the growth temperature but at a lower rate, to ensure the growth temperatures and the source temperatures were reached simultaneously. This method led to the possibility of the sublimation of the seed crystal if insufficient source material had flowed through the capillary to build up the growth-side pressure.

The growth period lasted between 20 and 72 hours, depending upon the size of the crystal required. After this period the source and growth temperatures were lowered at 2 °/min, the growth middle held at 600°C until the sources also reached 600°C, after which the source and growth zones were cooled to room temperature at 2 °/min. Holding the growth middle at 600°C prevented too much residual growth on the crystal surface and in the annulus, which caused difficulties in the removal of the crystal from the growth tube. The thermal capacity of the crossmember was lower than the growth and source tubes, which were better insulated with a greater thermal mass, consequently the cooling of the crossmember only commenced 3 hours after the other zones, ensuring no vapour condensed on the crossmember, especially the windows.

Once all of the zones had reached room temperature (usually after an overnight wait) the turbo vacuum was turned off, the dump tube closed and air admitted slowly into the vacuum jacket. After about 30 minutes the system

was usually at atmospheric pressure and could be opened, disassembled and the grown crystal removed.

3.6 CONCLUSIONS

The Multi Tube Physical Vapour Transport (MTPVT) system has been redesigned and rebuilt to permit the growth of binary and ternary II-VI compounds from elemental or binary sources, and is described in this chapter. The unique M-shape design, and crossmember capillaries, allowed decoupling of the source and growth zones, permitting lower growth temperatures to be used. Along with the annulus gap between the crystal and tube walls, this reduced the stress applied to the growing crystal, and helped account for non-stoichiometries in the source.

The temperature profiles in the system were important, ensuring nucleation only occurred on the seed crystal and not on any of the glassware. The furnaces were computer controlled, and the PI control algorithm and the C++ control program were introduced.

3.7 REFERENCES FOR CHAPTER 3

[1]   J. T. Mullins, J. Carles, N. M. Aitken and A. W. Brinkman. *"A Novel "Multi-Tube" Vapour Growth System and Its Application to the Growth of Bulk Crystals of Cadmium Telluride"*. Journal of Crystal Growth **208** (2000) 211.

[2]   E. V. Markov and A. A. Davydov. *"Sublimation of CdS Crystals"*. Inorg. Mater. **7** (1971) 503.

[3]   J. Carles Alabert. *"Optical Vapour Pressure Monitoring and Mass Transport Control During Bulk CdTe Crystal Growth in a Novel Multi-Tube PVT System"*. PhD Thesis. University of Durham. (1998).

[4]   A. W. Brinkman, J. Carles, J. T. Mullins, J. B. Mullin, K. W. Benz, T. Kunz, C. Raptis, Y. S. Raptis, E. Sarantopoulou and F. Rustichelli *"A New "Multi-Tube" Bulk Vapour Growth Technique with Special Reference to CdTe and Its Characterisation"* Report for Brite EuRam project BRE2.CT94.0609 (1998).

[5]   R. A. Chard. *"Software Concepts in Process Control"*. NCC Publications Manchester (1983).

[6]   T. K. Kiong, W. Quing-Guo and H. C. Chieh. *"Advances in PID Control"*. Springer - Verlag London (1999).

Chapter **4**

Development of Crystal Growth in MTPVT System

4.1 INTRODUCTION

The design of the MPTVT system has been outlined in Chapter 3, and this chapter will describe the growth of crystals in the system, and how the system has been developed to improve the crystal quality. The work was focussed on improving the quality of the CdTe crystals grown, although some preliminary experiments to test the ability of the system to grow CdZnTe are included.

The initial design of this MTPVT system used a quartz silica cone in a 32 mm diameter socket, with three 1 kW lamps providing the energy to heat the crossmember. Through the experiences of over 80 growth runs the design has been developed to the current use of a flat silica pedestal in a 52 mm diameter growth tube, with five 1.5 kW lamps heating the crossmember. Other developments include changes in the temperature profiles, both time profiles and temperature gradients, and changes to the system to improve

reliability and reduce leakage, and these developments will also be introduced.

4.2 PREVIOUS CRYSTAL GROWTH IN THE ORIGINAL MTPVT SYSTEM

Several CdTe boules had been grown in the original two-legged MTPVT system [1-4]. The boules, which were all grown on 49 mm diameter CdZnTe wafers on solid disc pedestals, were of varying quality, with several characterisation techniques performed for comparison with other reference crystal parameters. Dislocation densities were $3 - 9 \times 10^4$ cm^{-2}, around the same order of magnitude as in reference crystals, and the range of X-ray rocking curve widths between $43 - 107$ arcseconds [5] was higher than the reference standard of 22 - 50. The mosaic spread of 1.7 arcminutes was also slightly higher than the reference 1.2, with the dominant low-temperature photo-luminescent emission peaks at 1.59 eV for both [1].

4.3 PEDESTAL DESIGN

4.3.1 Original Pedestal Design

The initial growth tube design was of a 32 mm ID tube containing a hand-made socket, as outlined in Chapter 3. A complementary flat-topped hollow cone, with a top-face diameter of 30 mm, was also made by hand to fit tightly into the socket. A 1 mm deep wide and 1.5 mm deep cross cut into the top face of the pedestal allowed tantalum wire of 150 μm diameter or 250 μm platinum wire to be attached to the outer diameter of the pedestal (as displayed in Figure 4.1). This wire allowed tight control of the annulus, with a gap all around the pedestal almost guaranteed by the four lengths of wire.

The high cost of single crystals of CdTe and CdZnTe (about $2000 for a millimetre thick 52 mm diameter CdTe single crystal) severely limited their availability, and cheaper multi-grain seeds had to be used until the system was optimised. Two-millimetre thick multi-grain CdZnTe crystals were used as seed crystals in the initial growth runs because a stock of these crystals was available. At this time there was an outside interest in availability of 22 mm diameter CdTe crystals, therefore early growth runs concentrated on the growth on CdTe crystals instead of making an attempt to grow CdZnTe crystals. 22 mm diameter octagons were cut out of larger 60 mm diameter CdZnTe crystals using a diamond saw, and were mechanically polished with decreasing alumina grit size, beginning with 12 μm grit and ending with a 3 μm grit giving a smooth finish. The crystal was subsequently chemically polished for 3 minutes on a hydroplane polisher using a bromine – methanol etch, and finally cleaned overnight using hot IPA in a reflux system. The seed crystal was removed from the reflux system immediately prior to loading in the growth tube, and care was taken to ensure the 22 mm seed crystal sat in the centre of the 30 mm pedestal after the growth tube had been placed in its furnace in the MTPVT system, keeping the seed away from the growth tube walls.

During the early growth runs several problems arose, such as lamp failure, the existence of cold-spots on the glassware and leaks from the glassware, often perturbing material transport and causing the sublimation of the seed crystal. The first complete cycle of the MTPVT system, Run 36, took place with a source temperature of 870°C and a seed temperature of 700°C, and a polycrystalline CdTe boule was grown on the multi-grain CdZnTe, named 'Alex', and is displayed in Figure 4.1.

Figure 4.1: Photograph of 30 mm diameter CdTe boule 'Alex' grown on multi-grain CdZnTe seed, during Run 36, sitting on cone pedestal with tantalum annulus wires visible

Alex was 5 mm deep, weighed 23.5 g with a diameter of 32 mm, the same diameter as the growth tube and much greater than the seed diameter of 22 mm. After Alex was cut into strips, it was clear nucleation occurred on the bare glass regions of the pedestal and CdTe grew faster on this region than on the seed crystal, until this polycrystalline growth reached the level of the top face of the seed, after which this growth spread over the top of the seed crystal and the whole area began to grow upwards at the same rate. This evidence can be seen in Figure 4.2, with the border of the seed and overgrowth clearly visible.
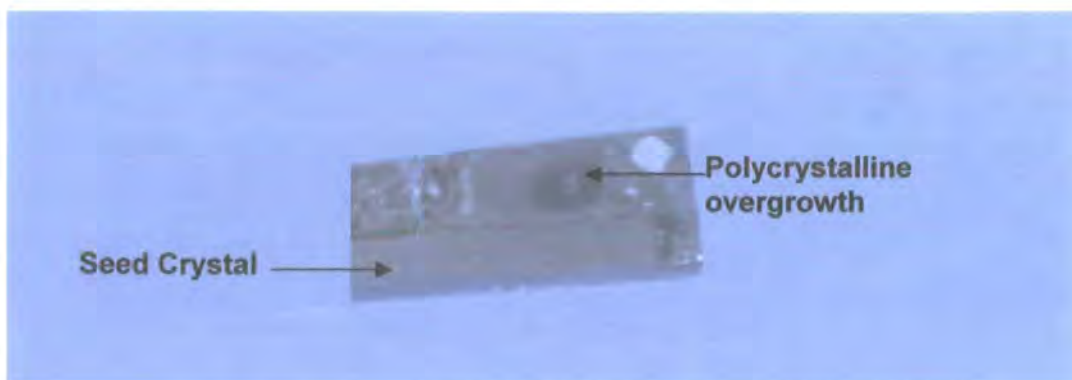
Figure 4.2: Photograph showing evidence of polycrystalline overgrowth in 30 mm diameter CdTe boule Alex after the material was cut

Subsequent growth runs using the same pedestal setup displayed the same overgrowth effects. This overgrowth may be because the pedestal was at a lower temperature than the seed crystal, since the transparent pedestal would absorb less radiation than the opaque seed crystal, leading to a higher nucleation rate. Once a layer of nucleation had occurred on the glass pedestal this polycrystalline material would grow at a faster rate and naturally overtake the growth on the seed crystal.

To counter the overgrowth a 20 mm diameter solid quartz disc, with a height of 10 mm, was placed directly onto this pedestal and the 22 mm seed crystal placed on top of this disc. The top face of the disc was therefore completely covered by the seed, and the extended distance between the seed and the pedestal would reduce the likelihood of the pedestal-nucleated growth overcoming the seed crystal. Growth Run 39 took place with this configuration, with a growth temperature of 700°C. During this run the seed crystal appeared to sublime away and the spurious nucleation on the bare pedestal continued to occur.

The evidence from these early growth runs allowed several conclusions to be drawn:

- The seed crystal should cover the pedestal surface

- The pedestal should be constructed of a solid material (hollow pedestals may absorb too little heat)

- Bare glassware should be kept to a minimum

4.3.2 Solid Disc Pedestal

Drawing on the evidence of overgrowth on the cone pedestal, the pedestal was re-designed into the form of a 32 mm diameter, 10 mm deep solid quartz disc. Initially this disc was placed directly onto the top of the socket in the growth tube. With this setup there was little control on the size of the annulus gap, which was determined by the dimensions of the pedestal and the inner diameter of the growth tube, and the gap between the base of the pedestal and the top face of the socket. No tools were available to accurately measure the inner diameter of the growth tube around the growth region, and the pedestals needed to be found by the trial and error method of grinding down the pedestal until it could be inserted into the growth tube. The uncertainty in this annulus gap was much larger than with the wire method for the cone pedestal.

At the time the disc pedestal was introduced the only seeds available were the 22 mm diameter CdZnTe crystals which had been cut for the previous pedestal design. In Run 42 a mosaic of smaller pieces of CdZnTe crystal were used to cover the pedestal, as had been found necessary to prevent overgrowth, and a 22 mm polished seed placed on top of this mosaic, as presented in Figure 4.3.
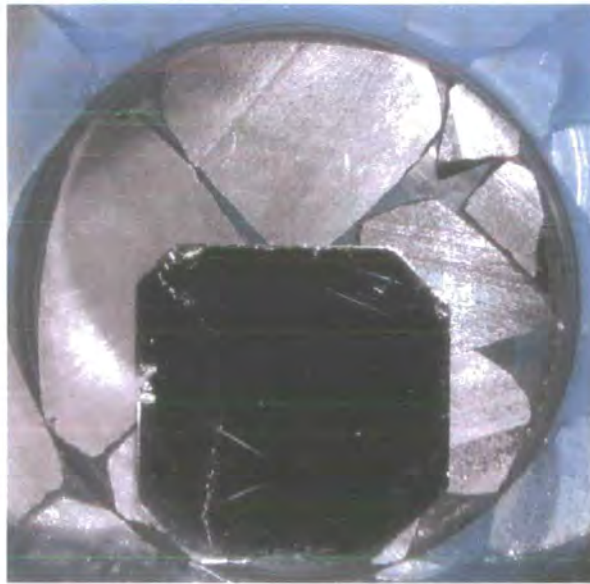
Figure 4.3: Photograph of mosaic and multi-grain CdZnTe seed used to grow 32 mm diameter CdTe boule 'Bea' in Run 42

After 20 hours at the growth temperature of 675°C the seed and mosaic had grown by 30.1 g in total, forming a large CdTe boule, named 'Bea', and displayed in Figure 4.4.

Figure 4.4: Photograph of 32 mm diameter CdTe boule 'Bea' grown on mosaic and seed arrangement displayed in Figure 4.3, showing polished top face (left) and base view (right) displaying presence of original mosaic

An outline of the mosaic and seed crystal was visible on the top growth face of Bea once the surface had been mechanically polished, indicating there had been growth on the CdZnTe crystals and overgrowth had not taken over

the crystal surface. This was evidence the crystal would grow according to the seed if the pedestal was covered. The base view of the crystal implied that nucleation on the pedestal had bound the regions of mosaic together to form the large boule.

In the following growth run (Run 43) Bea was placed directly onto the disc pedestal and another CdZnTe seed placed on top (Figure 4.5). During the growth run an optical window on the crossmember cracked, and the run had to be aborted, but the crystal height still increased by 5 mm. Nucleation had occurred around the socket at the top of the growth tube, causing the pedestal to stick inside the growth tube, and upon removal the grown boule (Charlotte) cracked along the lines of the gaps in the mosaic (see Figure 4.5). The boule had grown on the faces of the mosaic crystals, but pedestal nucleation had also occurred, preventing growth on the mosaic faces overlapping. This ruled out the possibility of using a mosaic of smaller crystals to grow larger-diameter crystals.
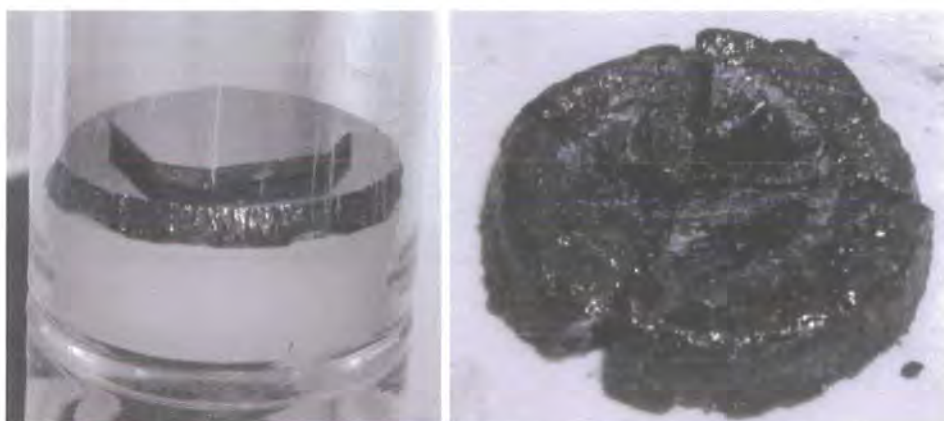
Figure 4.5: Photographs of multigrain CdZnTe seed on 32 mm diameter CdTe boule 'Bea' used as seed for CdTe growth in Run 43 (left), and resulting boule after CdTe growth (right) showing breakage along mosaic edges

The annulus around the growing crystal served two purposes; to enable flow past the crystal into the dump tube and to prevent growth of the crystal onto the walls of the growth tube. Placing the pedestal upon the socket prevented contact directly with the tube walls, but the flow restriction tended to stop as nucleation on the top of the socket regularly sealed the gap.

4.3.3 Silicon Substrate

Temporary unavailability of 32 mm diameter CdTe or CdZnTe seed crystals led to the trials of other materials as substrates for growth. Thin films of CdTe have been grown by MBE on both silicon and GaAs substrates [6] despite the lattice mismatch of the materials [7]. The mismatch was overcome as the lattice strain relaxed in the overlayer due to the action of misfit dislocations, and despite the different pressure regimes and growth rates in MBE and the MTPVT, the possibility existed to grow good-quality CdTe on substrates of these materials.

To test the feasibility of growth on silicon substrates, a thin (<0.5 mm) 30 mm diameter (111) Si wafer was placed on the 32 mm disc pedestal and a standard growth run completed, with the source temperature held at 870°C and the seed at 700°C. Observations of the seed during growth saw nucleation take place on the bare pedestal area around the Si seed, and this CdTe subsequently overgrowing across the Si face. Inspection of the growth tube after removal from the kit found polycrystalline growth throughout the pedestal region with the crystal sticking so strongly to the tube walls the tube cracked during the cooldown. Therefore the test of the use of Si as a substrate was inconclusive, but the experiment suggested another use of Si during the growth of CdTe. CdTe was observed to grow faster on the

glassware than the Si, and if CdTe would grow faster on a CdTe or CdZnTe seed than silicon, then Si could be used as a buffer between a quartz pedestal and an undersized seed.

A 25 mm diameter octagonal CdZnTe seed was separated from the pedestal by a 32 mm diameter Si buffer wafer during Run 45 (see Figure 4.6 a)) to test the use of the buffer. During the growth period CdTe was observed to nucleate on the Si buffer and overgrow the CdZnTe seed. The seed crystal did not sublime, as the outline of the seed was visible on the underside of the grown polycrystalline boule (Figure 4.6 b)), therefore the growth was faster on the Si buffer than the CdZnTe seed, and Si was not a suitable buffer to permit the use of undersized seed crystals.
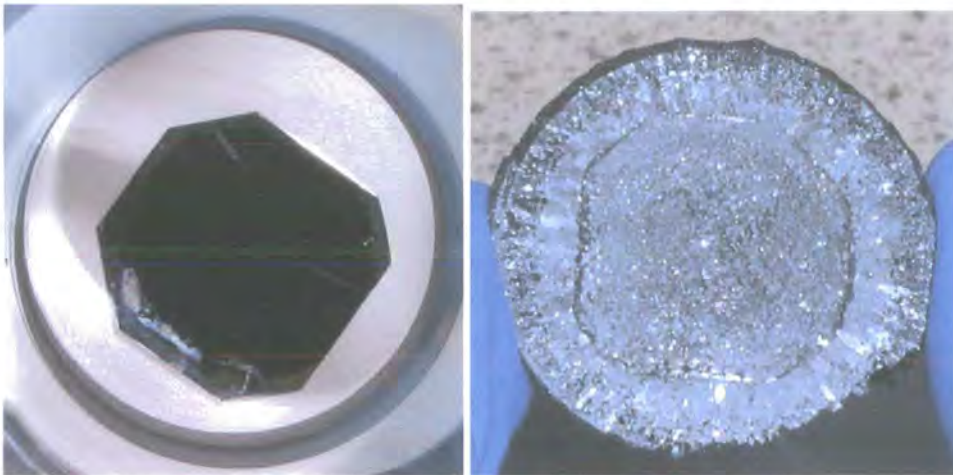
Figure 4.6: Photographs of 25 mm multigrain CdZnTe seed and 32 mm Si buffer used as seed arrangement in Run 45 (left), and boule base after CdTe growth run (right) showing presence of original seed

4.3.4 Open Annulus

The annulus formed by resting the solid disc pedestal upon the socket in the growth tube was regularly blocked during growth, and another method of

suspending the pedestal in the growth tube was sought. Three inward-pointing indentations in a straight growth tube held the disc pedestal whilst allowing vapour flow through the annulus gap around the pedestal (the arrangement is displayed in Figure 4.7). With this setup the size and shape of the annulus gap was entirely dependent upon the size and shape of the pedestal and inner wall of the growth tube. The standard tolerance of the diameter at any point on a 32 mm ID quartz silica tube was ±0.5 mm, with a potential difference in diameter of 1 mm between the top and pedestal region of the growth tube. Pedestals were individually ground to fit tightly into the growth tube, but this still left open the possibility of a tight fit (e.g. ~0.1 mm clearance) at the tube entrance but a large annulus (~1 mm) at the critical region around the growing crystal.

Figure 4.7: Photograph of 32 mm solid disc pedestal supported by dimples first used in Run 50

Repeated growth runs with this pedestal setup and a 32 mm diameter circular multi-grain seed illustrated the annulus gap was a very important determining factor for the crystal growth and annulus flow rates. In Run 55, which took place with the standard temperature conditions (see Figure 4.8), the mulit-grain CdTe seed was seen to sublime away as the growth temperature was ramped up to the 710°C standard. Clearly the annulus was too large, as 27 g of CdTe was found to have condensed beyond the annulus, 8 g of which was the mass from the sublimed seed crystal and the other 19 g was transported from the CdTe source tube. Run 54, however, took place with the same temperature profiles and pedestal design, but with a different pedestal and growth tube, the multi-grain CdTe seed crystal did not sublime. 31 g of CdTe entered the growth tube, with 23 g growing onto the crystal and only 8 g flowing beyond the annulus. Hazel, the crystal grown, was very polycrystalline and the annulus had become blocked.
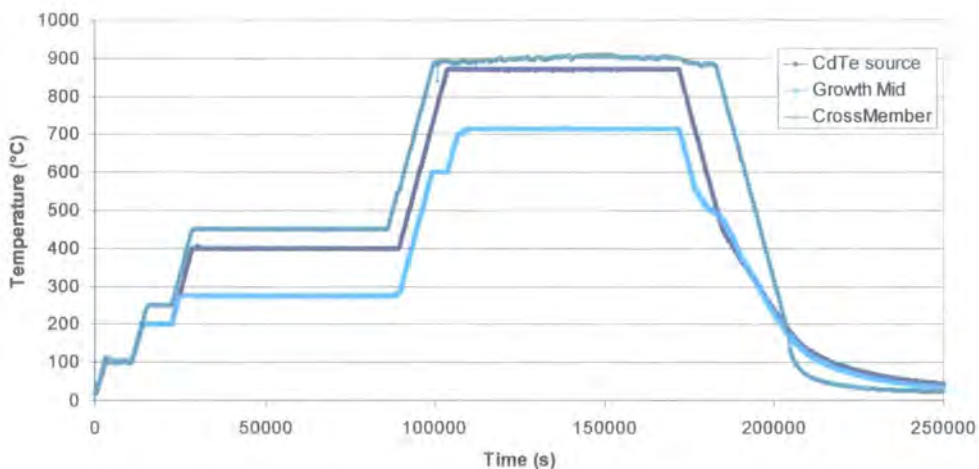
Figure 4.8: Source, growth and crossmember temperature profiles of Run 55. The hold in growth temperature is visible around 100 000s.

The standard temperature profile used in these growth runs involved heating the crossmember, growth tube and source tube at the same rate (2 K/min) from their differing bake-out temperatures, holding the growth middle temperature at 600°C for one hour, before raising this growth temperature to 710°C. Increasing this growth middle hold time and reducing the hold temperature decreased the probability of the seed crystal subliming but increased the probability of the annulus blocking and acting as a nucleation point for polycrystalline growth.

An alternative temperature profile, presented in Figure 4.9, involved heating the growth tube at a slightly slower rate than the crossmember and source tubes (about 1.8 K/min, compared to 2 K/min, depending upon the target) to allow the maximum source temperature to be reached at the same time as the growth temperature. This reduced the likelihood of subliming the seed crystal, since the seed crystal pressure increase was matched by the pressure increase in the source tube, and also allowed the annulus to remain free as no period of great capillary transport existed.
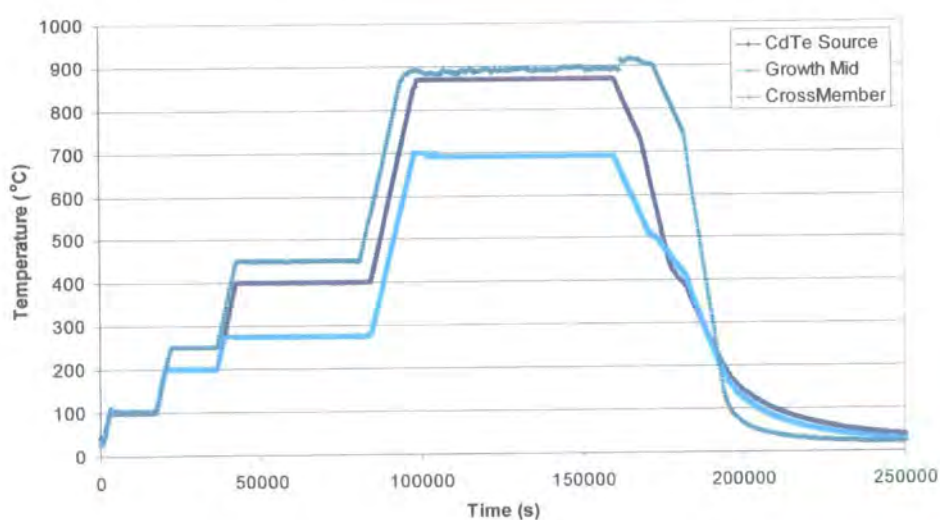
Figure 4.9: Temperature profile of Run 64 showing slower growth ramp rate with no hold period around 100 000s.

The indentations in the growth tube were formed by heating the area towards the softening point and pushing a rod gently into the side of the tube. This method allowed little control over the size and the tube position of the dimples, making it almost impossible to place three identical indentations at the same height. Consequentially the pedestals did not sit exactly horizontally in the tube, and during the growth runs the boules produced were regularly wedge-shaped.

4.3.5 Large Diameter Growth Tube

Evidence from the growth runs using the 32 mm ID growth tube implied the annulus gap was too variable and greatly influenced the growth process, leading to irreproducibility of the crystal growth. Tighter control of the annulus size was required to improve reliability of the growth. Results of the modelling of the growth process (which will be discussed in Chapter 7) illustrated the annulus had a greater influence on the growth in small growth tubes than in larger diameter tubes.

The MTPVT system was redesigned to accommodate a 52 mm ID growth tube, with the source tubes remaining at their original sizes. Special "Precision" quartz silica tubing, with a lower tolerance of ±0.25 mm on the tube ID, was used to form the growth region of the growth tube to give tighter control on the annulus gap. A new method of producing the growth tube also allowed the diameter around the pedestal to be more accurately measured. The pedestal rested on a 25 mm diameter 20 mm long quartz silica tube with both ends ground flat which in turn was placed on a cross formed by glass-welding three quartz rods together and to the growth tube inner wall (as displayed in Figure 4.10). This configuration ensured the pedestal sat

horizontally with no distortions around the annulus which could perturb free flow.
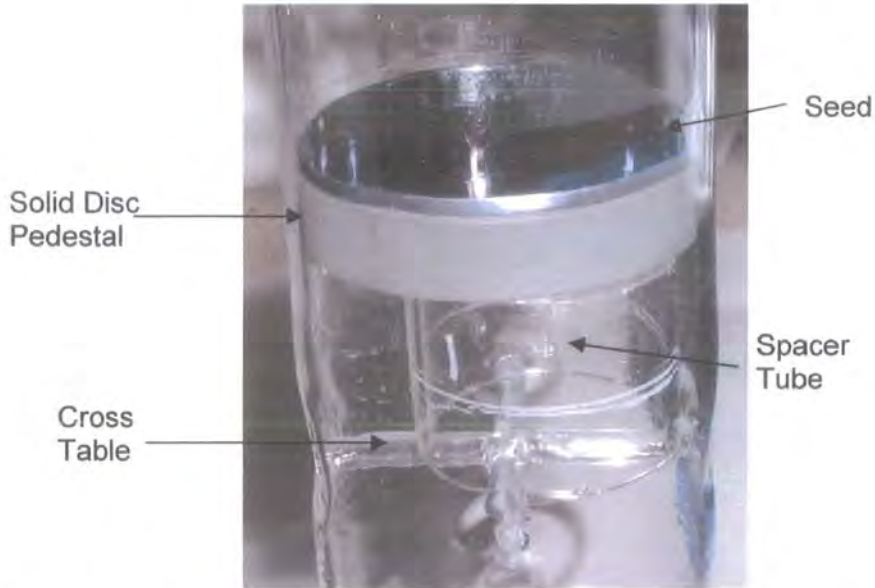
Figure 4.10: Photograph of 52 mm diameter growth tube containing pedestal with spacer tube and cross table

4.3.6 Radial Temperature Gradient in Growth Tube

The wedge-shaped growth observed during growth runs with the 32 mm tube was still observed during several growth runs with the 52 mm growth tube, and was more pronounced than in the smaller tube. The pedestal was horizontal to within approximately 5° with the new pedestal setup, and this uneven growth indicated that a radial temperature gradient existed in the growth tube.

Stresses exceeding the Critically Resolved Sheer Stress (CRSS) allow dislocations to multiply in the growing crystal, and, to reduce the stress, the temperature difference across the crystal should be kept to a minimum. The maximum temperature difference allowed (ΔT) can be estimated using Young's modulus E for the crystal, defined as $E=stress/strain$

$$\Delta T \leq \frac{CRSS}{E\alpha} \qquad\qquad (4.1)$$

as the thermal strain

$$\frac{\delta l}{l} = \alpha\Delta T \qquad\qquad (4.2)$$

The linear expansion coefficient α can be considered constant at temperatures above room temperature [3], and using the values given in Chapter 2 for α (5.5×10^{-6} K^{-1}), E (4.5×10^{10} Pa) and the CRSS (0.5 MPa), it can be seen that at growth temperatures

$$\Delta T \leq 2K \qquad\qquad (4.3)$$

During the initial testing period of the MTPVT system tests of the source heaters on their own gave rise to an increase in the temperatures around the growth tube. The temperature registered by the growth middle thermocouple (which measures the temperature at the growing crystal) reached 180°C when the graphite CdTe source heater was raised to 900°C without any power supplied to the growth heaters or crossmember lamps. With power supplied to the growth heaters the effect of the source heaters would have been reduced, but the wedge shape of the grown crystals implied this was not sufficient. Placing two extra steel plates between the source and growth regions, in addition to the shielding around the individual heaters, drastically reduced the wedge shape. Ophelia, which was grown in Run 66 before the extra shielding was introduced, measured 12 mm at one side and 10 mm at the other. After the shielding was introduced Yasmin, grown during Run 82, was found to measure 8 mm ±0.5 mm all around its perimeter. These effects can be seen in Figure 4.11.
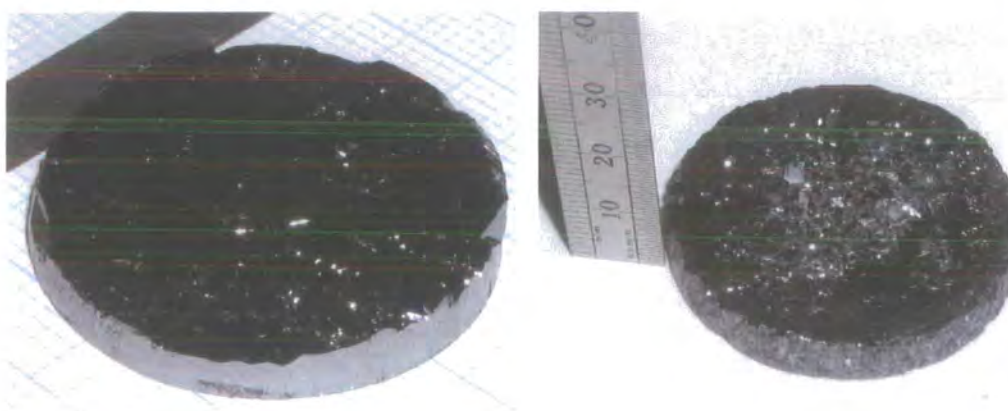
Figure 4.11: Photographs of 50 mm diameter CdTe boules Ophelia grown in Run 66 before introduction of additional shielding (left), and Yasmin grown in Run 82 after (right), showing reduction in wedge-shaped growth

4.4 SEED CRYSTALS

4.4.1 Growth on Multi-Grain Seed Crystals

The basic concept of the MTPVT system was to grow on and match the crystal structure of the seed crystal. Consequentially a single grain CdTe or CdZnTe crystal could not be grown on a multi-grain seed. A series of photographs of the growing boule were taken during Run 69 and are displayed in Figure 4.12, along with the time (hr:min) and seed temperature at which the photo was taken.

(a) *25:41,* 409°C   (b) *26:51,* 546°C   (c) *27:08,* 577°C
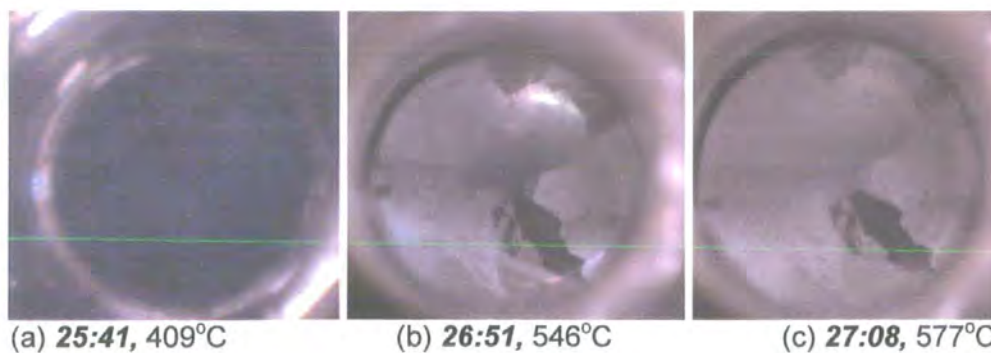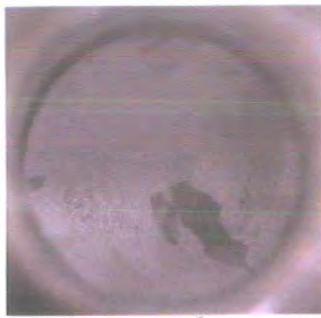
(d) *27:20,* 600°C
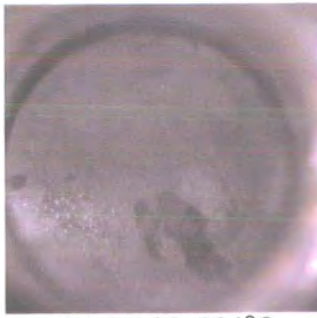
(e) *27:36,* 631°C
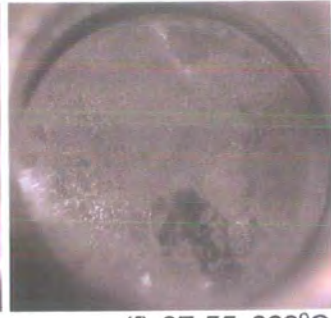
(f) *27:55,* 668°C
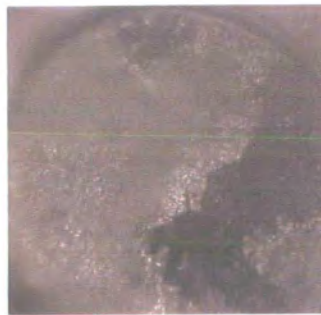
(g) *28:15,* 705°C
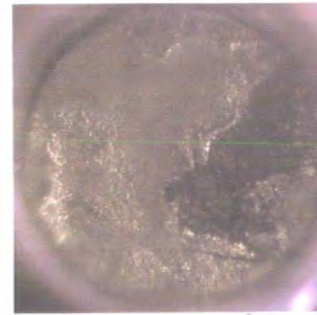
(h) *28:45,* 725°C
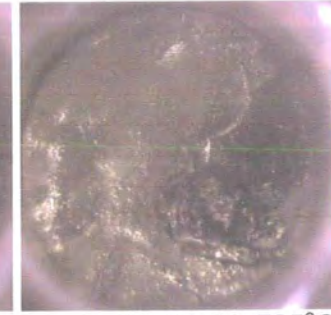
(i) *29:20,* 725°C

(j) *29:55,* 725°C
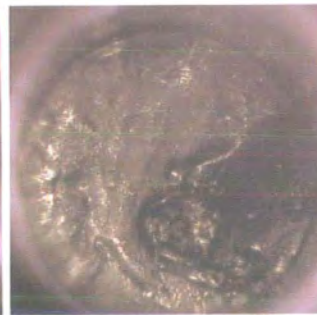
(k) *30:25,* 725°C
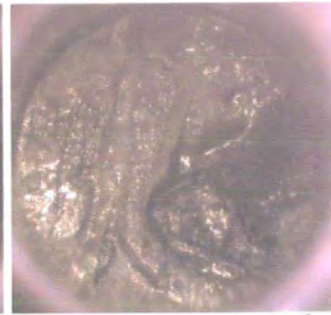
(l) *30:44,* 725°C
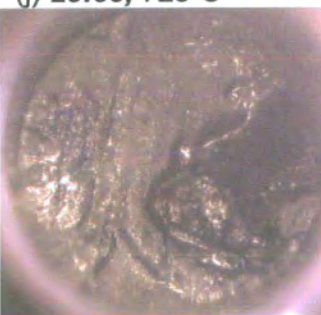
(m) *31:10,* 725°C

(n) *32:55,* 725°C

(o) *47:35,* 725°C
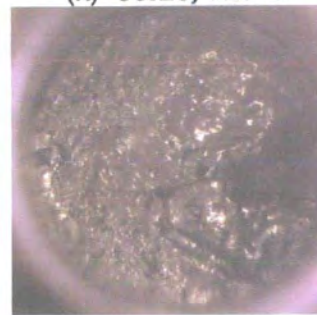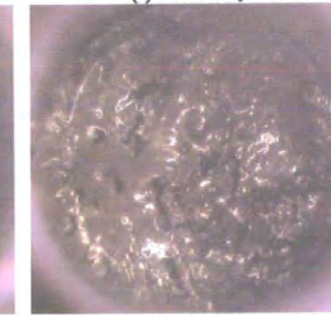
(p) **50:00,** 650°C   (q) **50:40,** 575°C   (r) **51:25,** 516°C
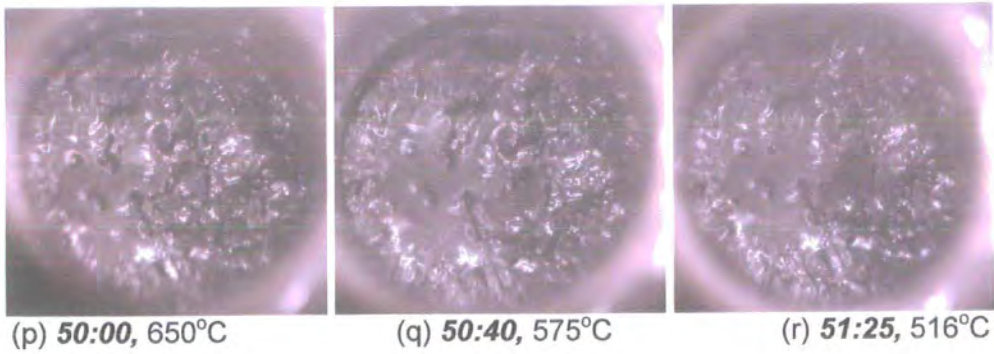
Figure 4.12: Photographs of evolution of growth on 52 mm diameter multi-grain CdTe seed crystal in Run 69, alongside time and seed temperature of each photograph

Pat, the grown boule, is displayed in Figure 4,13 after removal from the growth tube, and the corresponding temperature profile of Run 69 is given in Figure 4.14.
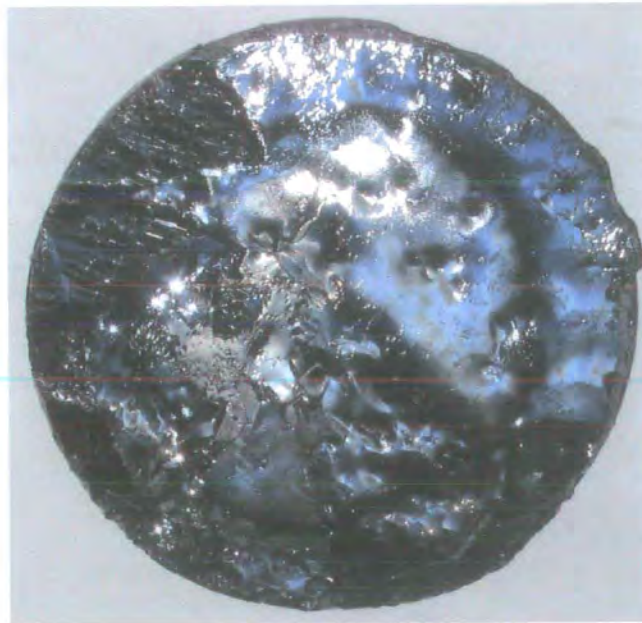
Figure 4.13: Photograph of 50 mm diameter CdTe boule 'Pat' grown on multi-grain CdTe seed during Run 69, after removal from growth tube showing features observed in Figure 4.12
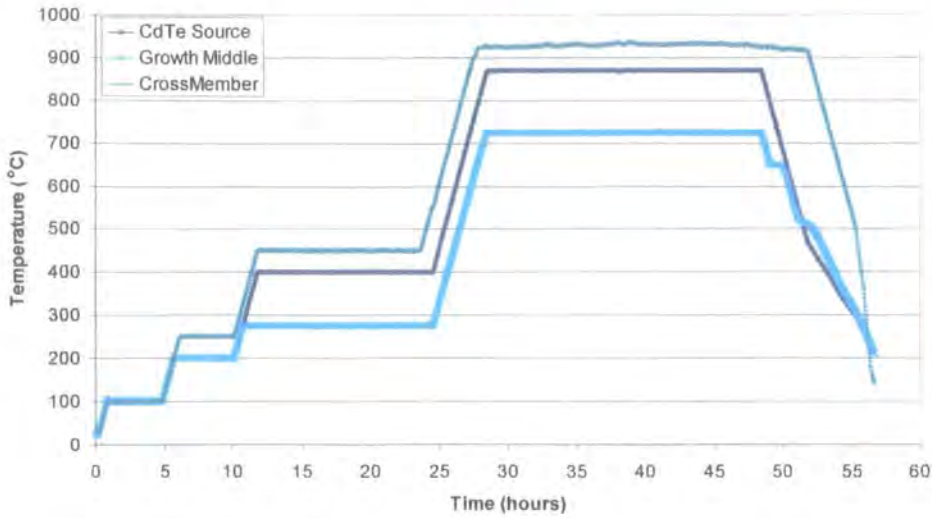
Figure 4.14: Temperature profile of Run 69

The mirror finish of the seed crystal seen in Figure 4.12(a) began to etch away as the growth temperature reached 550°C, and the individual grains started to emerge in 4.12(b). The surface appeared to roughen as the temperature increased, although it is not possible to tell if this was due to further etching of the crystal or nucleation on the crystal surface. Two prominent grains in the bottom right of the photographs appeared to grow at a higher rate in the early stages, and merged together to form a larger grain. This could be because some grains grew while other grains etched away as it is known that different crystal orientations grow preferentially, in particular the (111)b face which has previously been recognised as the face on which better growth takes place [8]. Further definition of the crystal face occurred throughout the growth period at 725°C, with hills and valleys appearing across the surface, with the area on the right of the crystal continuing to grow the quickest. These hills and valleys were not apparent on the crystal after its removal, with several pits and valleys visible in Figure 4.13 but without the density at which they appeared during growth. This is unlikely to be due to condensation during the cooldown process filling in the valleys, or

sublimation smoothing away the hills, since Figure 4.12(r) was taken when both the source and growth temperatures were around 515°C corresponding to low pressures with low sublimation and growth rate.

Other boules grown on multi-grain seeds illustrated the growth matching the seed crystal structure, with smooth growth on some areas of the surface and rougher growth in other areas.
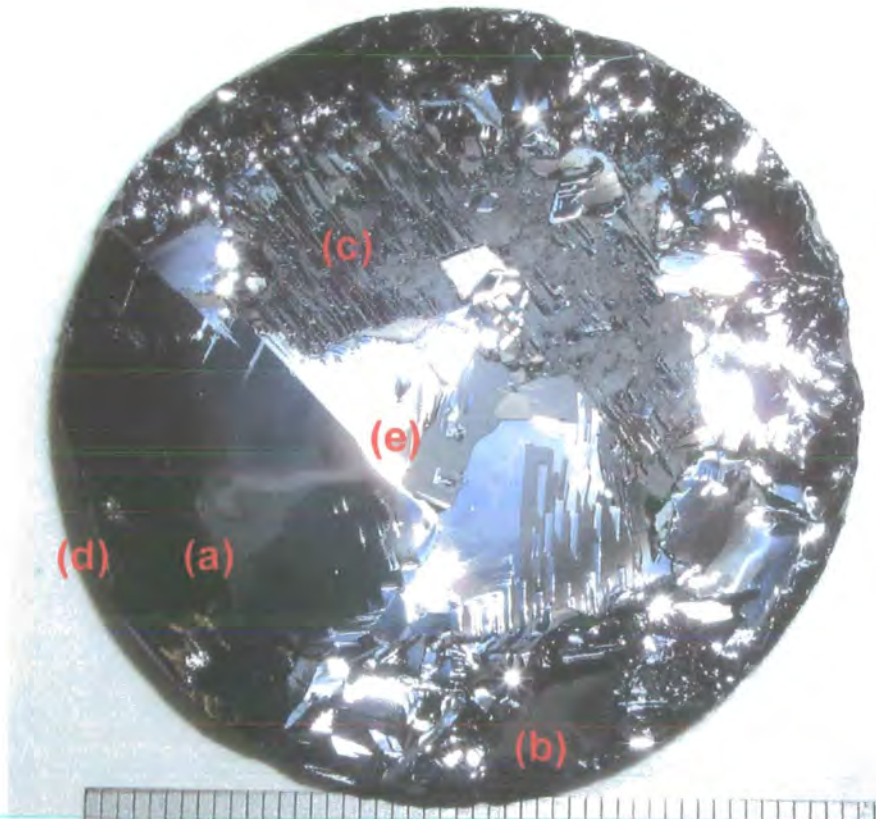
Figure 4.15: Photograph of 52 mm diameter CdTe boule 'Zoe', grown on multi-grain CdTe seed in Run 83, showing large grain with twins and facet on left hand portion

Several crystallographic features characteristic of CdTe growth are visible in the photograph of Zoe in Figure 4.15. The smooth region (a) has very sharp boundaries with the other regions, and the twin bands appearing to

propagate from the grain boundary at about 70° suggests the surface is close to (111). The facet at (d) on the left of this region implies regular growth of the crystal. Region (b) contains a number of visible twin bands which lie on {111} planes. Although region (c) is highly terraced it is possible this region is a large grain which has been thermally etched, although some spurious nucleation appears at different positions of this region. These features are accentuated on the surface after a small amount of lapping, as displayed in Figure 4.16.
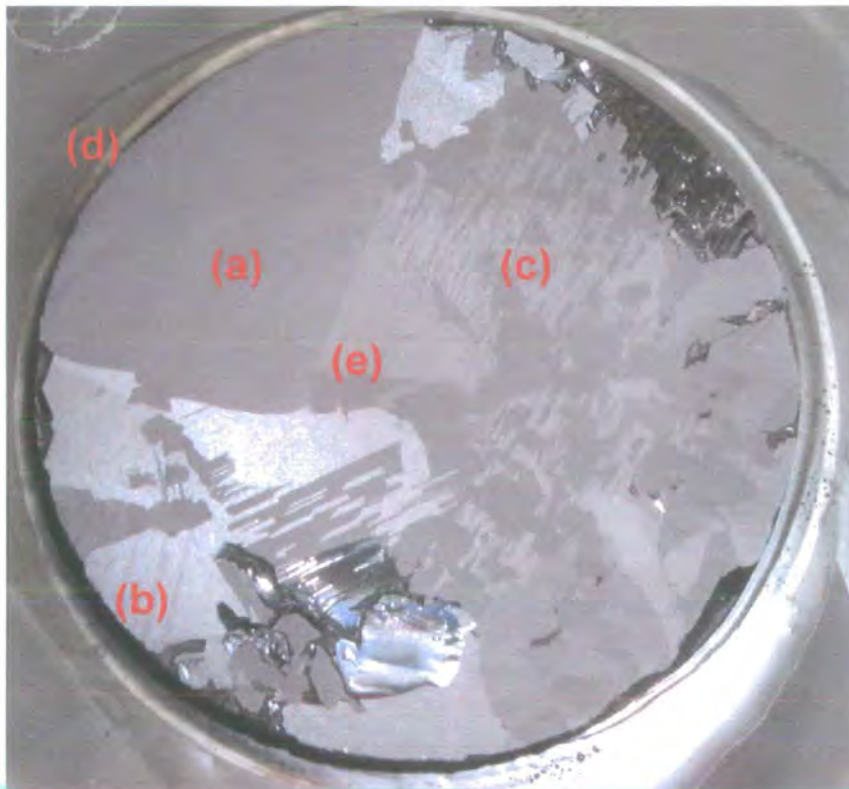
Figure 4.16: Photograph of lapped surface of Zoe, 52 mm diameter boule grown on multigrain CdTe seed in Run 83, displaying features visible in as-grown surface in Figure 4.15

Seed temperatures between 675 and 735°C were used for growth runs with the large multi-grain seeds. At temperatures below 700°C polycrystalline growth tended to arise around the annulus, and above 730°C very little

growth occurred with a large mass flowing down the annulus. The best results appeared to occur for seed temperatures between 710 and 725°C, although other factors, in particular the seed quality, seemed to play just as important a role.

4.4.2 Growth on Single-Grain Seeds

The difference in growth quality between multi-grain and single-grain seeds is clearly apparent in Figure 4.17, a photograph taken during the growth on a 50 mm diameter single-grain crystal. The separate grains in the multi-grain seed are pronounced and can be seen to grow at different rates, while no areas of variable growth are visible on the single-grain seed.   When viewed by the eye the surface appears almost molten, although the photograph displays an uneven surface, which was initially believed to be a camera effect.
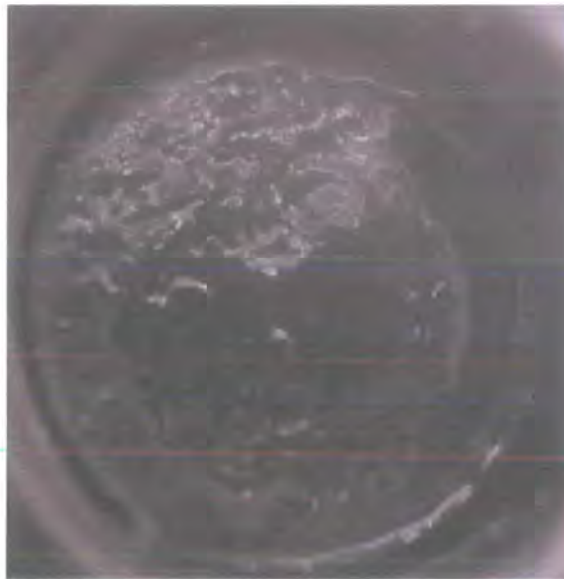
Figure 4.17: Photograph taken during growth of 52 mm diameter CdTe boule 'Amelie' in Run 85 on a single-grain CdTe seed crystal

Due to the high cost only a small number of {111} CdTe single crystals were available for use as seeds. Initial characterisation using X-ray diffraction with a beam size of about 2 mm confirmed the (111) surface throughout the crystals. The as-grown surface of Amelie displayed in Figure 4.18 contains a series of triangular pyramids similar to those observed by Teramoto [8, 9], although several small regions of spuriously nucleated growth are visible. A high density of pits is also visible around the edges of the crystal, and no large facets around the edges are observed.
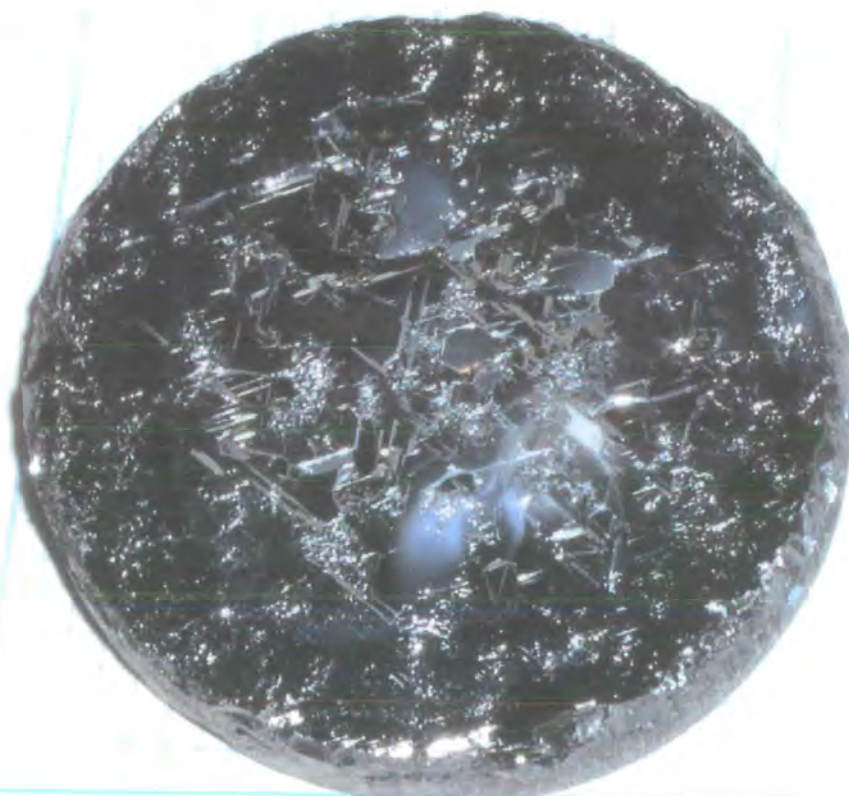
Figure 4.18: Photograph of 52 mm diameter CdTe boule 'Amelie', grown during Run 85 on single-grain CdTe seed, with growth pyramids visible

Slicing the crystal with a wire saw revealed what appeared to be a high density of twins in the body of the crystal. Polishing of the underside of the boule should have revealed the single crystal seed, but the seed also appeared to be highly twinned. Although it is unlikely twins were introduced

into the seed during the growth period, the results of the XRD on the seed revealed a (111) surface. It is possible that since the beam size (~2 mm) was larger than the size of the twins (~1 mm) there was always some diffraction from the (111) surface, and if the (511) surface (which is the common twin surface on {111} planes) was searched for similar results would have been observed.

4.4.3 Growth on a GaAs Seed

The use of Si as an alternative to CdTe as a seed crystal was described in section 4.3.4, and, with the poor quality of the crystals grown on Si, other alternatives were sought. Thin CdTe films have been grown on GaAs substrates, and three separate growth runs were made with 52 mm diameter 0.2 mm thick GaAs as the seed.

Growth at the standard MTPVT conditions (source at 870°C and growth at 710°C) produced a polycrystalline material very similar to the material grown on Si. Nucleation occurred on the GaAs surface at a fast rate, with polycrystalline growth overcoming the crystal early in the growth period. This growth rate was much greater than the rates obtained in thin-film techniques, which tend to produce strained films due to the lattice mismatch at the GaAs-CdTe interface, with the quality increasing the further from the substrate as the layer relaxes. To reduce the growth rate in the MTPVT system the source temperature was reduced to 850°C and the seed temperature raised to 750°C. During the growth, changes occurred on the seed surface, as can be seen in the photograph in Figure 4.19, but it is not known what caused these changes. White patches were seen on the surface, which were unlikely to be a grown film of CdTe, and may be due to As escaping from the seed. A ring

of polycrystalline CdTe growth appeared around the perimeter of the GaAs seed which may have nucleated on the pedestal, and this growth eventually enveloped the entire seed.

Figure 4.19: Photograph of 52 mm diameter GaAs seed taken during growth of CdTe in Run 75, with white patches visible on surface, and polycrystalline growth appearing around edges

4.5 GROWTH OF CdZnTe

One of the aims of the redevelopment of the MTPVT was to add a second source tube to permit the growth CdZnTe from the binary sources CdTe and ZnTe. The work plan of development was to optimise the system for the growth of CdTe crystals in the dual-source setup, and, once an acceptable standard of crystal quality had been achieved, to introduce a ZnTe source to grow CdZnTe. The demand for higher-quality CdTe single crystals altered the plan, leading to a change in emphasis of research from the growth of CdZnTe to the improved growth of CdTe. Preliminary experiments for the transport of

CdZnTe showed encouraging results, giving further opportunities for the development of growth of CdZnTe crystals in the MTPVT system.
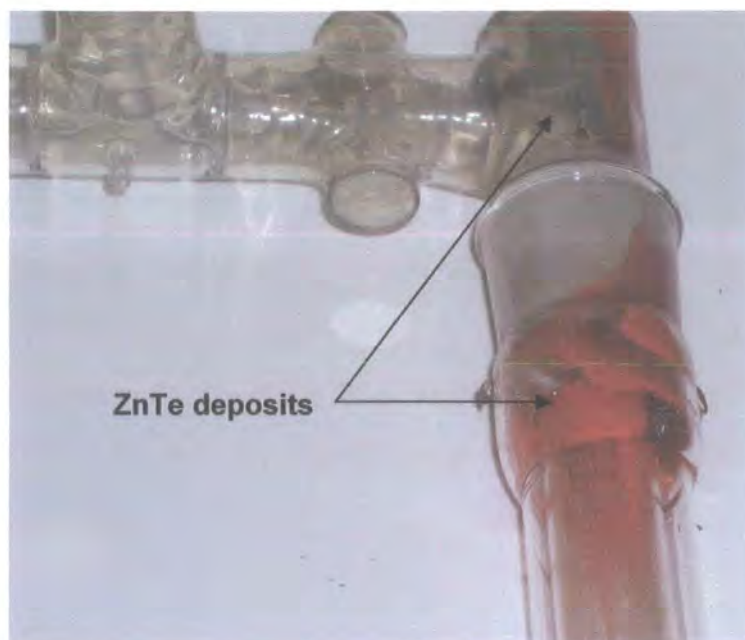
Figure 4.20: Photograph showing deposits of ZnTe on source tube and crossmember after growth of CdZnTe in Run 48

Two growth runs using both CdTe and ZnTe as sources took place in the MTPVT system. In both runs a large amount of ZnTe condensed at the top of the ZnTe source tube and upon the crossmember above (see Figure 4.20), and reduced the flow of ZnTe into the growth tube. Accurate measurements of the mass transport were difficult to obtain because the crossmember and ZnTe source tube could not be separated, but during Run 48 approximately 1 g of ZnTe flowed into the 32 mm growth tube along with 36 g of CdTe. The growth took place on an octagonal multi-grain CdZnTe seed with a Si buffer, and the material produced was highly polycrystalline CdZnTe containing approximately 3% zinc.

4.6 CHARACTERISATION OF GROWN MATERIAL

Visual inspection of the grown boule and any other material deposits in the glassware was the main method of characterisation of the material produced in each run, with the masses of the glassware and seeds before and after each run providing information on flow and growth rates. Polycrystalline growth, sublimation of the seed, wedged growth, spurious nucleation and regions of possible single-grain growth could be observed by eye, giving a general indication of the quality of the crystal produced. In addition, X-ray scattering measurements were undertaken on several crystals to provide a more qualitative description of the crystal structure, and 4-probe I-V measurements provided information on the resistivity of the material.

4.6.1 X-ray Diffraction Characterisation

X-ray scattering can provide a useful quantitative determination of a range of unknown crystal parameters, such as crystallite size and orientation, as well as the degree of in-plane mosaic. The orientation and lattice parameter can be obtained from the position in reciprocal space of the diffracted beam, with any extension of the diffracted beam along the direction of reciprocal space *parallel* to the surface (q_x) giving information about the mosaic spread, as illustrated in Figure 4.21. [10] Within each mosaic block, the crystal can be considered to be perfect, and the rocking curve caused by tilting the sample angle θ is defined by the intrinsic Darwin [11] width of the perfect crystal, which depends upon the material, energy and crystal orientation. [12] As the sample is rocked different parts of the crystal come into the diffraction condition, giving a total rocking curve width which is a convolution of all the Darwin widths from different regions of the surface in the x-ray beam.
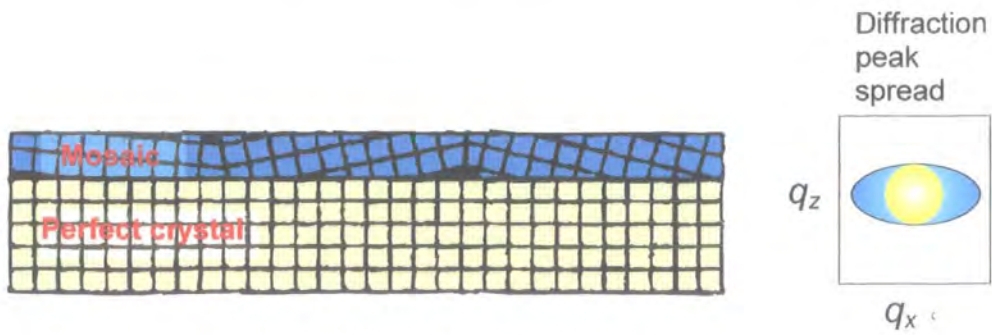
Figure 4.21: Broadening of diffracted beam by mosaic spread [11]

Natalie, a 52 mm diameter boule grown in Run 65 on a multi-grain CdTe seed was studied by Dr T. P. A. Hase using a Bede D1 X-ray diffraction system. Prior to an x-ray characterisation, the entire surface of the boule was polished to provide a smooth surface. As illustrated in Figure 4.22 the as-grown surface shows several crystalline areas, the region of study incorporated by the X-ray experiments covering the largest crystallite towards the top right of the photograph.
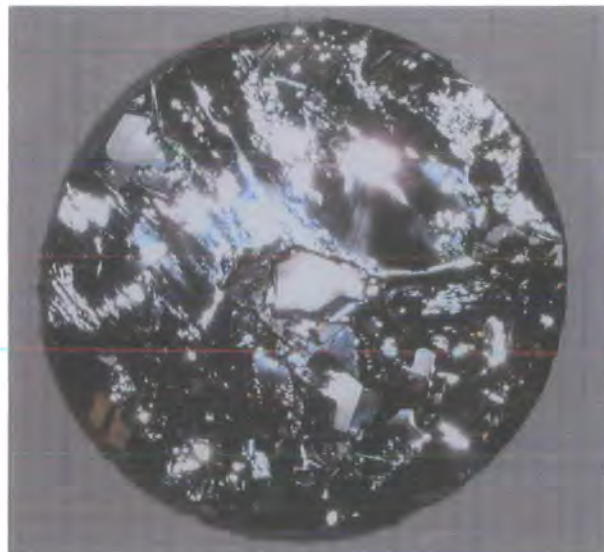
Figure 4.22: Photograph of 52 mm diameter CdTe boule 'Natalie', grown on multi-grain CdTe seed during Run 65, which was studied by XRD

X-ray diffraction was conducted with the D1 in the conventional double crystal geometry. A Cu tube source was monochromated using a two bounce Si 111 crystal to give a beam with low wavelength dispersion, $\Delta\lambda/\lambda \approx 1 \times 10^{-4}$, in a low divergent 2 mm beam spot. This sample was moved in the XY plane, so the beam probed a 30 x 20 mm region on the surface of Natalie. The angular acceptance of the detector was defined using a broad 3 mm slit.

The sample was aligned in the straight through (2θ=0) direction such that it was in the exact centre of the beam. Previous studies [9] indicated that the preferential growth of CdTe on such seeds is such that the {111} planes are normal to the sample surface. The sample angle was not reset from the initial alignment at 2θ=0. A strong diffracted intensity was found when the detector and sample angles were set to the {111} diffraction condition. However, it was only with the surface tilt set to $\chi = 27 \pm 1°$ to the vertical that the strongest intensity was found.

In order to quantify the quality of the crystal the mosaic distribution was measured as a function of the surface position (X,Y). The distribution of the mosaics were determined by a rocking curve whereby the sample, or specimen angle, was rocked by a small amount from the diffraction condition.

Figure 4.23 shows the rocking curve recorded at sample co-ordinates (25.26, -7.00) which lies towards the edge of the scanning region. It shows several features. The presence of multiple peaks shows that the surface is composed of many small regions, or crystallites, slightly misaligned with respect to each other. The peaks are sharp, showing that the within each crystallite the

surface is flat. A disadvantage of working at the {111} reflection is that the large number of mosaics detected may be due to the large footprint of the beam at these low sample angles. Working at the higher {333} reflection ensured a smaller footprint, but the intensity of the peaks was too low to allow characterisation to be undertaken over such a wide area.
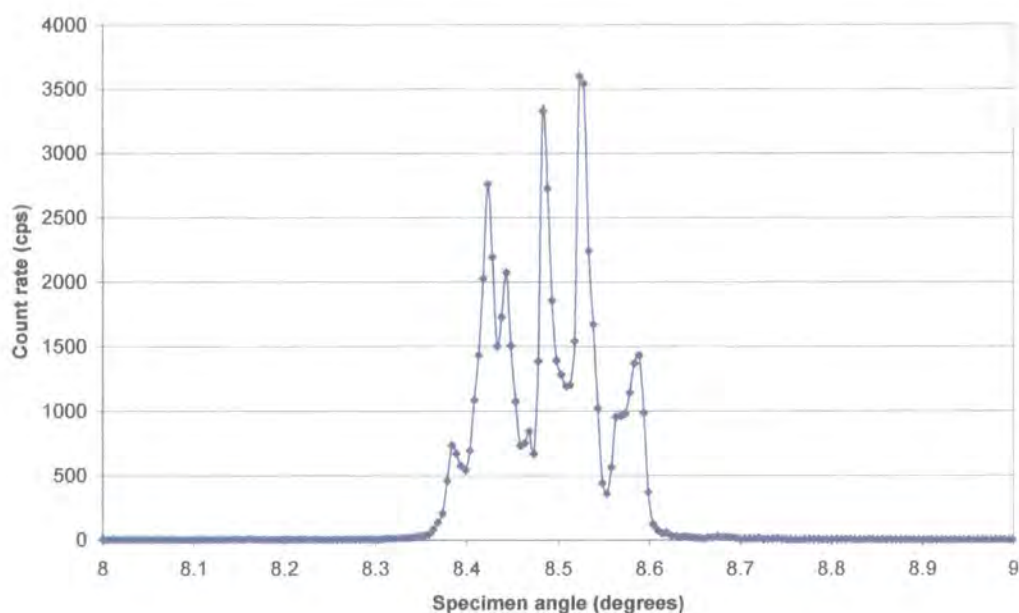
Figure 4.23: Variations in X-ray count rate with specimen angle at x = 25.26 mm , y = -7.00 mm

The contour plot of the position of the most intense peak, presented in Figure 4.24, shows a variation in specimen angle of about $0.75°$ over the scanned area, with the peaks at each point between 8.10 and $8.85°$. Even with the large number of peaks, there is a large systematic shift in peak position from the top left to bottom right, probably caused by a slight χ misalignment.
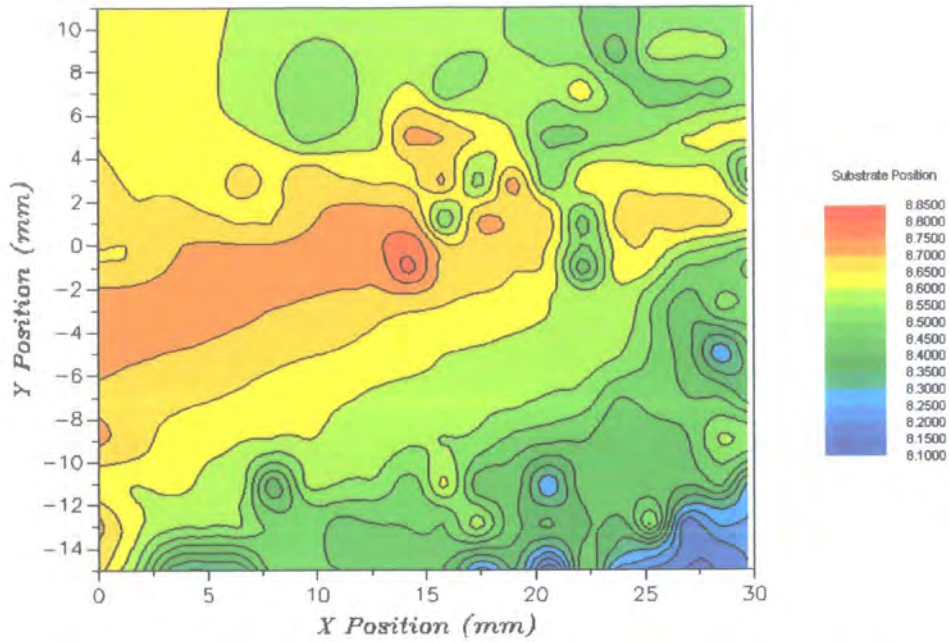
Figure 4.24: Contour plot of specimen angle of greatest peak across surface of CdTe boule Natalie

The widths of the peaks contained within the rocking curve give an indication of the local crystal order. The scan at position (17.37, -3.00), presented in Figure 4.25, implies the crystal was better towards the centre of the scanning region with only two peaks present in the rocking curve.
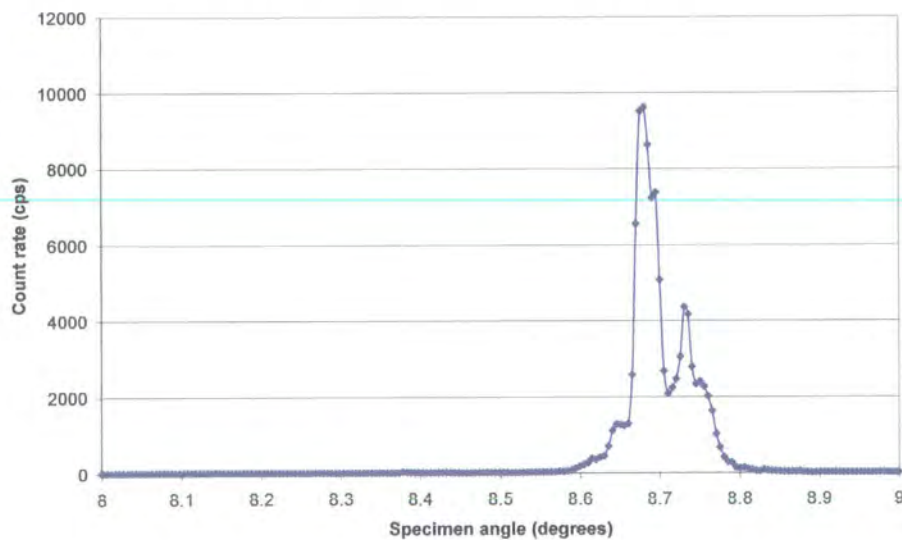
Figure 4.25: Variations in X-ray count rate with specimen angle at x = 17.37 mm, y = -3.00 mm.

The contour map of the full width half maximum (FWHM) given in Figure 4.26 confirms that the better region was in the centre of the scan area, with the FWHM around the limit of the detector at 36 arcseconds compared with over 500 arcseconds at another point. However, it should be noted that the FWHM contour plot shows the width of the most intense peak as a function of coordinate. The large number of peaks in the rocking curves makes more qualitative analysis impossible. There is no evidence that the large polished region seen in Figure 4.22 is in fact a single crystallite, with the X-ray data suggesting the presence of multiple grains. The offset of the {111} planes from the surface normal suggests that these grains may be oriented with the (110) normal to the surface, but further analysis is needed to confirm this.
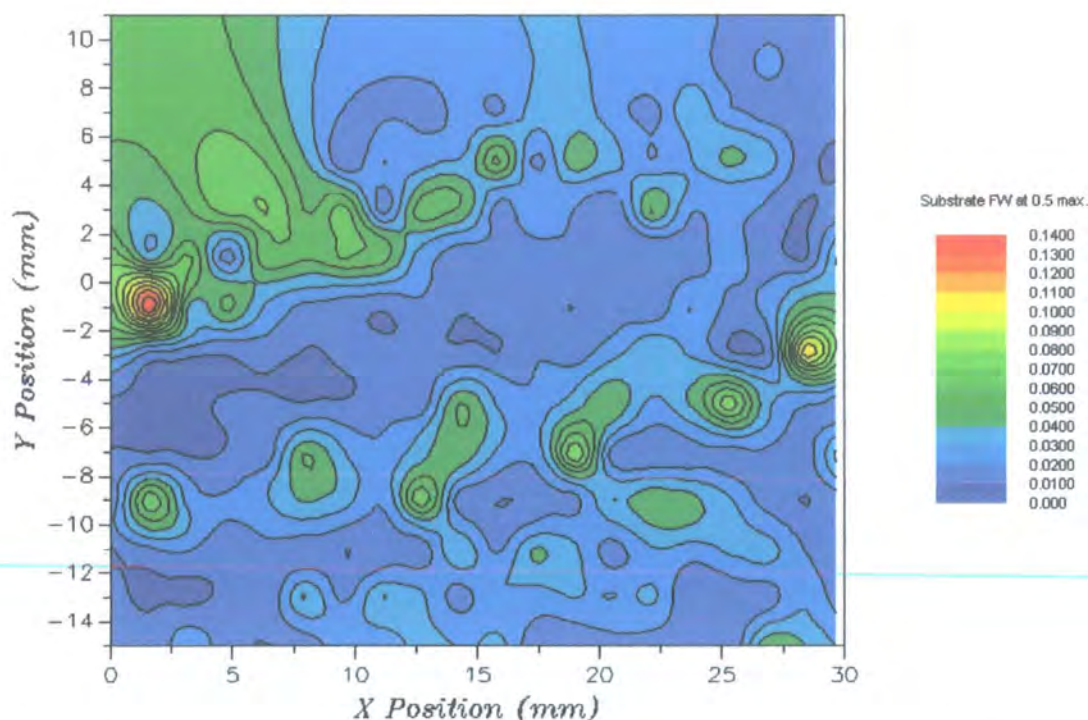
Figure 4.26: Contour plot of FWHM across surface of CdTe boule Natalie Armani *et al* [13, 14] studied crystals grown by both PVT and Vertical Bridgman (BG) methods, using XRD to probe the (333) reflection. They discovered a clear inhomogeneity in the BG sample, with a deviation in the sample angle of about 300 arcseconds and the FWHM ranging from 70 to

130 arcseconds. The PVT grown material had a FWHM of 245 arcseconds, greater than that of their BG material and also the majority of Natalie. They attributed this broadening to the presence of unstrained subgrains.

Fiederle *et al* [15] also studied material grown from the vapour phase (in a Modified Markov Technique), with one sample grown on a CZT seed and another in a self-seeding method . The rocking curve of the 220-reflex for the growth on a CZT seed found a FWHM of 31 arcseconds, while the self-seeded crystal possessed a FWHM of only 18 arcseconds.

A study of Bridgman-grown 10 mm diameter (111) CdTe single crystals, by Kumaresan *et al* [16], found the FWHM increased from 20 arcseconds in the centre of the crystal to 75 arcseconds on the edge of the crystal. Milenov *et al* [17] also investigated multi-grain crystals grown by the Bridgman method, and found the FWHM did not exceed 38 arcseconds.

As discussed in section 4.2, a study of many of the properties of 49 mm diameter CdTe crystals, grown in the original MTPVT system, found a range of X-ray rocking curve widths between 43 – 107 arcseconds [5]. The same study investigated other crystals available at the time and found the standard range was between 22 and 50 arcseconds.

Although the inconclusive data obtained by the XRD study of Natalie does not allow a foolproof comparison of the results with those in the literature, a simple comparison of the FWHMs places the best regions of Natalie within the middle of the range of literature values, although the greatest value of 500 arcseconds in Natalie is well above the literature standards. It should be

noted this value of the FWHM was only observed on one point on the surface of Natalie, with the next highest value at around 215 arcseconds, less than the value observed by Armani for PVT grown CdTe.

4.6.2 Resistivity Measurements

The resistivity of two samples, Estelle and Maria, were measured using a standard linear four-probe technique. Both samples possessed a low as-grown resistivity, Estelle 90 Ωcm and Maria 124 Ωcm. Doping the samples with chlorine, by heating to 550°C in a sealed ampoule containing $CdCl_2$, raised the resistivity above the detector standard 10^9 Ωcm threshold.

4.7 CONCLUSIONS

The growth of CdTe crystals in the redeveloped MTPVT system has been studied in this chapter. The design of the pedestal and seed crystal was of primary importance in growing on the seed crystal and not on the glassware. Several growth tube configurations were tested, and it was found that the best setup included a large-diameter tube containing a thick cylindrical pedestal held on a cross table.

CdTe boules have been grown on a number of different seeds, including multigrain CdTe and CdZnTe seeds, single CdTe crystals, and Si and GaAs wafers. The best results were seen on the multigrain CdTe seeds, and the growth on single crystal CdTe seeds needs further study.

Preliminary experiments to test the transport of the binary source CdTe and ZnTe for the growth of CdZnTe were carried out, with encouraging results, although further study would be required to optimise the process.

4.8 REFERENCES FOR CHAPTER 4

[1]   N. M. Aitken, M. D. G. Potter, D. J. Buckley, J. T. Mullins, J. Carles, D. P. Halliday, K. Durose, B. K. Tanner and A. W. Brinkman. *"Characterisation of Cadmium Telluride Bulk Crystals Grown by Novel 'Multi-Tube' Vapour Growth Technique"*. Journal of Crystal Growth **198/199** (1999) 984.

[2]   J. T. Mullins, J. Carles, N. M. Aitken and A. W. Brinkman. *"A Novel "Multi-Tube" Vapour Growth System and Its Application to the Growth of Bulk Crystals of Cadmium Telluride"*. Journal of Crystal Growth **208** (2000) 211.

[3]   J. Carles Alabert. *"Optical Vapour Pressure Monitoring and Mass Transport Control During Bulk CdTe Crystal Growth in a Novel Multi-Tube PVT System"*. PhD Thesis. University of Durham. (1998).

[4]   N. M. Aitken. *"Mass Transport Studies in the Growth of CdTe Crystals by Multi-Tube Physical Vapour Transport"*. MSc Thesis. University of Durham. (1999).

[5]   A. W. Brinkman, J. Carles, J. T. Mullins, J. B. Mullin, K. W. Benz, T. Kunz, C. Raptis, Y. S. Raptis, E. Sarantopoulou and F. Rustichelli *"A New "Multi-Tube" Bulk Vapour Growth Technique with Special Reference to CdTe and Its Characterisation"* Report for Brite EuRam project BRE2.CT94.0609 (1998).

[6]   M. Niraula, D. Mochizuki, T. Aoki, Y. Nakanishi and Y. Hatanaka. *"Low-Temperature Growth and N-Type Doping of CdTe by the Remote-Plasma-Assisted Metalorganic Chemical Vapor Deposition Method"*. Vacuum **59** (2000) 678.

[7]   P. D. Brown, H. Kelly, P. A. Clifton, J. T. Mullins, M. Y. Simmons, K. Durose, A. W. Brinkman, T. D. Golding and J. Dinan. *"TEM Studies of Cd:Zn:Te Based Superlattices and Epitaxial Layers"*. Mat. Res. Soc. Symp. Proc. **216** (1991) 427.

[8]   I. Teramoto and M. Inoue. *"Vapour Growth of Cadmium Telluride Crystals in the <111> Polar Directions"*. Philosophical Magazine **8** (1963) 1593.

[9]   I. Teramoto. *"Vapour Growth Patterns of CdTe Crystals"*. Philosophical Magazine **8** (1963) 357.

[10]   T. P. A. Hase. *"X-Rays & Neutrons"*. Durham (2000).

[11]   H. M. Rosenberg. *"The Solid State"*. Oxford University Press Oxford (1988).

[12]   A. Erko, N. V. Abrosimov and V. Alex. *"Lateral-Graded SiGe Crystals for High Resolution Synchrotron Optics"*. Crystal Research Technology **37** (2002) 685.

[13]   N. Armani, C. Ferrari, G. Salviati, F. Bissoli, M. Zha and L. Zanotti. *"Crystal Defects and Optical Transitions in High Purity, High Resistivity CdTe for Device Applications"*. Material Science and Engineering B **91-92** (2002) 353.

[14]   N. Armani, C. Ferrari, G. Salviati, F. Bissoli, M. Zha, A. Zappettini and L. Zanotti. *"Defect-Induced Luminescence in High-Resistivity High-Purity Undoped CdTe Crystals"*. Journal of Physics: Condensed Matter **14** (2002) 13203.

[15]   M. Fiederle, T. Feltgen, M. Rogalla, J. Meinhardt, J. Ludwig, K. Runge and K. W. Benz. *"Characterisation of Vapour Phase Grown CdTe and (Cd,Zn)Te for Detector Applcations"*. Nuclear Instruments and Metohds in Physics Research **434** (1999) 152.

[16]   R. Kumaresan, R. Gopalakrishnan, S. M. Babu, P. Ramasamy, P. Zaumseil and M. Ichimura. *"Quality Assessment of Bridgman-Grown Cdte Single Crystals Using Double-Crystal X-Ray Diffractometry (DCD) and Synchrotron Radiation".* Journal of Crystal Growth **210** (2000) 193.

[17]   T. I. Milenov and M. M. Gospodinov. *"Deformational Twinning in CdTe Crystals Grown by the Bridgman Method".* Material Science and Engineering B **84** (2001) 189.

Chapter **5**

Modelling the Growth of CdTe in the MTPVT System

5.1 INTRODUCTION

One of the main advantages of the MTPVT system is the ability to change the sublimation, growth and flow rates by altering a variety of independent parameters, such as the source and growth temperatures, annulus gap and the amount of material in the system. In order to fully utilise this adaptability, the effects of these parameters on the system must be known.

This chapter will present a new dynamic computer simulation developed to model the effects of the growth variables for the growth of CdTe in the MTPVT system. It will present the relevant theoretical background to the model and give an outline of the simulation itself. Results from the simulation will be given, and their relevance discussed. These results will be compared with actual data taken from growth runs in the MTPVT system, and compared with earlier attempts to model the growth.

5.1.1 Previous Models of MTPVT Growth

Three previous attempts have been made to model the growth of CdTe in the MTPVT system. Carles-Alabert [1] developed an analogue model of the transport of CdTe by considering the growth process as a series of conductances. The conductances of the crossmember capillary flow restrictor and annulus gap were derived, however no effort was made to quantify the transport. The partial pressure ratio in the growth tube was determined through the characteristics of the annulus gap, although the ratio in the source tube was not investigated.

Aitken [2] attempted to quantify the transport through the crossmember capillary through a numerical integration of the transport through the capillary. Aitken experimentally determined the characteristics of the capillary, and used this to quantify the flow rate. A Microsoft Excel Spreadsheet was used to calculate the flow rate according to the pre-entered growth temperature profile, recalculating at 10 second intervals, and numerically integrating over the growth time to determine the total mass transport. Broad unsubstantiated assumptions of linear growth of the crystal and the stoichiometry in the source and growth tubes were made, with no attempt to model these carried out. The flow through the annulus was also neglected.

Previous work by this author [3, 4] attempted to build on Aitken's work to obtain an algebraic expression for the integration of the capillary flow, which allowed the effects of the growth and source temperatures to be modelled. However, the basic assumptions of growth rate and stoichiometry inherent in the Aitken model were included, leading to incompleteness of the model.

5.2 THEORETICAL BACKGROUND

5.2.1 Stages of the MTPVT System

There are several regions in the MTPVT system which need to be incorporated into a simulation in order to accurately model the growth of CdTe. The species can exist in the source material, as a vapour in the source tube, as a vapour in the growth tube, in the growing crystal and in the dump tube beyond the annulus, and the simulation must model the transitions between these areas. Figure 5.1 gives a schematic of the MTPVT system indicating the main areas of interest and defines the flow and molar variables. Initially, there is the sublimation of polycrystalline CdTe into $Cd_{(g)}$ and $Te_{2(g)}$ [5]

$$CdTe_{(s)} \Leftrightarrow Cd_{(g)} + \frac{1}{2}Te_{2(g)} \qquad (5.1)$$

The source sublimation is followed by the presence of the crossmember capillary, which acts as a flow restrictor, reducing flow into the growth tube. In the growth tube the constituent vapours may condense onto the growing crystal or flow into a dump tube via the annulus gap. Each of these stages needs to be taken into account in the simulation. In this model the flow into the empty leg of the MTPVT system is neglected.

Conservation of mass requires that, assuming there are no leaks in the system, the total number of moles of Cd and Te_2 are constant, i.e. for species i ($i=Cd, Te_2$)

$$n_{Toti} = n_{scrysi} + n_{svapi} + n_{gvapi} + n_{gcrysi} + n_{anni} \qquad (5.2)$$

(see Figure 5.1 for explanation of symbols) and

$$\frac{dn_{Toti}}{dt} = 0 \qquad (5.3)$$

T_{cr}

Capillary flow
F_{capCd}
F_{capTe2}

Negligible flow to empty tube

Source vapour
n_{svapCd}
$n_{svapTe2}$

Ground glass joints

Growth vapour
n_{gvapCd}
$n_{gvapTe2}$

T_s

T_g

Sublimation
F_{subCd}
F_{subTe2}

Growth
F_{grCd}
F_{grTe2}

CdTe source
$n_{scrysCd}$
$n_{scrysTe2}$

Seed
$n_{gcrysCd}$
$n_{gcrysTe2}$

Pedestal

Annulus Flow
F_{annCd}
F_{annTe2}

To Dump Tube
n_{annCd}
n_{annTe2}
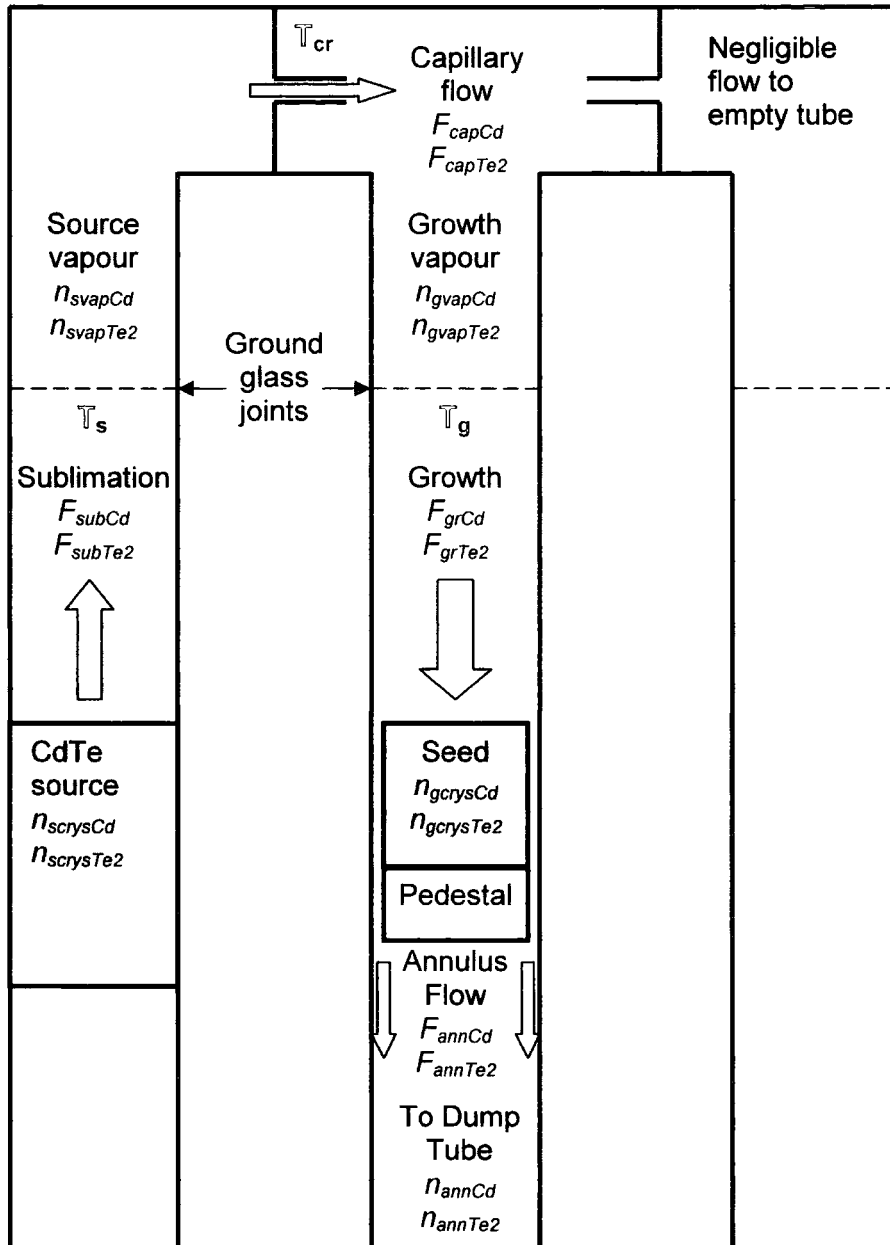
Figure 5.1: Schematic of MTPVT system showing flows and location of moles

At any time, the number of moles in each stage can be calculated using the number of moles in the previous time and the relevant flow rates.

Three temperatures are used to determine the rates in the system. The source temperature T_s determines the sublimation rate and the pressure in

the source tube, the crossmember temperature T_{cr} governs the capillary flow, and the growth temperature T_g determines the pressure in the growth tube and the growth and annulus flow rates.

5.2.2 Sublimation and Growth Rates

Although the CdTe seed crystals are hydroplane polished before their use the surface can not be said to be atomically flat. For the purpose of this simulation, the growth is assumed to be that of normal growth on a rough face [6], by the advancement of steps on the crystal surface through the incorporation of atoms / ions / molecules at preferential kink sites [7, 8].

Figure 5.2 displays the most important sites an atom can occupy on the crystal surface. The 5 sites are:

1) The atom is adsorbed onto the crystal face

2) The atom is adsorbed onto the step

3) The atom is in the half-crystal (kink) position

4) The atom is embedded into the step edge

5) The atom is embedded into the crystal plane
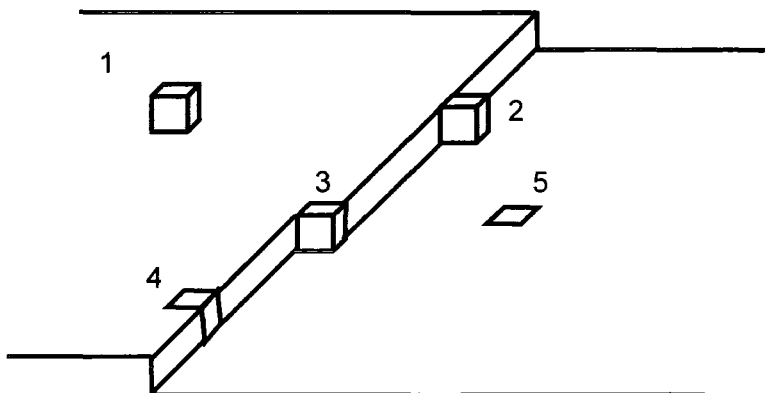
Figure 5.2: The 5 most important sites an atom can occupy on a crystal growth surface

Viewing the atoms as cubes with six faces, the atom at site 1 is bound to the crystal by one face or bond, and has five unsaturated bonds. The atom at site 5 however, has five saturated bonds and only one unsaturated. The attachment or detachment of either of these atoms, or atoms at sites 2 or 4, leads to a change in the number of unsaturated bonds of the crystal, therefore a change in the crystal surface energy. The atom at position 3, however, has three saturated bonds and three unsaturated bonds, so attaching or detaching an atom from this position does not alter the surface energy of the crystal. Thus, the crystal can be built up or eroded away by successive attachments or detachments of atoms at the kink site position.
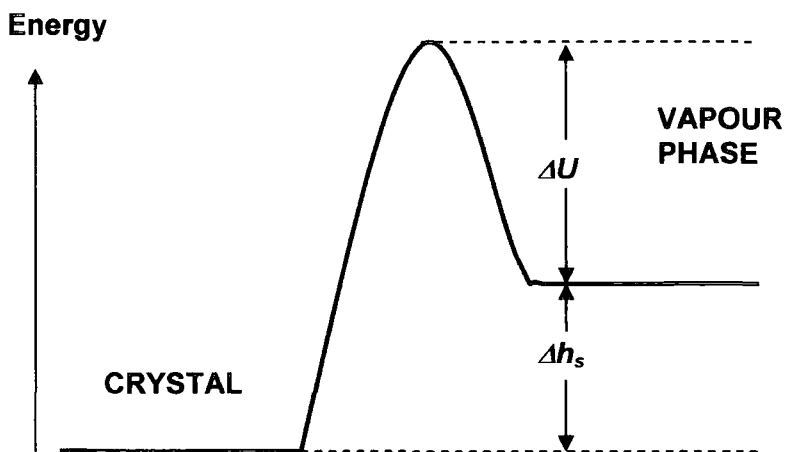
Figure 5.3: Variation of free energy for the transfer of atoms from the vapour phase to the kink position in the crystal

The growth rates are therefore determined by the rate of flux towards and away from the kink sites, and the probability of the atoms being incorporated into the kink sites once they arrive there. During growth from the vapour phase, the direct flux of atoms per kink site is [6]

$$j_+ = \frac{P}{\sqrt{2\pi mkT_g}} a^2 \exp\left(\frac{-\Delta U}{kT_g}\right)$$

(5.4)

115

where P is the pressure of the vapour, m is the mass of the molecule, k is Boltzmann's constant, T_g the growth temperature, a^2 the area of the kink site and ΔU the kinetic barrier.

The reverse flux away from the crystal is described by

$$j_- = v \exp\left(-\frac{\Delta h_s + \Delta U}{kT_g} \right) \tag{5.5}$$

where v is the molecular flux and Δh_s the enthalpy of sublimation. At equilibrium, the fluxes are equal $(j_+ = j_-)$, the pressure is the crystal equilibrium pressure $(P = P_\infty)$ and

$$\frac{P_\infty}{\sqrt{2\pi m k T_g}} a^2 = v \exp\left(-\frac{\Delta h_s}{kT_g} \right) \tag{5.6}$$

Therefore

$$j_- = \frac{P_\infty}{\sqrt{2\pi m k T_g}} a^2 \exp\left(-\frac{\Delta U}{kT_g} \right) \tag{5.7}$$

and the linear growth rate

$$R = \beta_v \left(P - P_\infty \right) \tag{5.8}$$

where β_v is the kinetic coefficient

$$\beta_v = \left(\frac{a}{\delta} \right)^2 \frac{a^3}{\sqrt{2\pi m k T_g}} \exp\left(\frac{-\Delta U}{kT_g} \right) \tag{5.9}$$

δ is the spacing between kink sites, and the probability of an inbound atom finding a kink site is $(a/\delta)^2$, which also gives the degree of surface roughness.

Equation (5.9) indicates that the growth rate is proportional to the difference between the vapour pressure and the crystal equilibrium pressure. Conversely, if the vapour pressure is less than the crystal equilibrium

pressure the crystal will sublime. Therefore equation (5.9) can be used to model both the sublimation of the source and growth on the seed in the MTPVT system.

The pressure in the tubes can be obtained from the ideal gas law [9, 10]. If the number of moles (*n*) in the gas is known, along with the volume of the tube *V*, then

$$P = \frac{nRT_g}{V}$$

(5.10)

Thus the linear growth rate can be converted into a molar flow rate for a crystal of radius *r*

$$F_{gr} = \frac{r^2 \pi \rho}{M} R = \frac{r^2 \pi \rho}{M} \beta (P - P_\infty)$$

(5.11)

where ρ is the crystal density and *M* the molecular mass.

5.2.3 Capillary Flow

The capillary in the crossmember acts as a flow restrictor to allow some decoupling of the sublimation and growth rates. The flow through capillaries has been well documented [11-14], and at low pressures there are two main flow regimes, namely viscous and molecular flow.

Viscous flow occurs when the mean free path of the molecules (λ) is much less than the radius of the capillary (r_{cap}) [15]. Collisions between molecules dominate over the collisions between the molecules and the capillary walls, and, if the velocity is not too great to be turbulent, the gas flows in a steady

state motion similar to the laminar flow of a liquid [13]. The flow rate across a capillary of length L_{cap} is given by Poiseuille's Flow Formula [14, 16]

$$F_{visc} = \frac{\pi r_{cap}^{4} \langle P \rangle \Delta P}{8 \eta k T_{cr} L_{cap}} \qquad (5.12)$$

for a vapour of viscosity η at crossmember temperature T_{cr}. In the MTPVT system, with both Cd and Te$_2$ vapours on either side of the capillary, the mean pressure in the capillary $<P>$ is the mean of the total vapour pressures on each side of the capillary.

$$\langle P \rangle = \frac{(P_{SvCd} + P_{SvTe2}) + (P_{GvCd} + P_{GvTe2})}{2} = \frac{P_{STot} + P_{GTot}}{2} \qquad (5.13)$$

and the pressure drop across the capillary ΔP is the total difference in pressure across the capillary

$$\Delta P = (P_{SvCd} + P_{SvTe2}) - (P_{GvCd} + P_{GvTe2}) = P_{STot} - P_{GTot} \qquad (5.14)$$

Therefore the total viscous flow

$$F_{viscTot} = \frac{\pi r_{cap}^{4} (P_{STot}^{2} - P_{GTot}^{2})}{16 \eta k T_{cr} L_{cap}} = k_v \frac{(P_{STot}^{2} - P_{GTot}^{2})}{T_{cr}} \qquad (5.15)$$

where the viscous flow constant

$$k_v = \frac{\pi r_{cap}^{4}}{16 \eta k L_{cap}} \qquad (5.16)$$

The higher source-side pressure is the driving force for the viscous flow, and therefore the viscous flow of each particular species depends upon the proportion of species i in the source vapour, x_{si},

$$F_{visci} = x_{si} F_{viscTot} \qquad (5.17)$$

The source constitutions can be derived from the stoichiometry of the source vapour α_s

$$x_{sCd} = \frac{\alpha_s}{\alpha_s + 1} \quad \text{and} \quad x_{sTe2} = \frac{1}{\alpha_s + 1} \qquad (5.18)$$

with

$$\alpha_s = \frac{P_{sCd}}{P_{sTe2}}$$ (5.19)

Molecular flow occurs when the mean free path of the molecules is large compared to the capillary radius [17], so collisions between the molecules and the wall dominate. The flow is dependent on the molecular mass (M) of the gas molecules [16]

$$F_{mol} = \frac{2\pi r_{cap}^3}{3}\left(\frac{8RT_{cr}}{\pi M}\right)^{\frac{1}{2}}\frac{\Delta P}{L_{cap}RT_{cr}}$$ (5.20)

Maxwell proposed a correction factor f applied to equation (5.20) to take account of the friction between the molecules and the walls [11, 14, 18].

$$F_{mol} = \frac{2\pi r_{cap}^3}{3}\left(\frac{8RT_{cr}}{\pi M}\right)^{\frac{1}{2}}\frac{\Delta P}{L_{cap}RT_{cr}}\left(\frac{2}{f}-1\right)$$ (5.21)

Since the molecular flow is species dependent there will be different flow rates for species of differing molecular weight M_i

$$F_{moli} = \frac{\pi^2 r_{cap}^3 \left(P_{Si} - P_{Gi}\right)}{L_{cap}\left(8\pi M_i RT_{cr}\right)^{\frac{1}{2}}}\left(\frac{2}{f}-1\right) = k_{mi}\frac{\left(P_{Si} - P_{Gi}\right)}{\sqrt{T_{cr}}}$$ (5.22)

with the molecular flow constants

$$k_{mi} = \frac{\pi^2 r_{cap}^3}{L_{cap}\left(8\pi M_i R\right)^{\frac{1}{2}}}\left(\frac{2}{f}-1\right)$$ (5.23)

There is no clear boundary between the molecular and viscous flow regimes, but an indication is given by the Knudsen number, K_d [17], the ratio of the

mean free path λ and the principal dimension of the orifice, in this case the capillary radius r_{cap}

$$K_d = \frac{\lambda}{r_{cap}}$$

(5.24)

Approximate boundaries for the flow regimes using the Knudsen number are generally taken to be [19];

Viscous flow	$K_d < 0.01$	(5.25)
Mixed flow	$3 > K_d > 0.01$	
Molecular flow	$3 < K_d$	

In the MTPVT system, the Knudsen number for the crossmember capillary $K_d \sim 0.04$, therefore the capillary flow is in the mixed regime. The capillary flow equations for Cd and Te$_2$ are

$$F_{capCd} = \frac{\alpha}{\alpha + 1} k_v \frac{\left(P_{STot}^2 - P_{GTot}^2\right)}{T_{cr}} + k_{mCd} \frac{\left(P_{SCd} - P_{GCd}\right)}{\sqrt{T_{cr}}}$$

(5.26)

and

$$F_{capTe2} = \frac{1}{\alpha + 1} k_v \frac{\left(P_{STot}^2 - P_{GTot}^2\right)}{T_{cr}} + k_{mTe2} \frac{\left(P_{STe2} - P_{GTe2}\right)}{\sqrt{T_{cr}}}$$

(5.27)

5.2.4 Annulus Flow

The gap between the growing crystal and the quartz silica growth tube walls (see Figure 5.4) allows excess components and impurities to flow away from the seed. However, if this annulus gap is too large there will be a large quantity of CdTe lost to the growth, vapour pressures will be unable to build and growth will be suppressed.
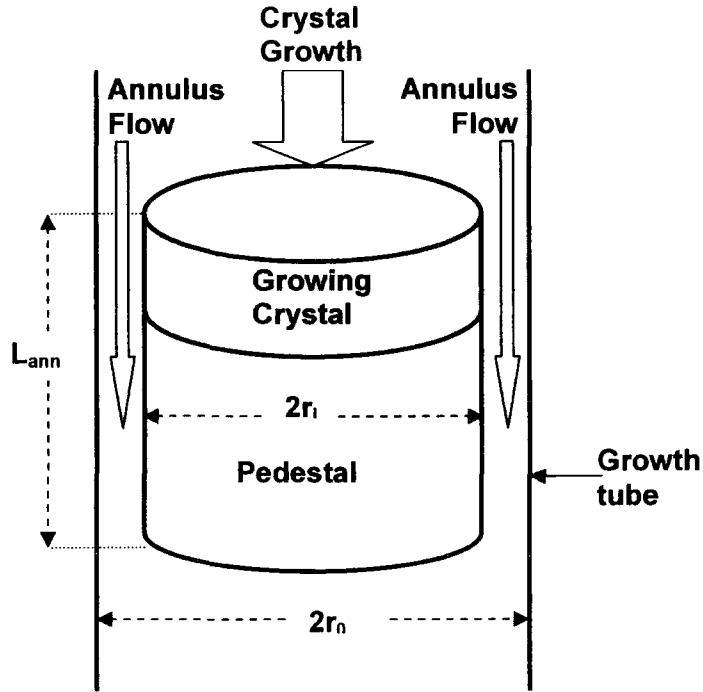
Figure 5.4 Annulus flow past growing crystal

As the area beyond the annulus is pumped via the dump tube, the pressure in the region is less than 10^{-5} mbar, and, when compared with the growth tube pressures around ~1-100 mbar, can be neglected. Therefore the corresponding flow equations are similar to the capillary flow equations

$$F_{Anni} = x_{gi} k_{vann} \frac{P_{GTot}^2}{T_g} + k_{manni} \frac{P_{Gi}}{\sqrt{T_g}}$$

(5.28)

The flow constants, k_{vann} and k_{mann} are radically different, however.

$$k_{vann} = \frac{1}{256 \eta R L_{ann}} \left(r_o^4 - r_i^4 - \frac{\left(r_o^2 - r_i^2 \right)^2}{\ln\left(\frac{r_o}{r_i} \right)} \right)$$

(5.29)

is the viscous annulus flow constant [17] for the crystal radius r_i and growth tube inner radius r_o with annulus length L_{ann}. For the molecular annulus flow the flow constant

$$k_{manni} = W \left(r_o^2 - r_i^2 \right) \sqrt{\frac{\pi}{2 R M_i}}$$

(5.30)

the transmission probability W [20] is given by [21]

$$W = \frac{1}{1 + \dfrac{L_{ann}}{r_o - r_i}\left(\dfrac{1}{2} - a\left(\tan^{-1}\left(\dfrac{L_{ann}}{b(r_o - r_i)}\right)\right)\right)}$$

(5.31)

where [17]

$$a = \frac{0.0741 - 0.014\dfrac{r_i}{r_o} - 0.037\left(\dfrac{r_i}{r_o}\right)^2}{1 - 0.918\dfrac{r_i}{r_o} + 0.05\left(\dfrac{r_i}{r_o}\right)^2}$$

(5.32)

and

$$b = \frac{5.825 - 2.86\dfrac{r_i}{r_o} - 1.45\left(\dfrac{r_i}{r_o}\right)^2}{1 + 0.56\dfrac{r_i}{r_o} - 1.28\left(\dfrac{r_i}{r_o}\right)^2}$$

(5.33)

As the crystal grows upwards in the growth tube, free from the tube walls, the length of the effective annulus L_{ann} increases. The annulus flow "constants" therefore require recalculation in the model as the crystal grows.

5.2.5 Crystal Equilibrium Partial Pressures

Functions describing the partial vapour pressures over the stoichiometric solid were introduced in Chapter 2.2.1. Equation (2.4) indicated from the law of mass action [22]

$$P_{Cd}P_{Te2}^{1/2} = K(T_s)$$

(5.34)

with the equilibrium constant K only dependent on the source crystal temperature T_s. The ratio of the Cd partial pressure, P_{Cd}, and the Te_2 partial pressure, P_{Te2}, gives the vapour partial pressure ratio, α.

$$\alpha = \frac{P_{Cd}}{P_{Te2}} \qquad\qquad (5.35)$$

The cadmium partial pressure in equation (2.10), derived from [23] as

$$P_{\infty Cd}(\text{Pa}) = \alpha^{\frac{1}{3}} \times 4.839 \times 10^{11} \times \exp\left(\frac{-23297}{T_s}\right) \qquad (5.36)$$

therefore the tellurium partial pressure can be determined by

$$P_{\infty Te2}(\text{Pa}) = \alpha^{-\frac{2}{3}} \times 4.839 \times 10^{11} \times \exp\left(\frac{-23297}{T_s}\right) \qquad (5.37)$$

The equilibrium partial pressures are dependent upon the stoichiometry of the vapour, which also needs to be re-evaluated throughout the simulation to provide an accurate model of the crystal equilibrium partial pressures.

5.3 COMPUTER SIMULATION OF CdTe CRYSTAL GROWTH

5.3.1 Assumptions of the Model

In order to produce a workable model for the growth of CdTe, several assumptions had to be made:

1) Crystals grew and sublimed stoichiometrically [24]

2) Growth rate was governed by the slowest growing species

3) Sublimation rate was governed by the fastest growing species

4) Material could only condense on the seed or source crystal – i.e. there was no growth on the glassware

5) Leaks of material through joints were negligible

6) Pressure beyond the annulus was negligible

7) Temperature gradient in the growth tube was linear around the growing crystal

Assumptions 1 to 3 can be justified because the vapour pressures of the elements are greater than the vapour pressures of the compound. Therefore, if one element preferentially sublimed, a region of the surface would be rich in the other element. This element would have a higher equilibrium pressure than it would in the compound and therefore would preferentially sublime. A dynamic equilibrium would result to maintain the stoichiometry. Similarly, if any element preferentially condensed on the crystal then this excess would re-sublime until the stoichiometry was restored.

Careful design and assembly of the system allowed assumptions 4 and 5 to be made. Condensation on the glassware at cold spots could be prevented by the appropriate use of heaters and shielding, and the glassware could be assembled to reduce leaks to less than 1%.

The temperature in the dump tube beneath the annulus was less than 100°C, at which the crystal (equilibrium) pressure was negligible compared to the crystal pressure at the growth temperatures (see equation 5.36). The dump tube was also pumped, limiting any back pressure to less than 10^{-5} mbar. Thus, assumption 6 that the pressure beneath the annulus was negligible was accurate. The actual temperature gradient in the growth tube has not been accurately measured, but the temperature was maintained by 3 consecutive heaters with no gaps. Consequently cold spots were unlikely to occur and the linear temperature assumption (7) should be a reasonable first approximation.

5.3.2 Flow Diagram of Computer Model

The code for the FORTRAN 95 simulation program is displayed in Appendix II. Figure 5.5 presents a flow diagram of the main sections of the program
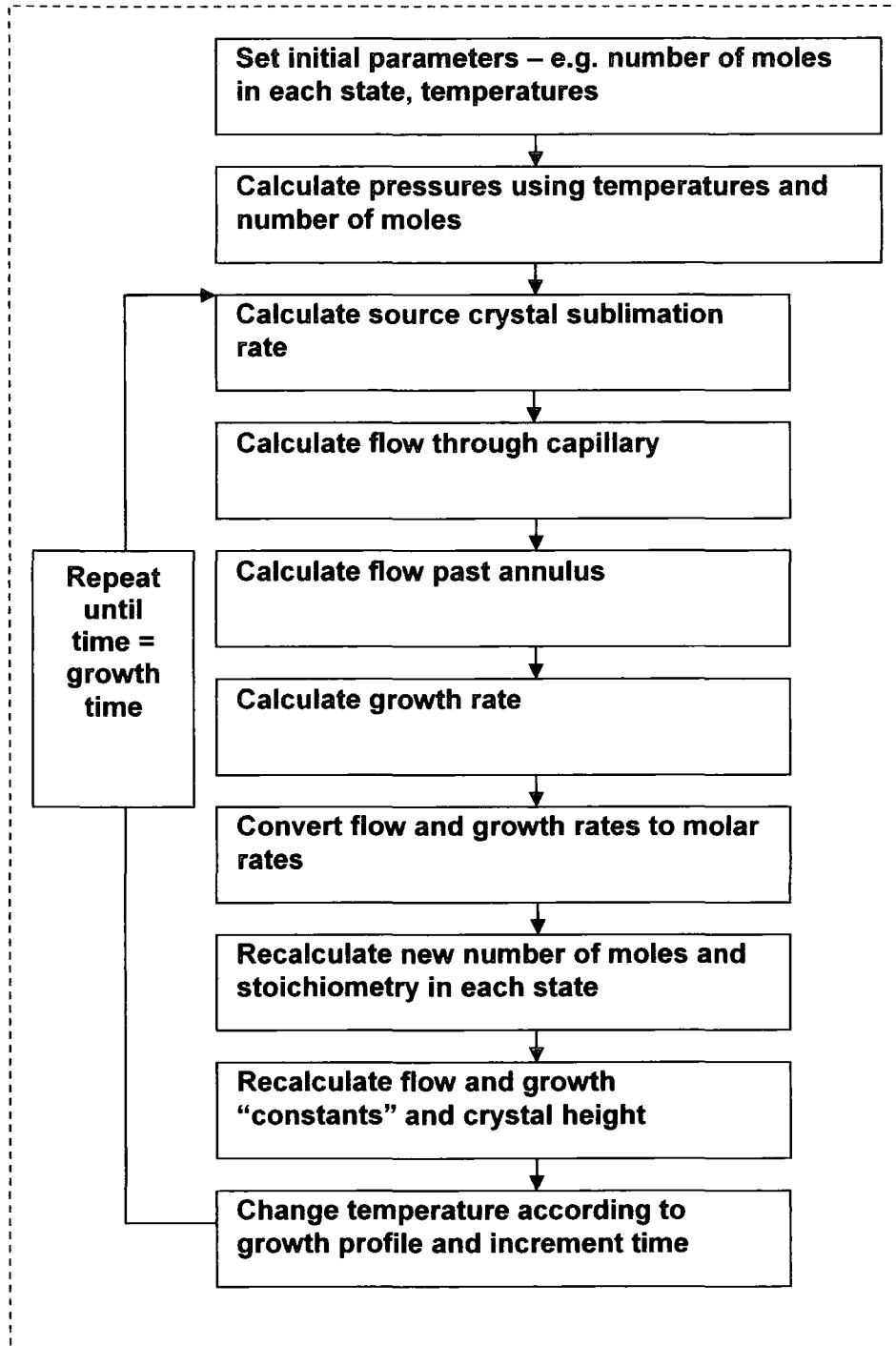
Figure 5.5: Flow diagram of computer model of CdTe growth

A number of constants are used in the simulation. Table 5.1 is a table of the standard constants used in the model.

Symbol	Description	Unit	Value	
M_{Cd}	Atomic mass of Cd atom	amu	112.4	[25]
M_{Te}	Atomic mass of Te atom	amu	127.6	[25]
η	Viscosity of CdTe	Pa s	9.00E-5	[1]
ρ	CdTe Density	kg m^{-3}	5.86E6	[26]
a	Kink Site Radius	m	6.48E-10	[26]

Table 5.1 Table of values of standard constants used in simulation

There are also a number of constants specific to the MTPVT system in use. The capillary radius, for example, can be different in different crossmembers, and the annulus gap may vary with different pedestals in different growth tubes. Table 5.2 displays a table of these values as they were initially used in the simulations.

Symbol	Description	Unit	Value
r_{Cap}	Capillary Radius	m	5.2 E-4
L_{cap}	Capillary Length	m	1.2 E-2
L_{ann}	Annulus Starting Length	m	10.2 E-3
r_0	Growth Tube Radius	m	2.5 E-2
V_s	Source-side volume	m^3	4.0 E-4
V_g	Growth-side volume	m^3	5.2 E-4
r_0-r_i	Annulus Gap	m	2.0 E-4

Table 5.2 Table of initial values used in the simulation

In the simulation there were a number of unknowns which could be used as fitting parameters for the simulation, such as the activation energy and the surface smoothness. The initial estimates of the values of these variables are presented in Table 5.3.

Symbol	Description	Unit	Value
$(\delta/a)_s$	Source Surface Smoothness		2
$(\delta/a)_g$	Growth Crystal Surface Smoothness		3
ΔU	Crystal Activation Energy	eV	0.4
f	Capillary Flow Friction Factor		0.74

Table 5.3 Other initial parameters used in the simulation

To test the validity of the simulation the growth conditions of Run 65 of the MTPVT system were used as the temperature profile of the model. During Run 65, the source was held at 870°C, the growth crystal at 705°C and the crossmember at 920°C for 24 hours. After the run, 61.4 g of material (0.256 moles) was measured to have left the source tube, the growing crystal gained 51.7 g (0.215 moles), and 8.8 g (0.036 moles) flowed beyond the annulus.

5.3.3 Simulation of Growth Run

Figures 5.6 to 5.11 display the simulated changes in the temperatures, pressures, location of moles, flow rates, species ratios (both species flow ratios and vapour partial pressure ratios) and kinetic coefficients as the crystal grew.
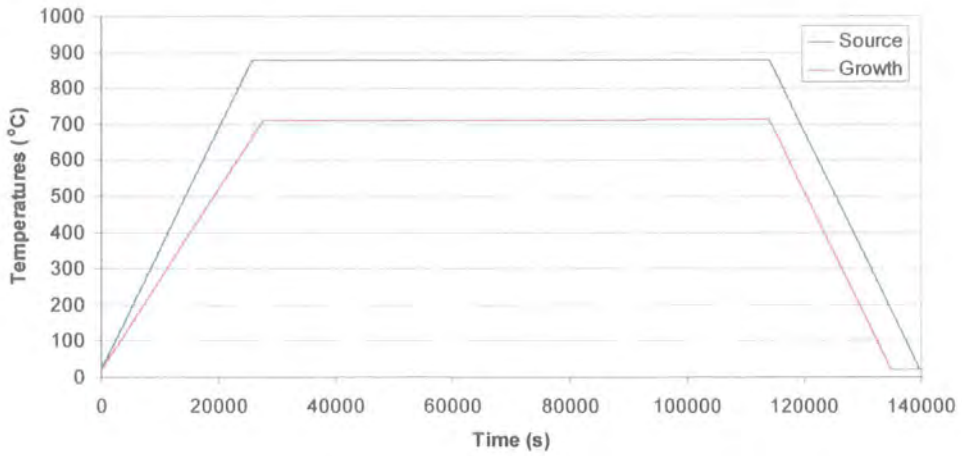
Figure 5.6: Source and growth temperatures in simulation of Run65
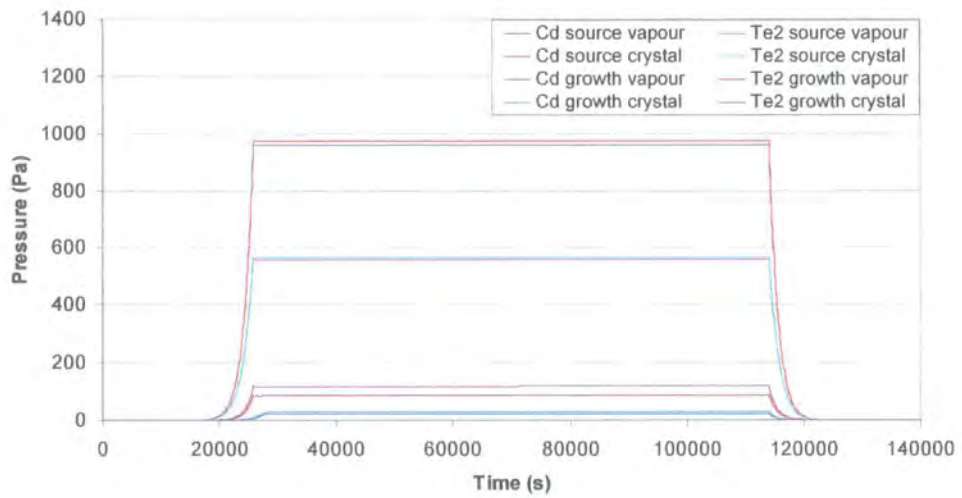
Figure 5.7: Pressures simulated for Run 65
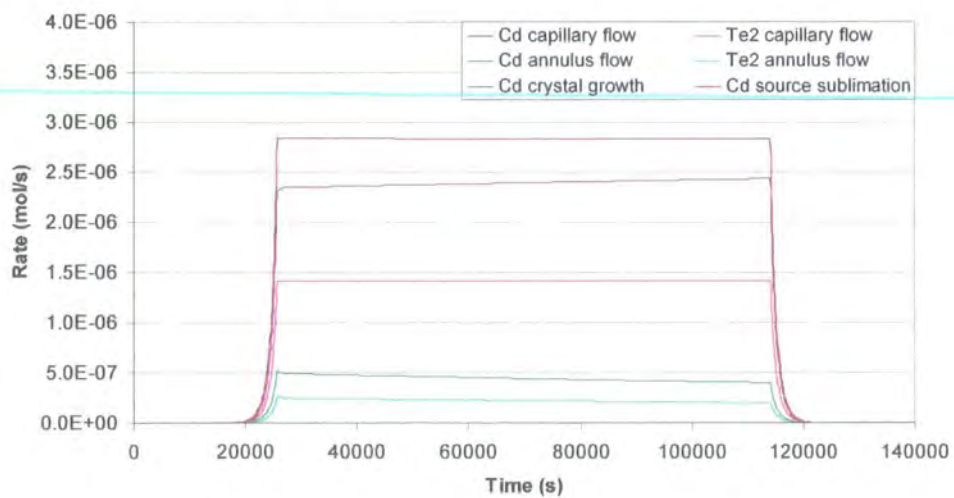
Figure 5.8: Flow and growth rates

(a)

(b)
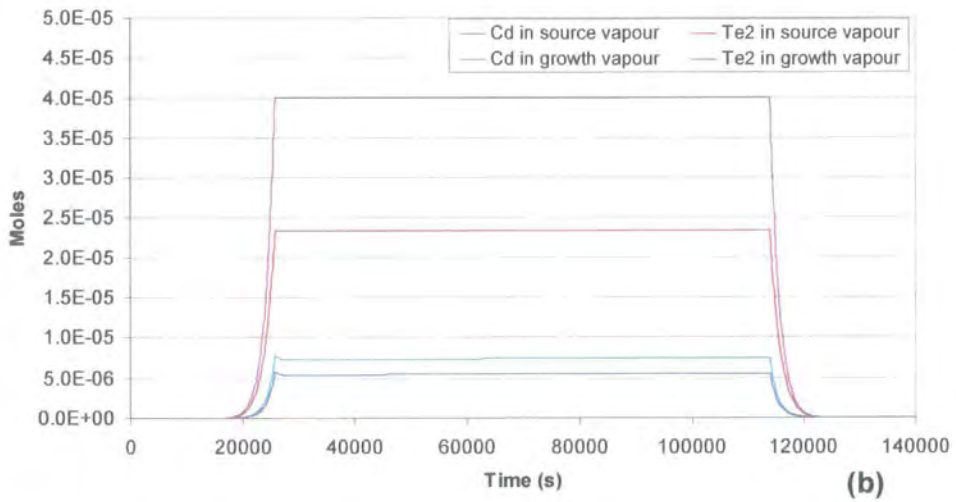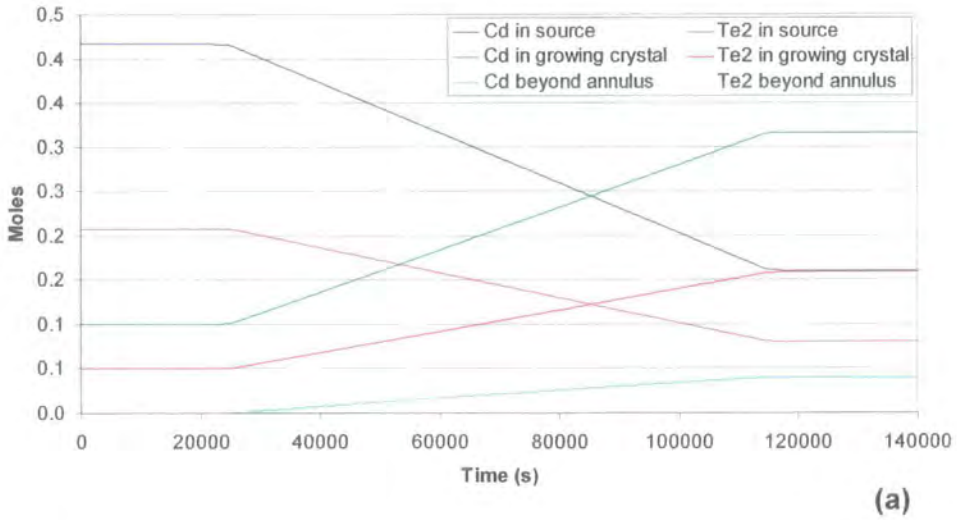
Figure 5.9: a) Number of moles in solid phases & b) Moles in vapour phase
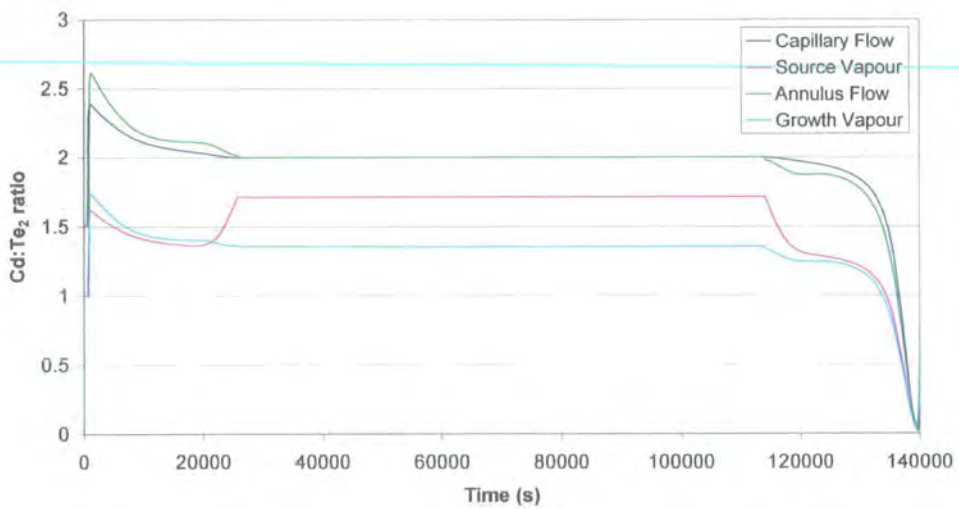
Figure 5.10: Cd :Te$_2$ ratios
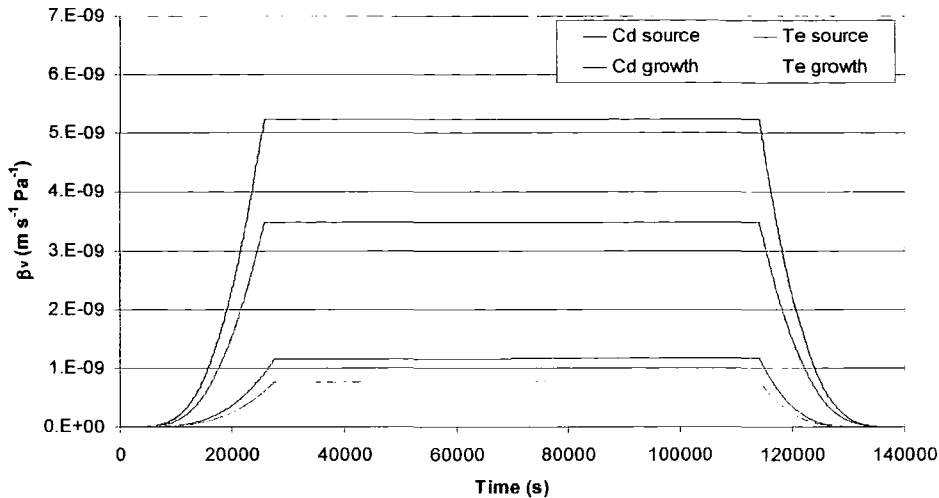
Figure 5.11: Kinetic coefficients

5.3.4 Discussion of Simulation Results

The simulation delivered a series of results which corresponded with expected trends and agree with experiment. Figures 5.6 and 5.7 indicated that the pressures became significant at temperatures above 500°C, reaching a maximum at the plateau temperatures. The source vapour pressures in Figure 5.7 were higher than the growth vapour pressures, providing the pressure drop across the capillary to drive matter to flow into the growth tube. At the growth temperatures, the source crystal equilibrium vapour pressures were slightly higher than the source tube vapour pressure (for Cd 972 Pa compared with 960 Pa), thus sublimation occurred. Conversely, the growth tube vapour pressure was much greater than the growth crystal equilibrium pressure (for Cd 119 Pa compared with 29 Pa), driving the crystal growth. This is also observed in Figure 5.12, which indicates at the same temperature the growth vapour pressure was much higher than the growth crystal equilibrium pressure, while the source vapour pressures and source crystal equilibrium pressures were almost indistinguishable.
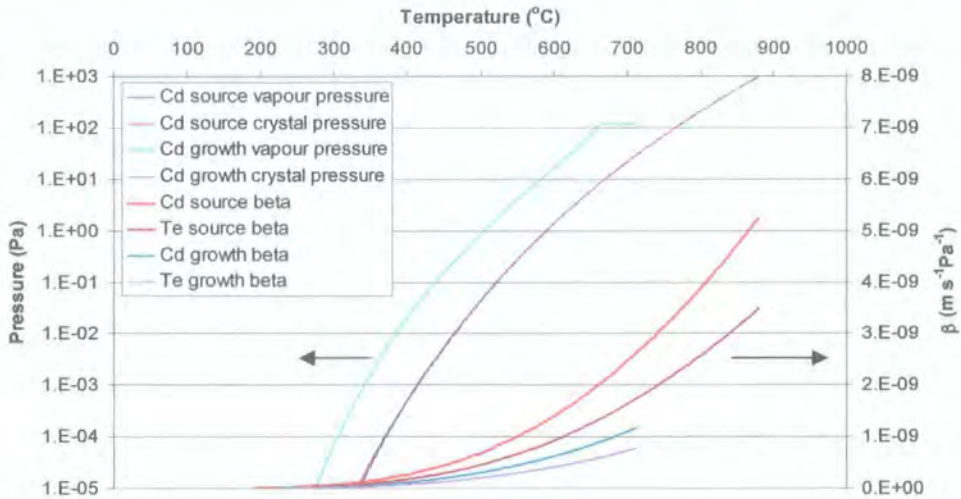
Figure 5.12: Variations of pressure and β with temperature

According to equation (5.8) the sublimation and growth rates are proportional to these pressure differences, but Figure 5.8 implies the sublimation rate was greater than the growth rate despite the lower pressure difference. This was due to the difference in the kinetic coefficients, which was dependent upon the material surface and temperature, with the growth coefficients considerably lower than the source coefficients given in Figures 5.11 and 5.12. The polycrystalline source material had a rougher surface than the polished growing crystal giving a lower coefficient at the same temperature in Figure 5.12.

Figure 5.8 also indicates that, as would be expected, at the growth temperatures an steady state existed where the sum of the crystal growth rate and annulus flow rate was equal to the capillary flow rate, which was also identical to the source sublimation rate. During the growth period, as the crystal grew through the temperature gradient in the growth tube, the growth crystal pressure increased, and the annulus increased in length, the capillary and annulus flows were seen to decrease. The crystal growth rate increased, however, as the kinetic coefficient increased with crystal temperature.

The simulation implies that during the plateau period several steady-state conditions existed. In equilibrium, because the source sublimation, capillary flow and crystal growth were all stoichiometric, the annulus flow must also have been stoichiometric. Figure 5.10 agreed, showing the annulus flow was stoichiometric, and that the growth-side vapour partial pressure ratio was around 1.35. The annulus flow was mainly molecular, with the viscous component very small. Thus, from equations (5.28) and (5.30) the ratio of the flows was

$$\frac{F_{AnnCd}}{F_{AnnTe2}} = \frac{k_{mannCd}\dfrac{P_{GCd}}{\sqrt{T_g}}}{k_{mannTe2}\dfrac{P_{GTe2}}{\sqrt{T_g}}} \tag{5.38}$$

Therefore, to ensure stoichiometric annular flow $(F_{AnnCd}/F_{AnnTe2} = 2)$, and using equation (5.28), rearranging (5.38) gives

$$\frac{P_{GCd}}{P_{GTe2}} = 2\sqrt{\frac{M_{Cd}}{M_{Te2}}} = 1.327 \tag{5.39}$$

which agrees with Figure 5.10. The partial pressure ratio of 1.33 is also observed in Knudsen cells [27], which, as with the vapour in the MTPVT growth tube, are effusion controlled .

During the plateau period, the capillary flow rate equalled the source sublimation rate, as is displayed in Figure 5.8. As a consequence, since the source sublimation was assumed to be stoichiometric, the flow through the capillary was stoichiometric (i.e. $F_{CapCd} = 2F_{CapTe2}$). If the capillary flow was purely molecular, the source-side vapour partial pressure ratio should be 1.33, the same as in the growth vapour. However, the capillary flow also had a considerable viscous component, which was independent of species. While

the growth-side partial pressure ratio was independent of growth conditions, the source-side partial pressure ratio changed as factors such as source temperature altered the molecular to capillary flow balance through the capillary.

$$\frac{k_{mCd}}{\sqrt{T_c}}\left(P_{sCd} - P_{GCd}\right) + \frac{k_v}{T_c}\frac{\alpha_S}{\alpha_S + 1}\left(P_{STot}^2 - P_{GTot}^2\right) =$$
$$2\left(\frac{k_{mTe_2}}{\sqrt{T_c}}\left(P_{sTe_2} - P_{GTe_2}\right) + \frac{k_v}{T_c}\frac{1}{\alpha_S + 1}\left(P_{STot}^2 - P_{GTot}^2\right)\right) \qquad (5.40)$$

Substituting for the source and growth-side partial pressure ratios

$$\alpha_S = \frac{P_{SCd}}{P_{STe_2}} \quad \text{and} \quad \alpha_G = \frac{P_{GCd}}{P_{GTe_2}} \qquad (5.41)$$

gives the total pressures in terms of the tellurium pressure

$$P_{STot} = \left(P_{SCd} + P_{STe_2}\right) = \left(\alpha_S + 1\right)P_{STe_2} \qquad (5.42)$$

$$P_{GTot} = \left(P_{GCd} + P_{GTe_2}\right) = \left(\alpha_G + 1\right)P_{GTe_2} \qquad (5.43)$$

therefore

$$k_{mCd}\left(\alpha_S P_{STe_2} - \alpha_G P_{GTe_2}\right) - 2k_{mTe_2}\left(P_{STe_2} - P_{GTe_2}\right)$$
$$= \left(\left(\alpha_S + 1\right)^2 P_{STe_2}^2 - \left(\alpha_G + 1\right)^2 P_{GTe_2}^2\right)\frac{k_v}{\sqrt{T_c}}\left(\frac{2 - \alpha_S}{\alpha_S + 1}\right) \qquad (5.44)$$

The ratio of the molecular flow constants is a function of the molecular masses

$$\frac{k_{mCd}}{k_{mTe_2}} = \sqrt{\frac{m_{Te_2}}{m_{Cd}}} \equiv M \qquad (5.45)$$

allowing all variables to be written in terms of their tellurium values, and equation (5.44) is found to be cubic with the source-side partial pressure ratio

$$\alpha_S{}^3 P_S^2 + \alpha_S{}^2 P_S M \frac{k_{mTe_2}\sqrt{T_c}}{k_v}$$

$$+ \alpha_S \left(\frac{k_{mTe_2}\sqrt{T_c}}{k_v}(P_S - (\alpha_G + 1)P_G) - 3P_S^2 + (\alpha_G + 1)^2 P_G^2 \right) \tag{5.46}$$

$$+ \left(2(\alpha_G + 1)^2 P_G^2 - \frac{k_{mTe_2}\sqrt{T_c}}{k_v}(P_S + P_G(M\alpha_G - 1)) - 2P_S^2 \right) = 0$$

where the Te_2 subscripts have been dropped and the pressures refer to the tellurium partial pressures.

The source-side vapour partial pressure ratio was therefore dependent upon the source-side and growth-side pressures, along with the capillary temperature and capillary flow constants. As a consequence the source-side vapour partial pressure ratio would vary for different growth runs as different source and growth temperatures were used. This was in contrast to the growth-side vapour partial pressure ratio, which is effectively constant around 1.33, and the source-side partial pressure ratio is observed to be dependent upon the growth partial pressure ratio.

With equation (5.46) as a cubic equation with respect to the source stoichiometry it was not possible to solve algebraically, but it could be solved graphically. Using the pressures and temperatures obtained in the simulation, and with the growth vapour partial pressure ratio set at 1.33, a plot of equation (5.46) for various source vapour partial pressure ratios displayed in Figure 5.13 gives three different partial pressure ratios which are possible solutions. Two solutions, -2.54 and -0.91, were negative and have no physical meaning as it was not possible for a negative partial pressure ratio, leaving the remaining solution, 1.73, as the only relevant solution for the

pressures and temperatures in the system. This broadly agrees with the source vapour partial pressure ratio of 1.72 displayed in Figure 5.10.

Source Vapour Partial Pressure Ratio
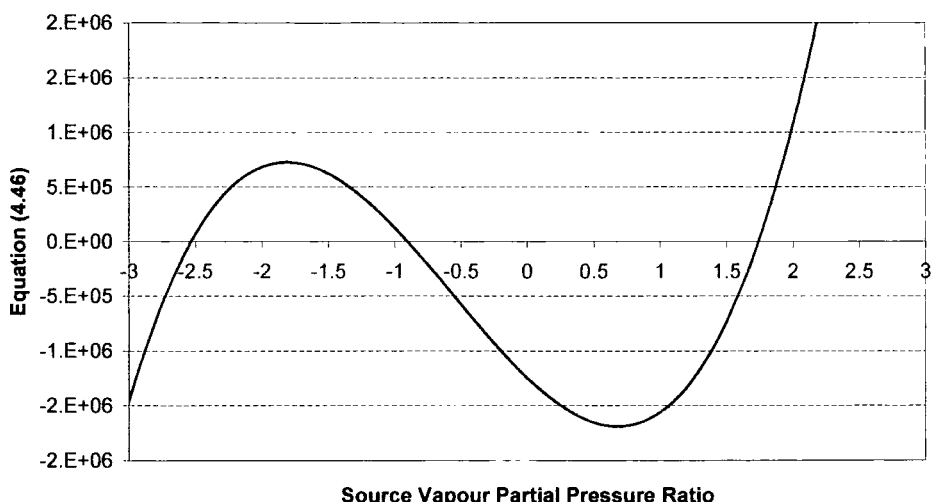
Figure 5.13: Graphical solution to stoichiometry cubic equation (5.46)

5.3.5 Comparison of Results with Experiment and Previous Models

As discussed in section 5.1.1, there have been previous attempts to model the growth of CdTe in the MTPVT system. Carles Alabert [1] treated the flow as a circuit with a series of restrictors, assigning a resistance to the crossmember capillary and annulus. However, no effort was made to quantify the flows. Aitken [2] used a numerical simulation to model the flow of cadmium through the capillary with an assumed linear growth rate. Previous work by this author developed the Cantwell-Sanghera [3, 4] model which included a derived algebraic expression to determine the total mass transport through the capillary over a growth run. All of these models ignored growth and sublimation rates, and made broad assumptions about the partial pressure ratio within the vapours.

As discussed in section 5.3.4, the simulation predicted the growth during Run 65 to within 1% of the measured 0.215 moles, and the annulus flow to within

7% of 0.036 moles, and this annulus error could have been due to inaccuracies in measuring the size of the annulus. The annulus size is very difficult to measure. The pedestal sits about 200 mm down the growth tube, so it is very difficult to measure the internal diameter of the tube at that position to be a great degree of accuracy. Precision-bore glassware is built to a tolerance of ± 0.25 mm, much greater than the desired annulus gap, and the pedestal required grinding until it could fit the tube. The measurement method used was to place the pedestal in position in the tube and try to feed wires of various diameters into the annulus gap, and to determine the maximum diameter wire which would fit. This allowed the annulus to be measured to within approximately 0.05 mm, which is still about 25% of the estimated value.

Aitken's model predicts for the growth condition in Run 65 the total flow through the capillary should be 0.346 moles, and the Cantwell-Sanghera model 0.342 moles. Assuming no leakage, the Aitken and Cantwell-Sanghera models overestimate the flow by 135% and 133% respectively of the measured amount. Thus, for Run 65 this simulation is much more accurate than the earlier models, and this is true for the other growth runs described in this thesis.

5.4 CONCLUSIONS

A new model for the growth of CdTe in the MTPVT system has been produced. The model takes account of source sublimation, capillary flow, crystal growth and annulus flow, giving a comprehensive simulation of the growth system. A computer simulation of the model illustrates how the pressures and flow rates vary throughout a typical growth run.

A simulation of Growth Run 65 of the MTPVT system gives a growth of 0.213 moles onto the crystal, and 0.0336 moles flowing beyond the annulus. The measured growth and annulus flow were 0.215 and 0.036 respectively, indicating the simulation underestimated the growth by 1% and overestimated the annulus flow by 7%, representing a positive validation of the simulation. These errors could be due to uncertainty in the annulus gap in the growth tube.

5.5 REFERENCES FOR CHAPTER 5

[1]   J. Carles Alabert. *"Optical Vapour Pressure Monitoring and Mass Transport Control During Bulk CdTe Crystal Growth in a Novel Multi-Tube PVT System"*. PhD Thesis. University of Durham. (1998).

[2]   N. M. Aitken. *"Mass Transport Studies in the Growth of CdTe Crystals by Multi-Tube Physical Vapour Transport"*. MSc Thesis. University of Durham. (1999).

[3]   H. K. Sanghera, B. J. Cantwell, N. M. Aitken and A. W. Brinkman. *"The Growth of CdTe Bulk Crystals Using the Multi-Tube Physical Vapour Transport System"*. Journal of Crystal Growth **237-239** (2002) 1711.

[4]   H. K. Sanghera, B. J. Cantwell and A. W. Brinkman. *"Modelling of the Growth of Ternary Compound Cadmium Zinc Telluride (in a Semi-Open Markov-Like System) from the Binary Sources CdTe and ZnTe"*. Journal of Crystal Growth **237-239** (2002) 1741.

[5]   P. Goldfinger and M. Jeunehomme. *"Mass Spectroscopic and Knudsen-Cell Vaporization Studies of Group 2b-6b Compounds"*. Trans. Faraday Soc. **59** (1963) 2851.

[6]   I. V. Markov. *"Crystal Growth for Beginners: Fundamentals of Nucleation, Crystal Growth and Epitaxy"*. World Scientific London (1995).

[7]   A. A. Chernov. *"Notes on Interface Growth Kinetics 50 Years after Burton, Cabera and Frank"*. Journal of Crystal Growth **264** (2004) 499.

[8]   E. Kaldis and M. Piechotka. *"Bulk Crystal Growth by Physical Vapour Transport"*. in *"Handbook of Crystal Growth, Vol 2"*. Edited by D. T. J. Hurle 2 Elsevier Amsterdam. (1994).

[9]   P. A. Tipler. *"Physics for Scientists and Engineers"*. Worth New York (1991).

[10]   B. B. Dayton. *"Kinetic Theory of Gases"*. in *"Foundations of Vacuum Science and Technology"*. Edited by J. M. Lafferty John Wiley and Sons New York. (1998).

[11]   G. P. Brown, A. DiNardo, G. K. Cheng and T. K. Sherwood. *"The Flow of Gases in Pipes at Low Pressures"*. Journal of Applied Physics **17** (1946) 802.

[12]   W. G. Pollard and R. D. Present. *"On Gaseous Self-Diffusion in Long Capillary Tubes"*. Physical Review **73** (1948) 762.

[13]   J. H. Jeans. *"An Introduction to the Kinetic Theory of Gases"*. Cambridge Univesity Press London (1940).

[14]   A. Roth. *"Vacuum Technology"*. Elsevier Amsterdam (1976).

[15]   R. G. Livesey. *"Flow of Gases through Tubes and Orifices"*. in *"Foundations of Vacuum Science and Technology"*. Edited by J. M. Lafferty John Wiley and Sons New York. (1998).

[16]   R. D. Present. *"Kinetic Theory of Gases"*. McGraw-Hill Book Company Inc. New York (1958).

[17]   L. Holland, W. Steckelmacher and J. Yarwood. *"Vacuum Manual"*. E. & F.N. Spon London (1974).

[18]   R. A. Dawe. *"The Slip Correction in Accurate Viscosity"*. Rev. Sci. Instrum. **44** (1973) 1271.

[19]   A. W. Brinkman and J. Carles. *"The Growth of Crystals from the Vapour"*. Progress in Crystal Growth and Characterization of Materials **37** (1998) 169.

[20]   A. S. Berman. *"Free Molecular Transmission Probabilities"*. Journal of Applied Physics **36** (1965).

[21]   A. S. Berman. *"Free Molecule Flow in an Annulus"*. Journal of Applied Physics **40** (1969) 4991.

[22]   M. M. Faktor and I. Garrett. *"Growth of Crystals from the Vapour"*. Chapman and Hall London (1974).

[23]   B. De-Largy, A. Finch and P. J. Gardner. *"Thermodynamic Functions for the Congruent Sublimation of Cadmiun-Telluride"*. Journal of Crystal Growth **61** (1983) 194.

[24]   M. M. Faktor, I. Garrett and R. Heckingbottom. *"Diffusional Limitations in the Gas Phase Growth of Crystals"*. Journal of Crystal Growth **9** (1971) 3.

[25]   *"CRC Handbook of Chemistry and Physics"*. CRC Press Inc. (1974).

[26]   D. J. Williams. *"Densities and Lattice Parameters of CdTe, CdZnTe and CdTeSe"*. in *"Properties of Narrow Gap Cadmium-Based Compounds"*. Edited by P. Capper 1 INSPEC London. (1994).

[27]   R. F. Brebrick and A. J. Strauss. *"Partial Pressures and Gibbs Free Energy of Formation for Congruently Subliming CdTe(C)"*. J Phys Chem Solids **25** (1964) 1441.

Chapter 6

Vapour Pressure Monitoring By Optical Absorption

6.1 INTRODUCTION

The growth runs described in the previous chapters implied the partial pressures of the vapours over the source and growing crystals are of great importance for vapour crystal growth, and the MTPVT system was designed to allow their monitoring through optical absorption. The three optical windows in the crossmember allowed the passage of light through the vapours for non-intrusive *in situ* monitoring of the vapour partial pressures above the sources and growing crystal during the growth.

This chapter introduces the theoretical basis of the optical absorption in vapours, and its relevance to the monitoring of pressure. The pressure-absorption spectra of Cd atoms and Te_2 molecules are presented, along with a benchtop experiment to determine this relationship for Zn atoms.

140

A system capable of measuring the optical absorption in the MTPVT system during the growth of both CdTe and CdZnTe is introduced, and the chapter concludes with the presentation of partial pressures measured during a CdTe growth run.

6.2 THEORETICAL BACKGROUND

6.2.1 Beer's Law

The Bouguert-Beer-Lambert (BBL) law of absorption [1], more commonly known as Beer's Law, is a combination of several laws which deal with the absorption of light through a homogeneous medium [2, 3]. The law is based on several key assumptions [4] :

i)   The incident radiation is monochromatic,

ii)   The absorbers act independently of each other,

iii)   The incident radiation consists of parallel rays, propagating perpendicular to the surface of the absorbing medium,

iv)   The pathlength traversed is uniform over the cross section of the beam (All rays traverse an equal distance of the absorbing medium),

v)   The absorbing medium is homogeneous and does not scatter the radiation,

vi)   The incident flux is not large enough to cause saturation effects.

Beer's Law states that for a beam of monochromatic light passing through a uniform medium of thickness l, containing the absorbing species of concentration c and with absorption coefficient k, the intensity of transmitted light I is related to the intensity of incident light I_0 by [5]

$$I = I_0 \exp(-kcl) \tag{6.1}$$

Beer's Law can be expressed in the form [6]

$$D_\lambda \equiv \log\left(\frac{I_0}{I}\right) = \varepsilon_\lambda cl \qquad (6.2)$$

with the optical density, D_λ and the decadic molar extinction coefficient, ε_λ, both dependent upon the wavelength λ. Using the ideal gas law [7],

$$D_\lambda = \frac{\varepsilon_\lambda pl}{RT_c} \qquad (6.3)$$

and the pressure p at temperature T_c can be determined through the optical density by

$$p = D_\lambda \frac{RT_c}{\varepsilon_\lambda l} \qquad (6.4)$$

where R is the ideal gas constant. If Beer's Law is obeyed, therefore, the pressure is directly proportional to the optical density, and the vapour pressures can be monitored *in situ* if ε_λ, T_c and l are known.

The species under investigation, cadmium, tellurium and zinc, have well defined Clausius-Clapeyron equations for the equilibrium pressure of a reservoir of the solid element, which are of the form

$$\log(p) = \frac{a}{T_r} + b \qquad (6.5)$$

where a and b are constants specific to each element and T_r is the temperature of the source reservoir, which may differ from the cell temperature T_c. Therefore, combining equations (6.4) and (6.5), for a given cell length and temperature, if the Beer's Law is obeyed, a plot of $\log(D_\lambda)$ versus ($1/T_r$) should give a straight line with slope a and intercept b'

$$\log(D_\lambda) = \frac{a}{T_r} + b' \qquad (6.6)$$

The relationship between the optical density and pressure can be determined directly by combining (6.5) and (6.6)

$$p = 10^{(b-b')} D_\lambda \qquad (6.7)$$

If Beer's Law is not obeyed, but a plot of $\log(D_\lambda)$ against the reciprocal reservoir temperature provides a straight line of slope a' and intercept b', the optical density may still be related to the pressure by

$$p = 10^{\left(\frac{ba'-b'a}{a'}\right)} D_\lambda^{a/a'} = \alpha_\lambda D_\lambda^{\beta_\lambda} \qquad (6.8)$$

6.2.2 Applicability of Beer's Law

The theoretical basis of the Beer's Law stipulates the absorption of monochromatic light, which in practical terms is unobtainable, hence Beer's Law does not always hold in real terms. The absorption band has a finite width due to natural, Doppler or collision broadening. When measuring the light intensity, the wavelength-selecting devices, e.g. monochromators or optical filters, allow a finite band of wavelengths to pass. Since the molar extinction coefficient ε_λ is a function of λ, Beer's law will in practice hold if ε_λ is constant over the wavelength band, but not if the absorption band is narrow compared to the monochromator bandpass [4]. Other factors which can cause deviation from Beer's law include the diffusing or scattering nature of the absorbing medium, photo-induced chemical changes in the medium and saturation effects when the incident radiation flux is large.

For the partial pressure monitoring in the MTPVT system, relationships of the form of equations (6.7) and (6.8) were required from the benchtop spectroscopy system (see section 6.3). The effects most likely to cause deviation in the MTPVT system from these equations are the temperature

dependence of the absorption line, and saturation through the use of quartz–halogen lamps for heating. The extinction coefficient ε_λ is only valid for the vapour temperature at which it is measured, and cannot be extrapolated to other temperatures. Therefore the pressure – optical density relationships need to be measured on the benchtop at the same temperature as the crossmember in the MTPVT system.

6.3 UV-VISIBLE ABSORPTION SPECTROSCOPY

A spectroscopic system has been developed to determine absorption spectra. Previous studies [8, 9] have used the system to study the spectra of Cd and Te_2, and the results of these studies, relevant to the MTPVT *in situ* partial pressure measurement system, will be presented. The spectroscopic system has been developed to study the absorption spectra of Zn, and the results of this study will be presented in this section.

6.3.1 Experimental Procedure

The arrangement of the spectroscopic system is illustrated in Figure 6.1.
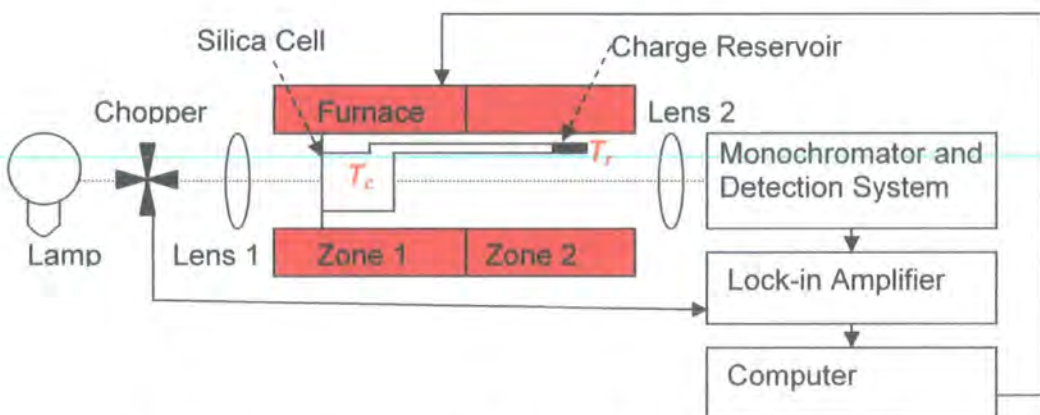
Figure 6.1: Spectroscopic Analysis Apparatus

A 50.1 mm long, 32 mm diameter quartz silica transmission cell, with a side arm attached containing a small amount of the element under investigation,

was placed in a two-zone furnace. Each zone was controlled by a computer, using a variation of the control program outlined in Chapter 3, enabling both the temperature of the reservoir and the cell to be accurately controlled independently of each other. Source charges of 99.999% purity were used in the cell and the cell was evacuated and baked out at 120°C to remove water vapour and other volatile impurities prior to sealing.

Rays from the light source were chopped and collimated by the use of a UV-enhanced silica-coated lens. The light emerging from the silica transmission cell was focussed on the input slit of the monochromator using a UV lens, with care taken to provide a light-tight seal between the furnace walls and the transmission cell to ensure no light reached the monochromator without having first passed through the transmission cell.

A Hilger-Engis Monospek 1000 monochromator with a 1200 lines/mm diffraction grating provided wavelength resolution better than 1 nm for the emergent light. A Photomultiplier Tube (PMT), supplied with 1 kV potential, enabled the detection of light of wavelengths between 200 and 660 nm, with the high intrinsic gain allowing the detection of low light levels. The PMT output was compared to the output signal of the chopper by the lock-in amplifier to filter out background light signals. A Keithley 195A multimeter detected the output signal of the lock-in amplifier, and the voltages communicated to the computer for storage. Voltages were recorded at 5 second intervals during the experiment, and, with the reservoir temperature ramp rate set at 2 K/min, optical densities could be calculated at temperature intervals of less than 0.2 K.

6.3.2 Zinc Vapour Absorption

The absorption spectra of zinc gas has been extensively studied [10, 11], and it is noted that zinc vapour has two main absorption lines: at 213.8 nm due to the transition from the ground state 4^1S_0 to the 4^1P_1 energy level, and at 307.6 nm from 4^1S_0 to 4^3P_1. [12] The 213.4 nm line is deep in the ultra-violet region, with a calculated Doppler half-width of about 0.3 nm at 1000°C, but broadens extensively towards the visible. The 307.6 nm line has been seen to develop as the temperature increases, [10] although other studies suggest this to be a very weak absorption. [9, 13].

A zinc lamp is a suitable light source with emission lines at both the 214 and 308 nm absorption wavelengths, along with other emission lines at higher wavelengths which are not absorbed by zinc gas as they correspond to transitions between higher energy levels in the zinc atom. The emission spectrum of the Pen-Ray zinc lamp used in the zinc absorption measurements, as measured by the Hamamatsu RS955 PMT at intervals of 0.25 nm via the Monospec monochromator, is presented in Figure 6.2.
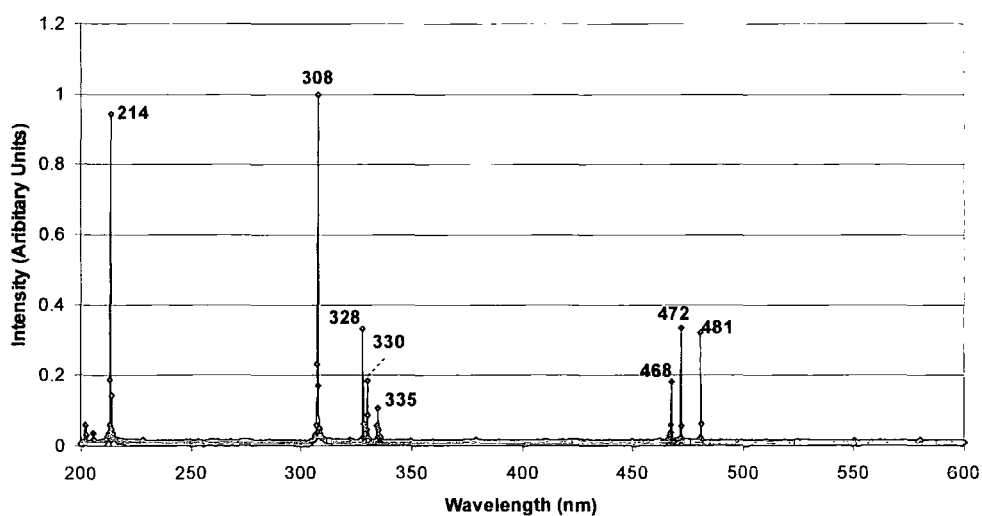
Figure 6.2: Emission spectrum of Pen-Ray zinc lamp

The 214 nm absorption line was chosen for study, as previous studies with this setup [9] provided no evidence of absorption at 308 nm at the temperatures relevant to the MTPVT system. Using the zinc lamp as the light source, and a Hamamatsu RS955 PMT with UV capability, the cell temperature was raised to 850°C at 2 K/min, and subsequently the reservoir temperature raised at the same rate to 700°C. The monochromator input slits were adjusted to give the same FWHM as the interference filters used in the MTPVT detection system (see section 6.5.3). The optical signal was seen to increase as the cell temperature was raised towards its maximum temperature, suggesting the windows of the cell were cleaned of any deposit at these high temperatures. The maximum signal level during this period was taken as the I_0 value for the optical density calculations. Figure 6.3 displays the variations of the optical density with the reservoir temperature.
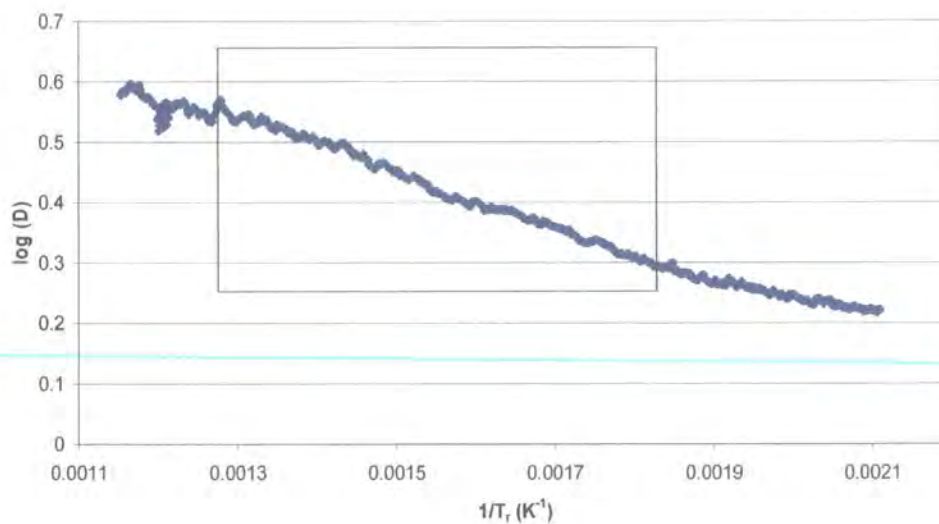
Figure 6.3: Optical absorption of zinc lamp 214 nm emission line by zinc vapour as a function of reciprocal cell temperature, with linear region highlighted

The region highlighted by the box on Figure 6.3 displays a linear relationship between the log of the optical density and the reciprocal reservoir temperature. The equation of best fit in this area, using the least squares method, is

$$\log(D_{214}) = -\frac{418.1}{T_r} + 1.08 \qquad (6.9)$$

This slope is much smaller than the published [14] slope of the log (P) vs reciprocal temperature

$$\log P_{Zn}(atm) = -\frac{6108}{T_r} + 5.2 \qquad (6.10)$$

This behaviour has been observed by other authors [10] as the Doppler half-width is much less than the band-pass of the monochromator, and the assumptions in Beer's Law are not matched. Using equation (6.8), the zinc pressure can be related to the optical density of the 214 nm line by

$$P_{Zn}(mbar) = 10^{-7.26} D_{214}^{14.4} \qquad (6.11)$$

The departure from linearity in Figure 6.3 at high temperatures may be due to the difficulty in measuring the low light levels associated with higher optical densities, with large errors associated with the low signal levels. At low temperatures the pressure is too low to create measurable absorption, hence the levelling out of the optical density at low temperatures.

6.3.3 Cadmium Vapour Absorption

Cadmium vapour had prominent absorption lines at 228.7 nm and 325.7 nm, corresponding to the transitions 5^1S_0 to 5^1P_1 and 5^1S_0 to 5^3P_1 respectively. The emission spectrum of a cadmium lamp, measured with the spectroscopic system but with an RCA 931-A photomultiplier tube and controlled by a BBC

microcomputer, is displayed in Figure 6.4. The spectral response of this photomultiplier tube was between 300 and 660 nm, and the glass casing of the cadmium lamp was manufactured to absorb UV for safety reasons, resulting in the absence of an emission line at 228.7 nm.
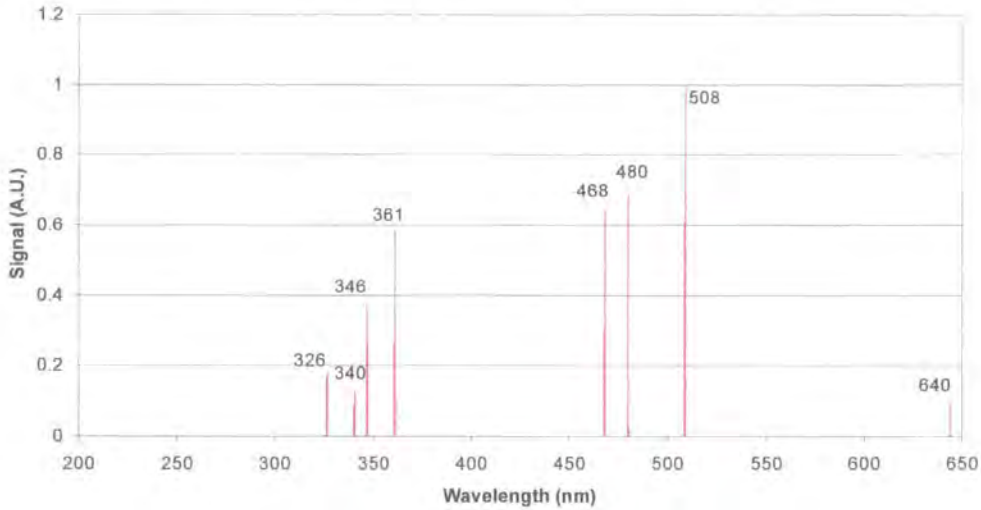
Figure 6.4: Emission of cadmium lamp

Previous studies [8, 9, 11, 15, 16] have concentrated on the 325.7 nm absorption line. A comparison of these results with the pressure-temperature relationship [14]

$$\log P_{Cd}(atm) = \frac{-5308}{T_R} + 5.108 \qquad (6.12)$$

gave a relationship between the optical density and pressure

$$P_{Cd}(mbar) = 2.49 D_{326}^{1.10} \qquad (6.13)$$

6.3.4 Tellurium Vapour Absorption

While atoms absorb photons through the promotion of electrons to higher energy levels, other absorption modes can take place in molecules. Among the possible excitation modes of the molecules are vibration, rotation and nuclear spin. The vibrational mode itself can be split into two parts: the

149

nuclear vibration and electronic vibration. As the nuclei vibrate the electronic configuration adjusts itself instantaneously, allowing the molecules to absorb photons at a range of different energies [3]. With tellurium vapour consisting mainly of Te_2 dimers [17], absorption was over a range of wavelengths and with a considerably different spectrum to the atomic vapours of cadmium and zinc. Previous studies with the Spectroscopic Analysis Apparatus, using a quartz halogen lamp with a broad emission spectrum as the light source, obtained the broad tellurium absorption spectrum [9] displayed in Figure 6.5.
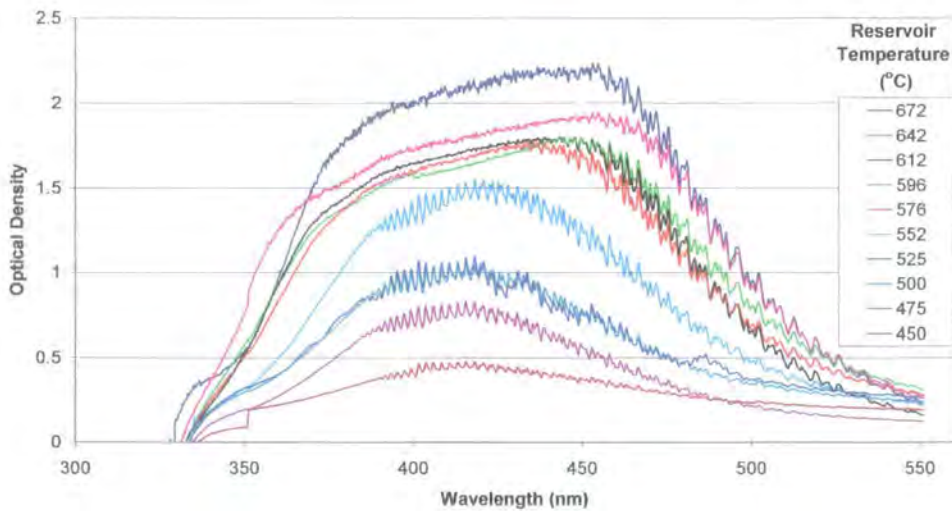
Figure 6.5: Tellurium Absorption Spectrum (from [9]) for varying reservoir temperatures

The Te_2 absorption range was between 330 and 550 nm, but there was negligible absorption at the Cd absorption line at 326 nm. Fine structure variations can be seen on the curves, particularly at the higher temperatures. This is likely to be due to different modes of vibrations being excited at different energies. The small peaks and troughs appear at the same wavelengths for different temperatures, ruling out experimental errors as the cause. If the lamp output or PMT dark current varied across the sampling

period it is highly unlikely the variations would have occurred at the same wavelengths. The size of the fluctuations also increases as the number of molecules increases at the higher temperatures, implying the effects were due to absorption, not signal fluctuations. At low wavelengths the fine structure does not appear, which may be because there are no vibrational modes in this region, or could also be due to the low signal to noise ratio in this region.

Te_2 absorption did occur at the wavelengths 467, 479 and 508 nm, these being Cd emission but not absorption lines, and also at the Zn emission-only wavelengths of 468, 472 and 481 nm. This permitted the use of cadmium and zinc lamps to determine the partial pressures of both the atomic species and the Te_2 molecules simultaneously.

Comparing the optical density data in Figure 6.5 with the published [14] pressure-temperature relationship

$$\log P_{Te_2}(atm) = -\frac{6415.4}{T_R} + 5.19$$
(6.14)

pressure - optical density relationships for the cadmium emission lines could be obtained through equation (6.8).

$$P_{Te_2}(mbar) = 2.32D_{467}^{0.89}$$
(6.15)

$$P_{Te_2}(mbar) = 2.89D_{479}^{0.91}$$
(6.16)

$$P_{Te_2}(mbar) = 3.09D_{508}^{0.98}$$
(6.17)

The corresponding zinc emission relations are

$$P_{Te_2}(mbar) = 2.40D_{468}^{0.89}$$
(6.18)

$$P_{Te_2}(mbar) = 2.63D_{472}^{0.90} \qquad\qquad (6.19)$$

$$P_{Te_2}(mbar) = 2.90D_{480}^{0.91} \qquad\qquad (6.20)$$

6.4 PARTIAL PRESSURE MONITORING OF CDTE VAPOURS

Optical absorption systems have been developed by several other parties for the partial pressuring monitoring of II-VI vapours. Zappettini *et al* [18] have developed a system similar to the one described in section 6.3.1, with several differences. A He-Cd laser was employed as the light source, giving emission lines at 325 and 440 nm, with 4 photodiodes detection the light emerging from the vapour cell. This system was not used to monitor pressures during growth, but to determine the stoichiometry deviation in a crystal. The system proved very accurate, with sensitivity to stoichiometry variations down to 0.0004 mol%. The system has also been used to determine the stoichiometry variations in CdZnTe crystals.

A system to determine the partial pressures in the original CdTe MTPVT system [8, 16] used a single cadmium lamp as a light source, with six silicon photodiodes behind appropriate filters detecting the emergent light. The lack of sensitivity of the photodiodes did not allow the partial pressures in the growth tube to be measured, and the results for the source side vapour appeared to be inconsistent in different growth runs under the same conditions. It was thought the use of photodiodes for the light detection may have been principally responsible for the limitations of the system.

6.5 MTPVT OPTICAL ABSORPTION SYSTEM

6.5.1 Outline of System

The pressure-optical density relations detailed above allow the monitoring of the partial pressures in the MTPVT system. The schematic of the optics system built to measure the optical absorption is presented in Figure 6.6.
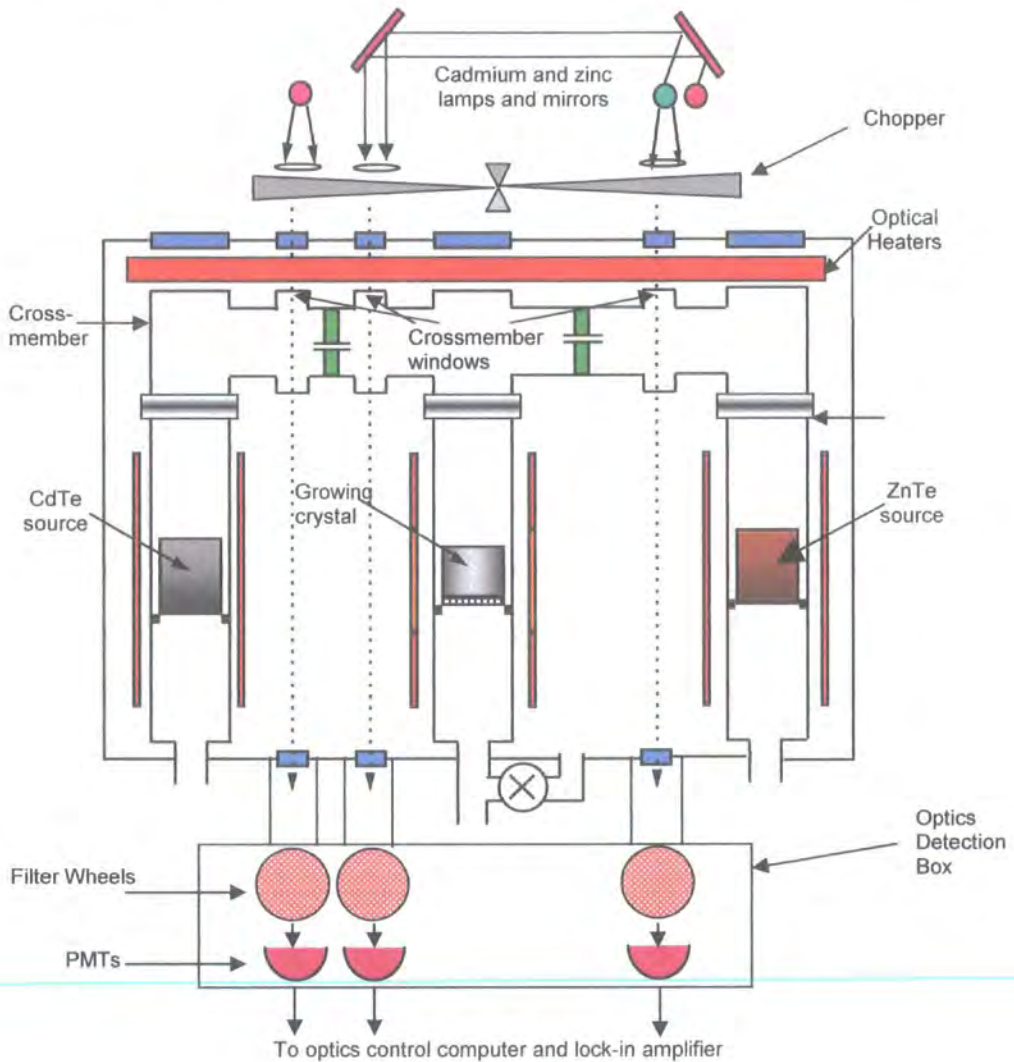
Figure 6.6: Schematic of optical absorption system

The light sources were placed on the top of the MTPVT system, with associated mirrors and lenses directing parallel light through a chopper and subsequently through the crossmember in the MTPVT system. The light emerging through the bottom windows of the MTPVT system was channelled

into a detection box with filter wheels used to select the wavelength of light to be measured by the photomultuplier tubes. Three separate filter wheels and PMTs allowed the optical absorption in the CdTe source tube, ZnTe source tube and the growth tube to be monitored individually throughout growth runs.

6.5.2 Light Source Design

During the growth of CdZnTe in the MTPVT system, $Cd_{(g)}$ and $Te_{2(g)}$ were present in the CdTe source tube, $Zn_{(g)}$ and $Te_{2(g)}$ in the ZnTe source tube, with $Cd_{(g)}$, $Zn_{(g)}$ and $Te_{2(g)}$ appearing in the growth tube. Light from a cadmium lamp located directly above the relevant window provided the necessary emission lines to monitor the Cd and Te_2 pressure in the CdTe source tube, with a zinc lamp enabling the equivalent for the ZnTe source tube. In order to measure the Cd, Zn and Te_2 pressures in the growth tube, however, emissions from both Cd and Zn lamps were required. The physical size of the lamps, (the ~50 mm diameter of the Cd lamp and the ~30 mm diameter of the Zn lamp), made it impossible to place both lamps directly above the 30 mm diameter growth tube window. Placing a Cd lamp alongside the Zn lamp above the ZnTe source window (displayed in Figure 6.7) allowed both beams to be directed to the growth tube window via two mirrors, which were CaF coated to permit the reflection of the UV zinc 214 nm emission line. This setup greatly reduced the intensity of the light entering the growth side compared to the source sides, but this was countered by the lower temperatures in the growth tube providing lower pressures and thus lower absorption in the growth side.
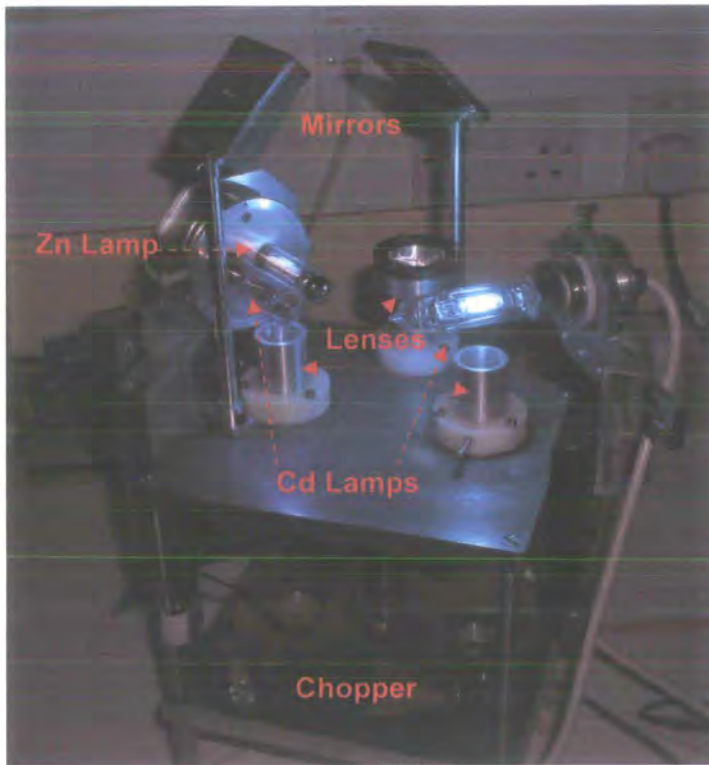
Figure 6.7: Light source

A single copper chopper wheel chopped all three beams simultaneously at the same height above the detectors, ensuring the phase of the beams matched each other, permitting the use of a single lock-in amplifier. An in-house built controller was able to vary the chopping frequency between 10 and 150 Hz, whilst providing the chopper reference signal for the lock-in.

6.5.3 Detection System

The computer controlled detection system built to determine the signal intensities at the relevant wavelengths, and encased in a light-tight matt black anodised aluminium box, is presented in Figure 6.8.

Figure 6.8: Optical Detection System

Two different models of PMTs were used in the MTPVT detection system. Hamamatsu RS955 PMTs, with enhanced UV detection capabilites, detected the light on the ZnTe source and growth sides which contained the Zn 214 nm emission line. An RCA 931-A PMT, without UV capability, detected the light on the CdTe source side.

Each filter wheel contained up to five filters which were rotated in sequence to sit directly above the PMT detection area. All three wheels contained five slots for filters, requiring rubber blanking discs to be placed in the unused

filter positions to prevent overexposure of the PMTs. The filters in each position are listed in the table in Table 6.1.

Filter Position	Wheel 1 (CdTe source side)	Wheel 2 (Growth side)	Wheel 3 (ZnTe source side)
1	Blank	214 nm – Zn absorption line	214 nm – Zn absorption line
2	326 nm – Cd absorption line	326 nm – Cd absorption line	Blank
3	510 nm – Te$_2$ absorption	480 nm – Te$_2$ absorption	510 nm – Te$_2$ absorption
4	Blank	307 nm – Zn absorption / ref	307 nm – Zn absorption / ref
5	640 nm – reference line	640 nm – reference line	640 nm – reference line

Table 6.1: Position of filters on filter wheels

The FWHM of the filters were between 5 and 10 nm, therefore the 214 and 326 nm filters admitted the whole of the absorption band, leading to probable deviation from Beer's Law as described earlier. However, the precautions taken in the preliminary measurements with the monochromator permit the use of the pressure-density relations derived earlier in this chapter. The absorption of Te$_2$ can be considered constant over the FWHM bandpass of the detection filters, resulting in Beer's Law being followed more closely.

The measurements at 640 nm allowed the normalisation of the optical density measurements with reference to this unabsorbed line, to account for any fluctuations in the light sources and any movement of the system.
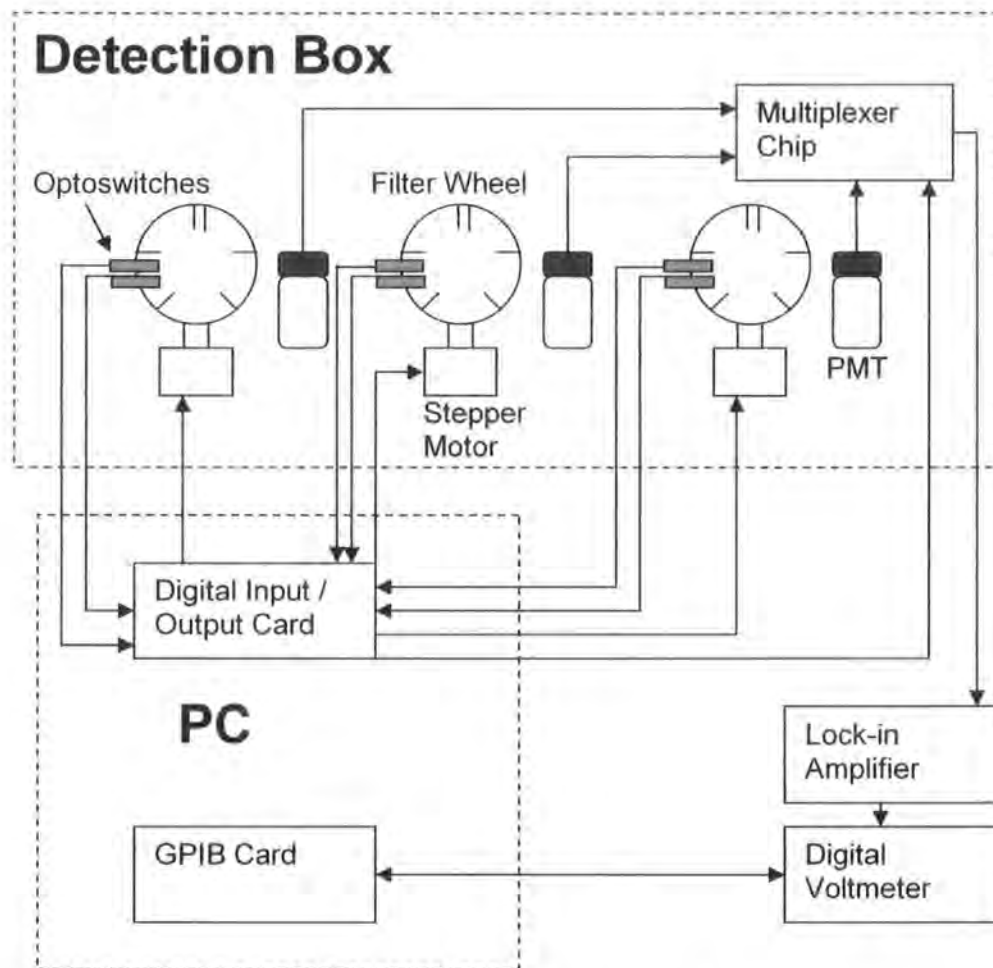
Figure 6.9: Schematic of MTPVT Optical Detection System

Each filter wheel was controlled by a stepper motor, with two optoswitches providing a definite location for each wheel. Five slots, 72° apart on each filter wheel, allowed one optoswitch to determine when a filter was positioned directly over a PMT, to 0.5° accuracy, with a sixth slit allowing the second optoswitch to determine a home position of the wheel, which corresponded to the filter position 1 being positioned over the PMT.

TTL signals from the optoswitches were detected by the Personal Computer via a Digital Input/ Output (DIO) card, as illustrated in Figure 6.9. The rotation of the filter wheel was also controlled by the PC DIO card, with each pulse sent by the card to the stepper motor rotating the wheel by 0.8°. The PC also controlled which of the three signals from the PMTs was sent to the lock-in amplifier, by passing a 3-bit code via the DIO card to a multiplexer chip, required due to the availability of one lock-in amplifier. The lock-in amplifier output voltage was measured by a Keithley 195A Digital voltmeter, with the measured value communicated to the PC through a GPIB card.

The detection process was controlled on the PC by a Windows-based program written in the Visual C++ language, and the main algorithm code is presented in Appendix III.

The signals from each filter on each wheel were read sequentially, with 15 voltages taken for each wavelength at one-second intervals, and filtered using infinite series averaging. After a set of readings for a wavelength were taken, the next filter was selected and a 15-second delay introduced to allow the lock-in amplifier output to settle.

6.5.4 Tests of Detection System

The five lamps used to heat the crossmember provided a much greater light level than the lamps used for optical absorption monitoring, consequentially the system was designed to allow the lock-in amplifier to remove the unchopped heater lamp light. This de-selection, however, took place after the combined light levels from both sources were detected by the PMTs, and too great a light level could swamp the PMTs with photons, and prevent to lock-in

from working. The filters in the filter wheels ensured only a narrow band of wavelengths illuminated the PMTs at any one time, but it was necessary to test the detection system to check this was enough to prevent saturation. The MTPVT system was heated according to standard growth run conditions, but without any source or growth material present in the system, and the light intensities in the CdTe source side measured.
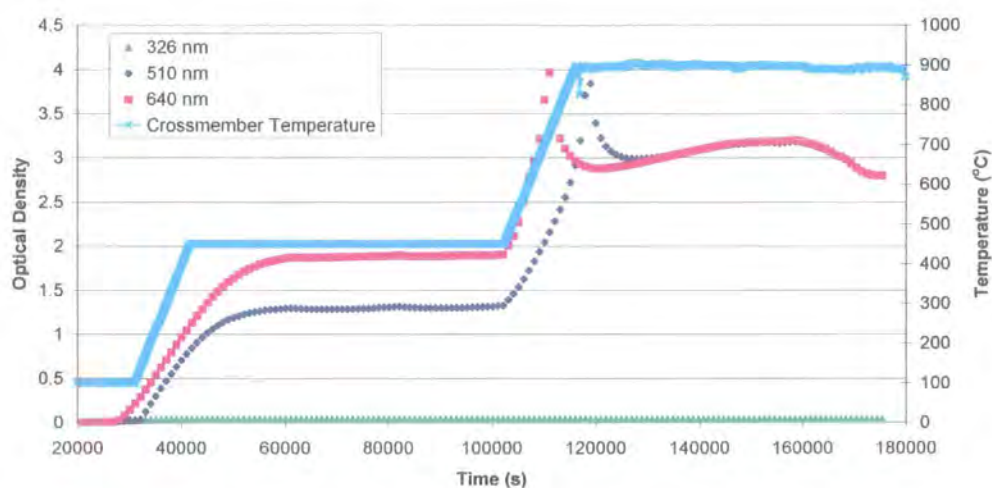
Figure 6.10: Optical density measurements with no vapour present

During the heating profile, the observed optical densities at 510 nm and 640 nm appeared to increase as the power to the heating lamps also increased, as displayed in Figure 6.10, suggesting swamping of the PMTs by photons did occur at these wavelengths. The observed optical density at 326 nm, however, was constant throughout the heating process, leading to the conclusion that the heating lamps did not emit a large amount of light at this short wavelength. It could also be inferred that the heating lamps failed to emit a substantial level of light at the 214 nm wavelength, used to monitor the zinc absorption line.

To counter the swamping effects, neutral density filters (NDF), each allowing 1% transmittance, were fitted to the light-entry holes on the detection box.

The NDFs prevented the swamping at the longer wavelengths whilst allowing sufficient chopped source light through to obtain pressure monitoring measurements. Too much light at the shorter wavelengths was absorbed by the NDFs, however, preventing accurate pressure measurements being taken, and since it was unnecessary to fit NDFs at these wavelengths, NDFs were only used in conjunction with the 510 and 640 nm filters.

6.6 PARTIAL PRESSURE MONITORING OF GROWTH RUN

6.6.1 CdTe Source Side Pressures

The optical partial pressure monitoring system was applied to several CdTe growth runs of the MTPVT system. This section introduces data taken during Run 80 of the MTPVT system, in which a CdTe crystal was grown at 710°C from CdTe in the cadmium source side at 870°C, with the zinc source tube empty. Figure 6.11 shows the source side Cd and Te_2 pressures calculated from the measured optical densities through the expressions given earlier in this chapter, with the source temperature profile on the secondary y-axis.
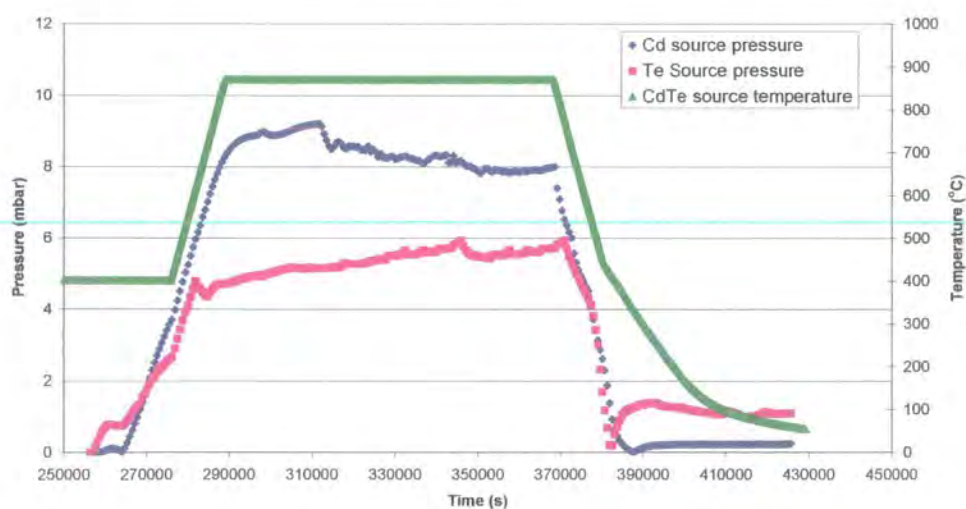
Figure 6.11: CdTe source pressures and temperatures during Run 80

Figure 6.11 presents a sharp increase in both the Cd and Te_2 pressures as the source temperature was increased, and a sharp decrease as the

temperature was dropped. During the period in which the source temperature was held at 870°C the Cd pressure gradually fell from about 9 mbar to 8 mbar, with the Te_2 pressure gradually rising to 5 mbar from 4 mbar.

6.6.2 CdTe Growth Side Pressures

The growth side pressures presented in Figure 6.12 follow a similar pattern to the source pressures previously described, with the pressures closely following the temperatures. In the growth side, the Cd and Te_2 pressures were broadly constant during the plateau region, at 4.5 and 1.8 mbar respectively. A spike appeared in both pressures during the heating up period, which could be due to a spot of CdTe condensing on the optical window, giving greater optical density, and quickly subliming away.
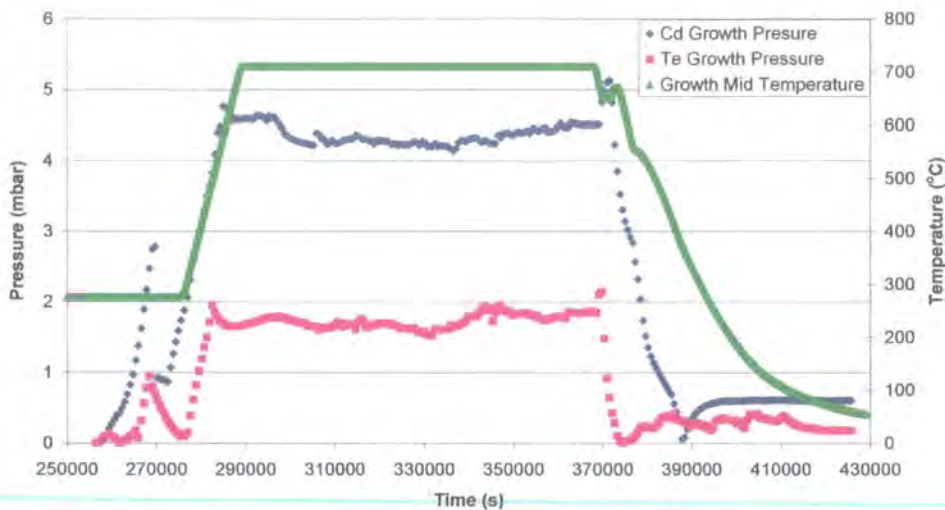
6.12: CdTe growth pressures and temperatures during Run 80

As discussed in Chapter 4, the focus of the growth was the development of CdTe, and only two preliminary CdZnTe runs took place. The optical monitoring system was not available for use in these growth runs, therefore it was not possible to test the detection of Zn by the system. The positive results for the monitoring of CdTe, coupled with the pressure-absorption

relationship calculated in section 6.3.2, gave reason to suggest the system would work well for the monitoring of CdZnTe growth.

6.7 CONCLUSIONS

The optical absorption of zinc vapour at 214 nm has been studied, and a relationship between the optical density and partial pressure was derived.

An optical detection system was developed to monitor the partial pressures in the MTPVT system independently in real time, using cadmium and zinc lamps as light sources. The detection system, which consisted of three wheels, each rotated by computer-controlled stepper motors to locate its filters above the photomultiplier tube, enabled the partial pressures over the CdTe and ZnTe sources and growing crystal to be calculated.

The results of the monitoring system applied to Run 80 of the MTPVT system, in which CdTe was grown with no ZnTe in the system, were presented. Source Cd and Te_2 pressures of around 9 mbar and 5 mbar respectively were observed during the growth period, with the corresponding growth pressures around 4.5 mbar and 1.9 mbar. No attempts were made to monitor the growth of CdZnTe or ZnTe, and therefore the pressure – density relationship of the Zn 214 nm line could not be verified under growth conditions.

6.7 REFERENCES FOR CHAPTER 6

[1]   H. H. Perkampus. *"Encyclopedia of Spectroscopy"*. VCH New York (1995).

[2]   G. F. Lothian. *"Absorption Spectrophotomery"*. Hilger & Watts London (1949).

[3]   R. E. Dodd. *"Chemical Spectroscopy"*. Elsevier Amstrerdam (1962).

[4]   J. D. Ingle and S. R. Crouch. *"Spectrochemical Analysis"*. Prentice Hall New Jersey (1988).

[5]   J. M. Hollas. *"Modern Spectroscopy"*. John Wiley & Sons Chichester (1987).

[6]   W. S. Struve. *"Fundamentals of Molecular Spectroscopy"*. John Wiley & Sons New York (1989).

[7]   J. H. Jeans. *"An Introduction to the Kinetic Theory of Gases"*. Cambridge Univesity Press London (1940).

[8]   J. Carles Alabert. *"Optical Vapour Pressure Monitoring and Mass Transport Control During Bulk CdTe Crystal Growth in a Novel Multi-Tube PVT System"*. PhD Thesis. University of Durham. (1998).

[9]   B. J. Cantwell. *"Vapour Pressure Monitoring by Optical Absorption"*. MSci Thesis. University of Durham. (2000).

[10]   R. F. Brebrick. *"Partial Pressures of Zn and Te_2 over ZnTe up to $917°c$"*. J Electrochem. Soc. **116** (1969) 1274.

[11]   R. F. Brebrick. *"Partial Pressures in the Cd-Te and Zn-Te Systems"*. Journal of Electrochemical Society: Solid State Science **118** (1971) 2014.

[12]   C. E. Moore Ed. *"Atomic Energy Levels" "Vol. II"*. United States of America National Bureau of Standards Washington (1952).

[13]   D. G. James. *"Measurement of Partial Pressure in CdZnTe by Optical Absorption"*. MSci Thesis. University of Durham. (2004).

[14]   *"Crc Handbook of Chemistry and Physics"*. CRC Press Inc. (1974).

[15]   R. F. Brebrick and A. J. Strauss. *"Partial Pressures and Gibbs Free Energy of Formation for Congruently Subliming $CdTe_{(c)}$"*. J Phys Chem Solids **25** (1964) 1441.

[16]   J. Carles, J. T. Mullins and A. W. Brinkman. *"Partial Pressure Monitoring in Cadmium Telluride Vapour Growth"*. Journal of Crystal Growth **174** (1997) 740.

[17]   P. Goldfinger and M. Jeunehomme. *"Mass Spectroscopic and Knudsen-Cell Vaporization Studies of Group 2b-6b Compounds"*. Trans. Faraday Soc. **59** (1963) 2851.

[18]   A. Zapperttini, F. Bissoli, L. Zanotti, M. Zha, C. Broglia and C. Paorici. *"Stoichiometric Derivations and Partial-Pressure Measurements in Solid-Vapour Cadmium Telluride System"*. Materials Chemistry and Physics **66** (2000) 138.

Chapter **7**

Discussion of Results

7.1 INTRODUCTION

In the previous three chapters the growth of CdTe crystals has been introduced, a model for the growth presented and the optical partial pressure monitoring system presented. In Chapter 5 a simulation of a growth run gave transport rates which closely matched the actual rates shown in the Chapter 4. In Chapter 6 the partial pressures monitored during a growth run by optical absorption measurements were shown. In this chapter the results of the growth and optical pressure measurements will be compared with the model and some of the findings accounted for.

This chapter will discuss the effects of the crystal radius and annulus gap observed during the crystal growth with reference to the model, and compare the stoichiometry and partial pressures measured with the modelled values. The variations in crystal height with an uneven radial temperature in the growth tube will also be accounted for by the simulation, and finally estimates

for the growth constant variables will be made by comparing the information obtained by all three sources.

7.2 VAPOUR PARTIAL PRESSURES

7.2.1 Source Vapour

The CdTe source side partial pressures derived from the optical absorption measurements taken during Run 80 are displayed in Figure 7.1, along with the calculated vapour partial pressure ratio $P_{Cd}:P_{Te2}$.
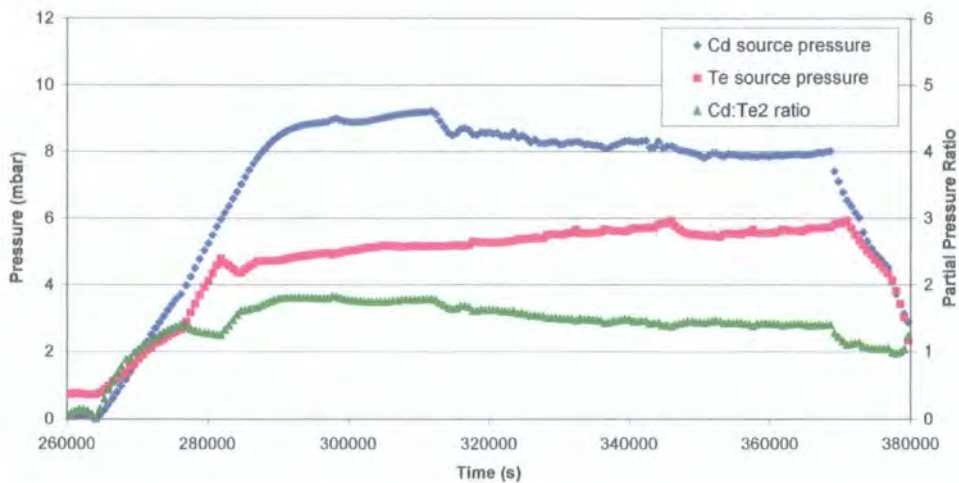
Figure 7.1: Source vapour partial pressures and their ratio derived from optical absorption measurements taken during Run 80

The Cd source vapour pressure is seen to fall slowly from 9.1 to 8.0 mbar during the growth period, while the Te_2 pressure rises from 4.7 to 5.9 mbar. Thus the partial pressure ratio is seen to decrease from 1.8 to 1.4 over the corresponding period.

A simulation of Run 80 using the model developed, shown in Figure 7.2, gave a constant Cd source plateau partial pressure of 9.6 mbar, and the Te_2 partial

pressure of 5.6 mbar, with the corresponding stoichiometry constant at 1.7.
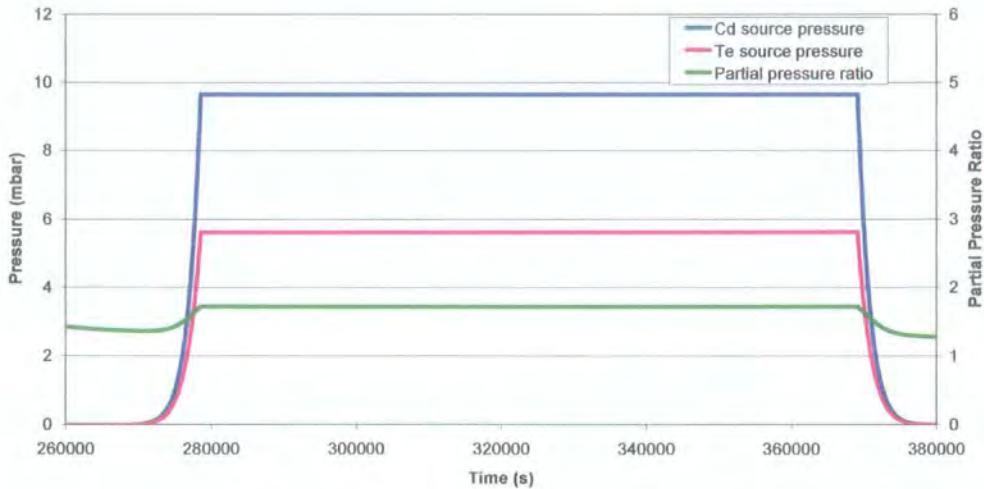
Figure 7.2: Source vapour partial pressures and ratio in simulation of Run 80

The simulation broadly follows the results observed by the optical absorption, with the magnitudes of the pressures and stoichiometry similar, but the pressures displayed in Figure 7.1 appeared to fluctuate throughout the growth period, despite the source temperature being held constant during this period, suggesting some error in the optical measurements. These fluctuations may be due to several factors: fluctuations in relative intensity of the emission lines of the lamp output; small movements of the various pieces of apparatus during the heating process due to differential expansions or other factors; a film of CdTe appearing on the optical windows; or variations in the outputs and sensitivities of the apparatus used in the detection system, such as the 1 kV supplied to the PMTs, the lock in amplifier or drift in the PMT sensitivities.

The simulation does not predict the fall in Cd pressure or rise in Te_2 pressure observed through the optical absorption measurements. Inspection of the

crossmember, after the completion of the growth run, found a thin layer of CdTe on the face of the optical windows. This film would not account for the variations in partial pressures described above, as the absorption coefficients of a CdTe film at the Cd 326, Te 510 and reference 640 nm wavelengths are 68.2, 9.6 and 4.6 μm^{-1} respectively. [1] The lower absorption at higher wavelengths would show a rising Cd pressure and falling Te_2 pressure as the film developed, which would not account for the contrary situation being observed.

One situation which could account for the trends observed is a variation in the lamp output at the different wavelengths. The optical densities were calculated using the initial readings for the voltage at the relevant wavelength, together with the current voltage at the reference wavelength. If the intensity of light at longer wavelengths increased relative to the intensity at shorter wavelengths, a fall in the Cd pressures would be seen, while the Te_2 pressures could have risen.

Slight movements in the optical apparatus could cause misalignment of the lamp output, through the optical windows and into the detectors. Slight changes in the local temperatures, or activity in the room housing the growth system could cause these movements, and "creaking noises" were often heard from the system during growth, suggesting such movements may have occurred. These movements could have caused measurement errors leading to the small fluctuations in pressures observed in Figure 7.1, but would be unlikely to cause the general fall in Cd and rise in Te_2 pressures through the growth process. Similarly, changes in the sensitivities of the electronic

measurement apparatus could account for the fluctuations in pressure observe, but would not account for the overall pressure trends.

7.2.2 Growth Vapour

The growth side partial pressures derived from the optical absorption measurements taken during Run 80 are displayed in Figure 7.3, along with the calculated vapour partial pressure ratio $P_{Cd}:P_{Te2}$.
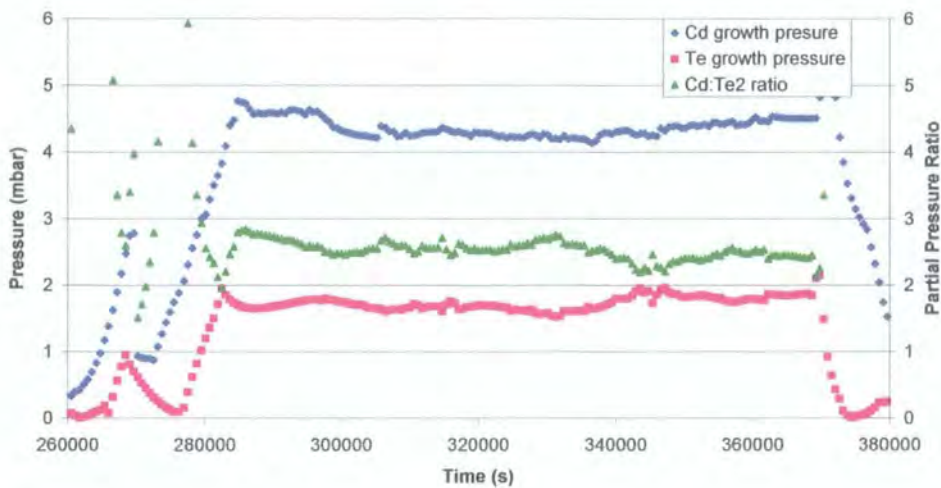
Figure 7.3: Growth vapour partial pressures and their ratio derived from optical absorption measurements taken during Run 80

Both the Cd and Te_2 partial pressures appear broadly constant throughout the growth period, at about 4.4 and 2.6 mbar respectively. The partial pressure ratio is therefore around 2.5. These results, however, differ greatly from the results of the simulation presented in Figure 7.4, which predicted pressures about an order of magnitude lower, but which rose steadily as the crystal grew up in the temperature gradient, and a steady partial pressure ratio of 1.34.
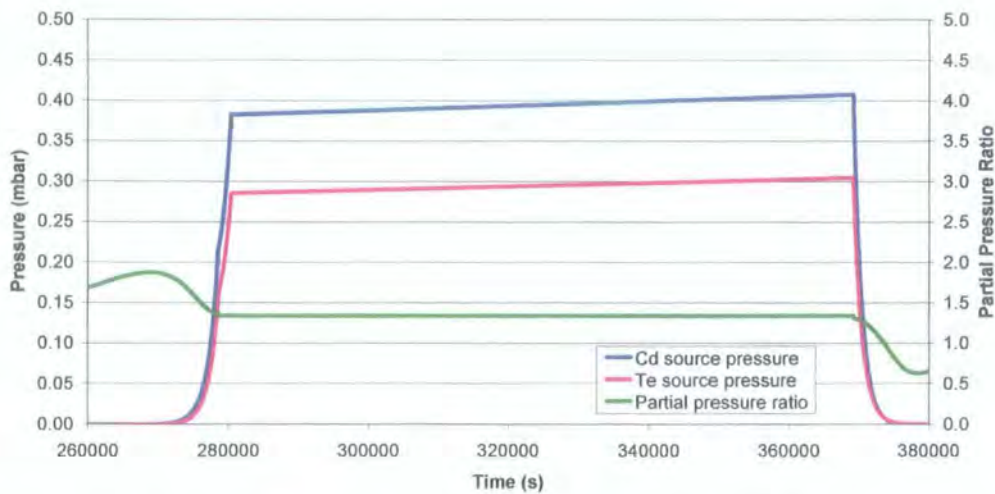
Figure 7.4: Growth vapour partial pressures and ratio in simulation of Run 80

These discrepancies are most likely to be due to errors in the optical absorption measurements. The partial pressure ratio of 1.33 is regularly observed in molecular flow regimes, and has been confirmed for a number of effusion-type semi-open systems [2-4], and is highly likely to be the ratio in the MTPVT growth tube. Chapter 6 outlined the light source setup for the absorption apparatus, with the light entering the growth tube less intense than the light entering the source tube, because it was directed via two mirrors. Saturation would have occurred at a much lower pressure, and, although the growth pressure was less than the source, this may have occurred. Examination of the basic data shows, at the growth time, the measured voltage was indistinguishable from the background, which would explain the broadly constant pressures.

7.3 EFFECT OF CRYSTAL DIAMETER AND ANNULUS GAP

The increase of the crystal diameter from 32 to 52 mm described in Chapter 4 appeared to decrease the effect of the annulus. A series of simulations were carried out to try to determine the dependence of growth rate on the annulus

gap and crystal radius. The flow rates at time = 6000 s (i.e. in the plateau region with the source at 870°C, the seed at 700°C and the crossmember at 900°C) were taken for simulations of the growth conditions of Run 65 for a range of annulus gaps and crystal radii.

Figure 7.5 shows that for a given crystal radius, the annulus flow rate and sublimation rate increased as the annulus increased, whilst the growth rate decreased. As might be expected, an increasing annulus gap acted to increase the growth side sink for the CdTe, thus reducing the growth side pressure, ensuring greater flow through the capillary and thus the sublimation rate increased to compensate. Similarly, the decrease in growth side pressure reduced the growth rate.
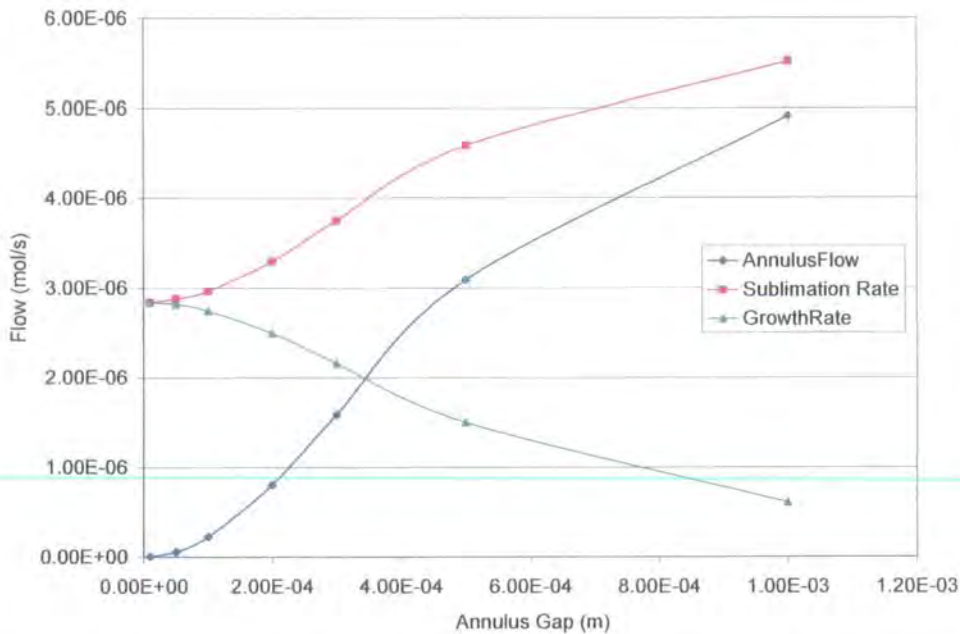
Figure 7.5: Variation in flows with annulus gap for 16mm radius crystal
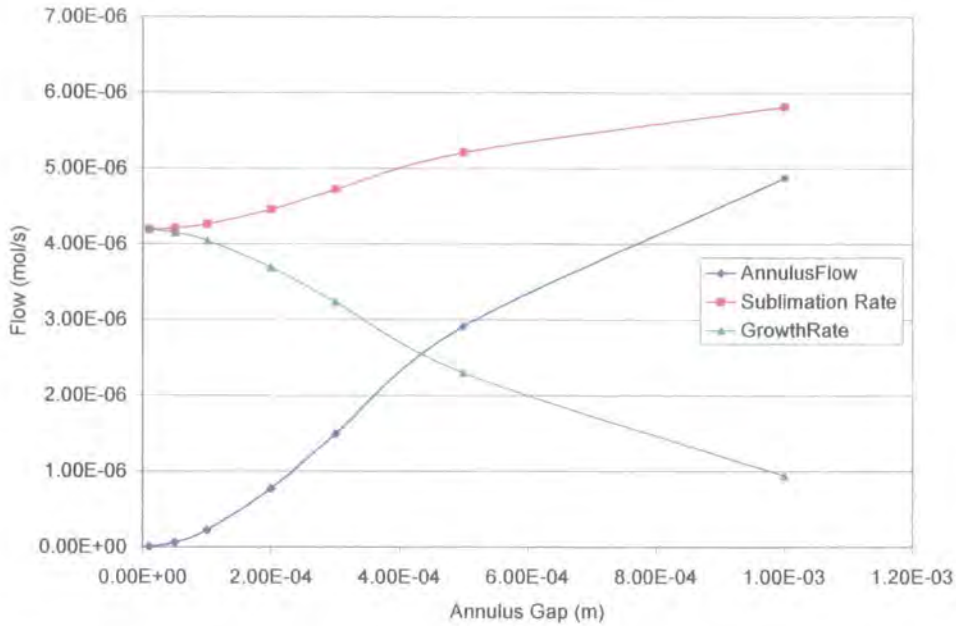
Figure 7.6: Variation in flows with annulus gap for 25mm radius crystal

Both Figures 7.5 and 7.6 show a cross-over point above which the annulus

flow rate is greater than the growth rate. A comparison of the graphs shows

for a crystal of radius 16 mm the annulus flow rate exceeded the crystal

growth rate at a smaller annulus gap, of about 0.35 mm compared to 0.45

mm for the 25 mm crystal. This has great implications for the crystal growth,

showing, for 16 mm radius crystals, if the annulus gap is greater than 0.35

mm the annulus flow will dominate and suppress the crystal growth. As

discussed in section 5.4.6 an accurate annulus gap is very difficult to obtain,

and is likely to be at least 0.2 mm. Therefore any growth in this MTPVT

system with a 16 mm radius pedestal was likely to be more difficult to control

than growth on a 25 mm pedestal. This indicated it was necessary to know

the effect of changes of the crystal radius. The smallest possible annulus gap

is believed to be about 0.2 mm, and Figure 7.7 shows the effects of the

crystal radius with this annulus gap.
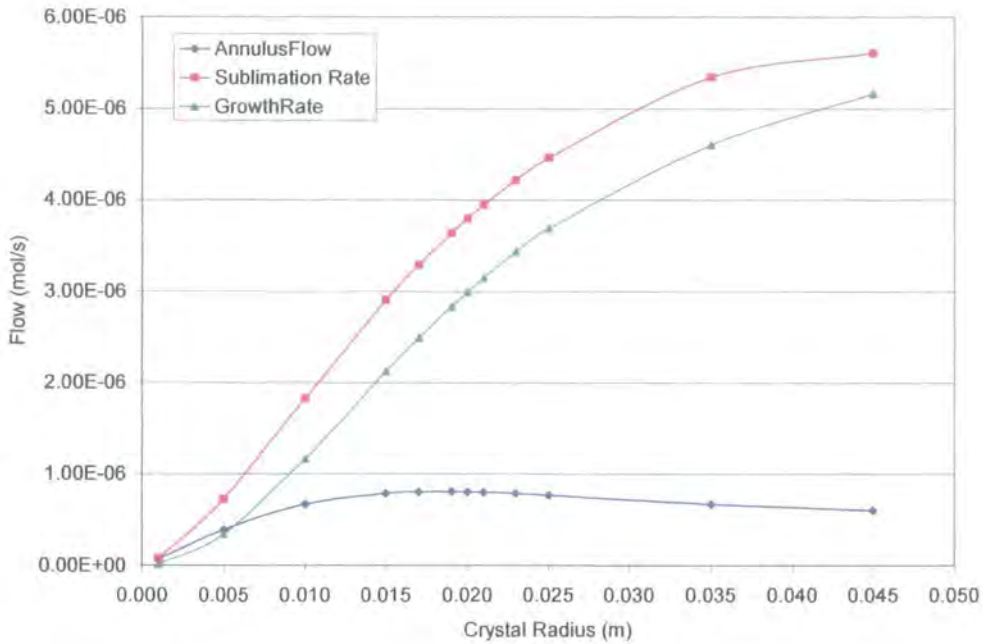
Figure 7.7: Effects of crystal radius on flow rates for a 0.2mm annulus gap

The sublimation and growth rates both increased steadily as the crystal radius increased in Figure 7.7. However, at low crystal radii, the annulus flow increased, reached a broad maximum around 15 mm and began to decrease. The growth was therefore increasingly independent of the annulus at large radii, as was observed through the growth runs at different growth tube radii described in Chapter 4. It is also noticeable that for crystal radii below 5 mm the annulus flow dominates over the growth rate. A progression of the simulation allowed the effects on the flow rates of both the annulus gap and crystal radius together to be modelled. Figures 7.8, 7.9 and 7.10 give the effects of the crystal radius for various annulus gaps on the growth rate, annulus flow rate and sublimation rate respectively.
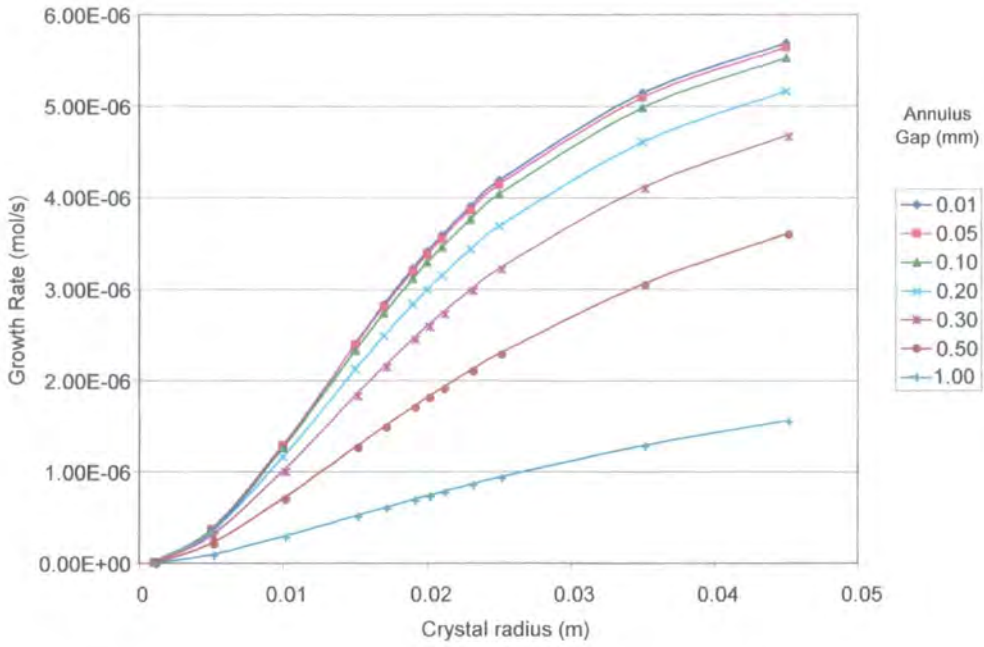
Figure 7.8: Effect of crystal radius on growth rate for various annulus gaps
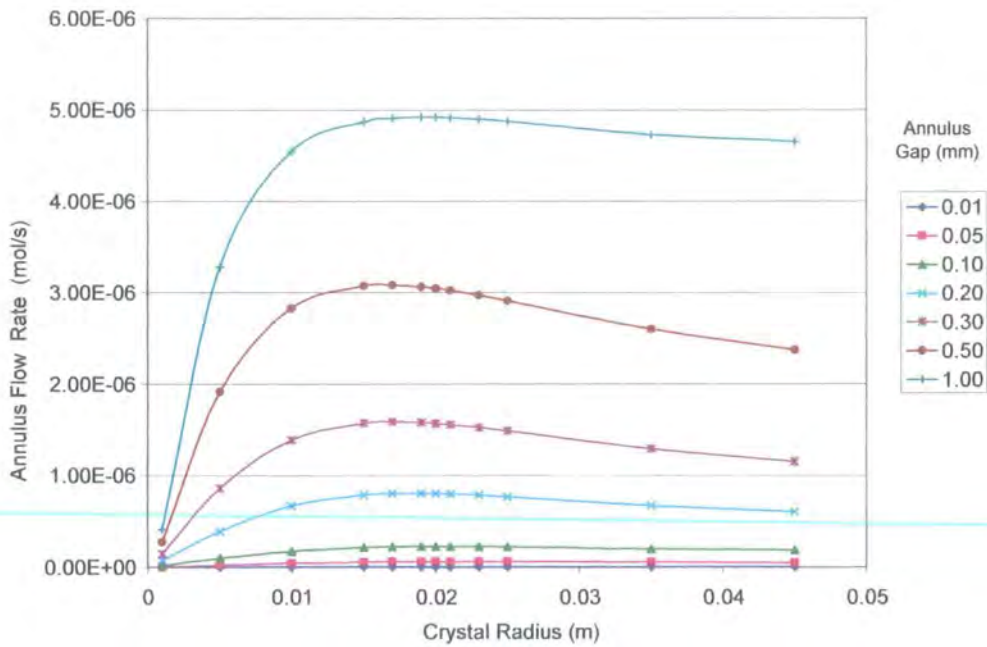
Figure 7.9: Effect of crystal radius on annulus flow rate for various annulus gaps

174
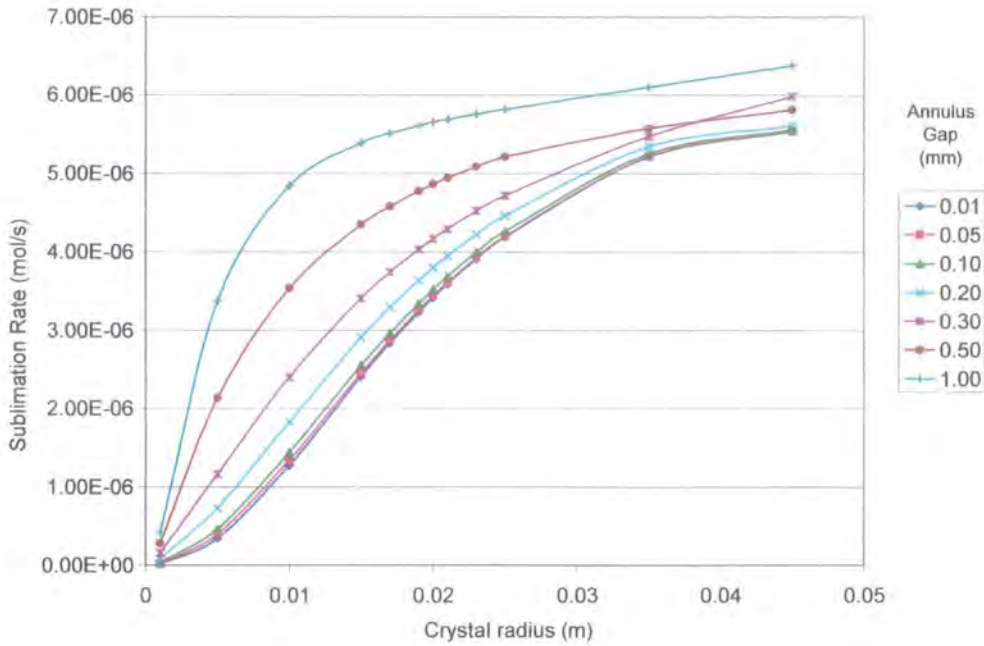
Figure: 7.10: Effect of crystal radius on sublimation rate for various annulus gaps

Several important trends became apparent in Figures 7.8, 7.9 and 7.10. It is clear for increasing radii the growth and sublimation rates increased, and for increasing annulus gaps the growth rate decreased and sublimation rate increased. In Figure 7.9 the annulus flow rates increase with radius at low radii, reach a plateau around 15 mm radius, and decrease beyond about 20 mm. As was observed during growth, the larger annulus gaps increased the annulus flow rate. The rate of decrease of flow, with the crystal radius beyond the plateau, appeared to increase with the annulus gap up until an annulus gap of 0.5 mm, yet for an annulus gap of 1 mm this decrease slowed down.

These trends can also be seen in Figures 7.11 to 7.13, which show the effects of annulus gap on the flows for various crystal radii.
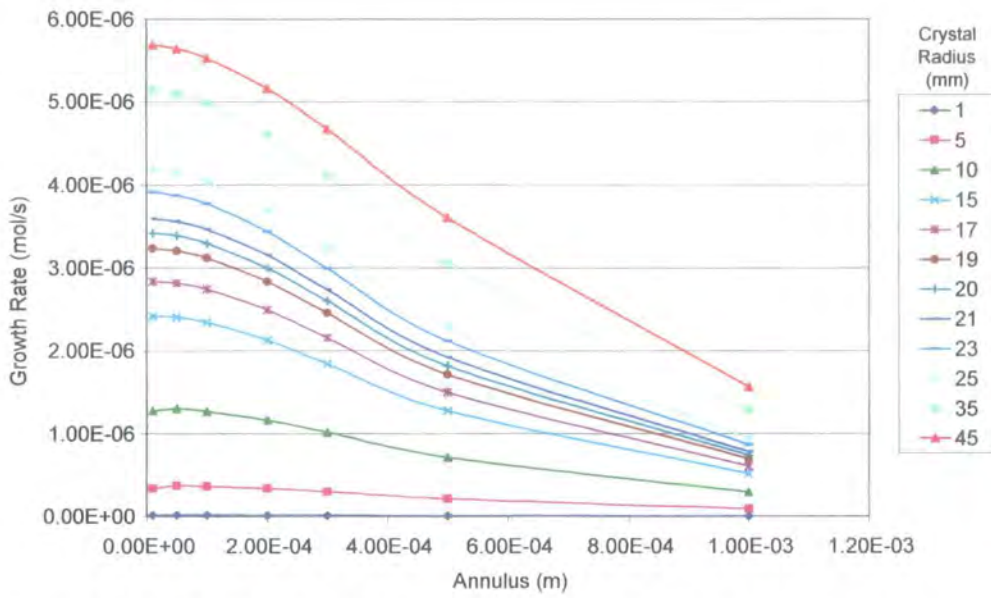
Figure 7.11: Effect of annulus gap on growth rate for various crystal radii
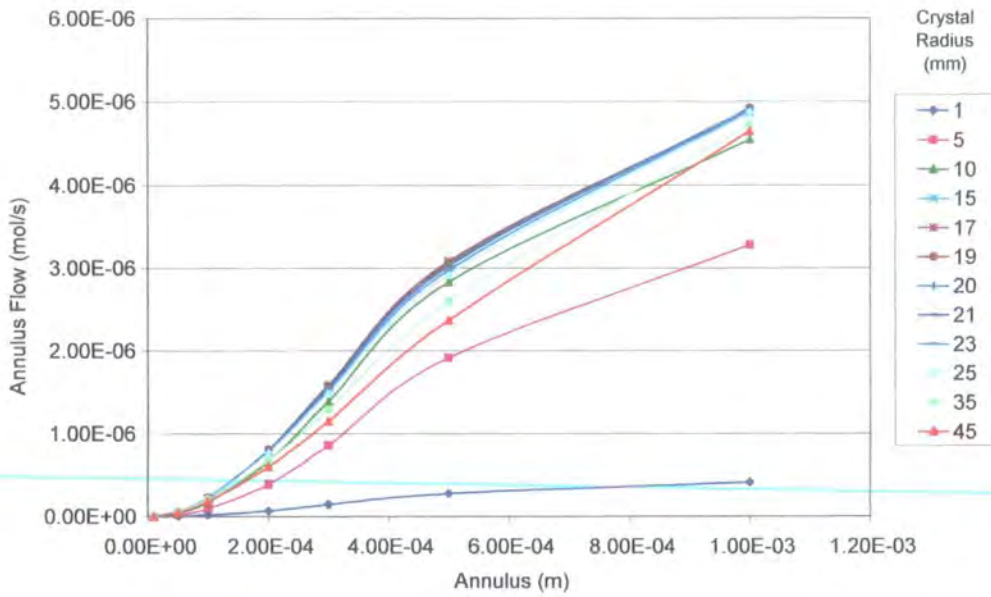
Figure 7.12: Effect of annulus gap on annulus flow rate for various crystal radii
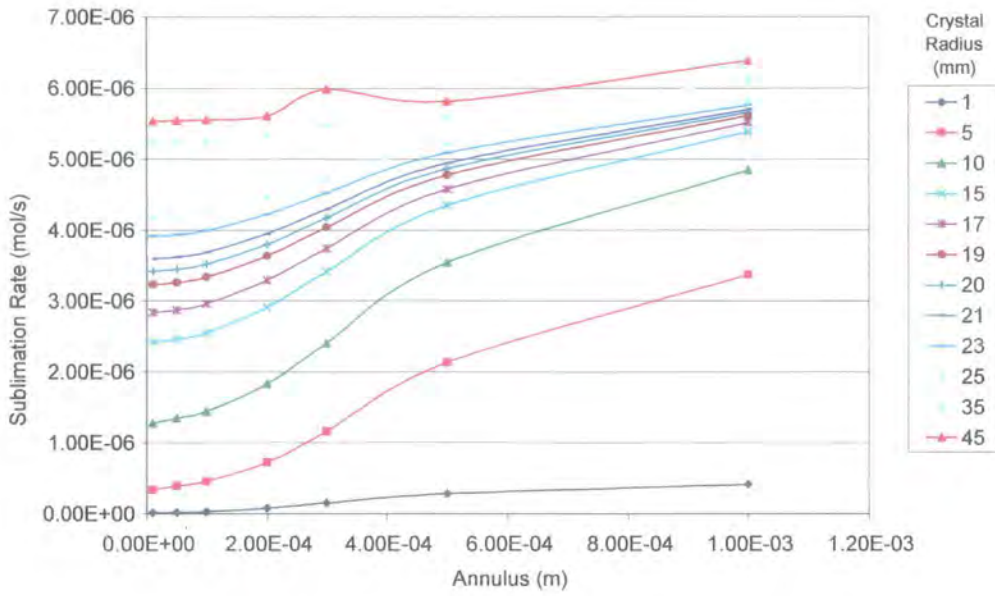
Figure 7.13: Effect of annulus gap on sublimation rate for various crystal radii

In the mid range of annulus gaps (around 0.5mm) in Figure 7.12, the highest annulus flow was for crystals of radius 15 and 17 mm. At the lowest crystal radii, the annulus flow remained very low, since the sublimation rate was very low. The largest radius, 45 mm, showed less annulus flow than the third lowest radius, 10 mm. These figures agree with the increase, plateau then decrease in the annulus flow seen in Figure 7.9.

The simulations show that, for larger radii, the annulus gap becomes less important in terms of growth rate, suggesting larger crystals are less likely to sublime and gain mass more rapidly. This is consistent with the observed growth rates, reported in Chapter 4, following the decision to increase the growth tube (and therefore crystal) radius.

7.4 VARIATIONS IN HEIGHT ACROSS CRYSTAL SURFACE

The CdTe boules grown in the earlier stages of the development of the MTPVT system were regularly wedge-shaped, with large variations in height observed across the crystal surface. Additional shielding placed between the growth and source tubes reduced the magnitude of the variations, implying the variations were the results of a temperature gradient across the surface.

For a crystal, growing in a growth tube containing a constant homogeneous vapour pressure P, any temperature variations across its surface would lead to a variation in linear growth rate. From equation (5.7), the linear growth rate at each point on the surface was a function of the crystal temperature T_{cr} at that point,

$$R(T_{cr}) = \beta_v(T_{cr})[P - P_\infty(T_{cr})]$$
(7.1)

as both the kinetic coefficient β_v and the crystal equilibrium pressure P_∞ were functions of the temperature.

The simulation of Run 65 outlined in Chapter 5 delivered a cadmium growth vapour pressure of 114 Pa, and a growth vapour stoichiometry of 1.33. Figure 7.14 shows the variations in the linear growth rate with crystal surface point temperatures, obtained by placing these values, along with the other standard constants presented in Chapter 5, into equation (7.1).
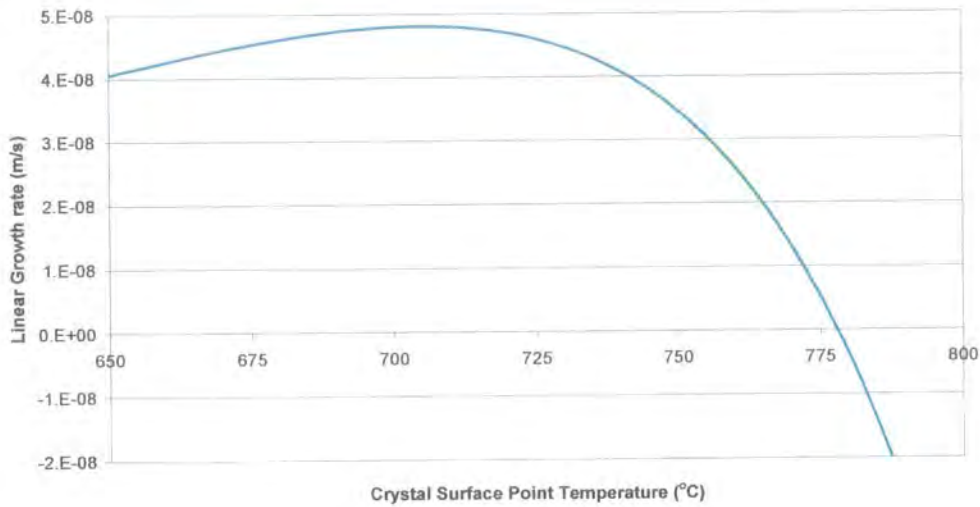
Figure 7.14: Effect of crystal surface point temperature on linear growth rate

The linear growth rate was seen to rise with temperature up to a maximum at 705°C, and decrease rapidly beyond 730°C, with the crystal subliming beyond 778°C. The crystal temperature during growth was measured by a thermocouple, placed alongside the growth tube at the relevant height, and it was not possible to measure the temperature gradient inside the growth tube, leading to uncertainties in the surface temperature. The boule Ophelia, which was introduced and discussed in Chapter 4, was grown at a measured seed temperature 710°C and measured 12 mm at one side and 10 mm on the other. Taking into account the original seed size of 2 mm, the growth on one side was only 80% of the other, which implies a 35°C variation across the crystal. This appears slightly high when compared to the vertical temperature gradient of only 50°C between the growth middle (seed) and growth top thermocouples, which implies other factors may also have affected the growth. Differential growth rates on different grains may have also been a factor.

After the extra shielding was added to the MTPVT system the wedge-shaped growth disappeared, although the grown crystal surfaces were not completely flat. The use of a tube heater would provide a concentric radial temperature profile, and also the pressure above the crystal surface may not have been homogeneous. With vapour flowing through the annulus around the crystals the pressure would also have a certain radial profile across the crystal surface. According to (7.1), at a constant temperature, the growth rate would increase linearly with vapour pressure, therefore a pressure variation ΔP would lead to a variation in linear growth rate of $\beta_v \Delta P$.

7.5 ESTIMATION OF GROWTH RATE PARAMETERS

7.5.1 Source and Growth Surface Smoothness

One parameter which affected the growth rate and sublimation was the surface smoothness (δ) which was related to the probability that an incoming atom would absorb on a kink site. The vapour growth kinetic coefficient β_v, was proportional to the reciprocal of the square of the smoothness

$$\beta_v = \left(\frac{a}{\delta}\right)^2 \frac{a^3}{\sqrt{2\pi mkT_g}} \exp\left(\frac{-\Delta U}{kT_g}\right) \qquad (7.2)$$

Smoother surfaces contained a lower density of kink sites, characterised by a higher δ value, giving a lower growth and sublimation rate. The complex nature of the MTPVT system meant changes in the kinetic conditions did not lead directly to changes in the mass transport rate, however, as the other elements in the process appeared to compensate for these variations.

Both the source and growth smoothness were included explicitly in the model for the simulation of the growth, and therefore their effects could be modelled. Figure 7.15 shows the results of a series of simulations in which the effects of

the growth temperature on the growth rate are observed for a series of growth-surface smoothness values, with the source smoothness δ/a set at 1.0. Figure 7.15 also shows the effects of the crystal temperature on the growth rate from growth runs in the MTPVT system.
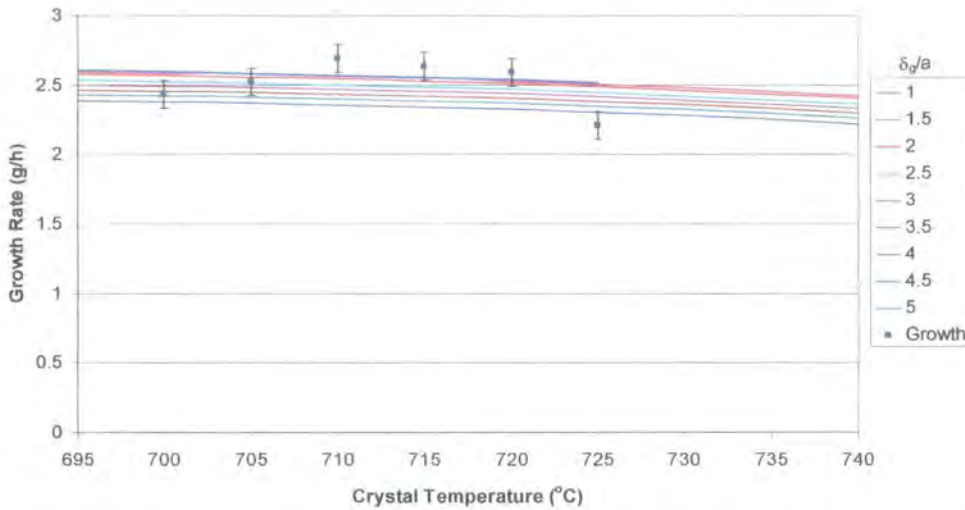
Figure 7.15: Effect of crystal temperature on growth rate modelled for a range of growth surface smoothnesses and from growth runs

The growth rate appears to increase as the surface smoothness decreased, as expected from equation (7.2), although the rate does not appear to be proportional to the $(a/\delta)^2$ factor given in (7.2). Markov [5] gave constant values of $\delta \cong 3a$ for the growth on rough faces, which would fit well with the results of the model displayed in Figure 7.15. Teramoto [6] stated that, for CdTe at 900°C during vapour growth, the mean distance between kinks was ~ 17 Å, corresponding to $\delta \sim 2.6a$, which would also fit with the model despite the differences in temperature.

Polycrystalline CdTe pieces were used as the source material in the MTPVT system, and therefore the source surface would have been much less smooth than the polished growth surface. This places an upper bound on the source smoothness, therefore its value must have been between a single lattice parameter and the growth crystal smoothness $3a$. Figure 7.16 shows the results of another series of simulations in which the effects of the growth temperature on the growth rate are observed for a series of growth surface smoothness values, with the growth smoothness δ/a set at 3.0.
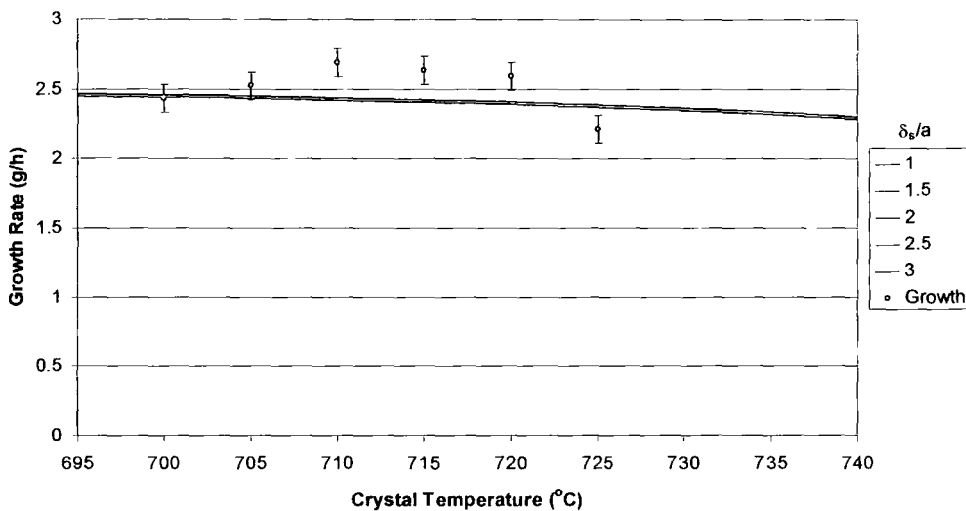
Figure 7.16: Effect of Crystal Temperature on Growth Rate Modelled for a Range of Source Surface Smoothness, with Growth Run Data Displayed for Comparison

The results displayed in Figure 7.16 show the growth is not greatly affected by the source smoothness. A doubling of the smoothness only decreased the growth rate by 0.4% at low temperatures, with even less effect at higher growth crystal temperatures. Therefore any (δ/a) value between 1.0 and 3.0 is sufficient to model the growth in the MTPVT system to a good degree of accuracy.

These results imply the growth and sublimation rates are not strongly dependent on δ. However, calculations on the sensitivity of β_v to changes in δ suggest otherwise. From the definition of β_v in equation (5.9)

$$\beta_v = \theta^2 \frac{a^3}{\sqrt{2\pi mkT_g}} \exp\left(\frac{-\Delta U}{kT_g}\right) \tag{7.3}$$

using the substitution

$$\theta = \frac{a}{\delta} \tag{7.4}$$

A small change $\Delta\theta$ will change β_v by $\Delta\beta_v$, i.e.

$$\Delta\beta_v = \frac{\partial\beta_v}{\partial\theta}\Delta\theta \tag{7.5}$$

With

$$\frac{\partial\beta_v}{\partial\theta} = 2\theta\frac{a^3}{\sqrt{2\pi mkT_g}}\exp\left(\frac{-\Delta U}{kT_g}\right) = \frac{2\beta_v}{\theta} \tag{7.6}$$

$$\therefore \quad \Delta\beta_v = \frac{2\beta_v}{\theta}\Delta\theta \quad \text{or} \quad \frac{\Delta\beta_v}{\beta_v} = \frac{2\Delta\theta}{\theta} \tag{7.7}$$

Therefore an error in δ of 20% e.g., from $\delta = 2\frac{1}{2}$ *a* to *3 a* compounds to an error in β_v of

$$\frac{\Delta\beta_v}{\beta_v} = \frac{2\times\frac{1}{15}}{\frac{2}{5}} = \frac{1}{3} \tag{7.8}$$

i.e. an error in β_v of ~33% compared to the error in δ of only 20%. The corresponding change in δ_g displayed in the simulation results in Figure 7.15 only shows an increase in the growth rate of 1.0%, implying the growth smoothness was not a controlling factor in the growth rate. Similarly, a corresponding change in the source smoothness did not affect the growth rate, as illustrated in Figure 7.16, and the capillary flow restrictor was likely to be a more important factor.

7.5.2 Estimation of ΔU

With estimates for all of the other growth parameters, it was possible to make an estimate for the crystal growth activation energy ΔU. Another series of simulations, with ΔU values between 0.05 and 1 eV, and using the estimates for the other parameters, allowed effects of the activation energy upon the growth rate, annulus flow rate and capillary flow rate to be modelled, with the results of simulations with the growth crystal temperature at 715°C displayed in Figure 7.17.
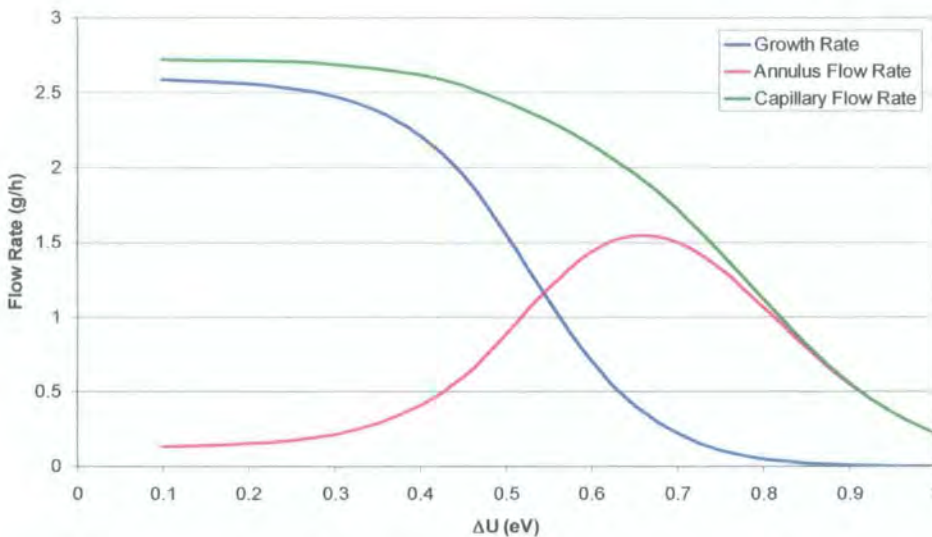
Figure 7.17: Effect of ΔU on the Mass Transport Rates

At low activation energies Figure 7.17 showed little change in transport rates with activation energy, and the transport rates appeared to be governed by other factors such as the crossmember flow restrictor capillary. As ΔU increased above 0.3 eV, the activation energy began to control the growth, with a fall in crystal growth rate observed above this level. The source sublimation rate (which has been shown to be equal to the capillary flow rate during the growth plateau period) did not appear to decrease significantly until 0.5 eV, due to the higher source temperature than growth. With the

capillary flow rate decreasing slower than the falling growth rate, the annulus flow rate was observed to rise, and at high activation energies almost all of the material flowing into the growth tube would have flowed through the annulus. At activation energies well above an eV the sublimation would stop and no flow would occur.

Simulations allowed the ΔU dependence of the growth rate / crystal temperature relationship to be modelled, with the simulation results given in Figure 7.18.
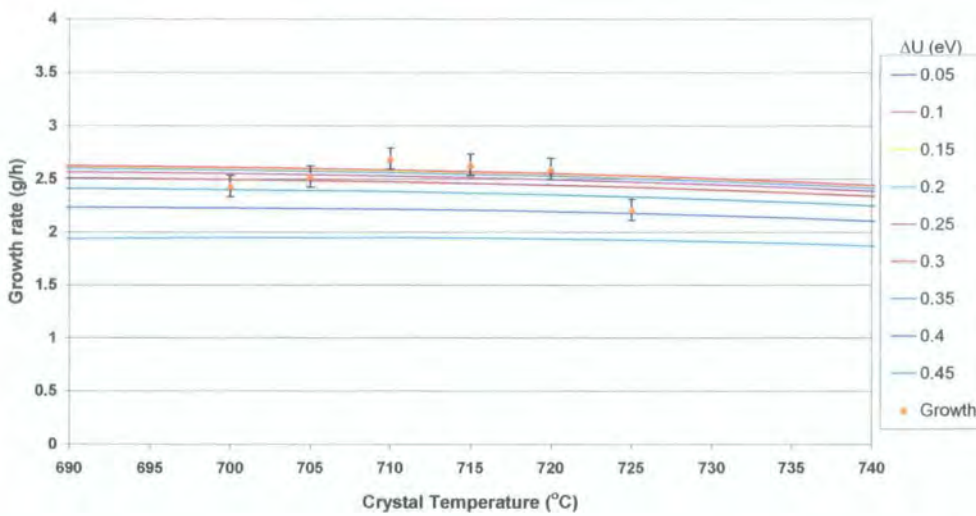
Figure 7.18: Effect of Crystal Temperature on Growth Rate Modelled for a Range of ΔU, with Rates Observed in Growth Runs Included for Comparison

The activation energies above 0.45 eV appear to inhibit growth to an extent not observed during growth runs, and this may be set as the upper limit for ΔU in this simulation. Both Figures 7.17 and 7.18 show the growth rate is insensitive to the activation energy at low values of ΔU, and therefore it is not possible to place a lower limit estimate on ΔU through this method.

The sensitivity of the growth parameter β_v to changes in the activation energy ΔU could be calculated using a method similar to the one used for the surface smoothness. From the definition of β_v in equation (5.9)

$$\beta_v = \beta_o \exp\left(\frac{-\Delta U}{kT_g}\right) \tag{7.9}$$

where

$$\beta_0 = \left(\frac{a}{\delta}\right)^2 \frac{a^3}{\sqrt{2\pi mkT_g}} \tag{7.10}$$

$$\therefore \quad \frac{\partial \beta_v}{\partial(\Delta U)} = \frac{-\beta_0}{kT}\exp\left(\frac{-\Delta U}{kT}\right) = -\frac{\beta}{kT} \tag{7.11}$$

For a small error $\Delta(\Delta U)$ in ΔU

$$\frac{\Delta \beta_v}{\beta_v} = -\frac{\Delta(\Delta U)}{kT} \tag{7.12}$$

Unlike the sensitivity to δ, the error in β_v is only dependent upon the change in ΔU, not on the actual value, although the sensitivity is now temperature dependent. For a growth temperature of 710°C, $kT = 0.085$ eV, and a 20% increase in the activation energy from 0.25 to 0.30 eV gives

$$\frac{\Delta \beta_v}{\beta_v} = -\frac{0.05}{0.085} = -0.59 \tag{7.13}$$

This high sensitivity is not observed in the results of the simulation (presented in Figure 7.18), providing more evidence that the growth is limited by the mass transport through the capillary flow restrictor and not kinetically limited by the kinetic coefficient of the growing crystal. Hence, as anticipated, the inclusion of the capillary in the MTPVT crossmember to control growth rate results in mass transport control of the growth process.

In the growth model the activation energy has been taken to be equal for both Cd and Te_2, but this was unlikely to be true in practice. The activation energy of Te_2 must include the breaking of the Te-Te bond which would precede the incorporation of a Te atom onto the crystal surface, while no bond breaking is required for Cd incorporation.

7.6 CONCLUSIONS

This chapter has compared the results of growth runs, optical absorption studies and computer simulations, to account for observations. The source side partial pressure measurements obtained by the *in situ* optical absorption system outlined in Chapter 6 broadly agreed with the pressures predicted by the simulation in Chapter 5, with the source partial pressure ratio approximately the same in both. The steady rise in tellurium partial pressure observed during growth, however, did not agree with the model which predicted a steady level throughout the growth. There was a large discrepancy between the growth side partial pressures predicted by the model and those measured by the optical absorption system. As the model predicted a similar partial pressure ratio to other models, it is probable the error was due to the optical absorption system, possibly because of the low intensity of light entering the growth side.

During the growth runs it was found that increasing the crystal radius from 16 to 25 mm reduced the likelihood of subliming the seed crystal and also reduced the flow through the annulus. A series of simulations for various crystal radii and annulus gaps showed the annulus gap was less of a factor in controlling the growth rate at higher crystal radii.

Variations in the crystal height across the surface, observed after the crystals were removed following growth, were investigated by modelling the growth rate as a function of temperature. A 35°C variation of growth temperature was required to match the observed height difference, but this value appears large in comparison to the linear temperature gradient around the crystal, and other factors may have had an effect.

Estimations on the growth parameters were made through comparing growth with simulations. The source smoothness was found to have little effect on the growth, with values between 1 and 3 times the lattice parameter fitting the results. The growth smoothness was found to agree with that in the literature between 2.6 and 3 *a*. The activation energy ΔU was found to have a maximum value around 0.45 eV, while no lower limit could be imposed.

7.7 REFERENCES FOR CHAPTER 7

[1]   E. D. Plalik. *"Handbook of Optical Constants of Solids"*. Academic Press (1985).

[2]   R. F. Brebrick and A. J. Strauss. *"Partial Pressures and Gibbs Free Energy of Formation for Congruently Subliming CdTe$_{(c)}$"*. J Phys Chem Solids **25** (1964) 1441.

[3]   A. W. Brinkman and J. Carles. *"The Growth of Crystals from the Vapour"*. Progress in Crystal Growth and Characterization of Materials **37** (1998) 169.

[4]   J. Carles Alabert. *"Optical Vapour Pressure Monitoring and Mass Transport Control During Bulk CdTe Crystal Growth in a Novel Multi-Tube PVT System"*. PhD Thesis. University of Durham. (1998).

[5]   I. V. Markov. *"Crystal Growth for Beginners: Fundamentals of Nucleation, Crystal Growth and Epitaxy"*. World Scientific London (1995).

[6]   I. Teramoto. *"Vapour Growth Patterns of CdTe Crystals"*. Philosophical Magazine **8** (1963) 357.

Chapter **8**

Conclusions and Scope for Future Work

8.1 CONCLUSIONS

There were three main aims to this project;

- redevelop a vapour growth system for the growth of II-VI compounds, in particular cadmium telluride, and ultimately ternary compounds,

- develop a model to simulate the growth of CdTe in the redeveloped system,

- design and construct a system to measure the vapour partial pressures *in situ*.

The Multi Tube Physical Vapour Transport (MTPVT) system, which took about 2 years to redevelop, was originally designed to grow CdTe crystals from a binary CdTe source. The addition of a second source, which was outlined in Chapter 3 and required a comprehensive redesign and rebuild of the apparatus, including the control software which was completely rewritten in C++, allowed flexibility of the source compounds and crystals grown.

The growth of CdTe crystals in the redeveloped MTPVT system has been studied, with particular emphasis given to the growth tube design and the seed crystal. Several growth tube designs were tested, with the best results obtained with a solid disc pedestal, and, to avoid nucleation on the pedestal, it was necessary for the seed crystal to completely cover the pedestal. Increasing the growth tube diameter, and consequently the diameter of the seed crystal, reduced the sensitivity to uncertainties in the annulus dimensions, making the growth process easier to control, with seed sublimation less likely to occur.

The maximum stable crossmember temperature was around 920 °C, permitting source temperatures of 870 °C to be used, without colder spots on the glassware causing a large amount of condensation. The optimal seed temperature to use in correspondence with these other temperatures was between 700 and 725 °C. Ramping up the source and seed temperatures at different rates, to reach the target values simultaneously, reduced the amount of spurious nucleation on glassware around the pedestal, while at the same time minimising the amount of seed sublimation during the heating up period.

Several different types of seed crystal were used, with the best results for single crystal CdTe seeds and CdTe seeds with only a few grains. The use of GaAs and Si as seeds only produced polycrystalline CdTe boules.

Several preliminary experiments, to test the transport of CdTe and ZnTe binaries for growth of CdZnTe, delivered some ZnTe transport, but the majority of the ZnTe appeared to condense at the top of the growth tube.

A computer simulation to model a standard CdTe growth run has been developed, with the predicted transport rates close to the experimental results. The MTPVT system was analysed in terms of a series of flows from the source to the growing crystal and beyond, incorporating the source sublimation, capillary flow, crystal growth and annulus flow. The variations in flows, partial pressures and vapour partial pressure ratios were modelled throughout the growth process, with the results matching expectations.

A system to measure the partial pressures *in situ* during growth by optical absorption measurements was developed. The system, which used computer controlled filter wheels to select the appropriate wavelengths for detection by photomultiplier tubes, employed cadmium and zinc lamps to provide incident light at the necessary wavelengths. The output from the 1.5 kW quartz halogen lamps, used to optically heat the crossmember, saturated the photomultiplier tubes at longer wavelengths, requiring the use of neutral density filters over some of the wavelength selecting filters.

The results obtained from the growth runs, the computer simulations and the optical absorption measurements were compared. Analysis of the experimental data obtained from the optical absorption system has shown the source partial pressures to be close to those predicted by the model, although the data gave growth side partial pressures about an order of magnitude higher than the model, with the growth partial pressure ratio also higher than the model's prediction.

A series of simulations were carried out to determine the effect of the crystal radius. The results predicted the annulus gap had less effect at higher crystal

radii, which agreed with the observed trend when the diameter of the growth tube was increased.

By comparing a series of simulations with the observed growth, estimations for some of the parameters in the CdTe vapour kinetic coefficient were made. The growth smoothness was found to be around three times the lattice parameter, while the source smoothness was found to be less significant and could be any value between a single lattice parameter and the value of the growth smoothness. An upper limit of 0.45 eV could be given for the activation energy, and the growth process appeared to be controlled by the mass transport rate and not the sublimation or growth rates.

The 214 nm absorption line of zinc vapour was found, using a benchtop absorption experiment, to deviate greatly from Beer's Law. Optical density-pressure relationships for MTPVT conditions were determined for the 326 nm cadmium absorption line and for several wavelengths in the broad tellurium dimer absorption spectrum.

8.2 SCOPE FOR FUTURE WORK

Although a quantity of good quality CdTe crystals have been grown, a number of issues remain unresolved. The growth on multi-grain seeds has been well developed, and further growth on single crystal seed is necessary to achieve single crystal boules.

Several of the growth parameters could be investigated further to optimise the growth process. A range of seed temperatures and several temperature profiles have been tested, with positive results, and further study could help

optimise the growth process. In this project the source temperature was always set at 870 °C, because it was felt necessary to keep some parameters constant throughout the development process, and this could be an area for further experimentation.

The addition of the second source tube to the MTPVT system gave flexibility in the growth of II-VI compounds, but this flexibility has yet to be fully utilised. Several preliminary experiments to test the growth of CdZnTe took place, with encouraging results, but a lot of further work will be required to grow this material to the required standard. Other fields which may be investigated include the growth of CdTe from the elements and the introduction of a dopant.

Due to the cost and length of time to complete a growth run, care should be taken when deciding the areas of study. Each growth run takes about a week to complete, and the source material and power costs upwards of £200 with single crystal seeds costing over £1200, so no line of study should be entered into lightly. Another factor limiting the studies has been the unreliability of the crossmember heater lamps. The lamps failed about every other growth run at the start of the project, although with increased experience this was reduced to about one in five. If money were available to develop the MTPVT system, a heating system to replace the lamps, with, for example, strip heaters made of PG/PBN, would improve the apparatus.

The *in situ* partial pressure measuring system showed good results for the detection of the CdTe source, but the results for the growth tube were probably erroneous. Changes to the light source design could improve these

results by increasing the intensity of the light entering the growth region. If the growth of CdZnTe is studied, then the capabilities of the system may be fully utilised, and the Zn pressure-absorption relation may be verified.

Estimates for the parameters in the kinetic coefficient have been made, and the simulation showed accurate modelling of the growth and transport rates. If the kinetic coefficient were to be more directly studied experimentally, then the values for these parameters may be better determined.

Finally, this project has developed a flexible system for the vapour growth of II-VI compounds, with some good results already been obtained, and should provide a firm base for further study.

Appendix **I**

Growth Control Program

The MTPVT system was computer controlled by a program named BenProgram written in the Visual C++ language, which was outlined in Chapter 3. The complete program is over 80 pages long, and only some of the important elements of the code are presented here.

The main algorithm of the program was contained in the BenProgramDlg.cpp implementation file. The start of the file called the external header files which were linked to the program, and defined as classes the different furnace zones.

```
// BenProgramDlg.cpp : implementation file
//Main file which contains main program

//Files to include
#include "stdafx.h"
#include "BenProgram.h"
#include "BenProgramDlg.h"
#include "DlgProxy.h"
#include <fstream.h>
#include <iostream.h>
#include <time.h>
#include "FurnaceControl.h"
#include <commdlg.h>

//Opening file output class
        ofstream fout;
        ofstream webout;
```

```
//Opening time variables
        time_t start, finish, thistime, lasttime;

//Creating the furnace zone classes
        CZone CdTel;                                 //CdTe Source Heater
        CZone ZnTel;                                 //ZnTe Source Heater
        CZone GrTop;                                 //Growth Top Heater
        CZone GrMid;                                 //Growth Middle Heater
        CZone GrBot;                                 //Growth Bottom Heater
        CZone CrMem2;                                //Twin Crossmember heaters
        CZone CrMem3;                                //Triple Crossmember heaters
```

The OnInitDialog Function sets the intial variables when the program is started and installs a timer to call the main algorithm every 10 ms.

```
BOOL CBenProgramDlg::OnInitDialog()
{
        CDialog::OnInitDialog();
//Run when program first starts

// opening the dialog box to select filename for output
        Saver();
        UpdateData(FALSE);

// writing column headers to output file
        fout << "Time (s),Cd Tar T(C), Cd T(C),Zn Tar T (C),  Zn T (C),  GrTop Tar (C),";
        fout << "GrTop T (C), GrMid Tar (C), GrMid T(C), GrBot Tar (T), GrBot T(C),";
        fout << "CrMem2 Tar (C), CrMem3 Tar (C), CrMem2 T(C), CrMem3 T(C),";
        fout << "Cd Pow(%),  Zn Pow(%), GrTop Pow(%), ";
        fout << "GrMid Pow(%),  GrBot Pow(%),CrMem2 Pow(%), CrMem3 Pow(%)" << "\n";

// Starting the temperature profile dialog box
                m_prof.DoModal();
                UpdateData(TRUE);

//Setting initial time variables
        timenow         = 0;
        prevtime  = 10;

//Setting target flags to false intially
        CdTFlag            = FALSE;
        ZnTFlag            = FALSE;
        GrTopTFlag         = FALSE;
        GrMidTFlag         = FALSE;
        GrBotTFlag         = FALSE;
        CrMemTFlag         = FALSE;
        CrMem3TFlag = FALSE;

// Setting stages to ramping
        ii = 0;
        jj = 0;
        kk = 0;
        mm = 0;

//input addresses for thermocouples
        CdTel.m_inadd = 14;
        ZnTel.m_inadd = 1;
        GrTop.m_inadd = 15;
        GrMid.m_inadd = 9;
        GrBot.m_inadd = 8;
        CrMem2.m_inadd = 0;
        CrMem3.m_inadd = 7;

//output addresses for DA card to thyristor packs
        CdTel.m_outadd  = 0x10A;
        ZnTel.m_outadd  = 0x108;
        GrTop.m_outadd  = 0x100;
        GrMid.m_outadd  = 0x102;
        GrBot.m_outadd  = 0x104;
```

```
                CrMem2.m_outadd = 0x106;
                CrMem3.m_outadd = 0x10C;

//Install the system timer
        int iInstallResult;
        time(&start);
        lasttime = start;
        iInstallResult = SetTimer ( 1,
                                    10,
                                    NULL);
        return TRUE;  // return TRUE  unless you set the focus to a control
}
```

The OnTimer function was called every 10 ms and controlled the main

algorithm. From this function all the temperatures were read, powers updated

and screen display updated through the calls to other functions.

```
//This function is called at intervals defined in the "SetTimer"
//function in the "OnInitDialog" function
void CBenProgramDlg::OnTimer(UINT nIDEvent)
{
        UpdateData(TRUE);

//Getting current time from time function
        time(&finish);
//Calculating difference in time now and time at start
        timenow = int(difftime(finish, start));
        m_timeshow = float(timenow);

//Calling function to convert time in s to h:m:s
        TimCon(timenow, m_hours, m_minutes, m_seconds);

//Calculating time between this cycle and last cycle
        now = float(difftime(finish, lasttime));
        m_dummy = now;

//Running the temperature control every second
        if (now >= 1.0){

//Calling function to step target temperature over time
                TarTemp();

//Calling function the calculate and output powers
                PowOut();
                UpdateData(FALSE);

//Calling function to control flags
                Flagsy();
                UpdateData(FALSE);

//Calling function to set stage status notifiers
                Stages();
                UpdateData(FALSE);

//Calling function to output to files
                OutFil();

//Getting timenow
                time(&lasttime);
        }

        CDialog::OnTimer(nIDEvent);
}
```

The PowOut function, which was called every second by the OnTimer

function, called the functions to obtain the current temperature and set the

output power.

```
//Function to calculate then output powers
void CBenProgramDlg::PowOut(void)

{

//Calling the functions retrieve the temperatures
        CdTel.GetTemp((float(calltime)/1000), m_dCdTar);
        ZnTel.GetTemp((float(calltime)/1000), m_dZnTar);
        GrTop.GetTemp((float(calltime)/1000), m_dGrTopTar);
        GrMid.GetTemp((float(calltime)/1000), m_dGrMidTar);
        GrBot.GetTemp((float(calltime)/1000), m_dGrBotTar);
        CrMem2.GetTemp((float(calltime)/1000), m_dCrMemTar);
        CrMem3.GetTemp((float(calltime)/1000), m_dCrMem3Tar);
        ti++;

//Calling the functions to output the powers
        if (ti == interval ){
                CdTel.Outputpower(ti, Cdgain, Cdsetin, Cdti, int(163.83f* CdMaxP));
                ZnTel.Outputpower(ti, Zngain, Znsetin, Znti, int(163.83f*ZnMaxP));
                GrTop.Outputpower(ti, GrTopgain, GrTopsetin, GrTopti, int(163.83f*GrTopMaxP));
                GrMid.Outputpower(ti, GrMidgain, GrMidsetin, GrMidti, int(163.83f*GrMidMaxP));
                GrBot.Outputpower(ti, GrBotgain, GrBotsetin, GrBotti, int(163.83f*GrBotMaxP));
                CrMem2.Outputpower(ti, CrMem2gain, CrMem2setin, CrMem2ti,
int(163.83f*CrMem2MaxP));
                CrMem3.Outputpower(ti, CrMem3gain, CrMem3setin, CrMem3ti,
int(163.83f*CrMem3MaxP));
                ti = 0;
        }
}
```

The GetTemp and Outputpower functions acted for each temperature zone.

These functions for each zone were contained in a separate header file,

FurnaceControl.h . During the process of the header file the functions to

communicate with the thermocouple card and DA output card were

processed.

```
//FurnaceControl.h
//Header file to input furnace temperatures and control output powers
#include <conio.h>
#include <cmath>
#include <math.h>
#include <cbw.h>
//Declare the class
class CZone
{
public:
//Defining member functions
//constructor function
        CZone();
//Declaring function to output power
        void Outputpower(int m_t, float m_gain, float m_setin, float m_ti, int m_maxpower);
//Declaring function to obtain temperature
        void   GetTemp( float c2, float m_settemp);
//Defining public member variables
        int   m_power;                              //power to heater
```

```
        float m_temp;                          //actual temperature
        int m_outadd;                          //output address
        int m_inadd;                           //input address
        float m_prevtemp;                      //previous temperature
        int m_powerhigh;                       //high 6 bits for power output
        int m_powerlow;                        //low 8 bits for power output
        BOOL    m_flag;                        //flag for temperature confirmation

//Destructor function
        ~CZone();

private:
//Defining private member variables
        float m_delta;                         //target & actual temperature diff
        float m_delta1;                        //target & actual temperature diff
        float m_meanderiv;                     //temperature smoothing variable
        float m_deriv;                         //temperature derivative array
        float m_timediff;                      //time difference between readings
        int m_powerinc;                        //power change increment
        int m_boardnum;                        //temperature board number
        int m_scale;                           //set scale to CELCIUS
        int m_options;                         //temp board options
        float m_meantemp1;                     //previous temperature
        float m_meantemp;                      //mean temperature
        int m_increment;                       //power increment
        int m_chan;                            // temperature input channel
};

//The constructor function
CZone::CZone (void)
{
//Setting intial variables
        m_power = 0;
        m_boardnum = 0;
        m_scale = 0;
        m_options = 0;
        m_deriv = 0;
        m_flag = FALSE;
        m_meantemp = 0;
        m_meantemp1 = 0;
}

//The destructor function
CZone::~CZone()
{   }

//Function Name: GetTemp
//Function to read temperature
void CZone::GetTemp(float c2, float m_settemp)
{
        int ULStat;
//External Function to get temperature from board
        ULStat = cbTIn (m_boardnum, m_inadd, m_scale, &m_temp, m_options);
//Checking if temperature is within range
        if (m_temp < -9998.0){
                m_temp = 99999;
                m_power = 0;
        }
        m_meantemp1 = m_meantemp;

//Calculating the mean temperature with infinite averaging
        m_meantemp = (m_temp + ( 0.5f * m_meantemp)) / 1.5f;

//Calculating the temperature derivative
        m_deriv = (m_meantemp - m_meantemp1)/c2;

//Calculating the mean derivative
        m_meanderiv = (m_deriv + (0.5f * m_meanderiv)) / 1.5f;

//Calculating the temperature difference
        m_delta =  m_settemp  - m_meantemp;

//Checking if temperature is within bounds
        if((fabs(m_delta) < 5) && (fabs(m_meanderiv) < 1)){
```

```
                        m_flag = TRUE;
            }
            else{
                        m_flag = FALSE;
            }
}


//Function Outputpower
//Function to calculate power then output via DA board

void CZone::Outputpower(int m_t, float m_gain, float m_setin, float m_ti, int m_maxpower)
{
//If temperature difference is less than Setin temperature then include integration in power output
            if (fabs( m_delta ) < m_setin){
                        m_increment = int(m_gain * (m_delta - m_delta1 + (m_delta * (float(m_t) /m_ti))));
                        m_power = m_power + m_increment;
            }
//Else power is proportional to temperature difference
            else { m_power = int(m_gain * m_delta) ;}
            m_delta1 = m_delta;

//Ensuring power is within limits
            if (m_power < 0) { m_power = 0;}
            if (m_power > m_maxpower) { m_power = m_maxpower;}

//Splitting power into low 8 bits and high 6 bits for output
            m_powerlow = m_power & 255;
            m_powerhigh = m_power>>8;

//Outputting power
            _outp(m_outadd, m_powerlow);
            _outp(m_outadd + 1, m_powerhigh);
}
```

Appendix II

Growth Simulation Code

The simulation of the growth process was introduced in Chapter 5. The simulation was written in the FORTRAN 95 programming language, and, as discussed earlier in Chapters 5 and 7, several different variations of the simulation took place. The code for the basic model of a single growth run is given below. All of the quantities are in SI units unless stated.

```
        PROGRAM CadTelSub01
!FORTRAN 95 program to simulate growth in CdTe system
        IMPLICIT NONE
        DOUBLE PRECISION::r, L, PI, MCD, MTE, MTE2, MZN, RG, U!        !flow constants
        DOUBLE PRECISION:: VISC,KMCD, KMTe, KMZn, KV, SROUGH           !flow constants
        DOUBLE PRECISION::KB, SPA, GROUGH, ACTEN, GDEN, GCSA           !growth constants
        DOUBLE PRECISION::W, RO, RI, LANN, LO, KMANNCD, KMANNTE        !Annulus constants
        DOUBLE PRECISION::VISCCD, VISCTE, MDCD, MDTE2                  !viscosity constants
        DOUBLE PRECISION::AMU, ANNGAP, VA, VB, VG, KVANN               !Annulus constants
        DOUBLE PRECISION::TCDTE, TZNTE, TGROWTH                        !Temperature var
        DOUBLE PRECISION::TGROWTHBASE, TCROSS                         !Temperature var
        DOUBLE PRECISION::TCDTEP, TGROWTHBASEP, TCROSSP               !Plateau temps
        DOUBLE PRECISION::PCDSV, PCDSC, PCDGV, PCDGC, PTESV           !Pressure Var
        DOUBLE PRECISION::PTESC, PSTOT, PGTOT,PTEGV, PTEGC            !Pressure Var
        DOUBLE PRECISION::NCDSC, NTESC, NCDSV, NTESV, NCDGC           !Molar var
        DOUBLE PRECISION::NTEGC, NCDGV, NTEGV, NCDT, NTET             !Molar var
        DOUBLE PRECISION::NCDANN, NTEANN                              !Molar var
        DOUBLE PRECISION::CDFLOW, TEFLOW                              !Flow variables
        DOUBLE PRECISION::CDANNFLOW, TEANNFLOW                        !Annulus flow var
        DOUBLE PRECISION::CDSUB, TESUB, SUB                           !Sublimation rates
        DOUBLE PRECISION::SS, SG , EX                                 !Stoichiometry var
        DOUBLE PRECISION::t, VAL                                      !time variable
        DOUBLE PRECISION::RA                                          !Crystal growth rate
        DOUBLE PRECISION::BETACDS, BETATES, BETACDG, BETATEG          !Crystal growth var
        DOUBLE PRECISION::SALPHAA, ALPHAB, SALPHAC, GAMMA             !Temp gradients
        DOUBLE PRECISION::GALPHAA, GALPHAC                            !Temp gradients
        DOUBLE PRECISION::CALPHAA, CALPHAC                            !Temp gradients
        DOUBLE PRECISION::SALPHA, CALPHA, GALPHA, HEIGHT              !Temp gradients
```

```fortran
CHARACTER (LEN = 20)::NAME, NAME2                                    !Filename
LOGICAL::SFLAG, CFLAG, GFLAG, FLAG                                   !Plateaux flags
INTEGER:: I = 0, J = 1                                               !do loop interval
INTEGER:: tb, HOLD                                                   !time holding variables
INTEGER:: V

DOUBLE PRECISION::CDPRESS                                            !Cd Pressure Function
DOUBLE PRECISION::TECDPRESS                                          !Te2 Function
DOUBLE PRECISION::FLOW                                               !Capillary Flow Function
DOUBLE PRECISION::RATE                                               !Growth Rate function
DOUBLE PRECISION::BETA                                               !Growth Rate variable fn
DOUBLE PRECISION::WANN                                               !Annulus constant fn
DOUBLE PRECISION::SUBRATE                                            !Sublimation Rate fn

!General constants
PI=4.0D0*ATAN(1.0D0)                                                 !calculating pi
MCD = 112.41D0                                                       !atomic mass of Cd
MTE = 127.60D0                                                       !atomic mass of Te
MTE2 = MTE*2.0D0                                                     !molecular mass Of Te2
AMU = 1.6605D-27                                                     !Atomic Mass Unit
RG = 8.31441D0                                                       !gas constant J/mol/K
KB = 1.38D-23                                                        !Boltzman Constant
VAL = 1.0D-1                                                         !Time interval (s)

!Capillary flow constants
r=1.0D0 * 5.20D-4                                                    !capillary radius  m
L=1.172D-2                                                           !capillary length  m
U= (2.0D0/0.7D0)-1.0D0                                               !friction factor
MDCD = 2.978D-10                                                     !Molecular diameter Cd
MDTE2 = 5.72D-10                                                     !Molecular diameter Te2
VISC=9.00D-5                                                         !viscosity in PaS
KMCD=(PI**2)*(r**3)*U/(L*SQRT(8.0D0*PI*MCD*RG/1.0D3))
KMTE=(PI**2)*(r**3)*U/(L*SQRT(8.0D0*PI*MTE2*RG/1.0D3))
KV=PI*(r**4)/(16*VISC*L*RG)

!Annulus Constants
LO = 10.22D-3                                                        !Initiial Annulus length
LANN = LO                                                           !Annulus length
ANNGAP = 3.0D-4                                                      !Annulus gap
RO = 50.0D-3 / 2.0D0                                                 !Annulus outer radius
RI = RO - ANNGAP                                                     !Annulus inner radius
VA = 4.0D-4                                                          !Volume of source side
VG = 1.7D-4 +(0.178D0*PI*((RI)**2))                                 !Volume of growth side
W = WANN (RI, RO, LANN)                                             !Annulus transmission
KMANNCD = W * ((RO * RO)-(RI * RI)) * SQRT(PI / (2.0D0*RG*MCD))
KMANNTE = W * ((RO * RO)-(RI * RI)) * SQRT(PI / (2.0D0*RG*MTE2))
KVANN = ((RO**4) - (RI**4) - ((((RO**2)-(RI**2))**2)/ ALOG(RO / RI)))
KVANN = KVANN / (16.0D0 * RG * VISC * LANN)

!Growth & sublimation constants
GCSA = PI * (RI)**2                                                  !Growth Crystal csa
GDEN = 5.86D6                                                        !Growth crystal density
SPA = 6.481D-10                                                      !Lattice parameter
SROUGH = 2.0D0 *SPA                                                  !Source Roughness
GROUGH = 3.0D0 *SPA                                                  !Growth Roughness
ACTEN =5.25D0* KB * 1000.0D0                                         !Crystal activation energy

!Temperature Constants
SALPHAA = (2.0D0 / 60.0D0)                                           !Source Temp grad K/s
CALPHAA = (3.0D0 / 60.0D0)                                           !Cross Temp grad K/s
GALPHAA = (1.5D0 / 60.0D0)                                           !Growth Temp grad K/s
ALPHAB = 0.0D0                                                       !Temp grad K/s
SALPHAC = -(2.0D0 / 60.0D0)                                          !Temp grad K/s
CALPHAC = -(1.5D0 / 60.0D0)                                          !Temp grad K/s
GALPHAC = -(2.0D0 / 60.0D0)                                          !Temp grad K/s
GAMMA = 700.0D0                                                      !Temp grad K/m
HOLD = INT(REAL(24*3600)/VAL )                                       !Plateaux length (s)
TCDTEP=273.0D0 + 880.0D0                                             !source plateau temp K
TGROWTHBASEP = 273.0D0 + 710.0D0                                     !Base growth cry plat T
TCROSSP=900.0D0 + 273.0D0                                            !Crossmember temp K

!Initial variables
!Stoichiometry variables
SS=2.0D0                                                             !Source vap stoichio
```

```
SG=2.0D0                                                  !Growth vap stoichio

!Temperature variables
TCDTE=293.0D0                                             !source temperature
TGROWTHBASE = 293.0D0                                     !Growth crystal base
TGROWTH= TGROWTHBASE
TCROSS=293.0D0                                            !Crossmember temp
SFLAG = .FALSE.                                           !source plateau flag
GFLAG = .FALSE.                                           !growth plateau flag
CFLAG = .FALSE.                                           !crossmem plateau flag
FLAG  = .FALSE.                                           !Plateau end flag

!Molar variables
NCDSC = 100.0D0 /(MCD+MTE)                                !# mol Cd in source cry
NTESC = NCDSC /2.0D0                                      !# mol Te2 in source cry
NCDSV = 0.0D0                                             !# mol Cd in source vap
NTESV = 0.0D0                                             !# moles Te2 in source v
NCDGC = 22.8D0 /(MCD+MTE)                                 !# moles Cd in grow cry
NTEGC = NCDGC / 2.0D0                                     !# moles Te2 in growth cr
NCDGV = 0.0D0                                             !# moles Cd in growth v
NTEGV = 0.0D0                                             !# moles Te2 in growth v
NCDANN = 0.0D0                                            !# moles Cd in annulus
NTEANN = 0.0D0                                            !# moles Te2 in annulus

!Other variables
V = 10                                                   !File output variable
J = 0                                                    !Do loop variable
HEIGHT = 0.0D0                                           !Growth crystal height
CALPHA = CALPHAA
GALPHA = GALPHAA
SALPHA = SALPHAA

!Request filename
WRITE(*,*)"INPUT FILENAME"
READ(*,*)NAME
!Open output file
OPEN(10,FILE = NAME)
!Write column headers
WRITE(10,50,ADVANCE='NO')
WRITE(10,60,ADVANCE='NO')
WRITE(10,70,ADVANCE='NO')
WRITE(10,80,ADVANCE='NO')
WRITE(10,90)
!File output format statements
50   FORMAT(' t TCDTE TGROWTH PCDSV PTESV PCDSC PTESC ')
60   FORMAT('PCDGV PTEGV PCDGC PTEGC ')
70   FORMAT('NCDSC NTESC NCDSV NTESV NCDGV NTEGV ')
80   FORMAT('NCDGC NTEGC NCDANN NTEANN CDFLOW TEFLOW ')
90   FORMAT('CDANNFLOW TEANNFLOW NCDT CDSUB HEIGHT SS SG ')
55   FORMAT(I8,D16.8,D16.8,D16.8,D16.8,D16.8,D16.8)
65   FORMAT(D16.8,D16.8,D16.8,D16.8)
75   FORMAT(D16.8,D16.8,D16.8,D16.8,D16.8,D16.8)
85   FORMAT(D16.8,D16.8,D16.8,D16.8,D16.8,D16.8)
95   FORMAT(D16.8,D16.8,D16.8,D16.8,D16.8,D16.8,D16.8)

!Time loop
DO I=0, (HOLD + INT(REAL(24*3600)/VAL ))
VISCCD= KB *DSQRT(TCROSS*MCD/(1.0D3*PI**3*RG))/ MDCD**2
VISCTE= KB *DSQRT(TCROSS*MTE2/(1.0D3*PI**3*RG))/ MDTE2**2
VISC = 2.0D0 * (VISCCD + VISCTE)/3.0D0
KV=PI*(r**4)/(16.0D0*VISC*L*RG)
!Calculate source crystal pressures
PCDSC = CDPRESS(SS,TCDTE)
PTESC = TECDPRESS(SS, TCDTE)
!Checking source doesn't run out
IF (NCDSC.LE.0)THEN
PCDSC = 0.0D0
PTESC = 0.0D0
END IF

!Calculate sourse side pressure through number of moles
PCDSV = NCDSV * RG * TCDTE / VA
PTESV = NTESV * RG * TCDTE / VA
```

```
!Calculate growth side crystal pressures
PCDGC = CDPRESS(SG, TGROWTH)
PTEGC = TECDPRESS(SG, TGROWTH)

!Calculate growth side vapour pressures through number of moles
PCDGV = NCDGV * RG * TGROWTH / VG
PTEGV = NTEGV * RG * TGROWTH / VG
PSTOT = PCDSV + PTESV
PGTOT = PCDGV + PTEGV

!Calculate proportions in source side
EX = 1.0D0 / (1.0D0 + SS)
!Calculate flow through capillary
CDFLOW =   FLOW(KV, KMCD, TCROSS, PSTOT, PCDSV, PGTOT, PCDGV, (1 - EX))
TEFLOW =   FLOW(KV, KMTE, TCROSS, PSTOT, PTESV, PGTOT, PTEGV, EX)

!Calculate growth rate parameter BETA
BETACDS = BETA(SPA, SROUGH, PI, MCD, KB, TCDTE, ACTEN, AMU)
BETATES = BETA(SPA, SROUGH, PI, MTE2, KB, TCDTE, ACTEN, AMU)
BETACDG = BETA(SPA, GROUGH, PI, MCD, KB, TGROWTH, ACTEN, AMU)
BETATEG = BETA(SPA, GROUGH, PI, MTE2, KB, TGROWTH, ACTEN, AMU)

!Calculate growth rate - determined by min growth rate
RA = RATE(TGROWTH, PCDGC, PCDGV, PTEGC, PTEGV, BETACDG, BETATEG)
HEIGHT = HEIGHT + (RA * VAL)
NCDT = RA * GCSA * GDEN / (MCD + (MTE2 / 2.0D0))
NTET = NCDT / 2.0D0

!Calculate Source Crystal Sublimation Rate
SUB = SUBRATE(TCDTE, PCDSV, PCDSC, PTESV, PTESC, BETACDS, BETATES)
CDSUB = SUB * GCSA * GDEN / (MCD + (MTE2 / 2.0D0))
TESUB = CDSUB / 2.0D0

!Calculate Mass Fow through annulus
CDANNFLOW = (KMANNCD * PCDGV / SQRT(TGROWTH))+ (KVANN * (PCDGV**2)/TGROWTH)
TEANNFLOW = (KMANNTE * PTEGV / SQRT(TGROWTH))+ (KVANN * (PTEGV**2)/TGROWTH)

!Recalculate number of moles
NCDSC = NCDSC - (CDSUB * VAL)
NTESC = NTESC - (TESUB * VAL)
NCDSV = NCDSV + ((CDSUB - CDFLOW )* VAL)
NTESV = NTESV + ((TESUB - TEFLOW )* VAL)
NCDGV = NCDGV + ((CDFLOW - NCDT  - CDANNFLOW) * VAL)
NTEGV = NTEGV + ((TEFLOW - NTET  - TEANNFLOW) * VAL)
NCDGC = NCDGC + (NCDT * VAL)
NTEGC = NTEGC + (NTET * VAL)
 NCDANN = NCDANN + (CDANNFLOW * VAL)
NTEANN = NTEANN + (TEANNFLOW * VAL)

!Calculate stoich ratios from no. moles
SS = NCDSV / NTESV
SG = NCDGV / NTEGV

!Output to file
IF (J.GE.1000)THEN
 J = 1
 WRITE(V,55,ADVANCE='NO')I /100 , TCDTE, TGROWTH, PCDSV, PTESV, PCDSC, PTESC
 WRITE(V,65,ADVANCE='NO')PCDGV ,PTEGV, PCDGC, PTEGC
 WRITE(V,75,ADVANCE='NO')NCDSC, NTESC, NCDSV, NTESV, NCDGV, NTEGV
 WRITE(V,85,ADVANCE='NO') NCDGC, NTEGC, NCDANN, NTEANN, CDFLOW, TEFLOW
 WRITE(V,95,ADVANCE='YES')CDANNFLOW, TEANNFLOW, NCDT, CDSUB, HEIGHT, SS, SG
ELSE
 J = J + 1
END IF

!Implement temperature profile
IF((TGROWTHBASE.GE.TGROWTHBASEP).AND.(.NOT.GFLAG))THEN
 GALPHA = ALPHAB
 GFLAG = .TRUE.
END IF

IF((TCDTE.GE.TCDTEP).AND.(.NOT.SFLAG))THEN
 SALPHA = ALPHAB
 SFLAG = .TRUE.
```

A10

```
       END IF
       IF((TCROSS.GE.TCROSSP).AND.(.NOT.CFLAG))THEN
        CALPHA = ALPHAB
        CFLAG = .TRUE.
       END IF
       IF(GFLAG.AND.CFLAG.AND.SFLAG.AND.(.NOT.FLAG))THEN
        tb = I + hold
        FLAG = .TRUE.
        GFLAG = .FALSE.
        CFLAG = .FALSE.
        SFLAG = .FALSE.
       END IF
       IF ((I.GE.tb).AND.FLAG)THEN
        CALPHA = CALPHAC
        SALPHA = SALPHAC
        GALPHA = GALPHAC
        FLAG = .FALSE.
       END IF

       TGROWTHBASE = TGROWTHBASE + (GALPHA * VAL)
       TGROWTH = TGROWTHBASE  + (GAMMA * HEIGHT)
       TCDTE = TCDTE + (SALPHA * VAL)
       TCROSS  = TCROSS + (CALPHA * VAL)

       IF (TGROWTH.LE.293.0)THEN
        TGROWTH = 293.0
       END IF

       IF (TCDTE.LE.293.0)THEN
        TCDTE = 293.0
       END IF

       IF (TCROSS.LE.293.0)THEN
        TCROSS = 293.0
       END IF

       !Recalculate annulus flow constants
       LANN = LO + HEIGHT
       W = WANN (RI, RO, LANN)
       KMANNCD = W * ((RO * RO)-(RI * RI)) * SQRT(PI / (2.0D0*RG*MCD))
       KMANNTE = W * ((RO * RO)-(RI * RI)) * SQRT(PI / (2.0D0*RG*MTE2))
       KVANN = ((RO**4) - (RI**4) - (((RO**2)-(RI**2))**2)/ ALOG(RO / RI)))
       KVANN = KVANN / (16.0D0 * RG * VISC * LANN)

       END DO
       CLOSE(10)
       STOP
       END PROGRAM CadTelSub01

!!!!!!!!!!!!!!!!!!!!!!!!!!!!!!!!!!!!!!!!!!!!!!!!!!!!!!!!
       FUNCTION CDPRESS(Q,R)
!Function to get partial pressure of Cd over CdTe
       IMPLICIT NONE
       DOUBLE PRECISION, INTENT(IN)::Q,R
       DOUBLE PRECISION::a,b
       DOUBLE PRECISION::CDPRESS
       a=4.83918D11                                              !constants
       b=-23297.77
       CDPRESS=(Q**(1.0D0/3.0D0))*a*exp(b/R)
       RETURN
       END FUNCTION CDPRESS
!!!!!!!!!!!!!!!!!!!!!!!!!!!!!!!!!!!!!!!!!!!!!!!!!!!!!!!!
       FUNCTION TECDPRESS(Q,R)
!Function to get partial pressure of Te2 over CdTe
       IMPLICIT NONE
       DOUBLE PRECISION, INTENT(IN)::Q,R
       DOUBLE PRECISION::a,b
       DOUBLE PRECISION::TECDPRESS
       a=4.83918D11                                              !constants
       b=-23297.77
       TECDPRESS=(Q**(-2.0D0/3.0D0))*a*exp(b/R)
       RETURN
       END FUNCTION TECDPRESS
!!!!!!!!!!!!!!!!!!!!!!!!!!!!!!!!!!!!!!!!!!!!!!!!!!!!!!!!
```

A11

```fortran
      FUNCTION FLOW(kv, km, tc, pstot, ps, pgrtot, pgr, rat)
! Function to calculate capillary flow
      DOUBLE PRECISION,INTENT(IN)::kv, km, tc, pstot, ps, pgrtot, pgr, rat
      DOUBLE PRECISION::part1, part2
      DOUBLE PRECISION::FLOW
      IF(pstot.GE.1D-30)THEN
       part1 = rat * kv * ((pstot**2)-(pgrtot**2)) / tc
      ELSE
       part1 = 0.0D0
      END IF
      part2= (ps - pgr)* km / DSQRT(tc)
      FLOW = part1 + part2
      RETURN
      END FUNCTION FLOW
!!!!!!!!!!!!!!!!!!!!!!!!!!!!!!!!!!!!!!!!!!!!!!!!!!!!!!!!!!!!
      FUNCTION RATE(tgrowth, p1c, p1g, p2c, p2g, bet1, bet2)
! Function to calculate crystal growth rate
      DOUBLE PRECISION, INTENT(IN)::tgrowth, p1c, p1g, p2c, p2g, bet1, bet2
      DOUBLE PRECISION:: doz1, doz2
      DOUBLE PRECISION:: RATE
      doz1 = bet1 * (p1g-p1c)
      doz2 = bet2 * (p2g-p2c)
      IF (doz1.GE.doz2)THEN
       RATE = doz2
      ELSE
       RATE = doz1
      END IF
      RETURN
      END FUNCTION RATE
!!!!!!!!!!!!!!!!!!!!!!!!!!!!!!!!!!!!!!!!!!!!!!!!!!!!!!!!!!!!
      FUNCTION BETA(spa, del, pi, m, k, T, ue, amut )
!! Function to calculate growth rate variable Beta
      DOUBLE PRECISION, INTENT(IN)::spa, del, pi, m, k, T, ue, amut
      DOUBLE PRECISION::dum1, dum2, dum3
      DOUBLE PRECISION::BETA
      dum1 = ((spa/del)**2)* (spa **3)
      dum2 = DSQRT(2.0D0 * pi * m * amut * k * T )
      dum3 = exp(-1.0D0 * ue /( k * T))
      BETA = (dum1 * dum3 / dum2)
      RETURN
      END FUNCTION BETA
!!!!!!!!!!!!!!!!!!!!!!!!!!!!!!!!!!!!!!!!!!!!!!!!!!!!!!!!!!!!
      FUNCTION WANN(ar1, ar2, al)
!Function to calculate annulus constant w
      DOUBLE PRECISION, INTENT(IN)::ar1, ar2, al
      DOUBLE PRECISION::aa, ab, ay, ar, av
      ay = al / (ar2-ar1)
      ar = ar1 / ar2
      aa = (0.0741D0 - (0.0014D0 * ar) - (0.037D0 *ar * ar))
      aa = aa /(1.0D0-(0.918D0 * ar)+(0.05D0 * ar * ar))
      ab = (5.825D0 - (2.86D0 * ar) - (1.45D0 * ar * ar))
      ab = ab /(1.0D0 + (0.56D0 * ar) - (1.28D0 *ar *ar))
      av = 1.0D0 + ( ay * (0.5D0 - (aa * ATAN (ay/ab))))
      WANN = 1.0D0 / av
      RETURN
      END FUNCTION WANN
!!!!!!!!!!!!!!!!!!!!!!!!!!!!!!!!!!!!!!!!!!!!!!!!!!!!!!!!!!!!
      FUNCTION SUBRATE(tgrowth, p1c, p1g, p2c, p2g, bet1, bet2)
! Function to calculate crystal sublimation rate
      DOUBLE PRECISION, INTENT(IN)::tgrowth, p1c, p1g, p2c, p2g, bet1, bet2
      DOUBLE PRECISION:: doz1, doz2
      DOUBLE PRECISION:: SUBRATE
      doz1 = bet1 * (p1g-p1c)
      doz2 = bet2 * (p2g-p2c)
      IF (doz1.LE.doz2)THEN
       SUBRATE = doz2
      ELSE
       SUBRATE = doz1
      END IF
      RETURN
      END FUNCTION SUBRATE
```

A12

Appendix ▌▌▌

Optical Absorption Control Program

The optical absorption system described in Chapter 6 was computer controlled by a program called BenOptical which was written in Visual C++. The important sections of the main program file are shown below.

The OnInitDialog function is started when the program is initialised. In this function the function to select the meter is called, the output file opened, the time synchronised with the growth computer and a system timer installed.

```
BOOL CBenOpticalDlg::OnInitDialog()
{
          CDialog::OnInitDialog();

//Opening meter select dialog
          m_met.DoModal();

//Open file for output and output column headings
          Saver();
          fout << "Time(s), W1F1 Cd Blank, W1F2 Cd326, W1F3 Cd510, W1F4 CdBlank, W1F5 Cd640, ";
          fout << "W2F1 Gr214, W2F2 Gr316, W2F3 Gr510, W2F4 Gr307, W2F5 Gr640, ";
          fout << "W3F1 Zn214, W3F2 ZnBlank, W3F3 Zn480, W3F4 Zn307, W3F5 Zn640 \n";

//Syncronising time with growth computer
          m_grtime.DoModal();

//Installing timer
          int iInstallResult;
          iInstallResult = SetTimer (1, 50, NULL);
```

```
            time(&start);
            lasttime = start;

// Send the output card config to address
            _outp(iBase2 + 3, 144);
            return TRUE;
}
```

The OnTimer function is called every 50 ms and contains the main control algorithm. In this function the filter wheels are selected and turned, and the voltages read.

```
void CBenOpticalDlg::OnTimer(UINT nIDEvent)
{
//Loop events after each time interval
            int w1, w2, w3;
            UpdateData(TRUE);
//Getting the time
            time(&finish);
            timenow = m_grtime.m_growthtime + int(difftime(finish, start));
//Sending commands for stepper motors to step
            _outp(iBase2 + 2, out * i);
            i++;
            if (i==2){ i = 0; }
//Inputting data from optoswitches
            code = _inp(iBase2);
            UpdateData(FALSE);
// Turning to the home position
            if (HomeFlag){
                        w1 = m_w1a | (m_w1b / 2);
                        w2 = (m_w2a / 2) | (m_w2b / 4);
                        w3 = (m_w3a / 4) | (m_w3b / 8);
                        out = w1 + w2 + w3;
                        if (out == 0){  //On all slits - ready
                                    HomeFlag = FALSE;
                                    filter = 1;
                        }
            }
//Turning to next filter
            if (TurnFlag){
                        if (j <= 159){
                                    out = 7;
                                    j++;
                        }
                        else {
                                    TurnFlag = FALSE;
                                    j = 0;
                                    out = 0;
                                    filter ++;
                                    if (filter == 6){
                                                filter = 1;
                                    }
                        }
            }
// Set the multiplexer to select wheel
            _outp(iBase2 + 1, multiplex);
//If statments to take readings if wheels are on filter
            if (!HomeFlag & !TurnFlag){
                        m++;
//Read only every second
                        if (m == 20){
                                    m = 0;
                                    if (k <= 15){
                                                k++;
                                                UpdateData(FALSE);
                                    }
                                    else if (k <= 30){
//Take readings by calling Reader function
                                                Reader();
                                                voltage = (voltage + reading);
```

```
                                        p++;
                                        k++;
                                        wheel = multiplex + 1;
                                        UpdateData(FALSE);
                        }
                        else {
//Go to next wheel / filter
                                voltage = voltage / p;
                                p = 0;
                                wheel = multiplex + 1;
                                if (wheel == 1){
//Passing reading to relevant filter variable
                                        if (filter == 1){m_W1F1 = voltage;}
                                        else if (filter == 2){ m_W1F2 = voltage; }
                                        else if (filter == 3){ m_W1F3 = voltage; }
                                        else if (filter == 4){ m_W1F4 = voltage; }
                                        else if (filter == 5){ m_W1F5 = voltage; }
                                        }
                                else if (wheel == 2){
                                        if (filter == 1){ m_W2F1 = voltage; }
                                        else if (filter == 2){ m_W2F2 = voltage; }
                                        else if (filter == 3){ m_W2F3 = voltage; }
                                        else if (filter == 4){ m_W2F4 = voltage; }
                                        else if (filter == 5){ m_W2F5 = voltage; }
                                        }
                                else if (wheel == 3){
                                        if (filter == 1){ m_W3F1 = voltage; }
                                        else if (filter == 2){ m_W3F2 = voltage; }
                                        else if (filter == 3){ m_W3F3 = voltage; }
                                        else if (filter == 4){ m_W3F4 = voltage; }
                                        else if (filter == 5){ m_W3F5 = voltage; }
                                        }
                                k = 0;
                                multiplex++;
                                if(multiplex==3){
// After wheel 3 go back to wheel 1
                                multiplex = 0;
                                TurnFlag = TRUE;
//Turn to next filter
                                if (filter == 5){
//Write averaged voltages to output file
fout << timenow <<","<< m_W1F1<<","<< m_W1F2<<","<< m_W1F3;
fout <<"," << m_W1F4 <<","<< m_W1F5;
fout <<"," << m_W2F1 <<","<< m_W2F2 <<","<< m_W2F3;
fout <<"," << m_W2F4 <<","<< m_W2F5;
fout <<"," << m_W3F1 <<","<< m_W3F2 <<","<< m_W3F3;
fout <<"," << m_W3F4 <<","<< m_W3F5 << "\n";
                                        }
                                }
                                voltage = 0;
                                UpdateData(FALSE);
                        }
                }
        }
        CDialog::OnTimer(nIDEvent);
}

void CBenOpticalDlg::Reader(void )
{
//Function to obtain readings from DVM
        int status;
//Poll the DVM for the voltage
        send (m_met.m_DVMadd, m_met.m_code, &status);
        char r[15];
        int I;
//Read a voltage
        enter (r, 25,&I, m_met.m_DVMadd, &status);
        reading = float(atof(r));
        UpdateData(FALSE);
}
```

A 15

Appendix IV

Table Of Growth Runs

The table below gives a brief description of the growth runs discussed in Chapter 4.

Run No.	Boule Grown	Seed	Description
36	Alex	Mulitgrain 22 mm CdZnTe polygon	First CdTe boule grown, using cone growth tube setup, very polycrystalline
42	Bea	Mulitgrain 22 mm CdZnTe polygon on mosaic of CdZnTe crystals	First growth on solid disc pedestal, mosaic structure permeated throughout grown boule
43	Charlotte	Mulitgrain 22 mm CdZnTe polygon on top of Bea	Mosaic structure in Bea present in Charlotte
45	Estelle	Mulitgrain 25 mm CdZnTe polygon on 32 mm Si disc	Si disc did not act as buffer to allow the growth on undersized seeds – growth on Si faster than on CdZnTe

Run No.	Boule Grown	Seed	Description
54	Hazel	Multigrain 32 mm CdZnTe disc	Dimples in growth tube used to support pedestal – annulus blocked
55	Ingrid	Multigrain 32 mm CdZnTe disc	Dimples in growth tube used to support pedestal – seed sublimed as annulus was large and unblocked
64	Maria	Single crystal (111)b 32 mm CdTe disc	Varied temperature ramp rates to prevent blockage of annulus
65	Natalie	Multigrain CdTe disc, 52 mm diameter	First growth in 52 mm diameter growth tube produced boule which appeared to replicated seed and was studied by XRD
66	Ophelia	Multigrain CdTe disc, 52 mm diameter	Wedge shaped growth apparent on grown CdTe boule
69	Pat	Multigrain CdTe disc, 52 mm diameter	Evolution of growth viewed through series of photographs
82	Yasmin	Multigrain CdTe disc, 52 mm diameter	Crystal height more uniform after adding extra shielding between source and growth zones
83	Zoe	Multigrain CdTe disc, 52 mm diameter	CdTe growth seen to match seed closely, with one large (111) region visible, containing several twin bands
85	Amelie	50 mm diameter (111) CdTe disc	Pyramids visible on growth surface

Appendix V

Publications and Conferences

Publications emanating during the course of this work:

H. K. Sanghera, B. J. Cantwell, N. M. Aitken and A. W. Brinkman. *"The Growth of CdTe Bulk Crystals Using the Multi-Tube Physical Vapour Transport System"* J. Crystal Growth 237-239 (2002) 1711-1715.

H. K. Sanghera, B. J. Cantwell and A. W. Brinkman. *"Modelling the Growth of Tternary Compound Cadmium Zinc Telluride (in a Semi-open Markov-like System) from the Binary Sources CdTe and ZnTe"* J. Crystal Growth 237-239 (2002) 1741-1744.

B.J. Cantwell, A.W. Brinkman and A. Basu. *"Control of Mass Transport in the Vapour Growth of Bulk Crystals of CdTe and Related Compounds"* J. Crystal Growth 275 (2005) 543-547.

B.J. Cantwell, A.W. Brinkman, A. Basu and M. Robinson. *"New Method for the Growth of High Quality Cadmium Telluride Crystals for use in X-ray and Gamma-ray Sensors"* Conference Proceedings of the 38th Annual IEEE Carnahan Conference on Security Technology, 2004.

Conferences attended during the course of this thesis:

Institute of Materials "Materials Congress" 2002, London, UK, April 2002.

Poster *"Measuring the partial vapour pressures during the growth of cadmium zinc telluride"* presented.

14th International Conference on Crystal Growth, Grenoble, France, August 2004.

Posters *"Control of Mass Transport in the Vapour Growth of Bulk Crystals of CdTe and Related Compounds"* and *"In Situ Optical Pressure Measurements During the Vapour Growth of Bulk CdTe Crystals"* presented.